SMALL SCALE FIRE TESTING ON COMPOSITES

By

ABDURAZZAG LOTFI NAAS

A Thesis submitted for the degree of

DOCTOR OF PHILOSOPHY

Centre for Composite Materials Engineering,
School of Mechanical and Systems Engineering,
University of Newcastle upon Tyne
UK

June 2005

"In the Name of God, Most Gracious, Most Merciful"

TO THE SOUL OF MY FATHER

Abdurazzag Lotfi Naas

University of Newcastle upon Tyne (UK), May 2005

Abstract

A small-scale propane burner test was developed to enable rapid characterization of composite systems under reproducible conditions for either hot face temperature or heat flux. The burner rig is a low cost device which enables a 100mm square specimen to be subjected to a near uniform heat flux over its surface. The small-scale tests were conducted to measure the thermal conductivities of woven roven (WR) glass fiber mats with a weight of 0.13kg and 11.8mm thickness at high temperatures up to 800°C. An empirical equation was derived for calculating the variation in thermal conductivity of the dry glass fiber mats.

A series of fire resistance tests on composite laminates was carried out using a small scale furnace. During the tests the samples were that prepared and laminated using hand-lay-up techniques were exposed to fire conditions defined by a furnace temperature versus time curve. Excellent fire resistance under hydrocarbon curve test conditions was demonstrated for several matrix materials (i.e. isophthalic polyester, orthophthalic polyester, vinyl ester).

This information was important for the marine sector and companies such as Devonport group (DML) and Vosper Thorneycroft (VT) to determine if materials could perform to the A60 requirements. The A60 requirements for fire resisting structural are refer to the subject the material to 60 minutes fire testing under the SOLAS temperature/time regime. This then press the material for CFRP pipe repair and metal vessels in petroleum and transportation industries.

The experimental results from tests using the small scale furnace were compared with predictions of thermal responses of composite panels in fires using an existing theoretical model. The 1D FD model is capable of modelling the thermal response behaviour of polyester/WR and vinyl ester/WR laminates subject to fire for small scale heat sources.

Substantial savings in the cost of implementation of new applications may be achieved by modelling thermal responses. A thermal model based on a finite difference technique takes into account the decomposition processes in the laminate. The thermal model used was an extension of a model already developed by the Composites Group at the University of Newcastle. This model can also be developed to incorporate the responses of composite structures under load.

AKNOWLEDEGEMENT

Firstly, I wish to express my thanks to Libyan People's Bureau and Culture Department in London for providing financial support for my PhD study at University of Newcastle upon Tyne.

I am heartily grateful to Professor A.G. Gibson for his supervision, continued support and invaluable help during the research. I would also like to thank Dr Y-S Wu for his helpful discussion and advice throughout my study. He has given much of his time. His confidence in me and his support for this study throughout these years deserve more than regard.

My special appreciation goes to my wife Entesar for her support, understanding and continual encouragement. Without her, the thesis would not have come to completion. Thanks also to my children Mohammed and Rawad for being patient. I also wish to thank my mother and my father for their emotional support through all the stages of my study. I dedicate this thesis to the memory of my father. My thanks are also extended to my sisters and brothers.

Thanks to the staff in the School of Mechanical and Systems Engineering for an enjoyable and memorable time.

Table of Contents

CHAPTER THREE

CALIBRATION OF INCIDENT HEAT FLUX FROM A PROPANE FLAME

CHAPTERE FOUR

MEASUREMENT OF THERMAL CONDUCTIVITY OF DRY FIBRE-MATS AT HIGH TEMPERATURES

CHAPTER FIVE

SMALL-SCALE FIRE TESTING

CHAPTER SIX

DATA PREPARATION FOR MODELLING

CHAPTER SEVEN

ONE-DIMENSIONAL MODELLING OF COMPOSITES IN FIRE

LIST OF FIGURES

Chapter Three

Chapter Four

Chapter Five

Chapter Six

Chapter Seven

Chapter Eight

LIST OF TABLES

NOMENCLATURE

$\partial T/\partial t$	Copper meter temperature rise during the period of exposure to
$\dot{M}_g$	Gaseous mass flux or rate of gaseous mass flow
C_{pg}	Specific heat of the gases generated
$\Delta T_{front\ face}$	Calorimeter final front face temperature minus the initial front face (ambient temperature T_0) (°K)
$(1.0 - V_f)$	Void volume fraction
ΔT	Calorimeter slug temperature rise during exposure to heat source (°K)
A	Front face area of the meter slug (m^2);
A_A	Pre-exponential factor or rate constants for the decomposition reaction (1/sec)
$C_{p\ mat}$	Specific heat of the fibre mat (J/kg °K)
C_p	Specific heat of copper block meter (J/kg °K)
E	Activation energy (J/mole)
h	Heat transfer coefficient through natural convection (W/m^2 °C)
h_c	Heat coefficient from the front face of the meter during the cooling-down test (W/m^2 °K).
$h_{com.}$	Respective enthalpies of the composite material
$h_{cylinder}$	Convective heat transfer coefficient from the fire to the cylinder = 10 (W/m^2 °K)
h_g	Enthalpy of the gases generated during decomposition.
j	Time instants at the beginning of the time step
j+1	End of the time step involved
K	Thermal conductivity of meter material (copper) (W/m °K)
K_{com}	Thermal conductivity of the composite material (W/m °K)
K_f	Thermal conductivity of glass fibre (W/m °K)
K_{void}	Thermal conductivity of the void (W/m °K)
l	Sink or block thickness (m)
l_{opt}	Optimum length of the slug (m)
m_i	Instant mass of the sample (mg)
m	Mass of the copper meter (kg);

m_f	Final mass of the sample at the end of decomposition (mg)
m_o	The original mass of the sample (mg)
m_{S1}	Mass of sample weighed in air (g)
m_{S2}	Mass of sample weighed in water (g)
n	Order of the chemical reaction (non-dimensional)
q	Calorimeter heat transfer rate (W/m^2)
q_c	Heat flux received through convection effects (W/m^2)
q_i	Total incident heat flux from the propane flame (W/m^2)
q_r	Heat flux by the radiation component (W/m^2)
Q_p	Endothermic energy of decomposition
R	Gas constant (8.314 J/mole ^oK)
r^2	Correlation factor
T_{fs}	Temperature of the front surface of the meter (^oC)
t	Time (minutes).
$T(x, t)$	Temperature as function of in through thickness and time (^oC)
T_0	Initial temperature (^oC)
T_1	Measured hot face temperature (^oC)
T_b	Body temperature of the meter (^oC)
$T_{Cylinder}$	Cylinder temperature (^oK)
T_f	Temperature of the moving fluid (^oC)
T_{Fire}	Fire temperature (^oK)
T_{fs}	Meter front face temperature minus initial front face temperature
T_{mc}	Temperature on the receiving surface of the meter
T_s	Heat source temperature;
V	Total volume of the meter body (m^3)
V_f	Fibre volume fractions (m^3)
x	Through-thickness coordinate (m)
α	Absorptivity of the front face of the meter
α_m	Absorptivity of the receiving surface of the meter
ΔT	Temperature increment (^oC)
Δt	Time increment (s)
Δx	Distance between any two adjacent thermocouples

Subscripts

b	Body
c	Convection
cf	Cold face
com	Composite material
Cylinder	Cylinder
f	Final
f	Fibre
fs	Front surface
g	Gaseous mass flow
i	Incident
i	Initial
j	Time instants at the beginning of the time step
j+1	End of the time step involved
m	Meter
mat	Fibre mat
mc	Surface of the meter (^{o}C)
nc	Natural convection
opt	Optimum
O	Original
P	Pressure
pg	Gases generated
r	Radiation
room	Room
S	Source
s1	Sample weighed in air
s2	Sample weighed in water
sc	Surrounding heating source
w	Water

Greek Symbols

α	Absorptivity of the front face of the meter
α_m	Absorptivity of the receiving surface of the meter
ε	Emissivity of the front face of the meter;
ε_f	Efficient emissivity of propane flame;
ε_m	Emissivity of the meter's surface
ε_r	Radiation source emissivity
ε_s	Emissivity of heating source
ξ	Accuracy coefficient.
ρ	Density of the meter material (kg/m3)
ρ_{com}	Density of the composite material (kg/m^3)
ρ_{mat}	Density of the mat (kg/m3)
ρ_w	Density of water(1000 g/cm^3)
σ	Stefan-Boltzmann constant (5.67×10^{-8} $W/m^2\ ^oK^4$)

CHAPTER ONE
INTRODUCTION

1.1 Background

Fibre reinforced plastic composites offer ideal properties for many structural applications. Such materials generally have low through life cost, high specific strength and stiffness, overall weight savings, and good corrosion. Their resistance to a wide range of fluids which can attack metals makes them an ideal and attractive choice for many applications of FRPs in many areas, especially in extreme conditions such as maritime or offshore environments and in fire protection for transport containers (Gibson and Fahrer, 2000).

One problem with the implementation of composite materials, especially in the offshore industry, is their inherent combustibility and the associated fire risk. In the past the use of organic matrix composites offshore has been ruled out by prescriptive regulations, but these are gradually being replaced with a move towards performance-led design procedures, which allows the use of composites in fire risk situations.

Recently, composites are finding wider use in engineering applications in both the onshore and offshore industries. They are beginning to be used in fire water piping and in panels and for cladding for fire and blast protection. An important factor to be considered in all these applications is their response to fire. Although organic matrix composites are flammable, they have been found to possess some interesting and potentially useful properties in fires, the most important of which is the slow burn-through effect. In laminates above a certain critical thickness the burn-through rate is greatly reduced, along with heat release and heat transmission through the laminate. This effect enhances the fire integrity of composites, as well as their potential for use in fire protection applications.

The factors which contributing to the slow burn-through of composite laminates in fire are believed to be:

- The low thermal conductivity and diffusivity of composites.
- The low thermal conductivity of the residual glass, depleted of resin, which remains on the surface of the material in fire.
- The endothermic process of resin decomposition and vaporisation.
- The cooling effect created by the convection of volatile gases diffusing through the material towards the hot face.

The use of FRPs in structural applications has given rise to interest in the fire reaction and fire resistance of such materials. Fire resistance is defined by the material's ability to retain structural integrity and to limit the transfer of heat to other remote objects when exposed to fire (Gibson, 2000).

Interest in fire reactions and fire resistance analysis has led to the development of numerous standard tests. Unfortunately, current fire test methods have several limitations. Both the small scale reaction tests and large scale resistance tests require expensive test equipment (Gibson, 2003; Babrauskas, 1992). It has been proposed that the use of a small-scale fire resistance test along with validated mathematical modelling may be sufficient to replace more expensive test methods (Gibson, Wu and Naas, 2003).

Composite materials have long been known to show surprisingly good tolerance to thermal loading and their qualification and acceptance in fire risk applications depends on satisfying standard tests (Dodds *et al*, 2000). Standard testing involves small-scale tests such as non-combustibility, ignitability, surface spread of flame (ISO 834, 1975; BS 476, 1990) and cone calorimetery (ISO 5660-1, 1993). These are combined with large scale testing where the material is subject to realistic thermal insult possibly under load. Large-scale fire resistance tests include furnace tests under specified temperature/time curves such as the SOLAS curve (SOLAS, 1974 and BS 476 part 20, 1990) representative of a fire driven by cellulosic materials, or the more severe hydrocarbon fire curve (BS 476 part 20, 1990).

Fire testing is essential for the safe implementation of new materials. A predictive model for the response of composite materials would help to minimise the number of standard tests required to qualify a new material. Also, such models may be generalised to predict thermal response under more realistic fire actions. Realistic

thermal modelling of fire behaviour provides the capability to demonstrate innovative, new designs, to a specified fire rating, with the minimum initial recourse to expensive fire testing (Dodds *et al*, 2000).

There are two basic manners in which fires can be fought: active and passive. Active fire fighting is commonly provided by automatic detection (smoke detectors and heat sensors), water sprinklers, deluges and sprays, and the use of fire suppressive foam and gas. In addition to active measures, passive fire protection is now being increasingly used to minimise the consequences of a fire. Passive protection is either achieved by the design of the structure itself, or by cladding, coating or a free standing system that is designed to impede the spread of the fire, saving both the structure and life within the fire environment.

The choice of active or passive fire protection systems or a combination of both is influenced by the protection philosophy, the predictability of fire and its duration, the equipment and structures requiring protection, and the time required for evacuation.

This thesis does not consider active fire protection, instead concentrating on fibre reinforced plastics (FRP), and examines the potential for the use of these structural panel skin applications.

One of the aims of this study was to use the small scale fire testing facility to experimentally examine some applications of GRP laminates for fire protection of (CFRP) pipes and metal vessels in petroleum and transportation industries.

1.2 Objectives of the Study

The objective and purpose of the study are:

- To develop a small-scale low cost fire test that enables rapid characterisation of many samples to be carried out.
- To determine the thermal conductivity of dry glass fibre mat as a function of temperature, in order to improve the present composite fire analysis tools.

- To investigate the fire resistance properties of composite laminates of varying construction used in fire protection.
- To validate the existing thermal model with data obtained experimentally.

1.3 Structure of the Thesis

This work discusses the potential benefits of using composite laminates for use in structures that may be subjected to fire. The plan of work for this thesis falls into four main areas involving eight chapters leading to an understanding of the behaviour of the composites under fire conditions.

To give an overview of the behaviour of composite materials in fire, chapter two gives a description of research on the applications of composite materials, the fire performance of composites (fire reaction and fire resistance), the kinetics of the thermal degradation of polymers, the thermal conductivity of composite materials, heat measurement techniques and the modelling of composites in fire.

Chapter three describes the small scale fire resistance testing carried out on composite systems. Chapter four describes the use of the propane burner in small-scale fire testing to measure the thermal conductivity of dry fibre-mats at high temperatures. Small-scale fire testing using the jet fire test and furnace tests on composite panels are presented in chapter five. Data input required for the analysis used in thermal modelling (such as rate factor, the order of the reaction, and activation energy), is presented in chapter six. Full details of using the 1D FD thermal model and a comparison with experimental data are presented in chapter seven. The final conclusions that can be drawn from the completed work, and recommendations for further work, are reported in chapter eight. Following that, the references used throughout this thesis are listed.

CHAPTER TWO

LITERATURE SURVEY

This chapter presents a review of the literature related to the fire behaviour of composite materials, including polymer matrix composites, composite applications, the fire performance of composites and the modelling of composites in fire.

2.1 Types of Fire Hazard

As fuels have become more sophisticated and powerful, and as demand for production has increased, the risk of a fire getting out of control has increased. The annual fire statistics for the UK reveal the full extent of injury and loss. Figure 2.1 shows annual trends in fire victims by cause of death. It is clear that the majority of casualties result from smoke/toxic gases, and burns caused by exposure to excess heat also show a major contribution. These are the primary fire hazards. A review of the typical patterns of fire growth and the evolution of fire hazards was conducted by Irvine and McCluskey (2000).

The use of fire science may improve our ability to predict the behaviour of different materials across a range of possible fire scenarios.

The growth of a fire in a compartment may be illustrated by referring to the variation of average temperature following ignition (Irvine and McCluskey (2000). Figure 2.2 shows a schematic diagram for the increase in the average temperature in a burning room as a function of time. All fires start with an ignition event. As the fire grows, three primary hazards are generated which are heat, smoke and toxic gases. The flashover starts following the increases in heat and temperature, typically to 500-600°C. The generation of heat reaches a peak at the stage of a fully developed fire around 1000°C and after this stage, eventually the temperature begins to fall as the fuel is consumed, flaming finally stops and all that remains in the compartment are glowing coals.

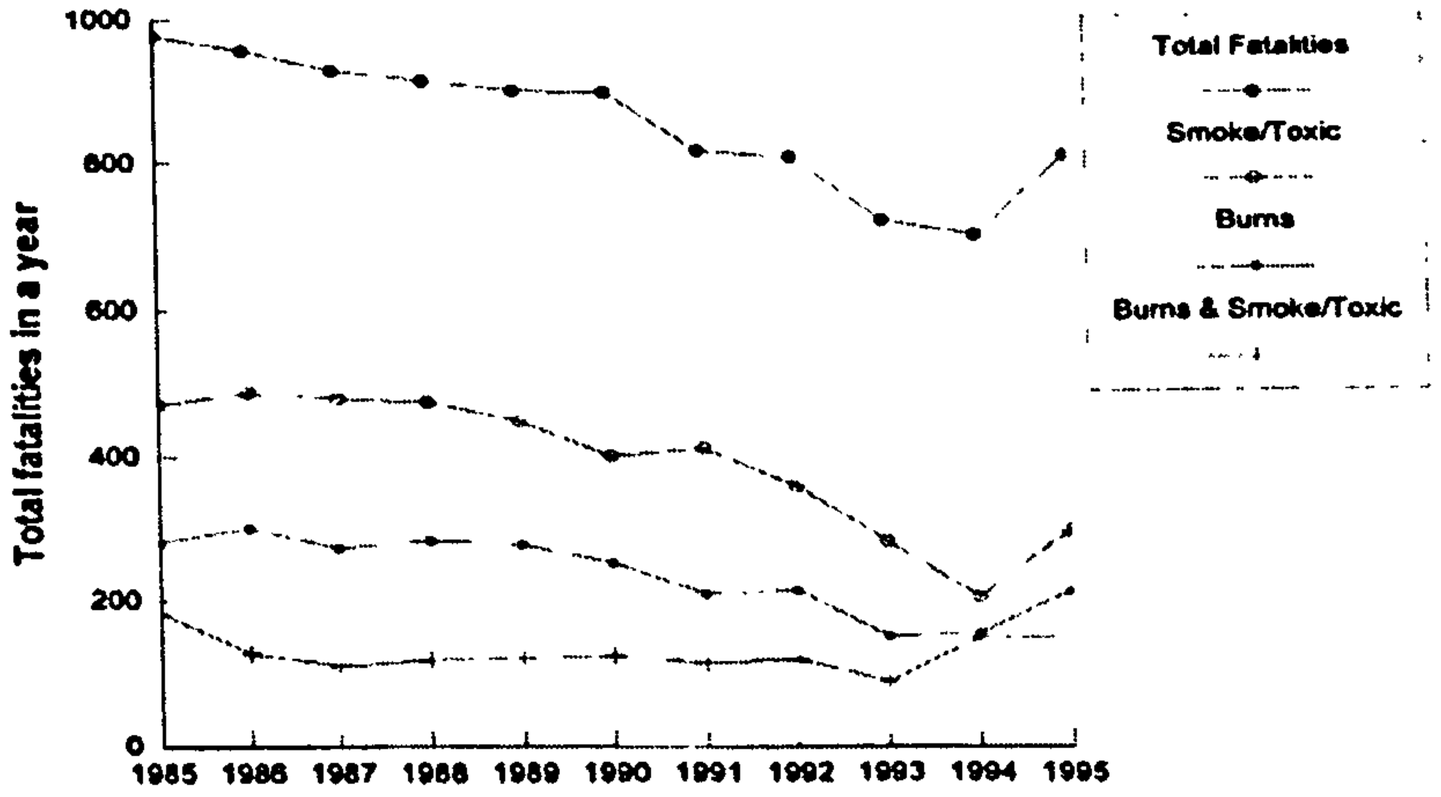

Figure 2.1 Annual total number of fire fatalities in the UK (1985-1995) by cause of death (Irvine and McCluskey, 2000).

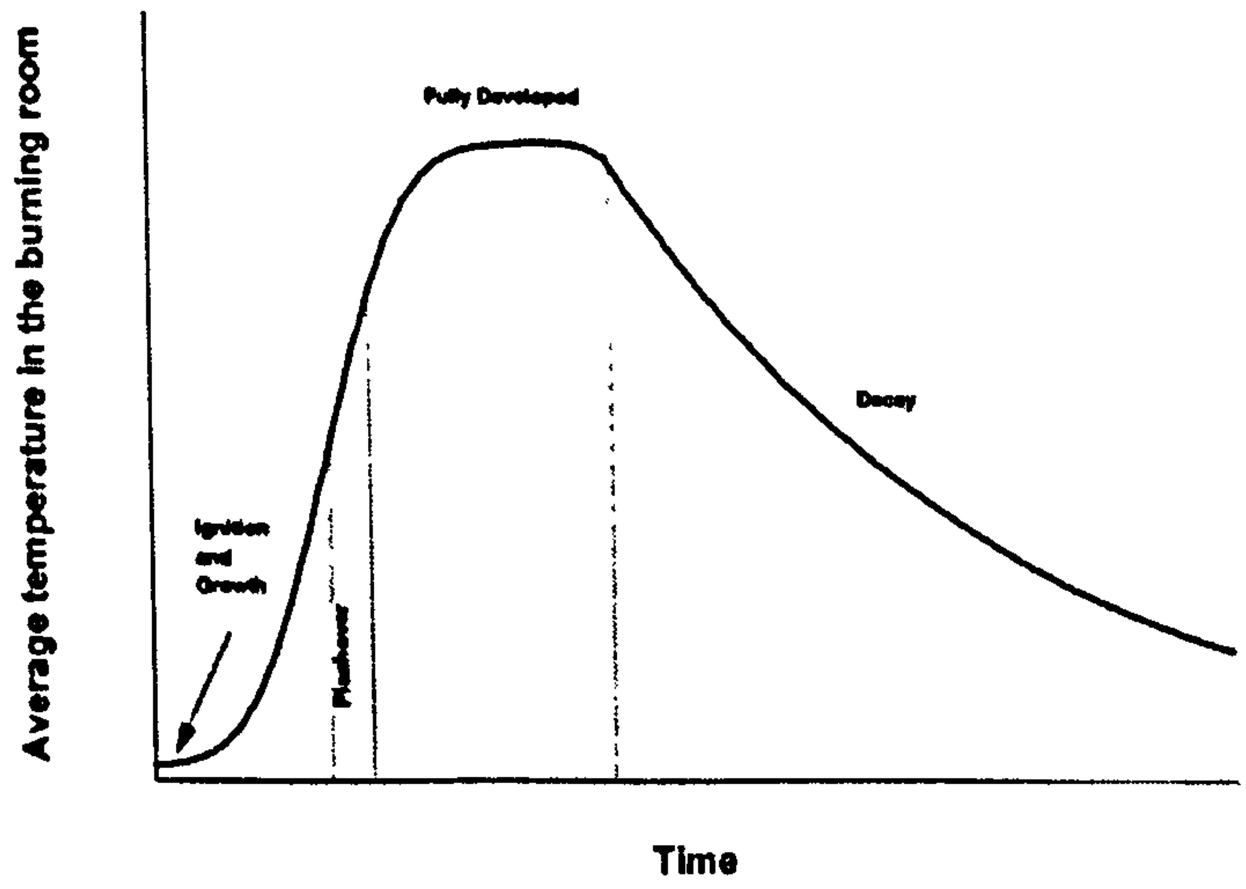

Figure 2.2 Schematic representation of a fire vs. time, from ignition and growth, flashover, full development and eventual decay (Irvine and McCluskey, 2000).

A variety of tests have been developed to ascertain the manner in which materials will behave in fire (Irvine and McCluskey, 2000). These are principally small scale standard tests such as BS 476 pt 6 (Troitzsch, 1983), and full scale and newer tests which examine a material's reaction to fire, such as the cone calorimeter. The numerous kinds of standard fire tests developed have been summarised by Troitzch

(1983). The definition of acceptable behaviour in fire for both materials and products is not universally agreed. In other words, what may constitute acceptable behaviour in one test method may be deemed unacceptable in another. Small scale tests will continue to be used to develop new materials and products in a cost effective manner. Full scale tests of fire behaviour are an alternative, but expensive, means.

Accidental fires have been a problem throughout human history, and they cause major loss of life and property worldwide almost every day. Prominent recent examples of fire hazards (Tewarson, 1995) include:

- Casualties in the Düsseldorf Airport fire: In Germany, April 1996 at Düsseldorf airport, 17 people were killed, 72 people were injured, and the estimated financial losses were of 150-500 million Euros. Poisonous smoke killed 17 people and infected the airport with dioxin-containing debris. The airport was later fire protected with non-combustible Rockwool insulation.

- Fire at the Piper Alpha platform oil offshore production facility in the North Sea (UK), 1988: The offshore oil industry is one which has inherent risks due to the nature of the work and the isolation of locations. Together with the unpredictability of offshore weather, these factors can, in a fire situation, lead to a disaster.

Wide ranging changes in offshore operating practices and regulations occurred as a result of an official report on the explosions and fires aboard Occidental Petroleum Ltd's Piper Alpha platform, at 11:20 p.m. on July 6th 1988 in the U. K. North Sea, 120 miles northeast of Aberdeen (Cullen, 1990; Oil & Gas Journal, 1988 and The Engineer, 1990). This caused what may turn out to be the heaviest death toll in the history of the offshore petroleum industry. After a series of large explosions, fires were still burning 17 hours later and flames, which soared to 700 ft at the peak of the fire, could be seen for 25 miles. The fires heavily damaged the platform. Over 160 workers aboard the platform died and only 61 survived. Following this tragedy, Cullen (1990) conducted a 13 month inquiry into the reasons for the explosions and a series of detailed recommendations were given. The major outcome of the Cullen report, however, was a retreat from prescriptive design towards performance based design. This change in design ideology gives more flexibility in the choice of

materials which can be used, and places more responsibility on the operators to ensure correct and safe design.

There are an infinite number of different fire scenarios due to fire being dependent not only on heat source and material but on all other conditions too. Fire, however, can be grouped into many categories. Those which may occur in the offshore/petrochemical environment (Dewhurst, 1997) are as follows:

- ***Pool Fire***: A turbulent diffusion fire burning above an upward facing horizontal pool of vaporising fuel under conditions where the fuel vapour or gas has zero or very little initial momentum. A boiling pool fire is difficult to control; it may accompany a jet fire where liquid rains out of the jet.

- ***Jet Spray Fire***: A turbulent diffusion flame resulting from the combustion of a fuel continuously released with some significant momentum in a particular direction.

The potential durations, temperatures and intensities of pool fire and jet fire together with other different types are given below in Table 2.1 (Dewhurst, 1997).

Table 2.1 Potential duration, temperatures and heat fluxes for different fire types.

Fire Type	**Duration**	**Temperature (°C)**	**Heat flux (kW/m^2)**
Blow-Out	Months	1000-1700	100-1000
Fire Ball/BLEVE	Seconds	1000-1400	113-1200
Pool Fire	Hours	1100-1200	150-220
Running Fire	Hours	800	-
Jet/Spray Fire	Hours	900-1500	80-1550

2.2 Composite Applications

Composite materials are finding wider use in many engineering applications, including offshore and onshore oil and gas industries. Because of their low through-life costs, high specific strength, overall weight savings and their chemical resistance to a wide range of fluids, they are an attractive choice for many applications (Gibson, 2000). Results of composite material fire testing have been reviewed in a number of papers (ARP, 2000, Gibson *et al*, 1995; Gibson, 2000; 2001; Dodds *et al* 2000 and Wang *et al*, 1999). Glass-reinforced polymer (GRP) composites are used increasingly in construction for many applications onshore such as fluid transport, and also for offshore platforms and in marine structures. In many cases the cost of composite components exceeds that of their metallic counterparts. However, the installation cost, especially for pipe systems, is often lower than with steel because of their relative ease of handling. Moreover, the cost advantages are even greater when composites replace expensive corrosion-resistant metals such as copper-nickel alloys, duplex or super duplex stainless steel or titanium (Gibson, 2000). Their features can also improve reliability and lead to lower through-life costs.

The most common polymer used in many composites applications are polyester, vinyl ester and phenolic because of their low cost and good durability in the environment. Vinyl ester resin is used infrequently instead of polyester in some applications such as in marine applications, because of its higher heat-distortion temperature, better water resistance and higher mechanical properties. However, vinyl ester resins are about 1.5-2 times more expensive then polyester, and therefore are used only for small high-performance requirements. Phenolic resins are used in composites requiring excellent fire resistance; however their mechanical properties are inferior to polyester and vinyl ester. Other types of resins, such as epoxies and thermoplastics (for example polyethersulphone and polyetherimide), are used in most composites applications, again because of their cost. Table 2.2 (Gibson, 2000) compares the most common types of resins used in composite structural applications. It appears that most resins are ruled out from use in areas where smoke and toxicity would be a problem (Gibson, 2000). From the viewpoint of toxicity, phenolic resins are the most favourable systems.

Table 2.2 Candidate resins systems for use in composites applications.

Resins	Mechanical integrity	Low smoke & toxicity in fire	Cost
Polyester	****	*	***
Vinyl ester	*******	*	******
Epoxy	*********	*	*********
Phenolic	*****	****	****

Excellent examples of the use of composites in offshore structures are the two small scale platforms (see Fig 2.3) deployed in shallow water by Amoco UK (now BP-Amoco). The low cost and easy transport were important features in their design, and minimum topside weight was important because of their monopod from. These topside assemblies, which included 10% by weight of composites, involved extensive use of glass/phenolic grating for floors, walkways and handrails, along with enclosure and heat protection walls. Table 2.3 lists the current offshore applications of composites, including those on the Amoco platforms, along with anticipated applications (Gibson, 2000).

Figure 2.3 Davy and Bessemer monopod platforms (Gibson, 2000).

Table 2.3 Current and expected future offshore applications (Gibson, 2000).

Recent applications of composite offshore		
Fire protection	Walkways and flooring	Lifeboats
Blast protection	Handrails	Buoys and floats
Corrosion protection	Sub sea anti-trawl structures	ESDV protection
Partition walls	Casings	Boxes, housings and shelters
Aqueous pipe systems	J-tubes	Loading gantry
Tanks and vessels	Caissons	Pipe refurbishment
Firewater systems	Cable trays and ladders	Riser protection
Pipe liners	Accumulator bottles	Bend restrictors
Separator internals	Well intervention	Subsea instrument housings
Future applications		
Rigid risers	Coilable tubing	Flexible risers
Tendons	Primary structure	Separators

2.2.1 Structural Applications

Composite materials can provide a cost and weight-effective solution, such as for blast and fire walls, when used in offshore platforms. Composite materials are also beginning to be used in the combined corrosion and fire protection of load-bearing steel structures, as in the platform legs shown in Fig. 2.4 (Gibson, 2000). Pultruded composite gratings have also been used offshore since the 1980s. Polyester and vinyl ester resins are still employed today for many applications. However, successful pultrusion techniques have been developed for phenolic resin for use offshore where fire integrity is important. In addition to the performance of phenolic gratings during fire, they have the ability to maintain a significant level of functionality after fire exposure.

Figure 2.4 Composite combined corrosion and fire protection applied to a platform jacket leg (courtesy of Vosper Thornycroft (UK) Ltd).

2.2.2 Applications for Pipes, Tanks and Vessels

The most important areas where composites are being used for applications such as fluid transport and storage are summarized below:

- Composite Pipework: Glass reinforced epoxy (GRE) is the material most used onshore for both low and high pressure applications with a wide variety of fluids (Stringfellow, 1992). By contrast, the main offshore applications have been limited so far to relatively low pressure aqueous services. Beside the best flexible chemical resistance provided by GRE, a number of other resin types may also be used, including: (i) isophthalic polyester, for general purpose products; (ii) vinyl ester, which often shows corrosion resistance approaching that of epoxy, and (iii) phenolic, which has recently been developed for fire-critical applications;

- Tanks and vessels: Composites have been used for the manufacture of tanks for water and diesel storage (Anisdahl *et al*, 1999; BS 4994, 1987 and ASME, 1992).

- Rigid risers: The development of composite rigid risers has been initiated by a number of companies, including Conco, Petrobras, Shell and Statoil. The Institute Français du Pétrol (IFP) has taken a role in research on prototype riser systems.

2.3 Fire Performance and Behaviour of Composite Materials

A key quality of composite materials for use in structural applications is their behaviour and response when exposed to severe fire. Three recent conferences have examined the fire resistance and reaction of composites (Dodds *et al.*, 2000; Gibson A. G. and Fahrer, 2000 and Gibson 2000). Testing to obtain both resistance and reaction properties are listed in Table 2.4.

Table 2.4 Properties and tests relating to the fire performance of materials in structural applications.

FIRE REACTION	
Start-up and progress of fire	Oxygen index, Combustibility, Time to ignition, Surface spread of flame, Peak heat release, Average heat release
Typical Test	Single burning item test (SBI)
Human survivability	Smoke generation, Toxicity index
FIRE RESISTANCE	Pool fire tests, Burner tests Furnace tests, Jet-fire tests

The behaviour and response of composite materials is measured and characterised by small and large scale testing. Small-scale tests are quick, repeatable ways to determine the flammability characteristics of organic materials. Usually, many types of information can be obtained using relatively small test specimens. Typical tests are the Cone calorimeter – ASTM E 1354, Intermediate-Scale tests, DTRC Burn through Test, U.S. Navy Quarter Scale Room Fire Test, and 3-Foot E 119 Test with Multiplane Load. The large-scale tests are designed to be the most realistic simulation of a shipboard fire scenario. Tests are generally not standardized and instead are designed to compare several material systems for a specific application. The aim of these tests is to model materials, geometry and the fire threat associated with a specific compartment. These include Corner Tests, Room Tests, SOLAS

Requirements for Structural Materials in Fires, International Maritime Organization (IMO) Tests, Room/Corner Test, and Hydrocarbon Inventory.

2.3.1 Fire Reaction

Fire reaction relates to the responses of materials, especially in the early stages of a fire, and their interaction with the environment. Properties considered for fire reaction can be subdivided into those that are involved in the progress of fire and those that relate to human survivability. These can be regarded as characteristic of the materials, as opposed to the structure, and can be determined from relatively small samples of materials.

The industry is currently in the process of standardizing tests that can quantify the performance of various composite materials systems in a fire. The U.S. Navy has taken the lead in an effort to certify materials for use on submarines. No single test method is adequate to evaluate the fire hazard of a particular composite material system. The behaviour of a given material system in a fire is dependent not only on the properties of the fuel, but also on the fire environment to which the materials system may be exposed. Proposed standardized test methods for flammability and toxicity characteristics cover the spectrum from small-scale to large-scale tests.

In 1982 the British Standards Institution published BS 6336 (1982) entitled 'Guide to the Development and Presentation of Fire Tests and their Use in Hazards Assessment'. Examples of methods to measure the key parameters (ignitability, heat release, flame spread, smoke production and toxic gas production) are the SBI (single burning item), room/corner test (ISO 9705), spread of flame/LIFT (IMO FTPC, Part 5 and ISO 5658-2) and the cone calorimeter (ISO 5660). The cone calorimeter, as shown in Fig. 2.5 (ISSO 5660) is considered to provide a good indication of the fire reaction behaviour of materials in a fire and its data would be expected to present the means to predict fire damage if measurements of damage depth and weight loss experienced by a composite as a result of a fire show good correlation.

Figure 2.5 Typical cone calorimeter standard fire tests.

The mass loss process, as observed during a cone calorimetry experiment and after exposure to a fuel fire of controlled duration, has been investigated by Burchill *et al* (2004). Several styrenic thermoset GRP composites were exposed to a range of heat fluxes corresponding to small, medium and large fires. A typical marine structural composite was also exposed to a fuel fire and results correlated with cone calorimetry data. Mass loss rates at a given flux were found to be linearly related to those at different heat fluxes. Relative mass loss rates appear to obey an Arrhenius relationship and the slope and intercept may be considered the same for all the materials tested given the errors in measurement.

There are several ways of modifying the basic fire reaction behaviour of resin systems through the use of additives or through chemical modification of the polymer. One method of improving fire performance is through the use of aluminium trihydrate (ATH) additive (Dodds *et al*., 2000). ATH operates by decomposing at temperatures in the range 200-400°C:

$$2AL(OH)_3 \longrightarrow Al_2O_3 + 3H_2O. \nearrow$$

The decomposition process is endothermic, and the water that develops gradually and naturally as a result of this decomposition provides both an intumescing effect and a blanket against oxygen. ATH has been used most effectively in conjunction with Modar resins (Dodds *et al*., 2000) which have a naturally low viscosity and low toxicity polyester resins (Brown; *et al*, 1999). The most well-known techniques adopted include the addition of alumina trihydrate (ATH) filler, phosphorous compounds, halogenation and antimony compounds. These techniques are used to improve the fire reaction properties. However, improvements in one particular property, such as ignitability for instance, may sometimes have effects on other properties, such as toxic product generation.

Polymeric materials are widely used in a variety of applications. Because polymers are combustible by nature, this could limit their use. This has led to efforts to find ways to modify their ignition, flame spread, and heat production as well as production of smoke and toxic and corrosive gases. The aim of these modifications of a polymer product is to improve its fire performance to pass the criteria of the specified fire tests for the application of concern. Different methods can be used to improve the fire performance of composite structures. Many publications have considered non-toxic solutions. For example, Lay and Gutierrez (2001) focused on the use of fire retardant fillers (alumina trihydrate (ATH)) added to a common polyester resin. Two types of ATH have been tested, at the same concentration, and many aspects have been studied such as production processing, mechanical properties (i.e., static and dynamic tests and fatigue) and fire reaction (i.e., cone calorimeter tests at different heat flux rates). The properties of polyester composites with ATH have been compared to those of standard polyester material. It has been shown that the use of ATH slightly decreases the mechanical properties of polyester composites, but significantly improves their fire behaviour.

Some experimental work has been done with respect to ATH additives. Lay and Gutierrez (2001) found that ATH added at a concentration of 60 pph (parts per hundred), is the best compromise to keep the ease of processing and good mechanical properties as well as obtaining a good improvement in the fire reaction of the composite. Fire reaction tests have shown that adding 60 pph of ATH in a

polyester composite, formed by hand lay up, significantly improves its fire reaction behaviour.

The fire properties of glass reinforced resins have been studied by Scudamore (1994); Sorathia *et al* (1992); Brownen and Mathys (1997); Sorathia and Beck (1996), who mainly concentrated on their burning characteristics. The most important parameter in characterising the flammability of materials is the rate of heat release, which is readily determined in the cone calorimeter along with ignitability, heat of combustion, smoke and toxic gas evolution (Burchill *et al*, 2003). The rate of heat release and ignition times are important parameters and can be used to estimate the time to flashover in large-scale fire tests (Wickstom and Goransson, 1987).

When fire reaction properties (i.e., time to ignition, heat release and smoke evolution) are the most important factors, phenolic composites and those based on ATH-modified resins are the most attractive. Figures 2.6 and 2.7 shows a comparison of time to ignition and heat release values for polyester, vinyl ester, epoxy and phenolic laminates of 3mm thick of woven glass fibre reinforcement together with the range of reported results for ATH-modified Modar and low toxicity polyester systems (Dodds *et al*., 2000). There are relatively small differences between the polyester, vinyl ester and epoxy composites, whereas the phenolic and Modar/ATH systems both show clear benefits in terms of both time-to-ignition and heat release. This is attributable to the high aromatic content, which promotes the formation of a significant amount of carbonaceous char, which in turn improves integrity and reduces heat release (Dodds *et al*., 2000).

In relation to survivability the main short-term to medium-term factors which have been recognized are smoke generation, which delays escape, and the level of carbon monoxide which is the most toxic parameter in the short term (Dodds *et al*., 2000).

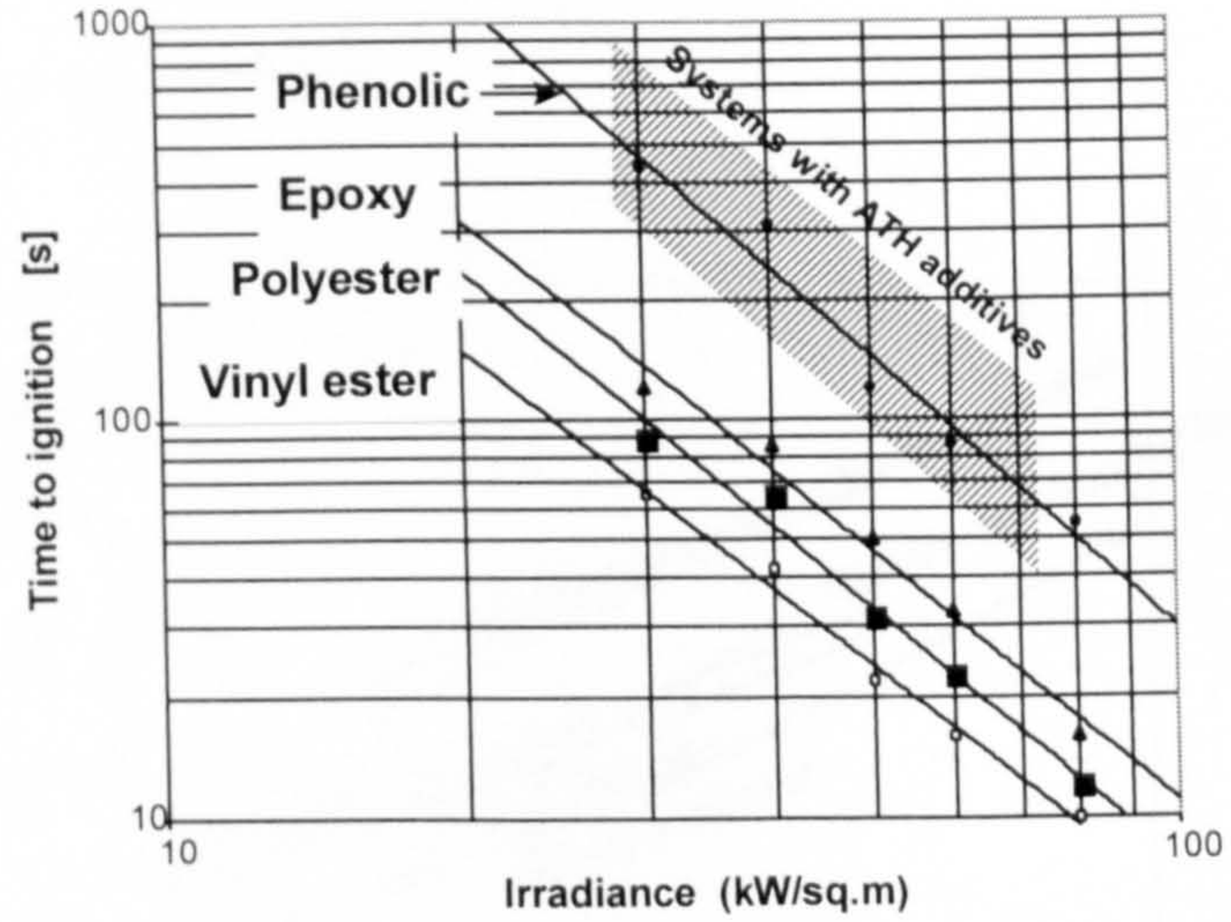

Figure 2.6 A comparison of time to ignition of cone calorimeter vs. irradiance.

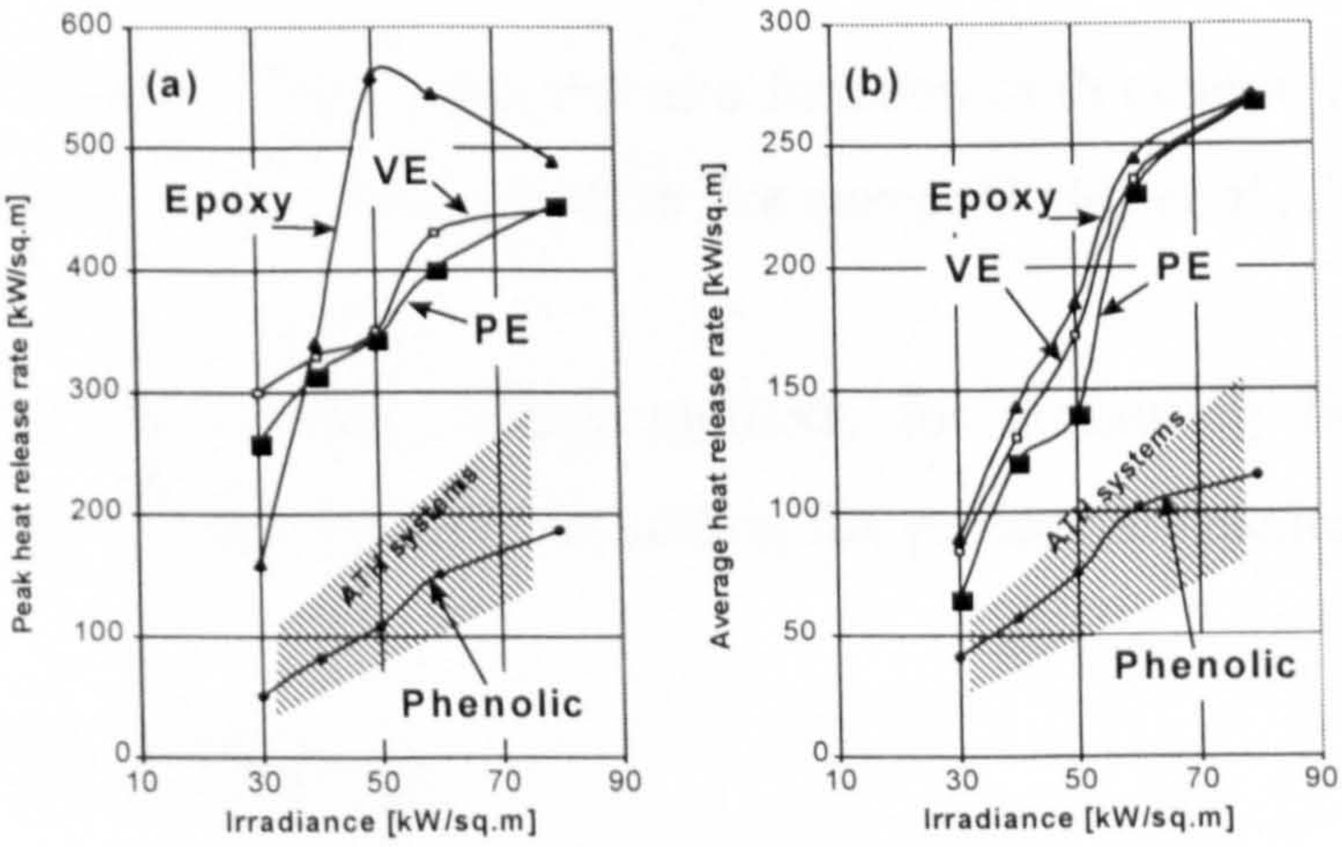

Figure 2.7 (a) Peak heat release rate and (b) average heat release rate vs. irradiance (Dodds *et al.*, 2000).

2.3.2 Fire Resistance

The term fire resistance relates to a structure's ability to maintain functionality during exposure to fire. Tests for fire resistance are generally large in scale, and more expensive, than those for fire reaction since they require the measurement of structural as well as material properties. Figure 2.8 shows the fire resistance characteristics of a range of types of composite materials studied for possible use in engineering applications (Dodds *et al.*, 2000). Despite the combustibility of the

organic component of the composites, the materials studied were able to offer significant fire-resisting properties.

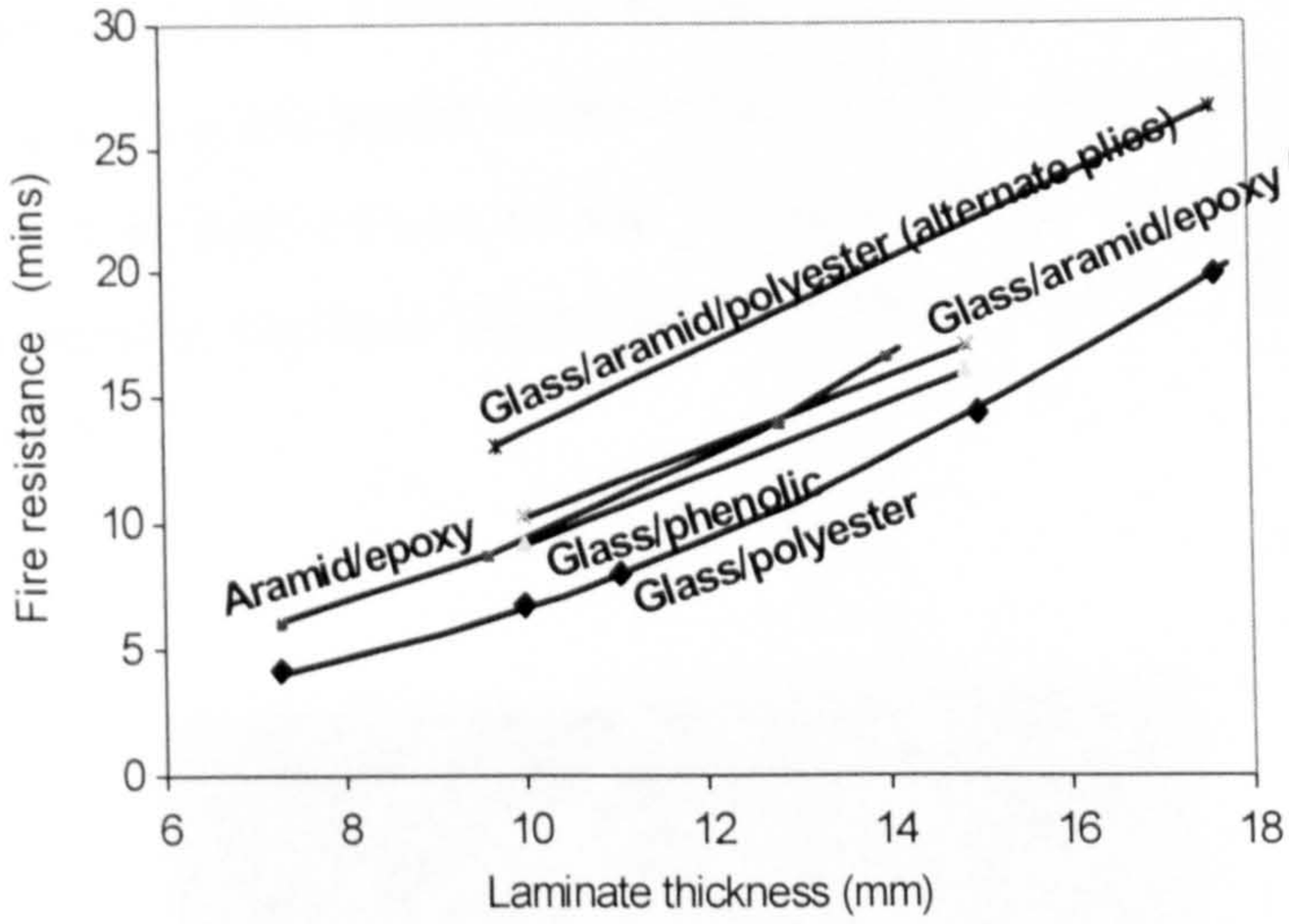

Figure 2.8 Fire resistance values, measured as a function of thickness, for a range of different laminates subjected to the HC/arbon fire curve (Dodds *et al.*, 2000).

The following sections describe testing methods for measuring fire resistance (section 2.3.2.1) and standard methods for adding fire protection (section 2.3.2.2).

2.3.2.1 Methods of Testing

Furnace Testing

There are two principle time-temperature regimes used for furnace testing, those for cellulosics (BS476, SOLAS, ASTM E-119), basically wood, fires and those for hydrocarbon fires (e.g. Mobil, DoE) and the cellulosics curve). Variations do exist between the different heating regimes and, in tests carried out by the present author, all furnace testing was performed to either SOLAS curve such as Eqn. (2.1) (BS 476, 1986) or those of the DoE interim hydrocarbon curve (i.e. Eqn. (2.2).

$$T - T_0 = 345\ log_{10}\left(8t + 1\right) \tag{2.1}$$

where T_0 = initial room temperature and t = time (seconds).

$$T = 1100\left(1 - 0.325e^{\left(-0.1667\frac{t}{60}\right)} - 0.204e^{\left(-1.417\frac{t}{60}\right)} - 0.471e^{\left(-15.833\frac{t}{60}\right)}\right) \quad (2.2)$$

The furnace test shown in Fig. 2.9 is of a broad range of fire tests. The structural samples in the furnace test are tested in the form of panels which are subjected to a temperature profile that follows one of the fire curves (i.e., Fig. 2.10). The fire resistance is measured by the time taken for the cool face of the panels to reach a temperature of 140 °C.

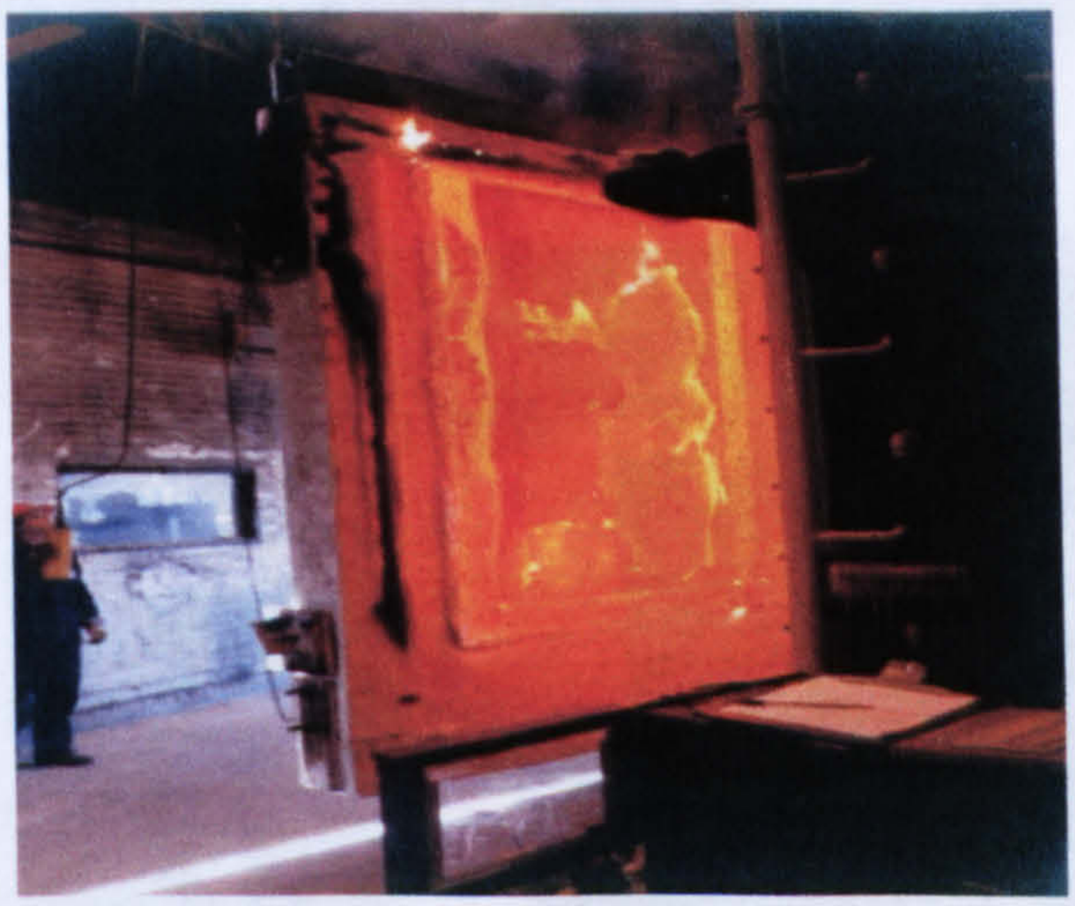

Figure 2.9 Large scale fire resistance furnace tests.

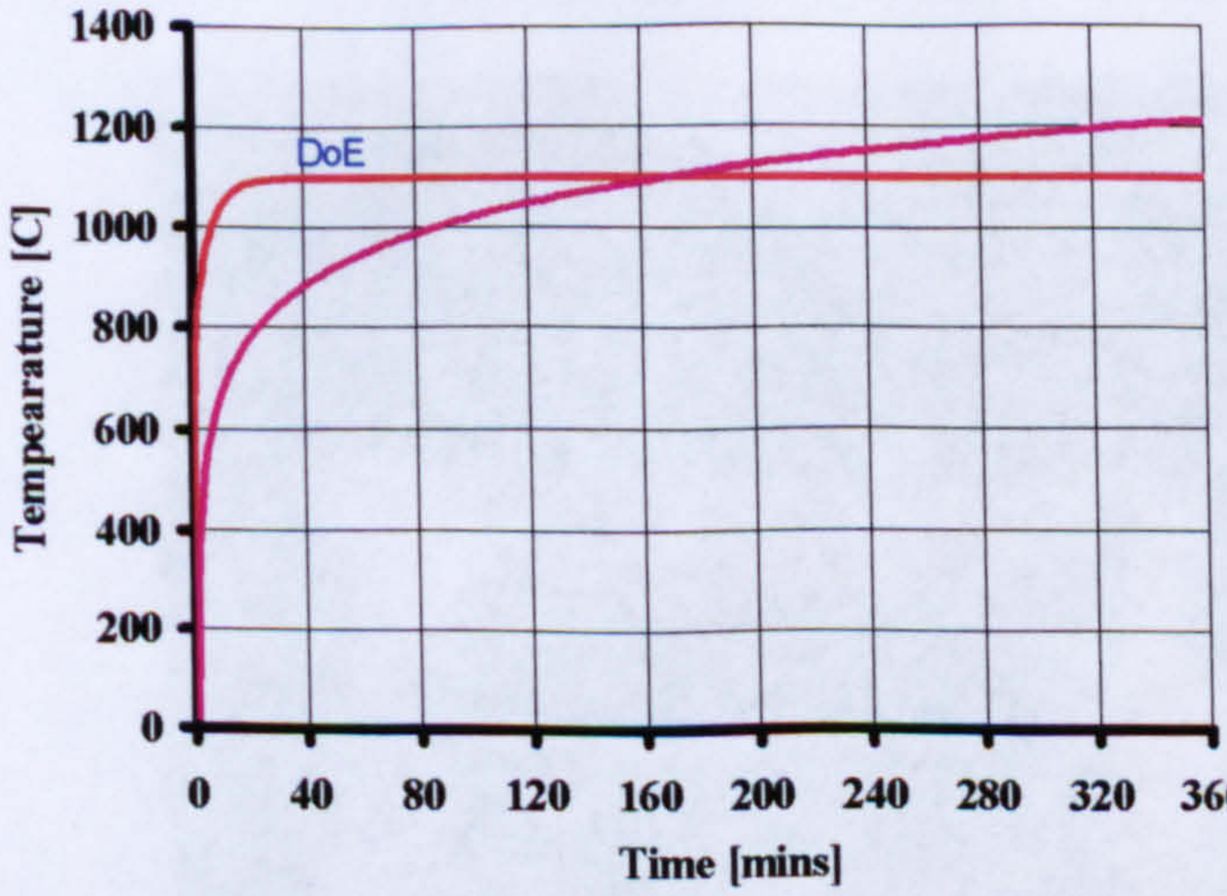

Figure 2.10 Hydrocarbon and cellulosics temperature/time curves.

Jet Fire Tests

The most extreme thermal conditions that an offshore structure is likely to encounter occur when a burning jet of hydrocarbon impinges directly onto its surface. Under these conditions an erosive effect is superimposed on a high level of heat flux. Jet fire testing of structures that are liable to be subjected to this type of hazard is essential and large-scale testing of this type can be very expensive. Recently Hill and White (1999) have been developed a procedure for a small-scale jet fire test, using a high-velocity propane jet. Figure 2.11 illustrates the steel tubular with composite fire protection during and after such a test. It is worth noting that composite materials with appropriate formulations have been found to be capable of surviving these tests.

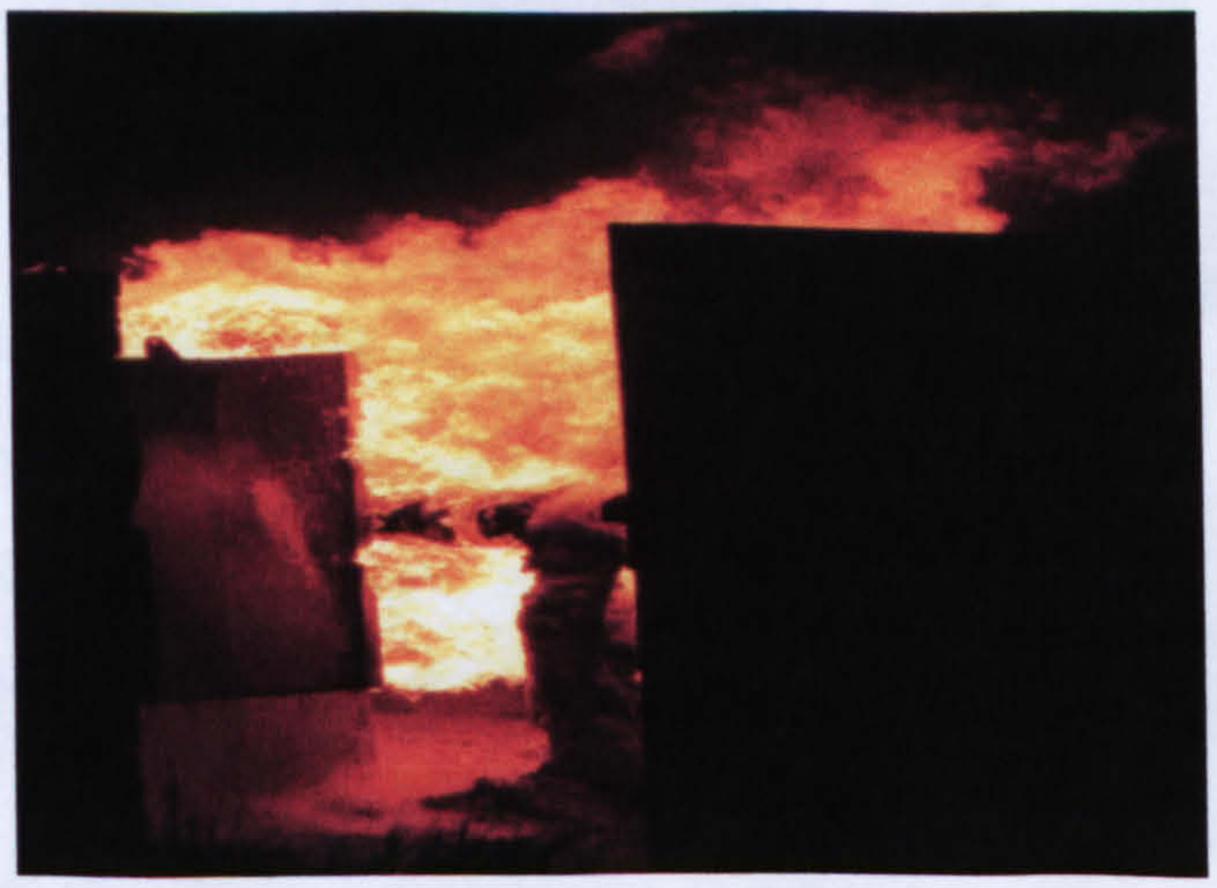

(a)

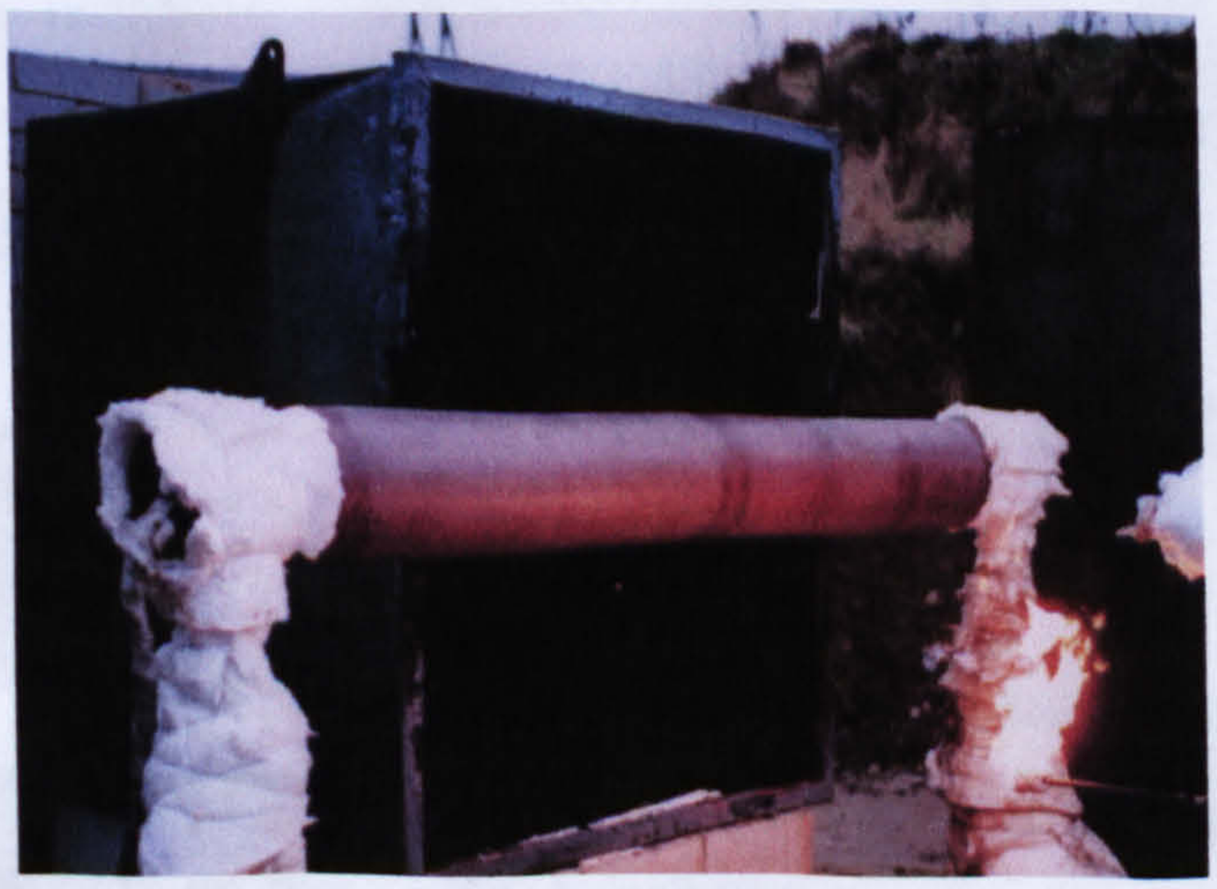

(b)

Figure 2.11 Jet fire test on a steel tubular with composite fire protection.(a) during test and (b) after 2 hours (courtesy Vosper Thornycroft (UK) Ltd.).

2.3.2.2 Fire Protection

Passive protection refers to the fire resistance of elements, whereas active protection measures are those contributing to a reduction in the severity of a fire. The most commonly used active system is sprinklers. There is a considerable body of statistical evidence to indicate that sprinklered buildings suffer less fire damage than others. Switzerland was the first nation to introduce a risk evaluation method for buildings in fire, which has been in operation for some twenty years (Lawson, 2001). Even if the sprinklers were only operational for a short duration (say 10 minutes), this would be well within normal fire-brigade response times and would reduce the potential damage.

Fire engineering is a widely used term in modern building design, but it has many meanings. The steel industry in the UK has expended considerable research effort on demonstrating the inherent fire resistance of unprotected steelwork. Conventional fire protection can add up to 30% to the cost of the bare steelwork, and there are many forms of structure where such protection can be shown to be unnecessary, leading to considerable economies. Historically, iron, as the predecessor of steel, was developed as a fire-proof material in the early nineteenth century after terrible fires in large timber mills in the north of England. Currently, Switzerland, Germany and Sweden have their own national regulations and design guidance for fire and steel structures. In the UK, BS5950 covers the use of steelwork in buildings (BS 5950, 1990).

2.4 Materials

2.4.1 Introduction

In its most basic form a composite material is one which is composed of at least two elements working together to produce material properties that are different to the properties of those elements on their own. In practice, most composites consist of the matrix, and a reinforcement of some kind, added primarily to increase the strength and stiffness of the matrix. This reinforcement is usually in fibre form. The most common man-made composites can be divided into three main groups:

(a) Polymer Matrix Composites (PMCs): These are the most common and represent the main area of discussion in this section. Also known as FRP - Fibre Reinforced Polymers (or Plastics) - these materials use a polymer-based resin as the matrix, and a variety of fibres such as glass, carbon and aramid as the reinforcement.

(b) Metal Matrix Composites (MMCs): Increasingly found in the automotive industry, these materials use a metal such as aluminium as the matrix, and reinforce it with fibres such as of silicon carbide.

(c) Ceramic Matrix Composites (CMCs): Used in very high temperature environments, these materials use a ceramic as the matrix and reinforce it with short fibres, or whiskers such as those made from silicon carbide and boron nitride.

This work we only considers the PMCs, although CMSs are showing potential for application in this field of research.

2.4.2 Polymer Matrix Composites

Resin systems such as epoxies and polyesters have limited use for the manufacture of structures on their own, since their mechanical properties are not very high when compared to, for example, most metals. However, they have desirable properties, most notably their ability to be easily formed into complex shapes. Materials such as glass, aramid and boron have extremely high tensile and compressive strength. It is when the resin systems are combined with reinforcing fibres such as glass, carbon and aramid those exceptional properties can be obtained.

2.4.2.1 Reinforcing Fibres

The role of the reinforcement in a composite material is fundamentally one of increasing the mechanical properties of the resin system. All of the different fibres used in composites have different properties and so affect the properties of the composite in different ways.

There are many types of fibres used for composite laminate applications. Many reinforcement are now available, some designed for a particular matrix system (Hull

and Clyne, 1996). The main criteria for selection are that the fibres should have good mechanical properties and be resistant to processing temperature. Common reinforcement fibres are made of carbon, glass and aramid, and they are now used extensively in polymer matrix composites, although there are others including polyester and polyethylene.

Glass Fibre

Most glass fibres are made by a direct melting process using silica sand, limestone, fluorspar, boric acid and clay. By varying the amount of raw materials and processing parameters, other glass types can be produced, such as E-glass, C-glass, S-glass (Mazumdar, 2002).

The E-glass (E for electrical), is known as electric grade. It is significantly cheaper than any other type and the most commonly used glass for loading bearing structures. E-glass fibre is available in the following forms: (i) Strand form (ii) Roving (iii) yarns. The diameter of E-glass is usually between 8 and 15 μm. It has good chemical and mechanical properties (i.e., good strength and stiffness). This type of glass was used for reinforcement of composite panels in this study. C-glass (C for corrosion) is preferred, having better resistance to corrosion than E-glass., but lower strength. S-glass (S for strength) is more expensive than E-glass, but has higher strength, Young's modulus and temperature resistance with lower density and high resistance at elevated temperatures. It is mainly used for aerospace applications.

Carbon Fibres

Carbon fibres are relatively smaller in diameter than glass fibre, typically about 8 μm. Carbon fibre is produced by the controlled oxidisation and carbonisation of polyacrylonitrile (PAN), mesophase pitch or cellulose. Carbon fibre has a low density and the highest specific stiffness of any commercially available fibre, very high strength and a high resistance to corrosion and fatigue.

Aramid Fibres

Aramid fibres consist a man-made organic polymer and are the most important high modulus polymer fibres developed from aromatic polyamides. They have superior tensile strength to weight when compared to other reinforced fibres. Several types of aramid fibres are available commercially, under different names such as Kevlar. Kevlar fibres provide excellent abrasion resistance in a composite but they are poor in compression. Hence, they are used in applications where subjection to high strain compressive or flexural loads are limited.

2.4.2.2 Matrix systems

The resin systems that are used in composite fabrication for composite panels have several tasks (Hull and Clyne, 1996; Mazumdar, 2002), such as to:

– Transfer and distribute the applied load to fibre.

– Bind the fibres together and keep them in the proper position.

– Protect the fibre from mechanical damage such as abrasion.

– provide a good protection against chemical and environment attack.

Therefore, the matrices which are used to carry out the above tasks should have the following features:

– Good mechanical and chemical properties.

– Good heat, corrosion and moisture resistance.

– High strain to failure to be able to transfer loads to the fibres.

– High strength of adhesion to the fibres.

– High toughness.

– Low viscosity.

In the present work, only thermosetting matrices were studied, as the properties of thermoplastic resins do not generally yield good fire properties.. Detailed descriptions of polyester, vinyl ester, epoxy and phenolic are given in the next section.

a. Thermosetting Materials

Thermosetting matrices or thermosets are formed from a chemical reaction in-suit, where the resin and catalyst (hardener) are mixed to form a hard, infusible product. Once cured, thermosets will not become liquid again if heated, although above a certain temperature (the Glass Transition Temperature) their mechanical properties will change significantly (Powell, 1983). Although there are many types of resins in use in the composite industry, the majority of composite panel components are made with four main types, namely: polyester, vinyl ester, epoxy and phenolic resins. The resins used in this study were polyester and vinyl ester resins.

Polyester Resins

Polyester resins are the most widely used resin system in many composite processes. This wide usage is probably related to their low cost, sufficient mechanical properties and environmental durability. Polyester resins are unsaturated oligomers dissolved in a monomer which is usually styrene. Unsaturated polyester is usually referred to as polyester resin or simply as polyesters. The styrene solvent performs the vital function of enabling the resin to cure from liquid to a solid by cross-linking the molecular chain of the polyester. There are several types of polyester, the most common being orthophthalic and isophthalic. The orthophthalic polyester resins are used as standard economic resins for general purposes. They have relatively poor corrosion resistance and lower mechanical properties. They are used only in structural applications where corrosion resistance is not applicable. On the other hand the isophthalic polyesters are becoming the preferred resins in industries such as marine applications and the oil industries, where their superior water resistance and mechanical properties are desirable.

Vinyl ester resins

Vinyl esters resins are similar in their molecular structure to polyester. Their cost is higher than polyester resins. They have superior corrosion resistance and mechanical properties and are used in some corrosion resisting applications, especially in very regressive environments such as marine applications (MacInally and Miller, 1998).

Epoxy Resins

Epoxy resins are the most commonly used type in filament wound tubes. Epoxy is formed by the reaction of epichlorohydrin with bisphenol A in the presence of sodium hydroxide (Varma and Gupta, 2000).

Epoxy resins are very reactive and can be cross-linked via the epoxy or the hydroxyl side groups. The choice of curing agent depends on the processing method, curing conditions, desired physical and chemical properties, toxicological and environmental limitations and cost. Although some epoxies are formulated to crosslink at room temperature, many require subsequent postcuring to complete crosslinking and to achieve optimum properties.

Phenolic Resin

Phenolic resins have potential as matrices for composite pipe work, especially in fire sensitive applications such as fire water piping, because of their good high temperature properties and low smoke emission (Gibson, 2000). Phenolic resins are made by chemical reactions between phenols and formaldehyde. There are two types of phenolic resins: resoles and novolacs. The resole phenolic resin is formed by the reaction of phenolic with an excess of formaldehyde in the presence of an alkaline catalyst. Heating of the resins will cause cross-linking via the methylol group or more complex routes.

Other resins

Besides polyesters, vinyl esters, epoxies and phenolics there are a number of other thermosetting resin systems that are used where their unique properties are required: (i) cyanate esters are mostly used in the aerospace industry, but are very expensive, typical costs: £40/kg; (ii) polyurethanes are highly tough materials; (iii) bismaleimides (BMI) are mainly used in aircraft composites where operation at higher temperatures is required (for example in engine inlets, and high-speed aircraft flight surfaces. Typical costs: >£50/kg; and (iv) polyimides are used where operation at higher temperatures (up to 250°C) is required. These are extremely expensive resins and typical applications include missile and aero-engine components.

2.5 Modelling of Composites in Fire

A predictive model for the responses of composite materials validated against standard fire test methods will help to minimise the number of standard tests required to qualify a new material. Moreover, once fire behaviour under the heat transfer conditions of specific cases of a standard furnace fire test is understood, then the model may be generalised to predict thermal responses under more realistic fire actions. Many contributions to the literature have reported the use of mathematical models to study the pyrolysis of charring materials, applying these models to the study of wood, plastics, and various ablative heat shields with apparent success.

Bamford *et al* (1946) were the first to propose a mathematical model to predict the thermal response of decomposing material. Their model consisted of a one-dimensional transit heat conduction equation with an additional term to account for the energy associated with thermal decomposition. Constant thermal properties and a first order decomposition reaction were assumed. Later, Panton and Ritmann, (1969) developed a model which accounted for the variable thermal and physical properties of the material during decomposition. Kanury (1969) and Munson and Spindler (1961) proposed models which accounted both for the variable properties of the material and the effects of gas flow through the char structure. Kung (1972) proposed a model which separated the material into its active and residual components. Kansa *et al* (1977) utilized a one-dimensional mathematical model to study the pyrolysis of charring, including porous and permeable structural effects on the volatile flow. Their model combined transient mass and energy conservation equations, the Darcy momentum equation, and global Arrhenius decomposition for a porous, permeable reacting solid. The model was validated with experimental data and the results indicated good agreement at low surface heating rates (i.e., 0.53 cal cm-1 sec-1), but poor agreement at fire level heat fluxes (2.0 cal cm-1 sec-1). In contrast, Henderson *et al* (1985) developed an appropriate mathematical model for the thermal response of polymer composite undergoing decomposition in the absence of surface recession.

Looyeh *et al* (1996) developed a finite element model associated with computer coding to quantify the fire-performance and thermal responses of a standard GRP laminate. It was found that the predicted temperature agreed very well with the experimental data.

A simple one dimensional computer model was developed and employed by Gibson *et al*, (1994) to compute the thermal profiles in thick polyester woven roven (WR) and CSM laminates subject to fire tests using the hydrocarbon curve. The model took into account the effect of the resin decomposition endotherm, which delays heat conduction through the panel and produces a plateau in the cold face response, as well as the effect of flow of the volatiles thus generated through the laminate. This approach is similar to that adopted and developed in many other studies (Adams, 1959; Kansa *et al,* 1977 and Sullivan, 1993). The computer model takes account of these effects and has been developed in parallel with a series of fire tests. The model was capable of simulating the thermal response of composite systems using an experimentally validated thermal model which provides basic data for performance based design.

The model is described in full in chapter eight. It has been developed from the unsteady state heat equation by including terms describing the ablative processes which take place. The basic governing equation is:

$$\rho C_p \frac{\partial T}{\partial t} = \frac{\partial}{\partial x}\left(k \frac{\partial T}{\partial x}\right) + M_G \frac{\partial}{\partial x} hG - A\,\rho_0 \left[\frac{\rho - \rho_f}{\rho_0}\right]^n e^{-(E/RT)}\left(Q_p + h_c + h_G\right) \qquad (2.3)$$

where: T, t and x are the temperature, time and through-thickness coordinate, respectively; ρ, Cp and k are the composite density, specific heat and heat conductivity; M_G is the mass flux of volatiles from the decomposition reaction; h_c and h_G are the respective enthalpies of the composite and evolved gas, Q_p is the endothermic energy of decomposition; A, E and n are the rate constants for the decomposition reaction; and R is the gas constant.

The three terms on the right hand side of Eqn. (2.3) relate to heat conduction, volatile convection and endothermic decomposition, respectively. The model also assumes that the thermal property values (C_p, k) remain constant as the laminate heats-up. Figure 2.13 shows the comparison for three individual panel thicknesses

of 11, 17 and 22mm exposed to the hydrocarbon curve furnace fire tests (Dodds and Gibson, 1998). The dotted lines are the calculated temperatures and the solid lines the experimentally measured temperatures. The intermediate curves are inter-laminar temperatures. For each panel thickness the computer model predicts the cold face temperature response very accurately.

One of the objectives in this study is to establish an approach for modelling the fire behaviour of composite laminates exposed to different fire conditions. This could be done by validating the existing computer model (i.e., Gibson, 1995) for prediction of fire resistance by means of comparison with experimental test results.

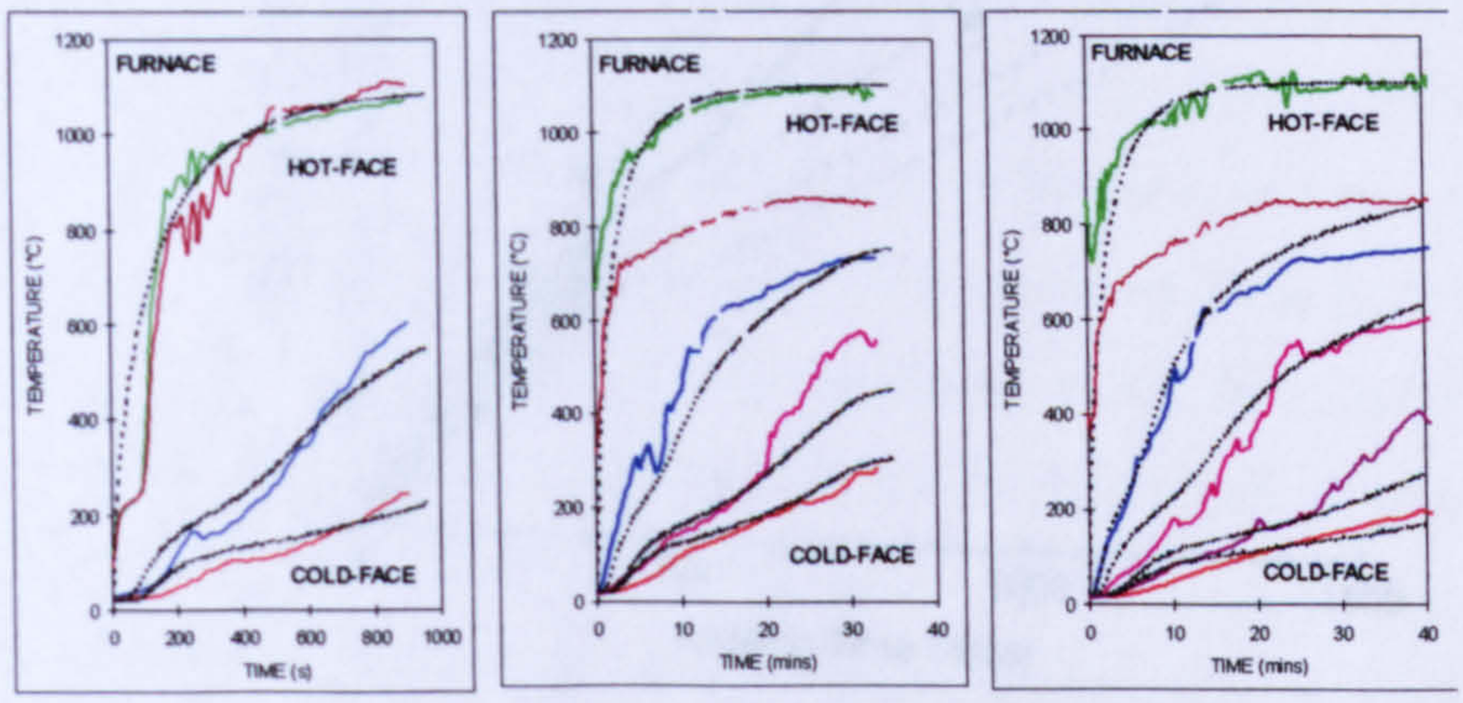

Figure 2.12 Experimental and modelling response of HC/curve furnace fire tests results for isophthalic polyester/glass WR laminated panels (Dodds and Gibson, 1998).

One of the products of polymer matrix decomposition is the formation of solid carbonaceous char, which affects the fire response of laminates in various ways (Levchik *et al*, 2000). The char formed can slow the burn-through rate by insulating the underlying composite from fire. The gas permeability of char influences the diffusion rate of volatiles out of the decomposing laminate into the fire, thus affecting the ignition time and flame spread rate. It can provide stability to burning laminate by holding the fibres in place after the polymer matrix has been depleted. This influence reveals that understanding the char formation process is essential in characterising the fire response of laminated composites. The formation and growth of char in thermoset laminate composites in fire has been experimentally and

theoretically studied (Mouritz *et al,* 2004). Figure 2.13 shows the measured increased in char thickness with heat flux and heating time for a laminate (Mouritz *et al*, 2004). The data points show the experimental values for char thickness. Also shown are theoretical curves of the remaining resin content with depth below the hot surface of the laminate. McManus and Springer (1992) proposed a thermomechanical model to determine the effects of temperature and duration of a fire on the extent of charring in polymer matrix and carbon matrix composites.

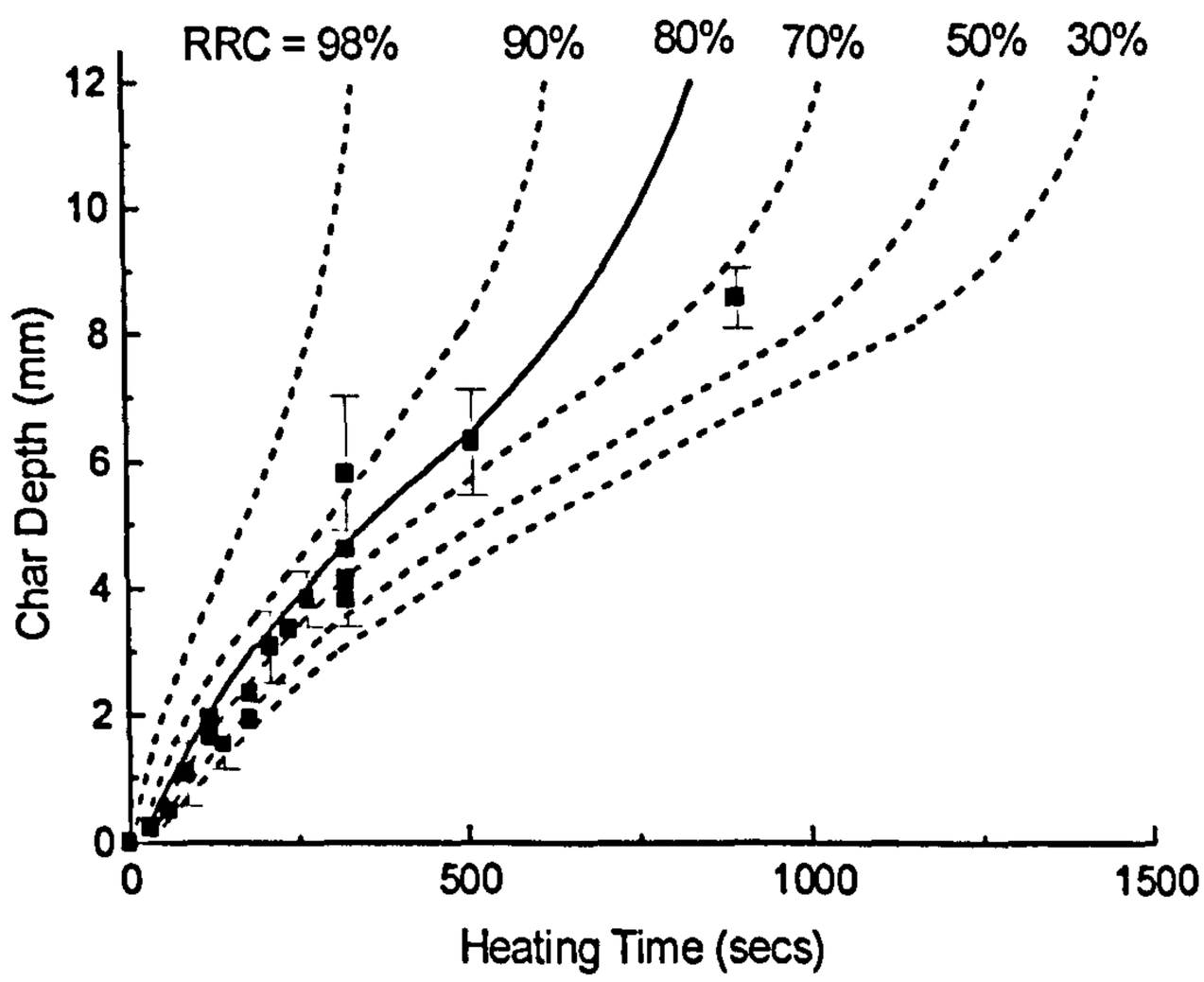

Figure 2.13 Thermal damage depth vs. heating time for a heat flux of 50 kW/m^2, for 12mm thick glass-polyester laminates (Mouritz *et al,* 2004).

2.6 Kinetics of Thermal Degradation of Polymer from Thermogravimetry (TGA)

Description of kinetic properties requires knowledge of the decomposition reactions taking place, which then allows prediction of the rate of change of mass of the composite. Thermogravimetric analysis ultimately affords a record of residual weight fraction versus temperature for a sample heated at a fixed rate under a particular set of other experimental conditions. For the purposes of modelling the fire behaviour of polymer resin composite laminates, some of the input data required are the reaction constants (A, E, n) for the decomposition of the polymer matrix, and these values are empirically determined using Thermogravimetric analysis (TGA).

The three kinetic parameters (A, E, n) can be derived from Eqn. (2.4) (i.e., the Arrhenius equation), which describes the decomposition of the polymer matrix (Freeman and Carroll, 1957).

$$\frac{d\rho}{dt} = -A\,\rho_0 \left[\frac{\rho - \rho_f}{\rho_0}\right]^n exp^{-(E/RT)} \qquad (2.4)$$

where: ρ, t and T are the mass density, time and temperature variables respectively; A, E and n are the rate constant activation energy and the order of the reaction; and R is the gas constant.

Thermogravimetry (TGA) had been used by Somiya and Hirano in 1930 to determine the volatile yield of many coals (Ottaway, 1982). Most of the studies which have been carried out have used DTA techniques, and several reviews of the field are available illustrating the variety of areas which have been researched using TG. The kinetics of the thermal degradation of solids have been evaluated from TGA at linear rates of temperature rise in a number of studies. van Krevelen *et al.*, (1951) studied the decomposition of coal, and Freeman and Carroll (1958) investigated the degradation of calcium oxalate monohydrate. Their technique was applied to the decomposition of styrenated polyester by Anderson and Freeman (1959), and this was modified by the same authors (1961) for polystyrene and polyethylene. Doyle (1961) studied the degradation of a large number of plastics. Friedman (1965) investigated the decomposition of glass-reinforced phenol-formaldehyde. In all of these earlier studies, calculations were based on experiments which were performed at a single rate of temperature rise. Friedman (1965) developed a technique for obtaining rate and kinetic parameters which described the thermal degradation of plastics from TGA data. This technique allowed the determination of the activation energy of certain processes without knowing the form of kinetic equation. The technique was applied to fibreglass reinforced CTL 91-LD phenolic resin, where the rate law (i.e., Eqn. 2.5) was found to apply to a major part of the degradation. The equation was successfully tested by several techniques, including a comparison with constant temperature data that were available in the literature. The calculations showed that 'n' = 5.0 and 'A' = 5.98 X 10^{18} $hr.^{-1}$.

$$-(1/w_o)(dw/dt) = 10^{18} e^{-55000/RT}\left[(w - w_f)/w_o\right]^5, \text{nr.}^{-1} \qquad (2.5)$$

Chapter six describes a procedure for evaluating such preliminary kinetic data from thermogram, and this will be discussed and applied to many cases.

2.7 Thermal Conductivity of Composite Materials

Fibre-reinforced plastic materials are considered as potential replacements for metals in situations where excellent specific strength properties, for instance strength/weight and stiffness/weight ratios, are required. While such composites have other advantages over metals, for example in corrosion resistance, they also have characteristics which may not be so beneficial in some applications.

GRP composites may undergo pyrolysis reactions with their polymeric matrix materials at high temperatures when exposed to a fire. As a result, the original solid elements may gradually become a skeleton material with the glass fibres as a part of the residues. The thermal properties of such gradually degraded composite materials vary at all times during decomposition. The effects of the variation of thermal properties at high temperatures on the thermal responses of composites in fire are important factors in modelling. However, a major difficulty encountered in modelling the thermal behaviour of GFP composites in fire is the lack of information of the above properties of glass fibres and resin materials at high temperatures. All of these can easily be found, with the exception of the high temperature thermal conductivity of glass.

In general, it is much more difficult to dissipate heat in fibre-reinforced plastic than in metal, and therefore it is important to adapt the thermal conductivity of composites. However, their basic properties must be known. As a result, accurately modelling heat transfer through the composite is a critical part of conducting structural analysis on a composite exposed to fire.

Equations and methods for modelling heat transfer are well established (Henderson *et al*, 1985; Boyer and Thomas, 1985; Boyer, 1984; Kung, 1972; Kanury and Blockshear, 1970). In general, a composite material will degrade (as shown in Fig.

2.14) when exposed to a heat source on one side (x=0) (Brian and Jason, 2004). During the degradation process, three regions will be present: char/glass region, pyrolysis front region which contains a mixture of virgin material and char/glass material, and virgin material region. To model the heat transfer through such a decomposition material, the physical and thermal properties need to be known for the virgin material, the char/glass material, and for the pyrolysis region where it is typically assumed that there is a mixture of the two types of materials (Gibson *et al*, 1995; Brian and Jason, 2004; Henderson *et al*, 1985; Boyer and Thomas, 1985; Boyer 1984). These properties need to be quantified over the temperature range expected, which could be up to 1000°C during a fire exposure.

Due to the increasing use of composite materials in industry, there is an urgent interest in the theoretical and experimental determination of the effective thermal conductivity of fibre and particle filled polymer composites. Although the thermal conductivity of particle filled polymers has been investigated theoretically and experimentally by many researchers (Tavman, 2000), there are few studies on the thermal conductivity of fibre filled polymers.

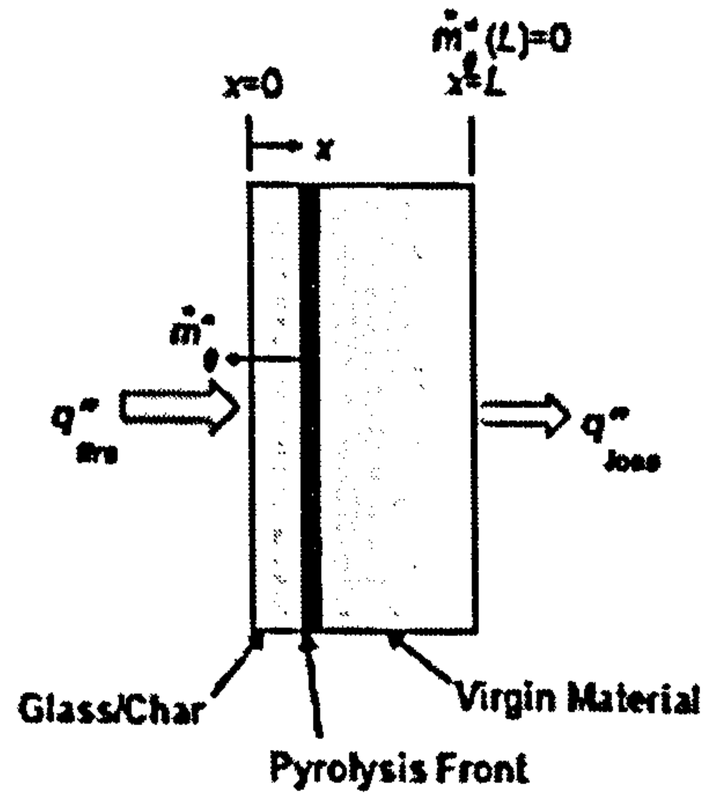

Figure 2.14 Thermal decomposition of a composite material (Brian and Jason, 2004).

Only very limited publications are available concerning the thermal conductivity of composite materials at high temperatures. Ott (1981) reported experimentally measured thermal conductivity of GFRP of many different types in the temperature range between 90 and 400 K. The author used different models to calculate the

thermal conductivity of GFRP for comparison with the relevant experimental results. For the temperature range up to 400 K, it seems unnecessary to consider any thermal effect of the voids contained inside the composite materials.

On the other hand, the measurement of thermal properties in milli-scale devices such as Thermogravimetric analysis (TGA) and differential scanning calorimetry (DSC) have been used in previous studies to develop thermal properties for composite materials (Kung, 1972 and Henderson *et al*, 1981). Boyer (1984) used inverse heat transfer techniques and carefully conducted experiments to determine a new set of thermal properties. Using these thermal properties, Boyer was able adequately to predict temperature profiles through the composite material.

The focus of this thesis is to develop a methodology for determining the thermal conductivity of composite materials, to be used in modelling the thermal response of composites during fires. Following the findings of Brian and Jason, (2004), the transit method was adopted to derive the thermal conductivity of composite material (i.e. dry fibre mat). Chapter five focuses on using this methodology to determine the thermal conductivity of non-decomposing samples.

2.8 Heat Flux Measurement Techniques

2.8.1 Introduction

Heat flux can be defined as the energy in transit because of a temperature difference per unit cross-sectional area normal to the direction of the flux. There are no devices that can measure energy and hence heat or heat flux directly (Childs *et al*, 1999).

The physical methods currently available for this are principally based on the monitoring of temperatures and spectral emissions.

Heat transfer can occur by means of any one, or a combination, of conduction, convection and radiation (see Bejan, 1993 or Diller, 1993, for comprehensive discussions on the subject). The objective of measurement is to quantify the heat flux. In a solid this will be due to conduction alone. However, at a solid/fluid interface, the resulting heat transfer will occur due to at least two of these three

modes. Most heat flux sensors measure the total heat flux at the solid/fluid interface or surface (Childs *et al*, 1999). The types of heat flux sensors available are reviewed in this study. Several techniques are in common use, including the following.

(i) Differential temperature sensors. The basis of these techniques is to monitor the difference in temperature between locations in a component and, with knowledge of the thermal properties, Fourier's one dimensional law of conduction and an equation such as Eqn. (2.6) can then be used to determine the heat flux through the medium (Childs *et al*, 1999). The limitation of this technique is that the heat flux must be one-dimensional across the region of concern.

$$q = -k\frac{dT}{dx} = -k\frac{T_1 - T_2}{x_1 - x_2} \tag{2.6}$$

This method was reported by Martinelli *et al* (1942) and presented by Godefroy *et al* (1990) and Bhatt *et al* (1993).

(ii) Calorimetric methods. A number of heat flux measurement techniques based on this principle include slug calorimeters, plug gauges, thermocouple gauges and thin-film sensors (ASTM E 457-96, 1997).

(iii) Energy supply or removal method. These use, for example, a heater to generate a thermal balance (ASTM E 422-99, 1999).

(iv) Mass transfer analogy, which can be linked to heat transfer using the analogy between the two (Goldstein and Cho, 1995).

No one method is suitable to all applications because of the differing considerations of accuracy, sensitivity, size, cost and robustness. Details on the use of the Slug Calorimeter in measuring heat transfer rates for specific applications are described in the following section.

2.8.2 Thermal Capacitance (Slug) Calorimeter.

This test method describes the measurement of heat transfer rate using a thermal capacitance type calorimeter which assumes one-dimensional heat conduction into a cylindrical piece of material (slug) with known physical properties. This technique is fully described in ASTM E 457-96, (1997). The method measures the rate of thermal energy per unit area transferred into a known piece of material (slug) for purposes of calibrating the thermal environment into which test specimens are placed for evaluation. This type of calorimeter is simple to fabricate, inexpensive and readily installed. The primary disadvantages are its short lifetime and relatively long cool-down time after exposure to the thermal source. The technique is shown schematically in Figure 2.15.

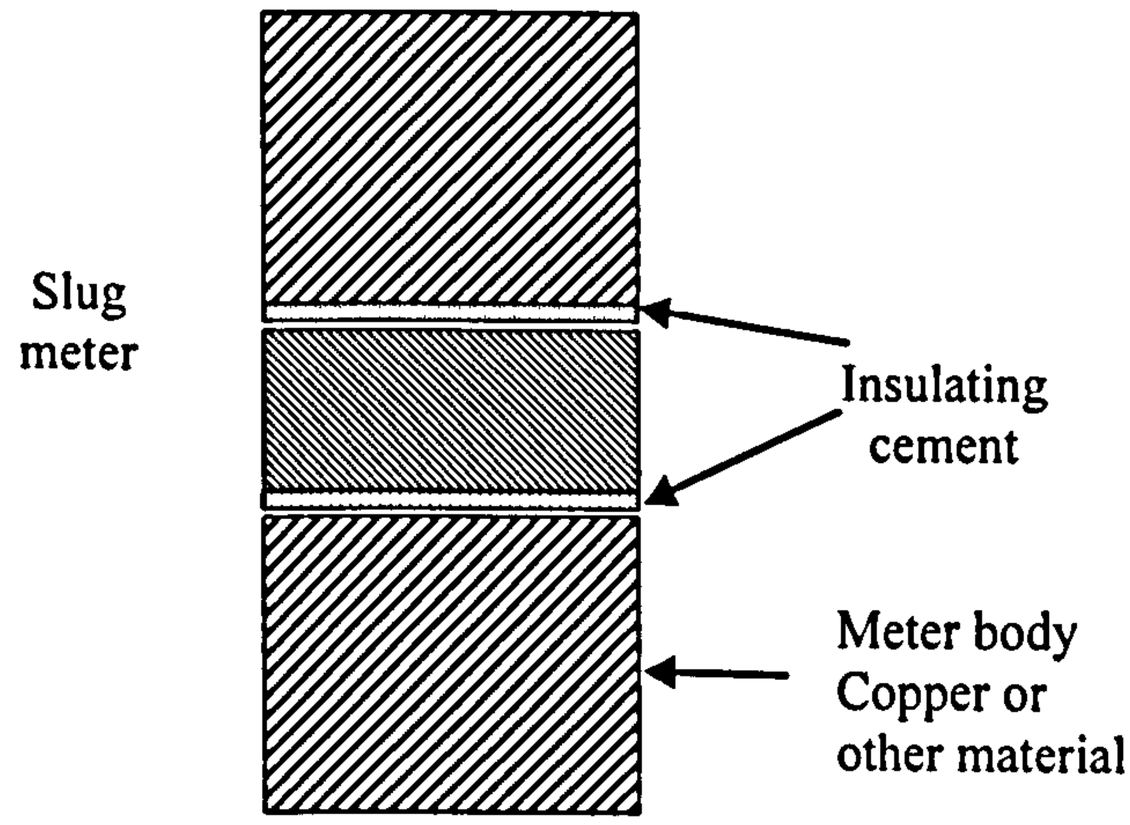

Figure 2.15 Schematic diagram of a thermal capacitance calorimeter (ASTM E 457).

For the control volume specified in this method, a thermal energy balance during the period of initial linear temperature response can be stated as follows (ASTM E 457-96, (1997): Energy Received by the Calorimeter (front face) = Energy Conducted Axially into the Slug. It can be expressed numerically by multiplying the density, specific heat, and length of the slug by the slope of the temperature-time curve obtained by the data acquisition system as following:

$$q = \rho C_p l(\Delta T/\Delta t) = (mC_p/A)(\Delta T/\Delta t) \tag{2.7}$$

where; q = calorimeter heat transfer rate; W/m^2; ρ = density of slug material (i.e. Copper) kg/m^3; C_p = average specific heat of slug material (Copper) kJ/kg °K; l = length or axial distance from front face of slug to the thermocouple location (back-face), m; ΔT = calorimeter slug temperature rise during exposure to heat source, °K; Δt = time period corresponding to ΔT temperature rise, s; m = mass of the cylindrical slug, kg; and A = cross-sectional area of slug, m^2.

In order to determine the steady-state heat transfer rate with a thermal capacitance type calorimeter, Eqn. (2.7) must be solved and calculated based on the known properties of the slug material, such as its density and specific heat (Tolukian and Goldsmith, 1961), the length of the slug and the slope (linear portion) of the temperature-time curve of the calorimeter obtained during the exposure to a heat source. The initial and final temperature transient effect must be eliminated by using the initial linear portion of the curve.

For the maximum linear test time (temperature-time curve) within an allowed surface temperature limit, the following relationship may be used (ASTM E457-96):

$$\tau_{max,opt.} = 0.48\rho l Cp(\Delta T_{frontface}/q) \tag{2.8}$$

where; $\Delta T_{front\ face}$ is the calorimeter final front face temperature minus the initial front face (ambient temperature T_0). $l_{opt.}$ is the optimum length of the slug, which can be obtained by applying the following equation:

$$l_{opt.} = 3k\Delta T_{front\ face}/5q \tag{2.9}$$

2.9 Conclusion

This review has discussed the areas where composites are penetrating the onshore and offshore engineering applications.

Despite their combustibility, organic matrix composites have been demonstrated to have considerable potential for use in structures that may be subject to fire.

When used in sufficiently thick sections composites are capable of withstanding severe temperature and ablative effects by virtue of their low intrinsic thermal conductivity and the endothermic nature of the resin decomposition process.

The challenges for the future are the move toward using composite materials as solutions for many applications. These challenges bring with them the possibility of greatly increased markets for glass based and high performance composites.

CHAPTER 3

CALIBRATION OF INCIDENT OF HEAT FLUX FROM A PROPANE FLAME

3.1 Introduction

Fire resistance testing is an essential requirement for ensuring fitness for purpose and the conformity to requirements of many structural systems. Unfortunately, both the scale of the tests and their cost are often too expensive at the materials development stage, a problem that slows down the innovation and development of fire resistant systems. Most fire resistance tests involve subjecting the sample to a known heat flux or temperature profile, and measuring the response in terms of integrity or heat transmission. Full-scale resistance tests may require mock-ups of the structure to be tested, or at least large panels. Alternatively, test may be carried out on 1.2 m square sample. Data from this type of test may be used when modelling the fire response of systems (Dodds *et. al.*, 2000 and Gibson *et. al.*, 2003).

The operation of furnace fire resistance tests based on one of the standard fire curves presents various problems in terms of reproducibility. These are mainly due to the variability in emissivity of the liner materials and to the difficulty of maintaining good control of temperature in the case of samples which may burn and thus contribute to the heat release within the furnace. It has been observed, however, that reliable quantitative information can be obtained on samples of smaller scale. The cone calorimeter, for example, produces highly reproducible heat release information on samples of only 100mm square. Unfortunately, even the modest cost of a cone calorimeter exceeds the budget for many small systems.

This chapter describes the use of a propane burner as the heat source in small scale fire resistance tests to enable rapid characterisation and testing to be carried out on composite systems under reproducible conditions of either hot face temperature or

heat flux. The burner rig is a low cost device which enables a 100mm^2 specimen to be subjected to a near uniform heat flux over its surface. Fluxes in the region of 25kwm^{-2} up to 180kWm^{-2} are possible. In addition to measuring the integrity of composite laminates in fire it can also be used to measure the heat flux through a protection laminate into essential surface.

3.2 Propane Burner Rig

The burner rig enables a 100mm square specimen to be subjected to a near uniform heat flux over its surface.

Heat transfer from the flame to a laminate involves both radiation and convection. Although radiation is the most important factor in fire situations, effects due to heat convection might not be negligible.

To treat flames as a heat radiation source, a characteristic temperature has to be specified, equivalent to the surface temperature for a solid radiating heat to the surroundings. The characteristic temperature of a gas flame can be correlated with the heat flux emitted from the flame through the Stefan-Boltzmann law (Eastop and McConkey, 1978).

A surrounding field temperature, T_s, is specified in this study as the characteristic temperature of a flame in a fire test. The surrounding field temperature is defined as the temperature measured at a position about 10mm away from the receiving surface of the sample.

When the surrounding field temperature, T_s, is measured in a fire test it can be correlated with the heat flux received from the flame, and an effective emissivity of the flame can be derived. The emissivity (ε) indicates the efficiency of the emitting surface as a radiator, with a value in the range from zero to 1.0. In fire situations most hot surfaces, smoke particles or luminous flames have an emissivity between 0.7 and 1.0 (Eastop and McConkey, 1978).

Specifying the surrounding field temperature alone will not uniquely define the heat flux input to the receiving surface of the sample being exposed to the flame. For fire

tests in a particular furnace, the effective emissivity of the flame inside the furnace has to be calibrated. Such an effective emissivity is usually a function of the surrounding field temperature and depends on many furnace factors.

To measure the heat flux output from a propane flame for calibration purposes, a thermal capacitance-type calorimeter (Designation: E457-96, 1996) or heat flux meter was used. The heat flux meter was a block of copper. Figures 3.1 and 3.2 show the experimental apparatus.

The heat flux meter consists of a 100mm diameter cylinder, one end of which was reduced to 72mm diameter at the region of incoming flux. The copper temperature during the test was measured by three thermocouples placed as shown. The outside was insulated with calcium silicate board and Kaowool. The mass of copper was chosen to be large enough to ensure that its temperature during the test did not generally exceed 70°C.

3.3 Heat Transfer between the Propane Flame and the Meter

In most fire situations where a fluid flows across a surface, the superimposed effect of natural convection is usually quite small. The total incident heat flux from the propane flame therefore consists of two parts.

$$q_i = q_r + q_{fc} \tag{3.1}$$

where, q_i represents the total incident heat flux from the propane flame, q_r denotes the radiation component and q_{fc} denotes the convection component.

The total heat flux, q, received by the front face of the sample is taking into account the heat flux part due to radiation and the convection part as follows:

$$q = \sigma\left(\varepsilon_r \alpha_m T_s^4 - \varepsilon_m T_m^4\right) + h_c\left(T_s - T_m\right) \tag{3.2}$$

where

q = total heat flux received by the front face (W/m^2)

ε_r = emissivity of propane flame;

σ = Stefan-Boltzmann constant (=5.67 × 10^{-8} W/m^2 °K^4);

α_m = absorptivity of the receiving surface of the meter;

T_s = surrounding field temperature;

ε_m = emissivity of the receiving surface of the meter;

T_m = temperature on the receiving surface of the meter;

h_c = forced heat convection coefficient (W/m^2 °C)

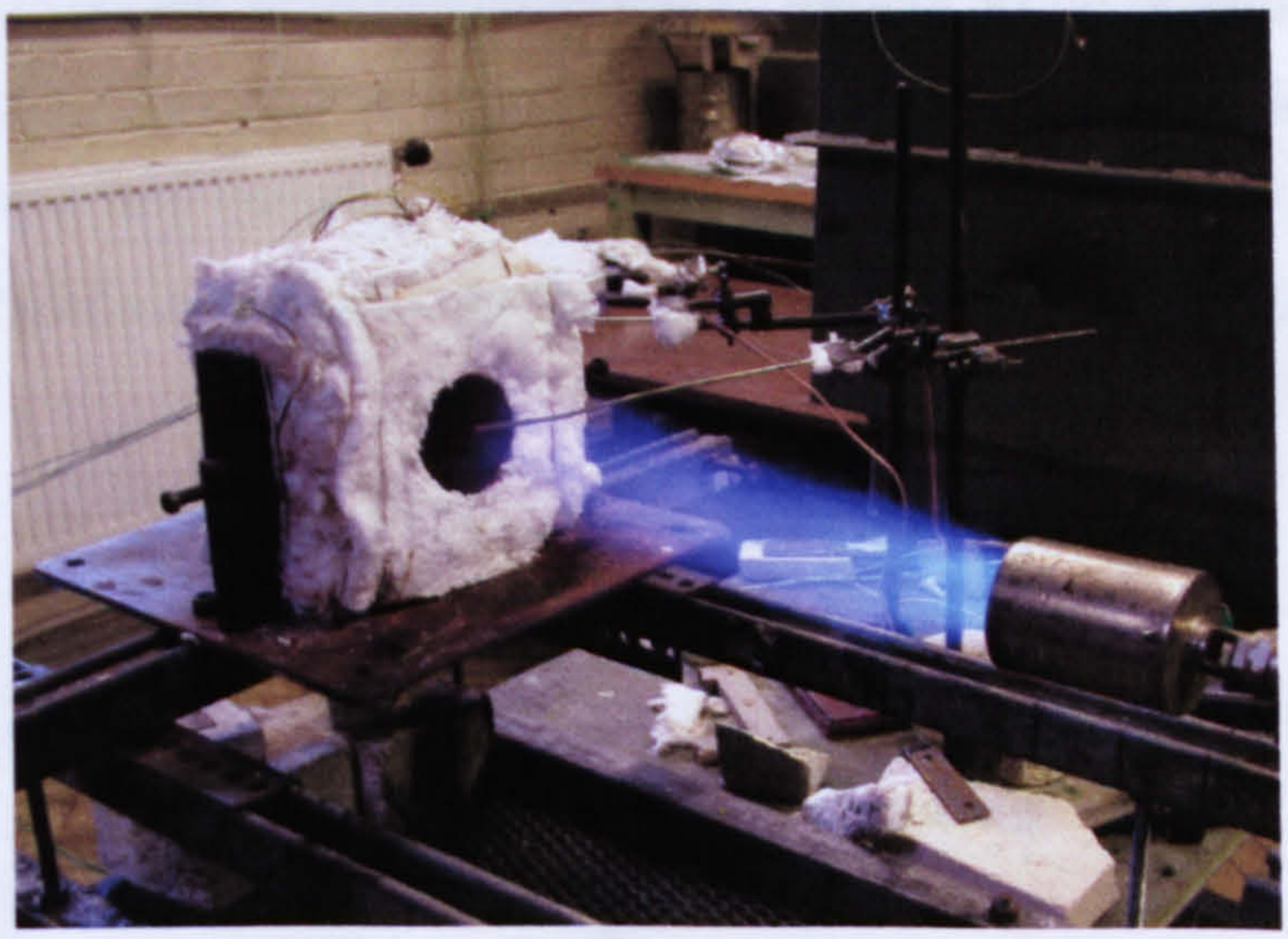

Figure 3.1 The propane burner used as a small scale fire testing apparatus

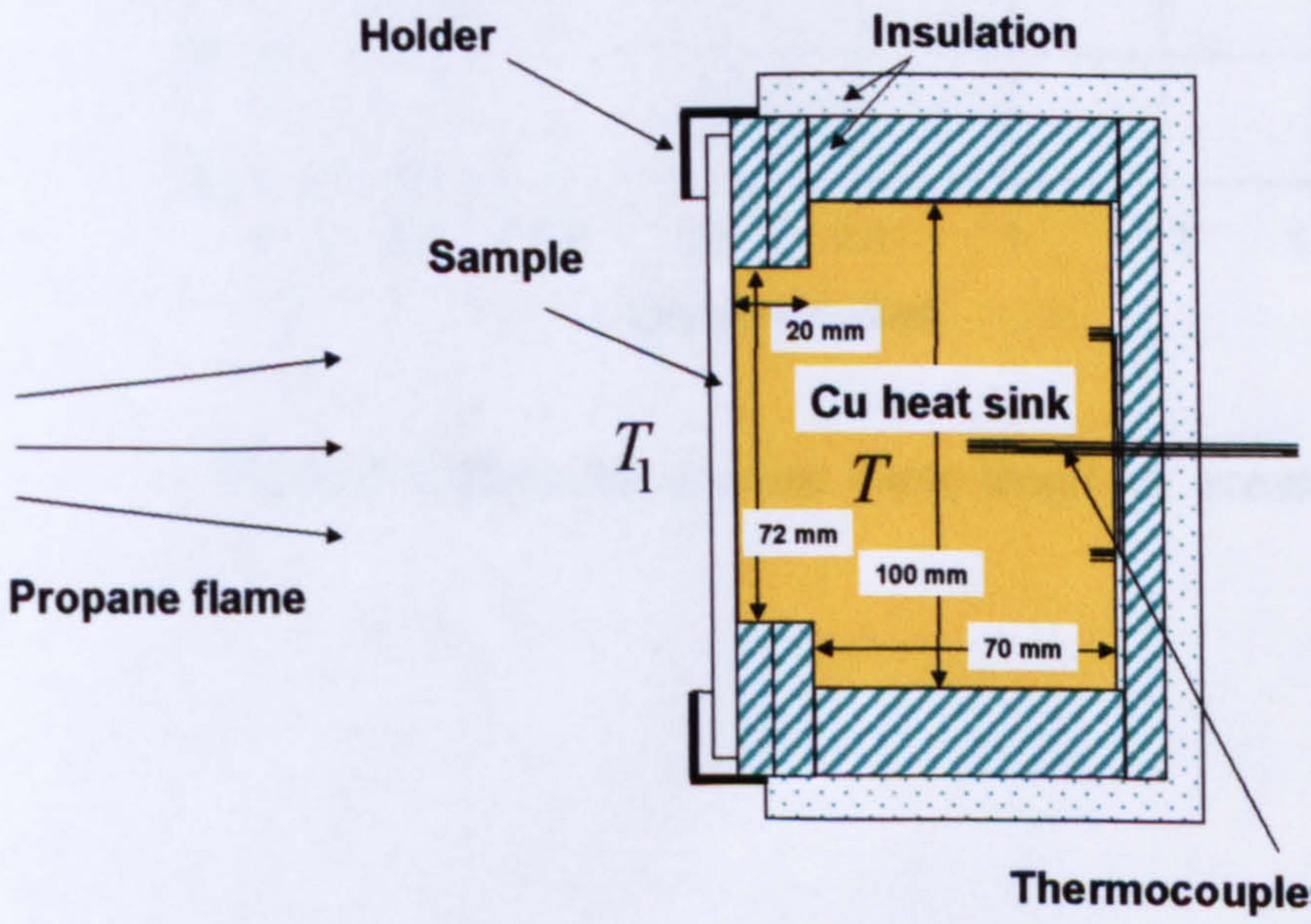

Figure 3.2 Schematic of the heat flux meter used in the calibration tests.

When propane gas is released at a pressure (Pr) (usually ranging between 0.2-1.2bar) and ignited, the initial velocity of the ejected fluid is apparently high. However, the velocity of the moving fluid decreases rapidly due to air resistance. Figure 3.3 shows the measured visible flame length, L_f, against pressure, P_r (by visual inspection). The curve shown in Fig. 3.3 indicates whether forced convection effects can be ignored or not in a fire test for specified condition (of P_r and L_f).

An investigation was conducted using a Newton's Law of Cooling to quantify the small heat loss through the insulation and the emissivity value of copper, for the purpose standardising the calibration procedure. The copper block was heated to 200°C, and allowed to cool naturally. This work and the results derived for the heat transfer coefficient and emissivity of the front face of the meter are presented later in section 3.7.

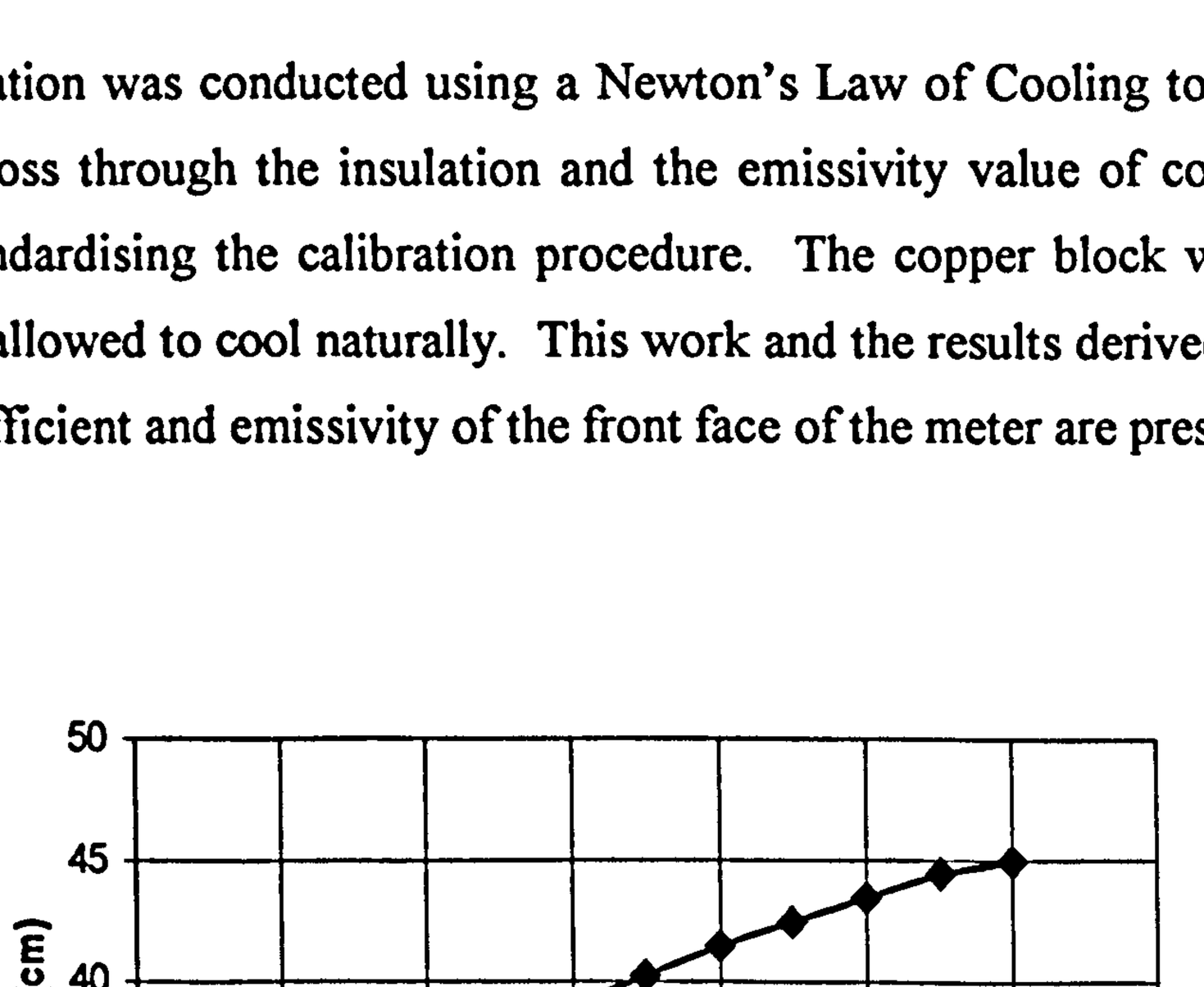

Figure 3.3 Observed propane flame length vs. pressure (P_r).

3.4. Temperature Field In Front of the Heat Flux Meter Created By the Propane Burner

3.4.1 Introduction.

In order to coordinate reproducible tests with the propane burner, the following questions need to be answered. Can a propane burner be regarded as a constant heat flux source when the distance between the sample and the burner, and the gas supply pressure are fixed? What is the relationship between the measured heat flux and the temperature near to the front surface of the sample?

In order to understand the propane burner test, measurements were conducted of the steady state temperature field in front of the hot face of the heat flux meter created by the propane burner at a specified gas supply pressure level. The results for different cases are presented below, followed by a discussion.

3.4.2 Effect of Supply Pressure

Two tests were carried out to investigate the steady state temperature field in front of the hot face of the heat flux meter created by the propane burner.

The test arrangement adopted here is shown in Fig. 3.4. The heat flux meter was thermally insulated with only its front face exposed to the heating source during the test. Three K-type thermocouples (i.e., CF1, CF2 and CF3) were installed inside the meter for measuring heat flux input, while two thermocouples (i.e., HF1 and HF2) were used for measuring temperatures on the hot face of the meter and the temperatures surrounding the hot face of the meter.

During the tests the distance (S) between the propane burner and the hot face of the meter was kept at 355mm, whilst the pressure gas supply set at 0.49 bar.

In Test 1 HF2 was positioned at 12 different points away from the hot face (i.e., D = 5, 10, 15, 20, 25, 30, 55, 105, 155, 205 and 255 mm). In Test 2 HF2 was placed at 16 different locations along the centre line to measure the front field temperatures. The first position of HF2 (i.e., D = 5mm) was kept for nearly 500 seconds during

both tests following by about one minute for each of the rest of the positions. The tests lasted for nearly 1400 seconds.

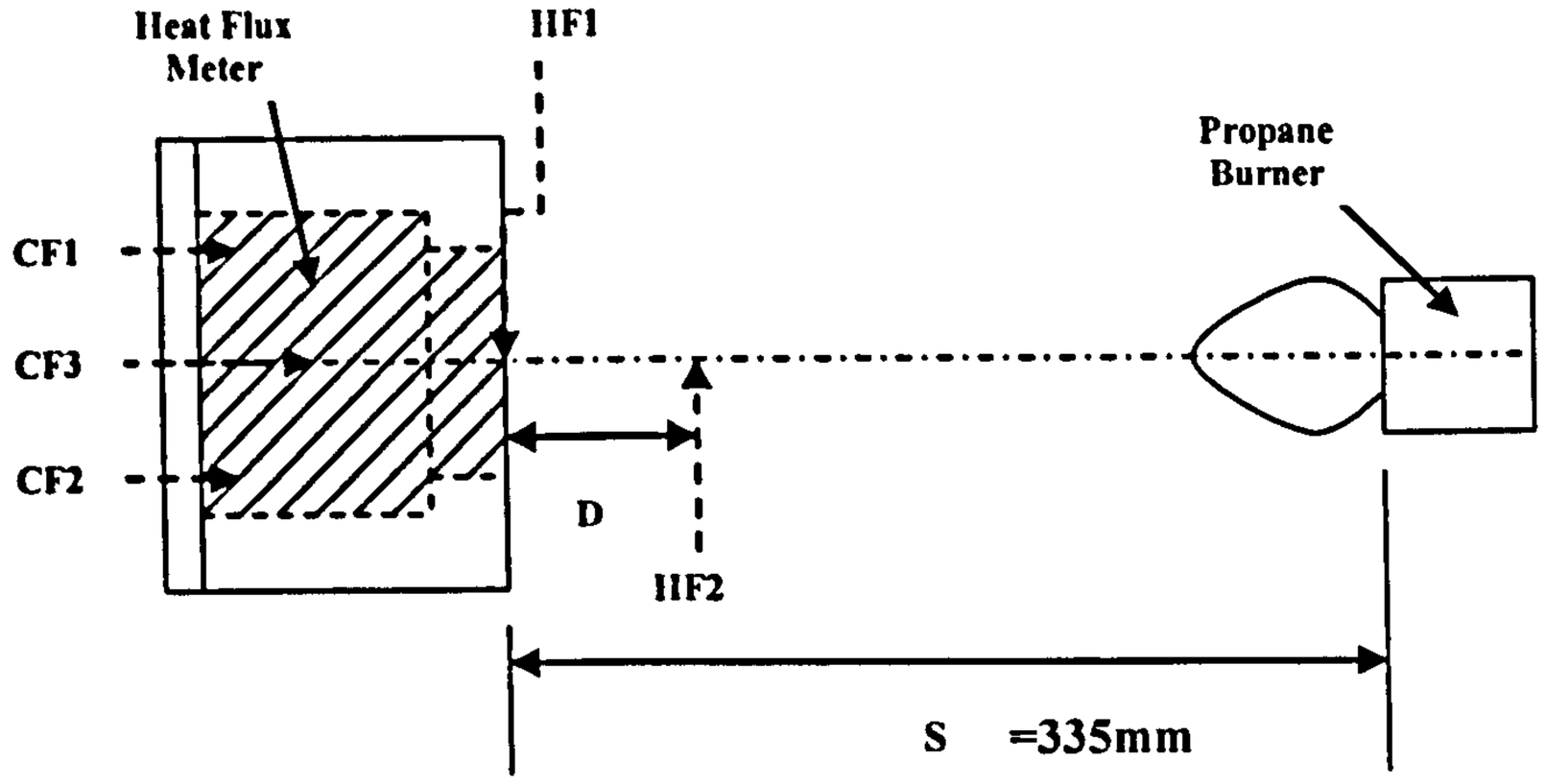

Figure 3.4 Calibration heat arrangements.

3.4.2.1 Results

Figure 3.5 shows typical results for measured temperature vs. time (i.e. CF average/HF1 and HF2). Within 40 seconds after the start of the test, the temperature on the hot face of the meter (i.e. HF1) became steady and the average temperature (i.e. between 45 and 1175 second.) was 780°C.

It can be seen from Fig. 3.5 that the measured steady-state temperatures surrounding the front of the hot face of the meter (i.e. HF2) were all higher than the steady-state temperatures on the hot face (i.e. HF1) of the meter. This is obviously attributed to the effects of heat conduction within the meter body.

It is clear from Fig. 3.6 that the steady-state temperatures along the central line of the rig in front of the hot face of the meter (i.e. HF2) from the two tests conducted are in a good agreement with one another, indicating that the relevant results are reliable.

It is also clear from Fig. 3.6 that the steady state temperature increased slightly with increasing (D) or when the thermocouple (i.e. HF2) was moved away from the block hot surface, until the position of D = 200 mm. As D increased, or the distance

between the block hot face (HF) and the propane burner (i.e. S) decreased, the steady-state temperature in the field increased. This is probably due to the fact that at such positions the propane burning process has not fully developed.

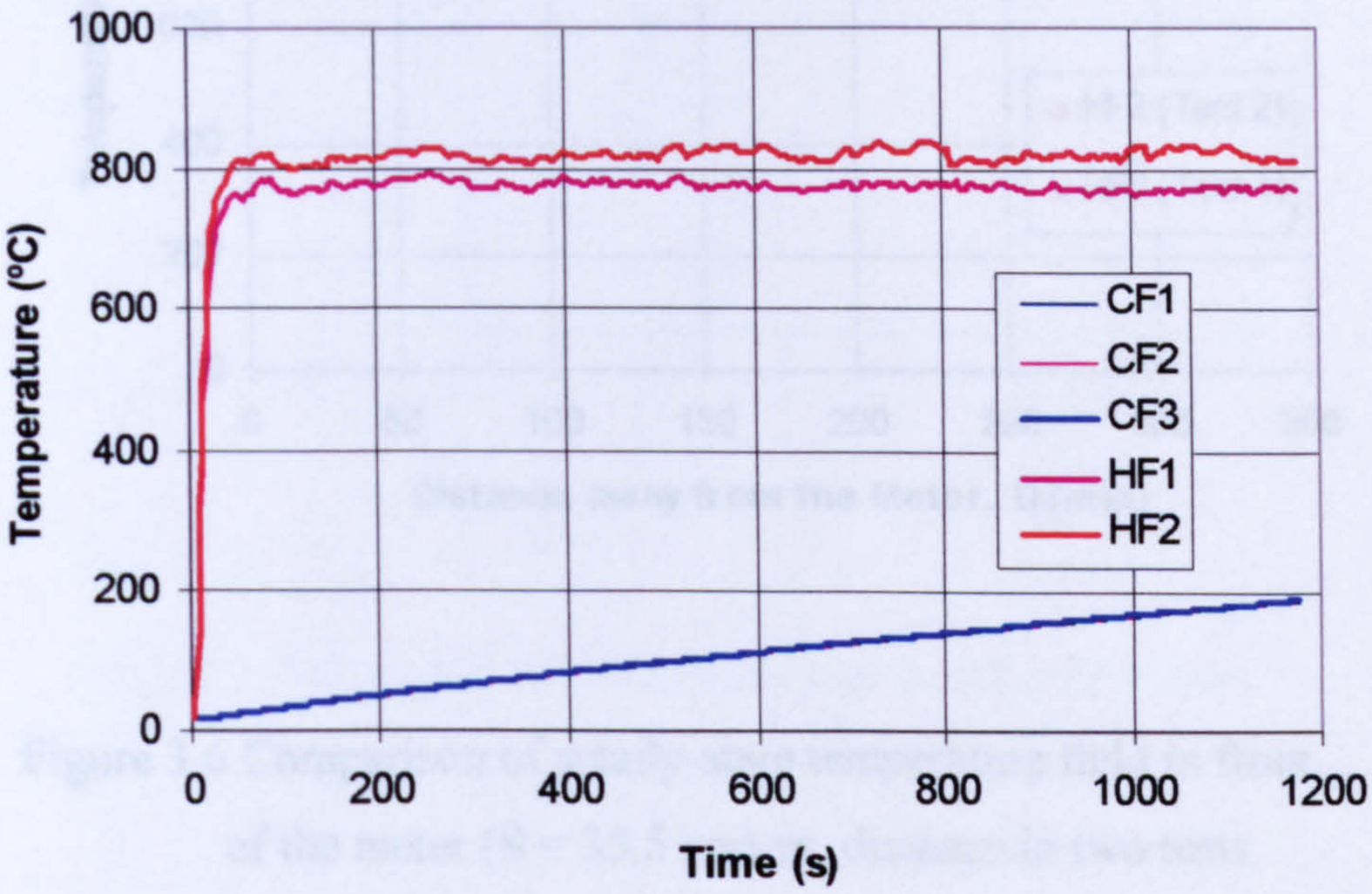

(a)

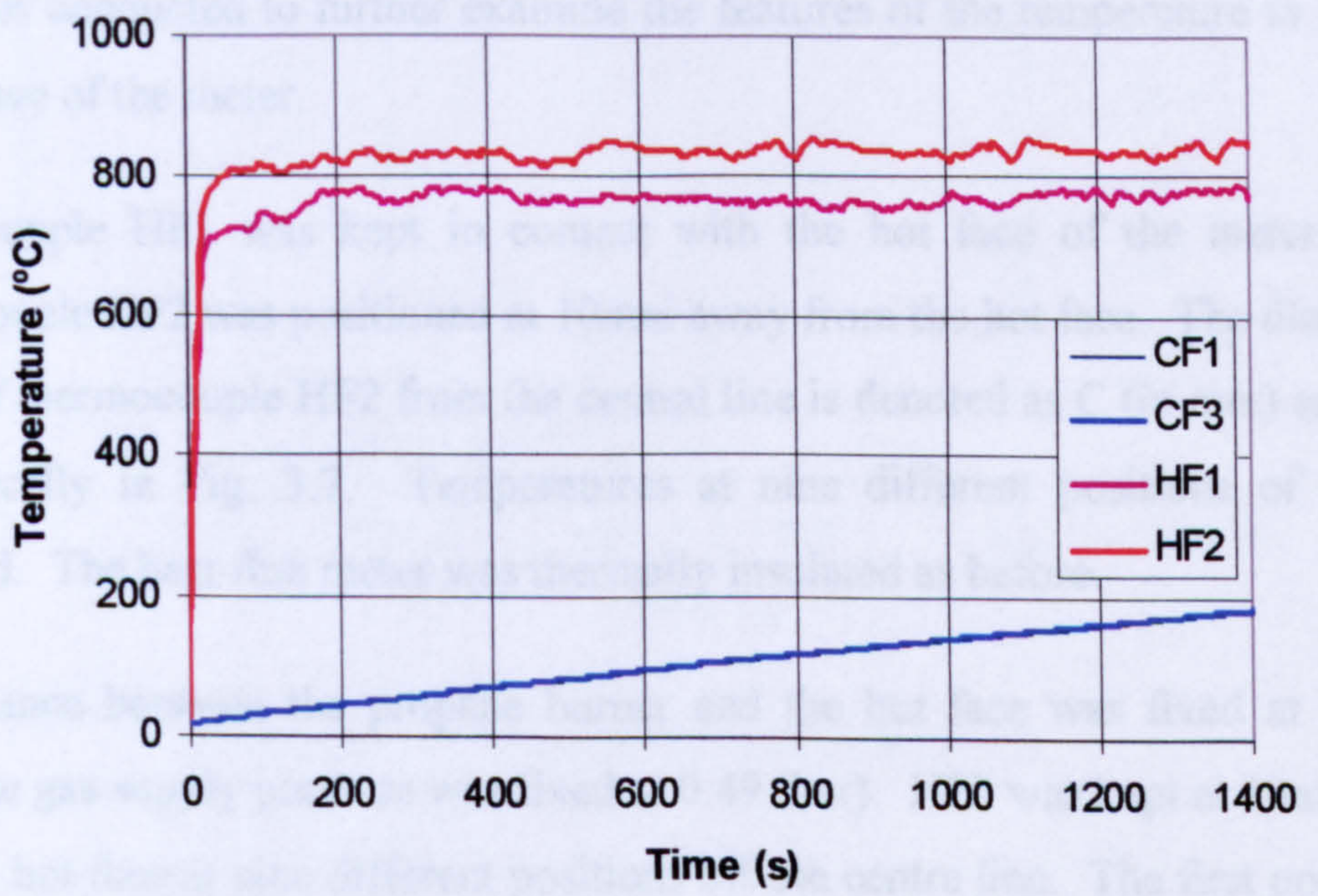

(b)

Figure 3.5 The measured temperature profile (a) Test 1 (b) Test 2.

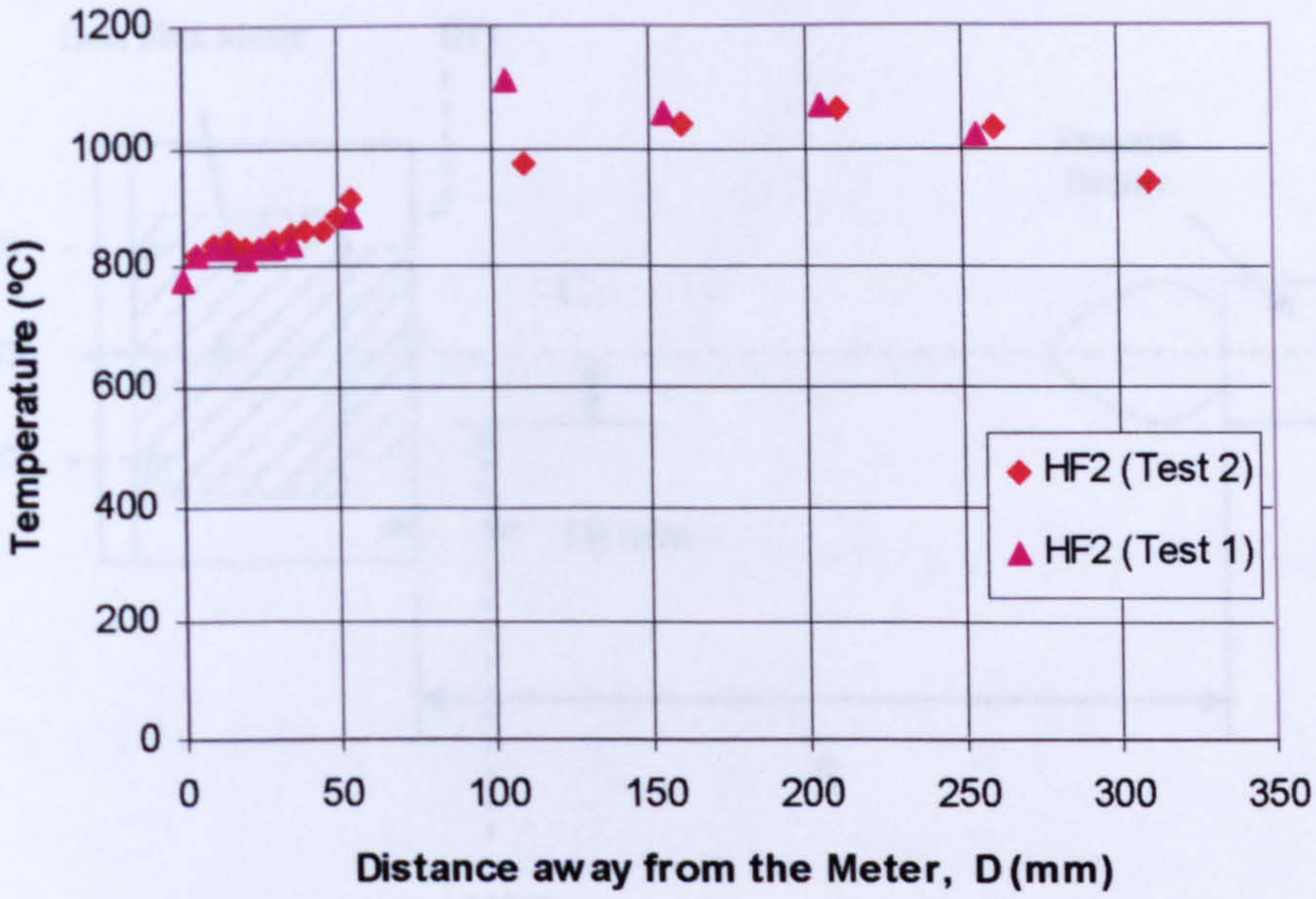

Figure 3.6 Comparison of steady-state temperature field in front of the meter (S = 35.5 cm) vs. distance in two tests.

3.4.3 Variation with Vertical Position

A test was conducted to further examine the features of the temperature in front of the hot face of the meter.

Thermocouple HF1 was kept in contact with the hot face of the meter, whilst thermocouple HF2 was positioned at 10mm away from the hot face. The distance of the tip of thermocouple HF2 from the central line is denoted as C (in mm) as shown schematically in Fig. 3.7. Temperatures at nine different positions of C were measured. The heat flux meter was thermally insulated as before.

The distance between the propane burner and the hot face was fixed at 35.5cm, whilst the gas supply pressure was fixed at 0.49 (bar). HF2 was kept at 10mm away from the hot face at nine different positions off the centre line. The first position of HF2 was kept for about 500 seconds, whilst HF2 was kept for about one minute for each of the other eight positions of C. The temperatures measured are shown in Fig. 3.8.

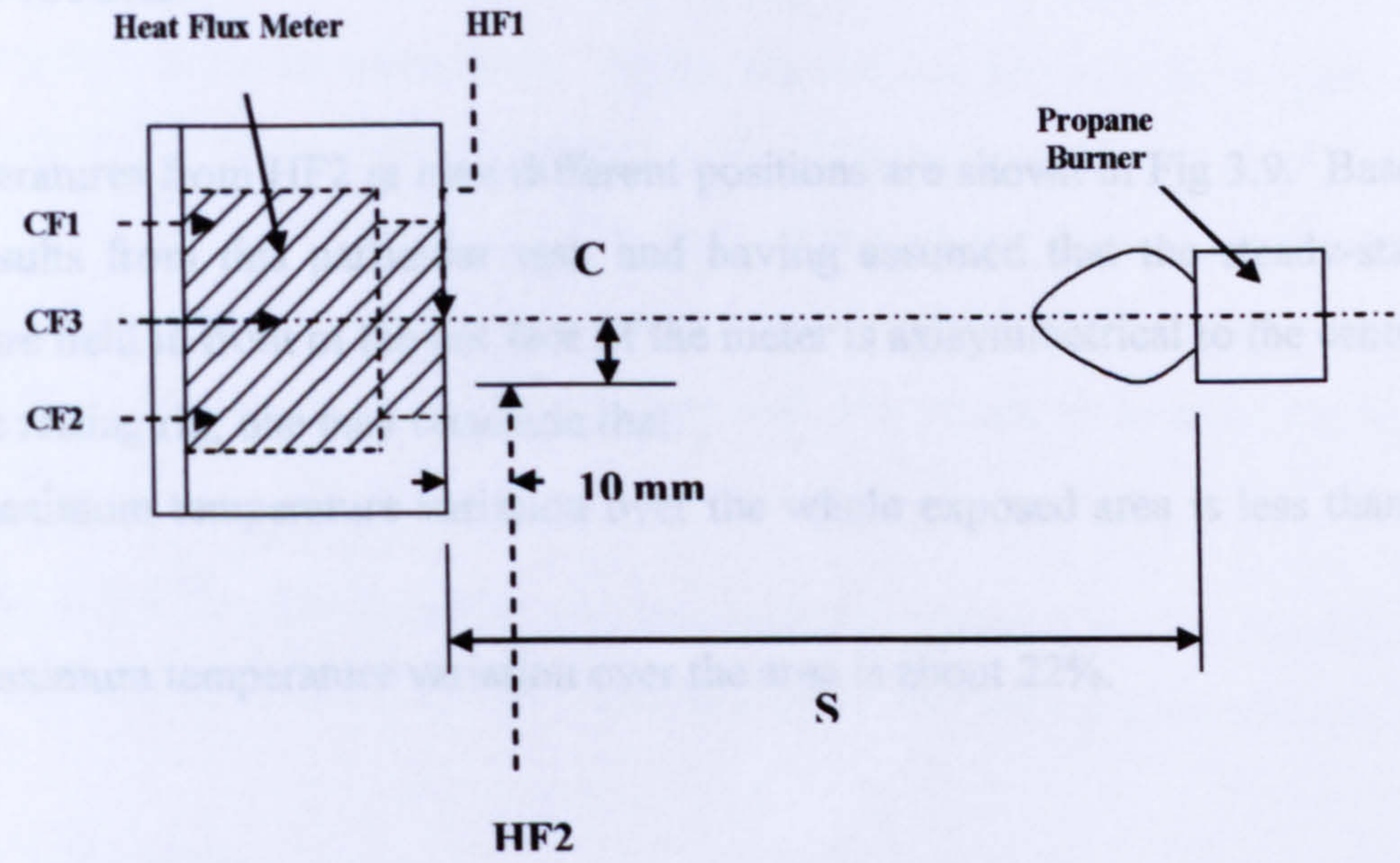

Figure 3.7 Top view of the test arrangement for case two.

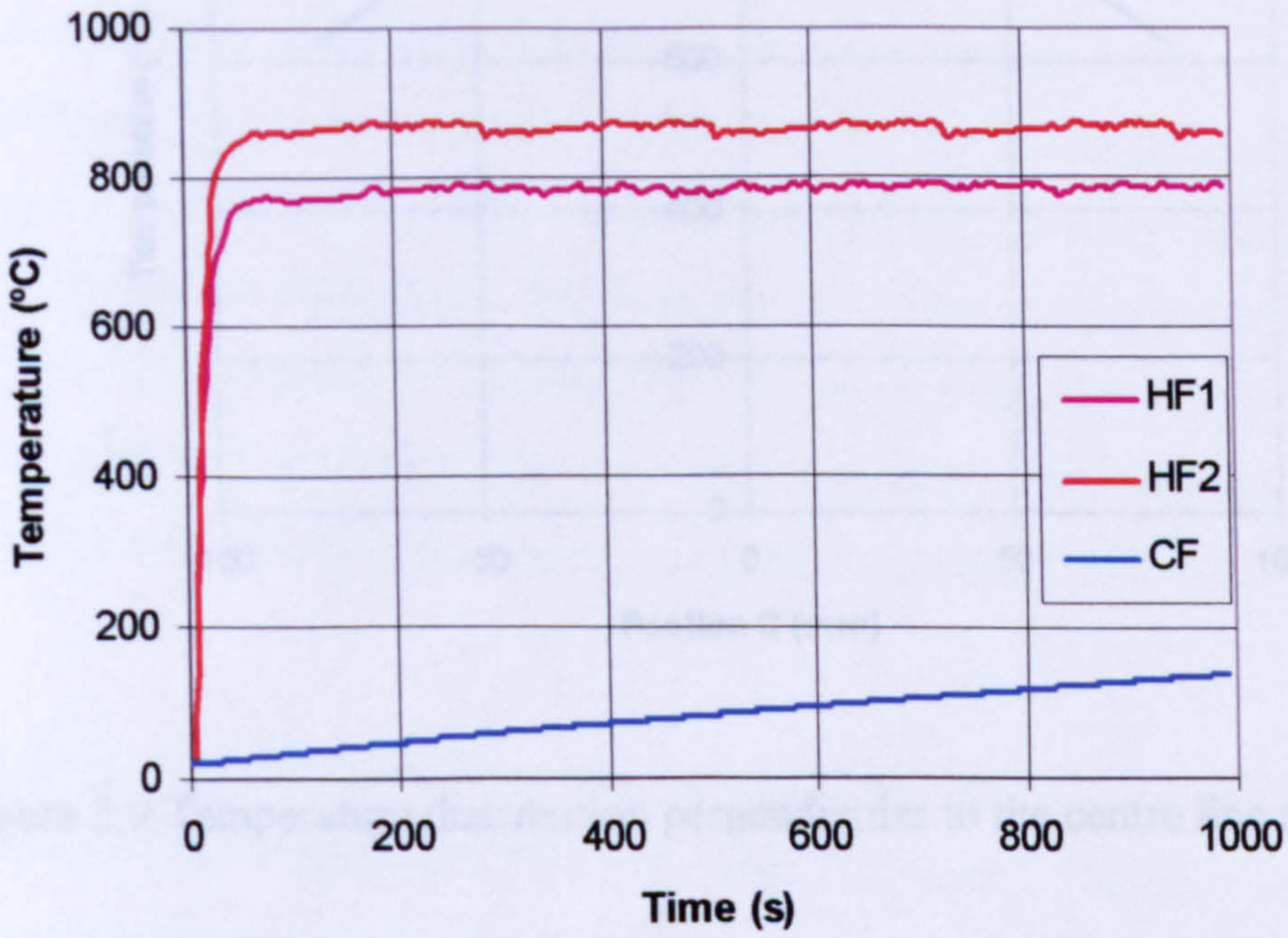

Figure 3.8 Measured temperature profile.

3.4.3.1 Results

The temperatures from HF2 at nine different positions are shown in Fig 3.9. Based on the results from this particular test, and having assumed that the steady-state temperature field in front of the hot face of the meter is axisymmetrical to the central line of the testing rig, one may conclude that:

- the maximum temperature variation over the whole exposed area is less than 7 %;
- the maximum temperature variation over the area is about 22%.

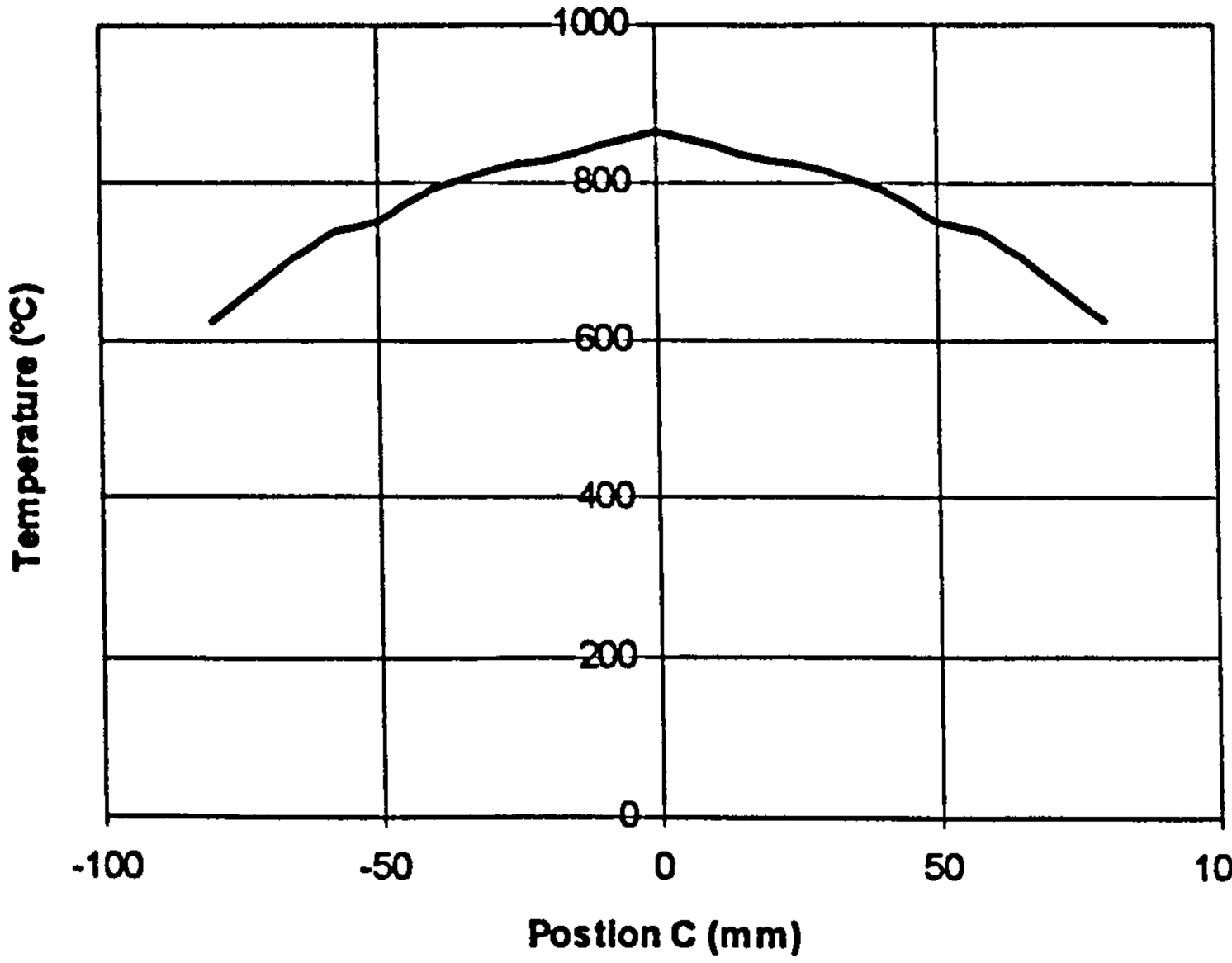

Figure 3.9 Temperature distribution perpendicular to the centre line of the rig.

3.4.4 Hot Face Temperatures

A new thermocouple, CF0 of Type K, was installed as indicated in Fig. 3.10 within the heat flux meter body near the front face to examine the temperature within the copper block and to derive the temperatures on the hot face as a function of time by extrapolation, in order to compare these with the measured temperatures from thermocouple HF1.

The thermocouple, CF0, was positioned along the central line and 5mm from the front surface inside the meter body. Again, the distance between the propane burner and the hot face of the meter was fixed at S = 355mm, and the gas supply pressure was kept at p = 0.49bar during the test. Meanwhile, thermocouple HF1 was positioned at the right centre of the hot face touching the meter body all times and HF2 was positioned along the central line and was 10mm in front of the hot face during the test.

The test lasted for 1000 seconds. The measured temperature profiles obtained from thermocouples CF0, CF1, CF3, HF1 and HF2 of the fire test are shown in Fig. 3.11.

3.4.4.1 Results

(A) General features of temperature profiles within the meter body.

The three temperature profiles measured at CF0, CF1 and CF3 are shown in Fig. 3.12. It can be seen from Fig. 3.12 that apart from the first 50 seconds during the fire test the temperatures measured at CF3 and CF1 are nearly the same, whilst the differences between temperatures measured at CF0 and CF1 (or between CF0 and CF3) remain almost unchanged. For example, the differences between temperatures at CF0 and CF1 are about 7°C during the 1000 second long fire test. It can also be seen from Fig. 3.12 that apart from the initial response stage, the slope of the three temperature-time curves looks nearly constant, suggesting a linear response time period.

At the initial response stage of the test, however, the thermal response status at the different positions within the meter body looks different. Figure 3.13 shows the temperature measured profiles at CF0, CF1 and CF3 for the first 60 seconds of the fire test. It can be clearly seen from Fig. 3.13 that the rate of temperature rise measured at CF0 at this stage is much higher than those measured at CF1 and CF3.

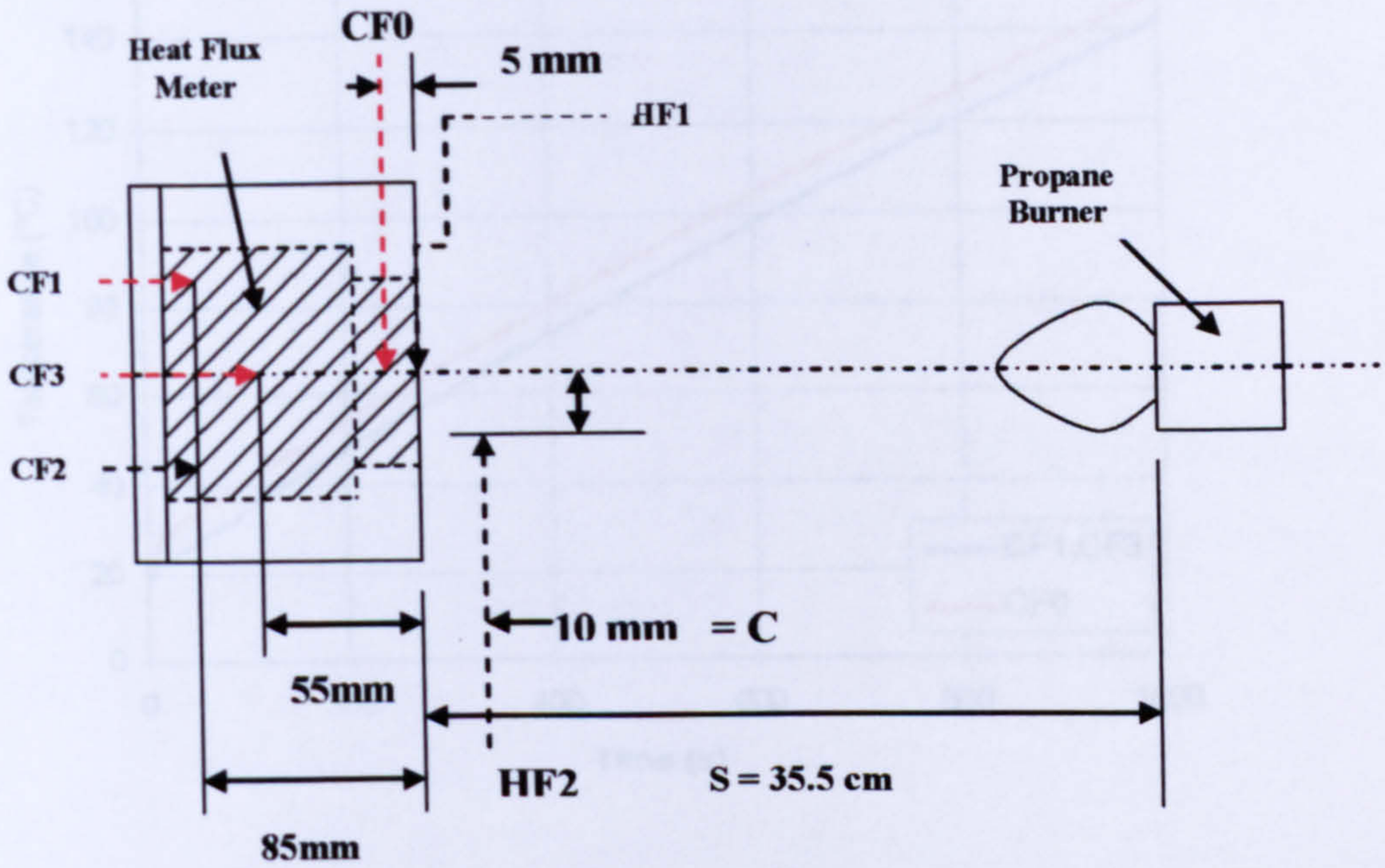

Figure 3.10 Top view of the test arrangement (test four).

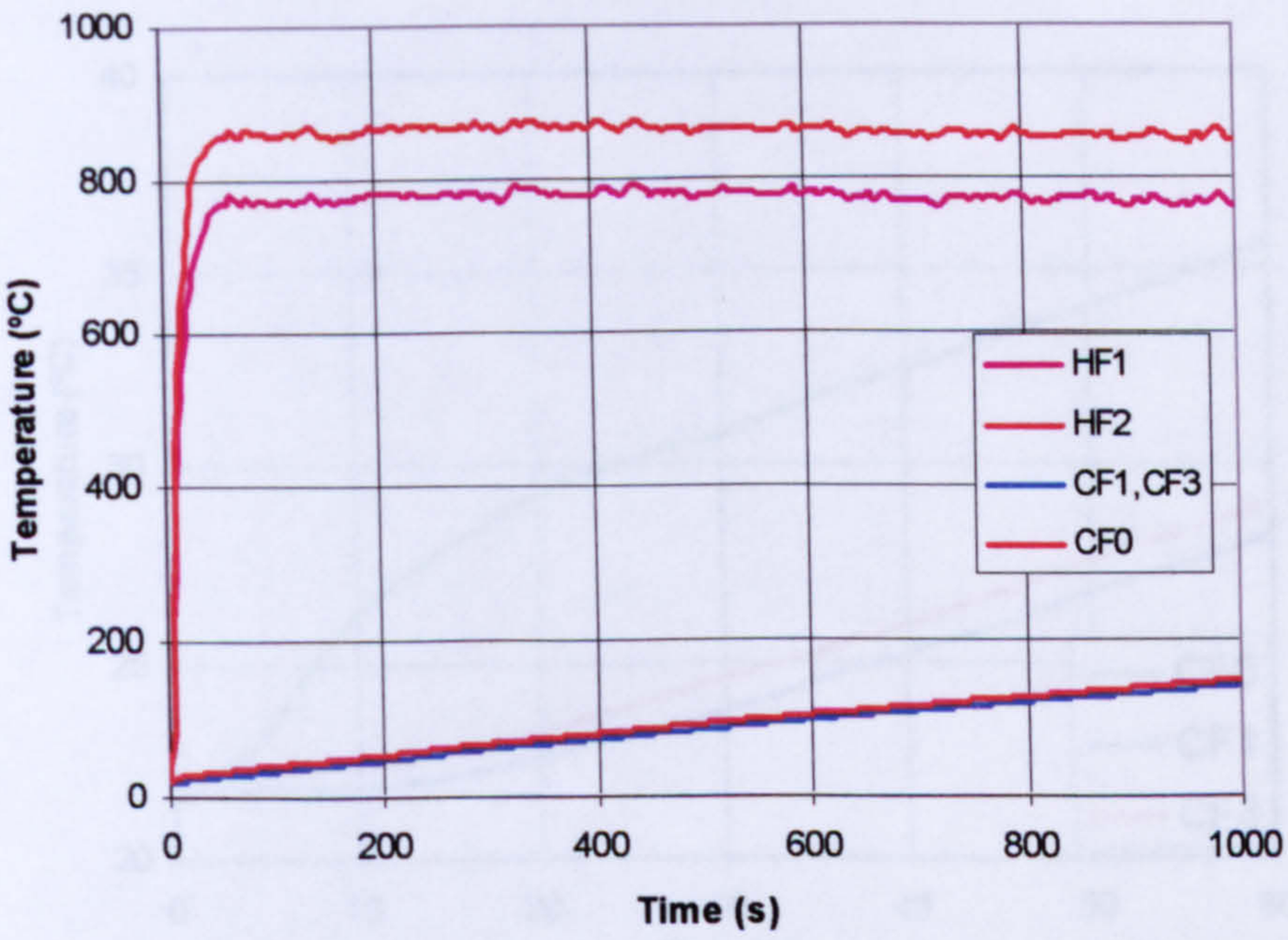

Figure 3.11 Result of fire test with CF0 newly installed.

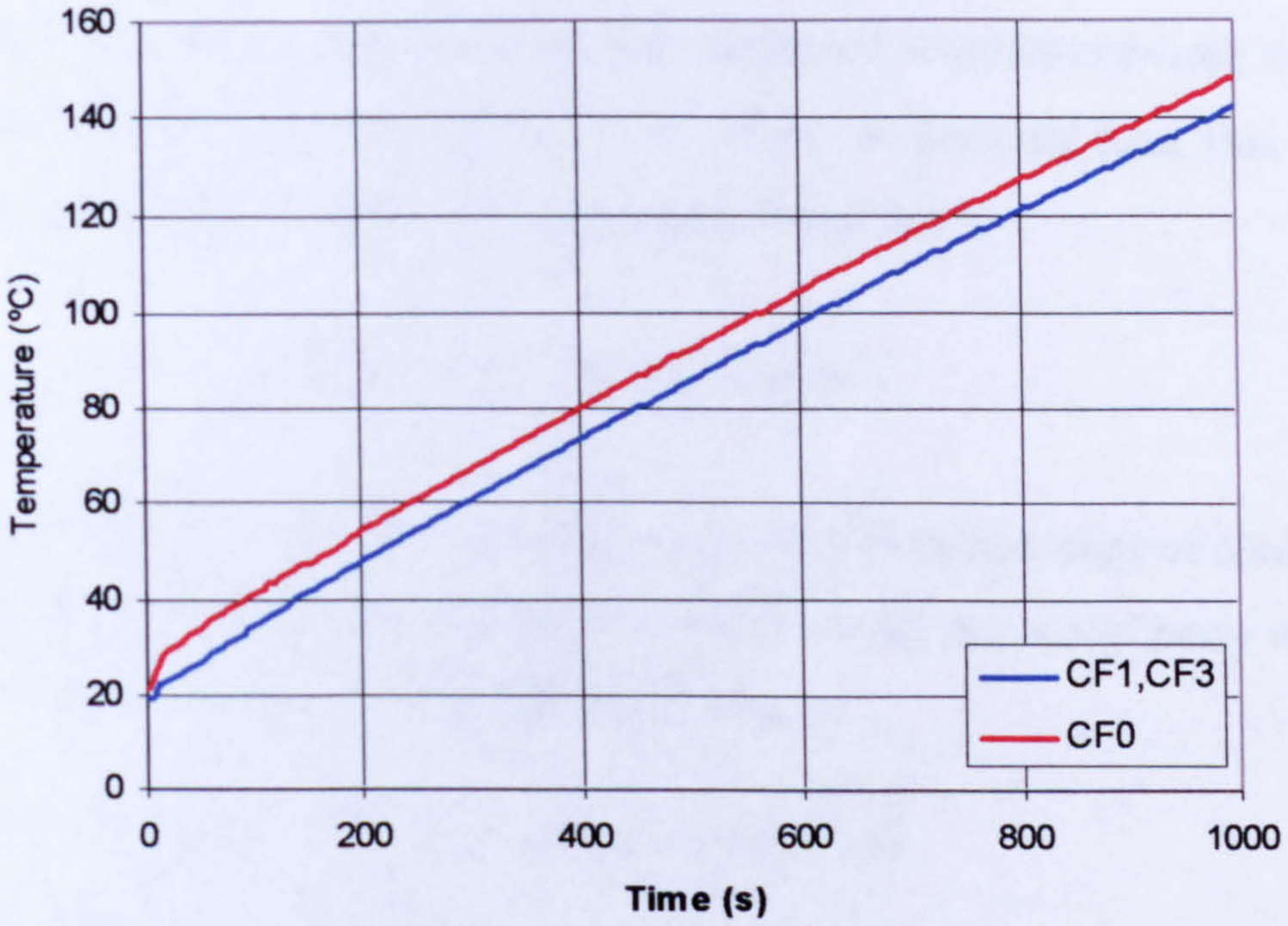

Figure 3.12 Thermal responses at CF0, CF1 and CF3.

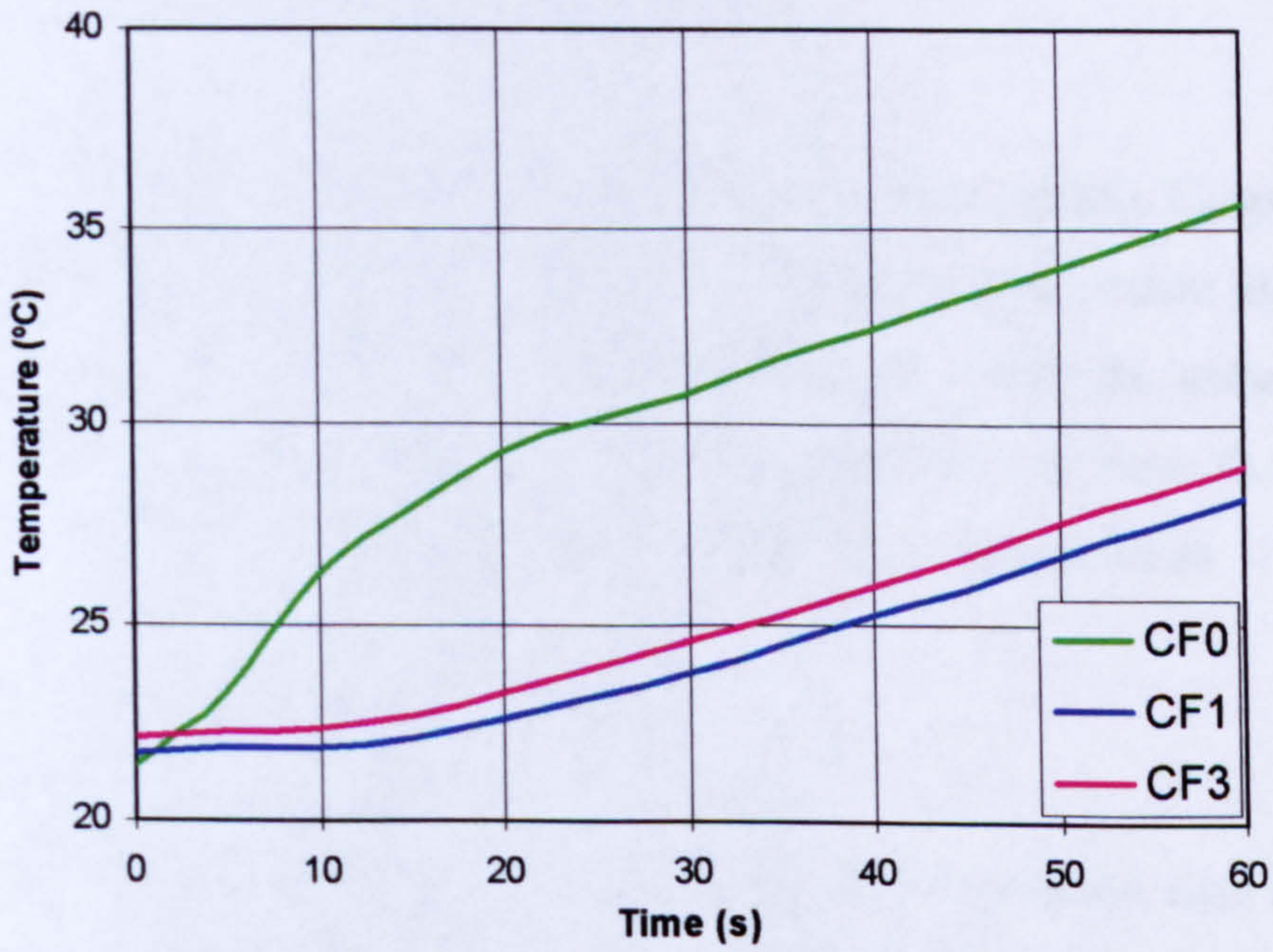

Figure 3.13 Thermal responses at CF0, CF1 and CF3 at the initial stage.

B) Rate of change of temperature within the meter body

The heat flux levels derived from the measured temperature-time curves at CF0, CF1 and CF3 are shown in Fig. 3.14. Here, in deriving heat flux levels, q, the following equation is adopted for the meter being used:

$$q = 530.2 \times (\Delta T/\Delta t) \quad (\text{in: kW/m}^2) \tag{3.3}$$

It can be seen from Fig. 3.14 that after the initial response stage of about 50 seconds, the rate of change of temperature everywhere inside the meter body was almost the same, declining slightly during the whole course.

C) Derived meter body's front surface temperatures

As indicated above, after the initial response stage of about 50 seconds, the rates of temperature change at CF0, CF1 and CF3 look almost the same. For transient thermal responses, the governing 1D equation for the metal body element of the meter is given as

$$\rho C_p \frac{\partial T}{\partial t} = \frac{\partial}{\partial x}\left(k \frac{\partial T}{\partial x}\right) \tag{3.4}$$

where, ρ denotes density of the meter material (i.e., pure copper), C_p specific heat of copper, k thermal conductivity of copper. For a given time instant after the initial stage, since the rates of change of temperatures are nearly the same everywhere within the meter body, the term on the right hand side of Eqn. (3.4) should be constant. Therefore, at a given time instant, $T(x)$ can be expressed as

$$T(x) = C_0 + C_1 x + C_2 x^2 \tag{3.5}$$

By assuming that the thermal status of the meter can be simulated with a 1-D model, and knowing the temperatures CF0 at x = 5mm, CF3 at x = 55mm and CF1 at x = 85mm, one can derive the temperatures on the front surface of the meter body using the experimental data of temperatures at CF0, CF3 and CF1. The temperatures on the front surface of the meter (FS) and the measured temperatures on the hot face (HF1) are shown in Fig. 3.15 for comparison. They look significantly different.

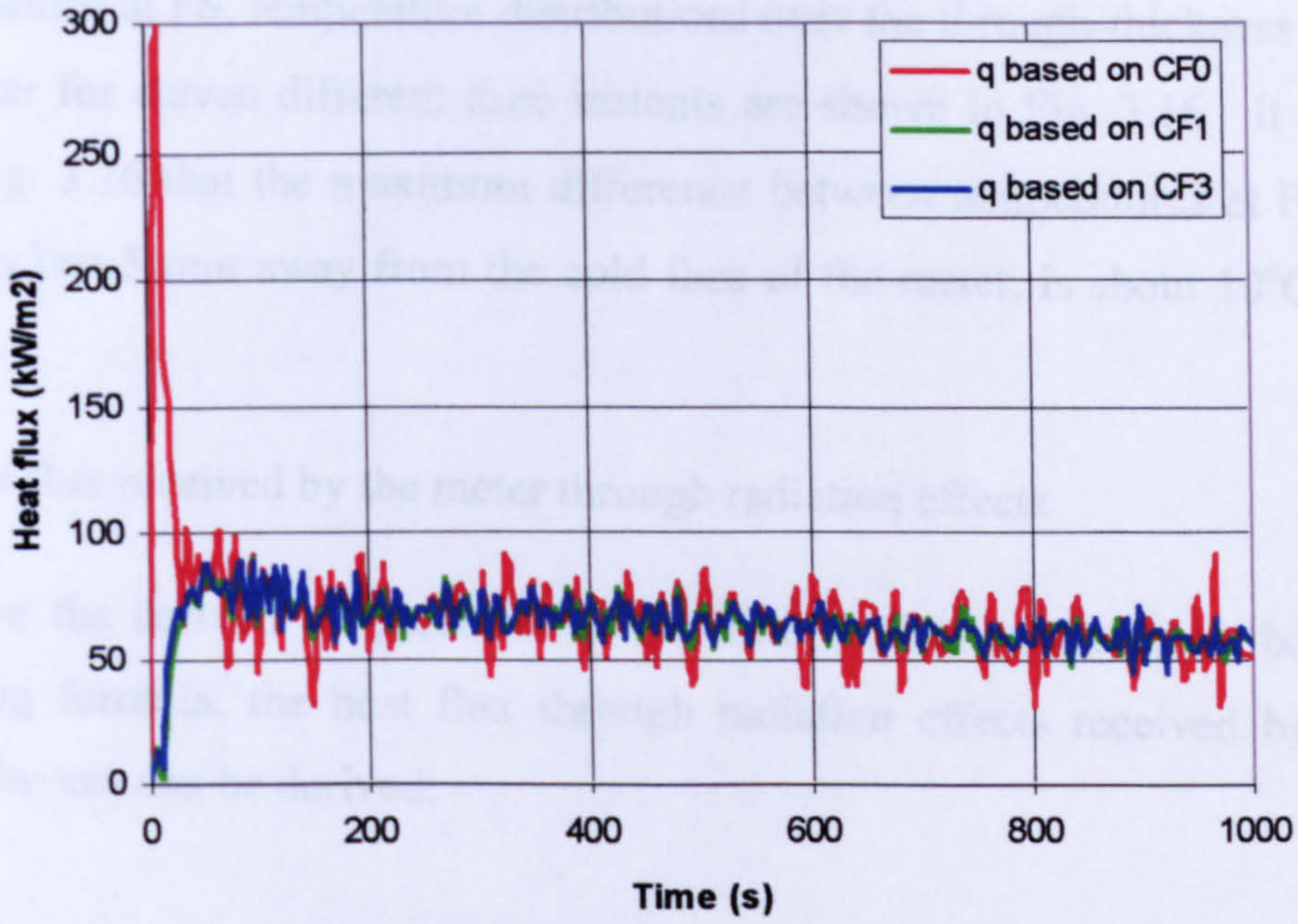

Figure 3.14 Derived heat flux levels based on measurements at CF0, CF1 and CF3.

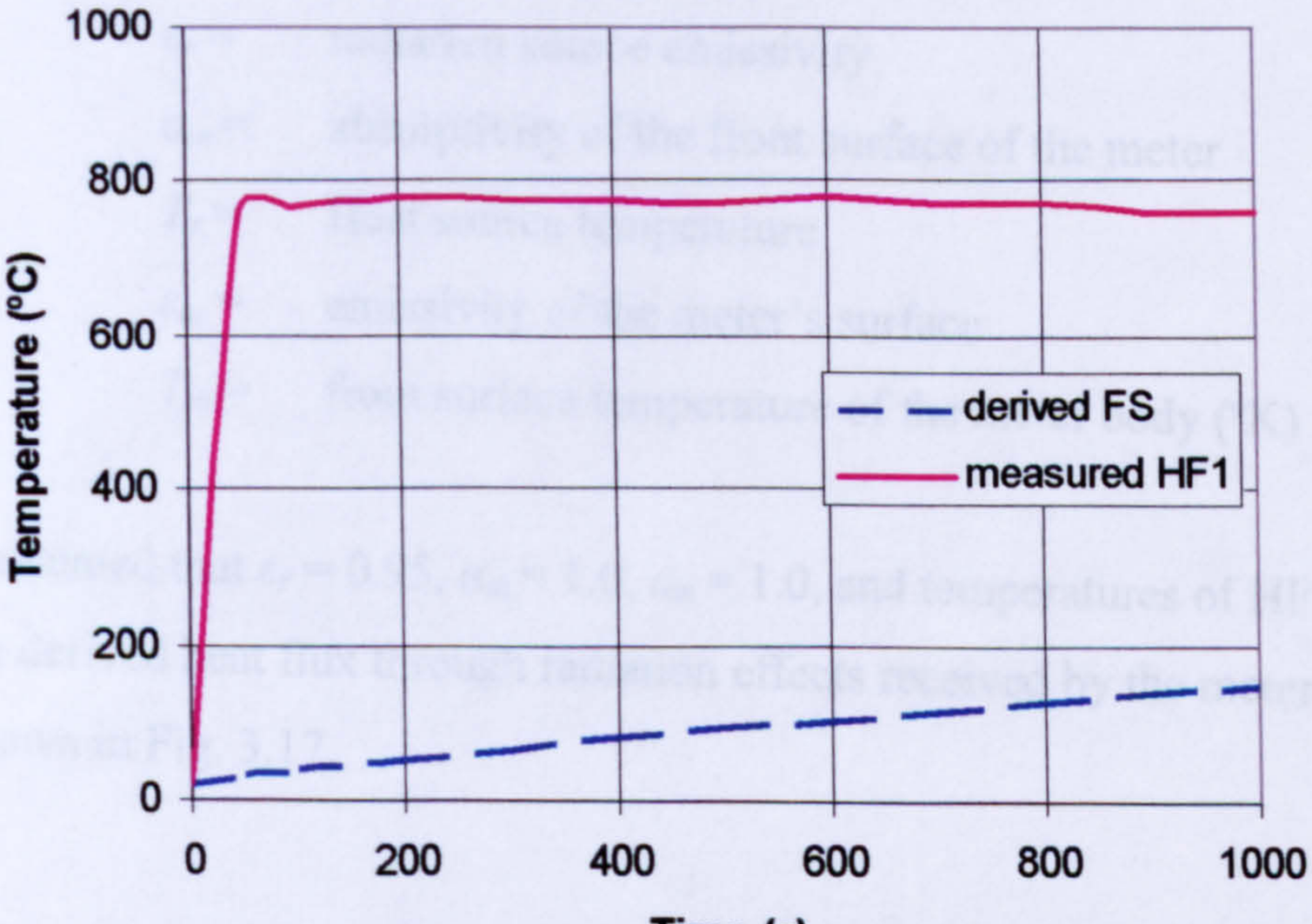

Figure 3.15 A comparison between measured HF1 FS temperatures.

D) Temperature distribution in the through-thickness direction of the meter

Based on the temperatures measured at CF0, CF1 and CF3, and also the derived temperatures at FS, temperature distributions over the through-thickness direction of the meter for eleven different time instants are shown in Fig. 3.16. It can be seen from Fig. 3.16 that the maximum difference between temperatures at FS and CF1, which is just 5 mm away from the cold face of the meter, is about 10°C during the fire test.

(E) Heat flux received by the meter through radiation effects

Based on the derived temperatures at the front surface of the meter body and the following formula, the heat flux through radiation effects received by the meter during the test can be derived:

$$q_r = \sigma \left(\varepsilon_r \alpha_m T^4_s - \varepsilon_m T^4_m \right) \qquad (3.6)$$

where

q_r = heat flux received by the meter through radiation (W/m^2)

σ = Stefan-Boltzmann constant (5.73×10^{-8} $W/m^2.°K^4$)

ε_r = radiation source emissivity

α_m = absorptivity of the front surface of the meter

T_s = Heat source temperature

ε_m = emissivity of the meter's surface

T_m = front surface temperature of the meter body (°K)

Having assumed that $\varepsilon_r = 0.95$, $\alpha_m = 1.0$, $\varepsilon_m = 1.0$, and temperatures of HF2 are taken as T_s, the derived heat flux through radiation effects received by the meter during the test is shown in Fig. 3.17.

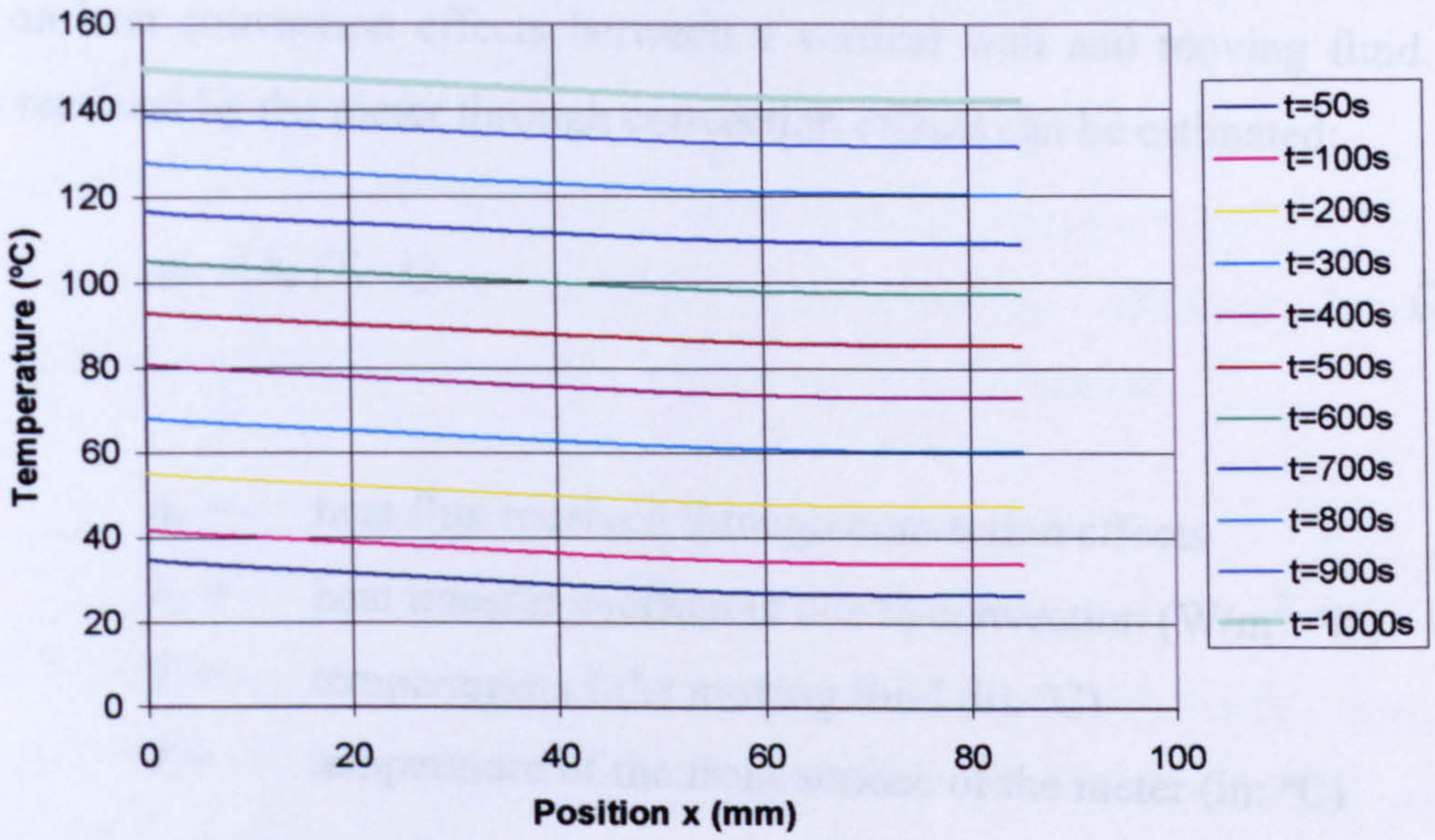

Figure 3.16 Temperature distributions in the through-thickness direction of the meter.

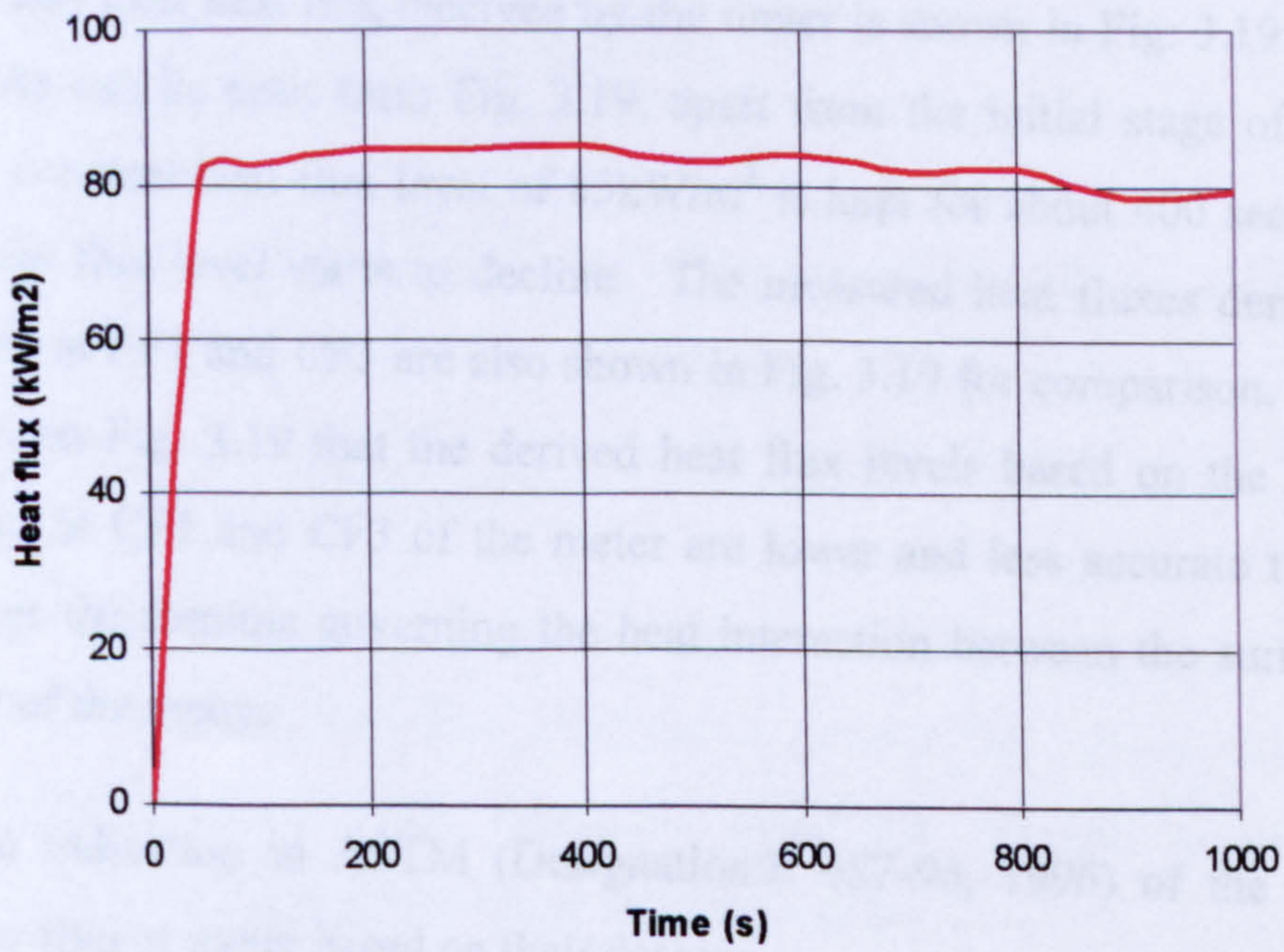

Figure 3.17 Derived heat flux received by the meter through radiation effects.

(F) Heat flux received by the meter through convection effects

Based on the derived temperatures at the front surface of the meter and the following formula on heat convection effects between a vertical wall and moving fluid, the heat flux received by the meter through convection effects can be estimated:

$$q_c = h_c (T_f - T) \tag{3.7}$$

where

q_c = heat flux received through convection effects

h_c = heat transfer coefficient due to convection (W/m^2. °K)

T_f = temperature of the moving fluid (in: °C)

T = temperature of the front surface of the meter (in: °C)

Having assumed that h_c = 10.0 (W/m^2. °K), and the measured temperatures at HF2 are taken as T_f, then the derived heat flux received by the meter through convection effects during the test is shown in Fig. 3.18.

By inspection of Figs 3.17 and 3.18, one may find that the total heat flux input to the meter during the test is dominated by radiation effects.

The calculated total heat flux received by the meter is shown in Fig. 3.19 as a solid red line. As can be seen from Fig. 3.19, apart from the initial stage of about 50 seconds, a constant heat flux level of 85kW/m^2 is kept for about 400 seconds, and then the heat flux level starts to decline. The measured heat fluxes derived from temperatures at CF1 and CF3 are also shown in Fig. 3.19 for comparison. It can be seen clearly in Fig. 3.19 that the derived heat flux levels based on the measured temperatures at CF1 and CF3 of the meter are lower and less accurate than those derived from the formula governing the heat interaction between the surroundings and surface of the meter.

There is an indication in ASTM (Designation:E 457-96, 1996) of the optimum length of the slug or meter based on their design:

$$l_{opt} = \frac{3k\Delta T_{fs}}{5q} \tag{3.8}$$

where:

k = thermal conductivity of the meter material (copper);

T_{fs} = the meter front face temperature minus the initial front face temperature;

q = heat transfer rate of the meter.

Having noticed that k (copper material) = 399 (W/m/K), $T_{front\ face}$ = 128 (°C) for the current case, and q is about 80 (kW/m^2), then the derived l_{opt} = 303 (mm). In reality, the actual equivalent length of the meter being used is given below:

$$l = 20.3 + (99.5/71.9)^2 \times 69.9 = 154.2 \text{ (mm)}$$

The result indicates that the thickness of the current meter is much smaller than that required, and this is the main reason behind the decline of the heat flux curve. For a given level of heat flux input, the longer the fire exposure time period lasts, the thicker the meter has to be.

There is another statement in ASTM (E 457-96) on maximum linear test time estimation. For a meter which is insulated at the back face, the following formula can be used to derive the so-called linear test time:

$$\tau_{max,out} = 0.48 \rho l Cp \left(\frac{\Delta T_{front\ face}}{q} \right) \tag{3.9}$$

Having known that ρ = 8890 (kg/m^3), C_p = 385(J/kg/K), l = 154 (mm), and q = 80 (kW/m^2), the estimated linear test time, therefore;

$$\tau_{max\ opt} = 404 \text{ (sec)}$$

This indicates that the estimated linear test time is about 400 seconds for the current case. One may conclude from Eqn. (3.9) that in general, for a given meter: (i) the higher the heat flux input is, the shorter the linear test time will be; and (ii) the thicker the meter is, the longer the linear test time will be.

With different levels of heat flux input for a given meter, the valid length of linear test time period varies according to the design guidelines. In general, to measure a higher level of heat flux input, a thicker meter is required. Effects of side heat losses

during the course of a test, in particular at relatively high body temperature levels, are the main reason for the inaccuracy of the method.

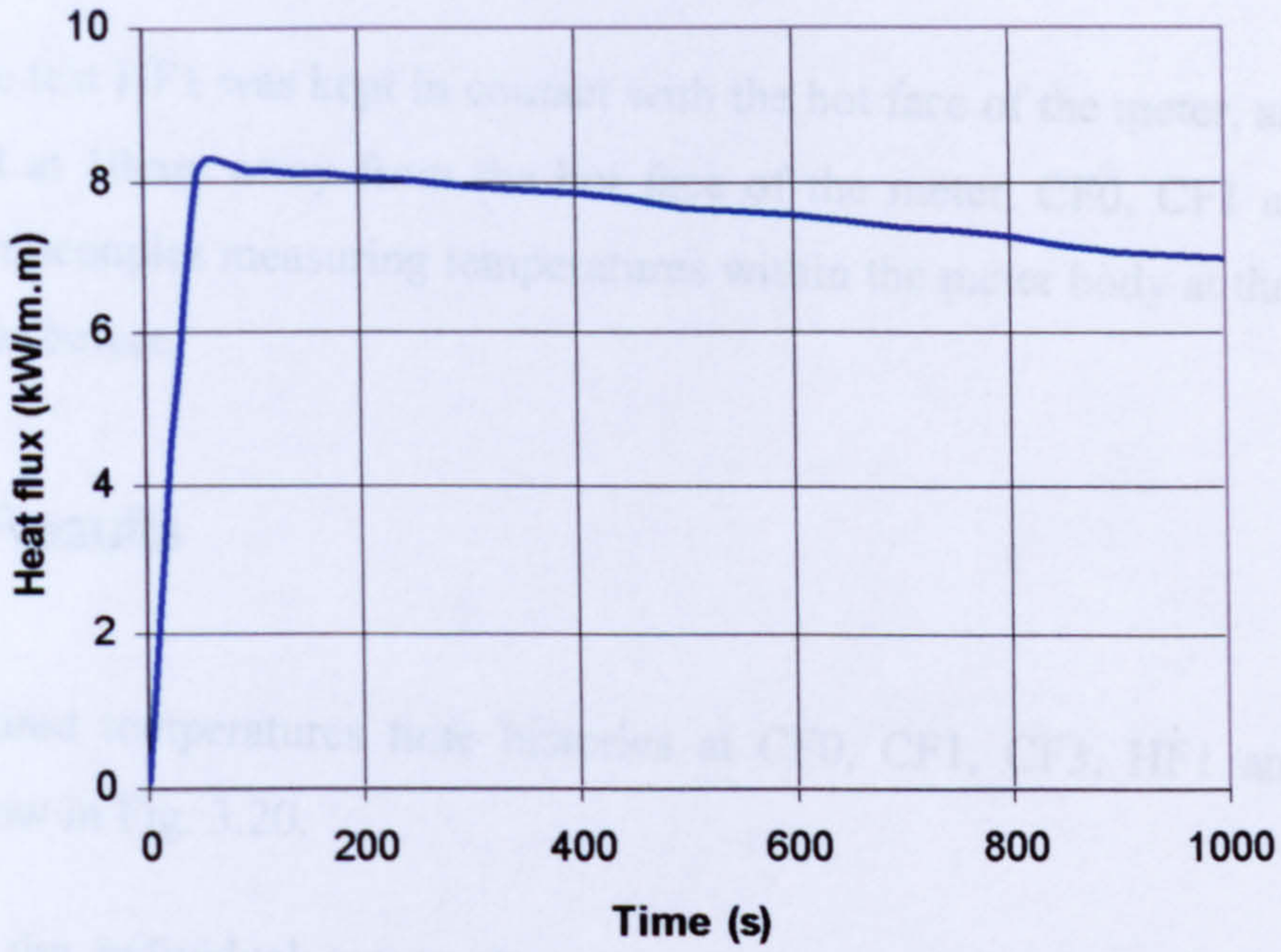

Figure 3.18 Heat flux received by the meter through convection effects.

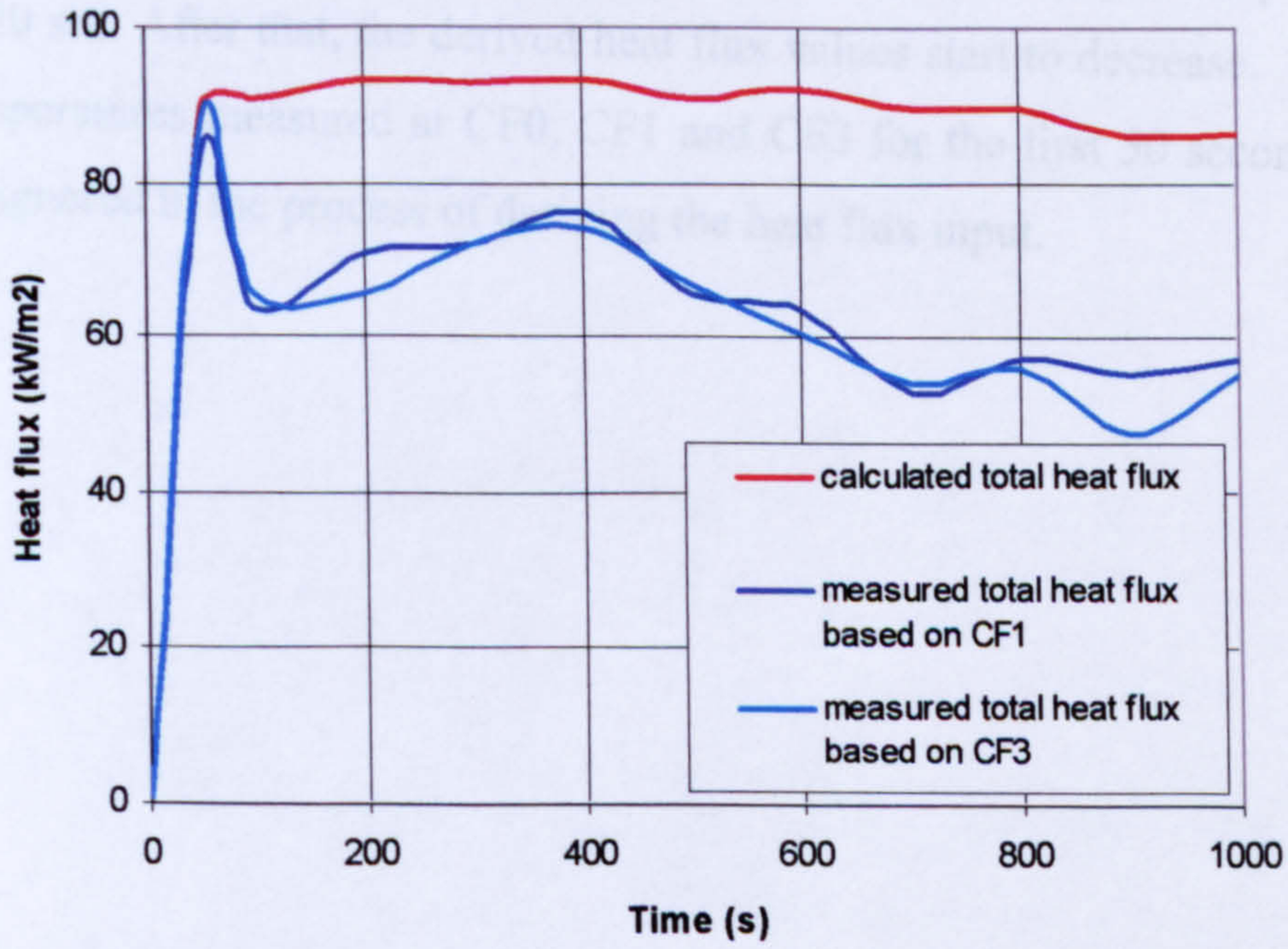

Figure 3.19 Total heat flux received by the meter.

3.4.5 Case Four

A fire test on the heat flux meter was conducted to further examine features of heat flux measurement at a lower input level: $P_r = 0.20$bar while s = 355mm.

During the test HF1 was kept in contact with the hot face of the meter, and HF2 was positioned at 10mm away from the hot face of the meter. CF0, CF1 and CF3 are three thermocouples measuring temperatures within the meter body at three different positions as before.

3.4.5.1 Results

The measured temperatures time histories at CF0, CF1, CF3, HF1 and HF2 are shown below in Fig. 3.20.

Based on the individual temperature measurements at CF0, CF1 and CF3, the derived heat flux levels are shown in Fig. 3.21. The test lasted for only six minutes. One can see clearly from Fig. 3.21 that for the given lower heat flux input ($P_r = 0.20$ bar) the derived heat flux inputs from CF0, CF1 and CF3 are kept nearly constant until $t = 320$ sec. After that, the derived heat flux values start to decrease. The data for the temperatures measured at CF0, CF1 and CF3 for the first 50 seconds or so have to be ignored in the process of deriving the heat flux input.

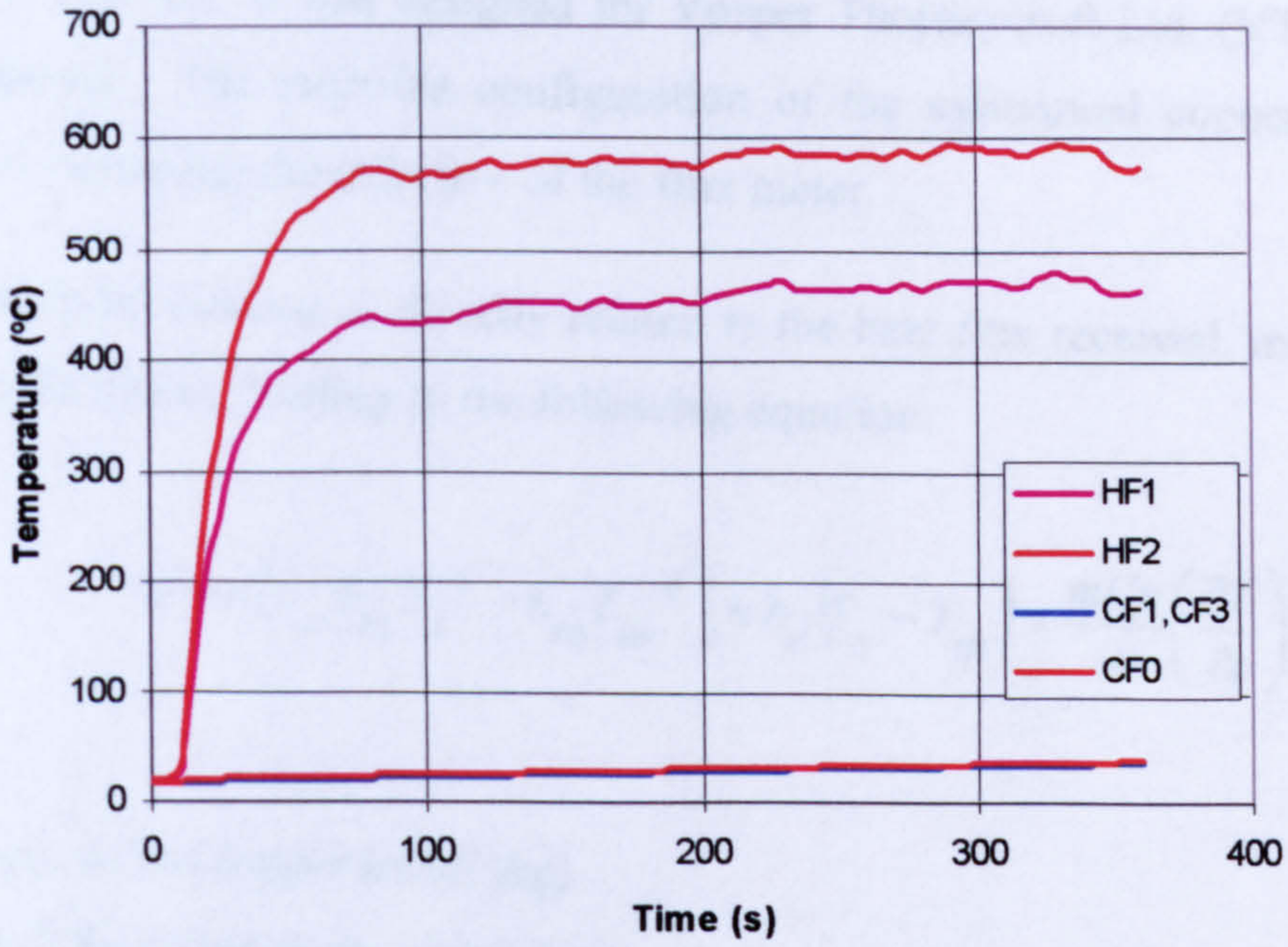

Figure 3.20 The measured temperature vs. time curves.

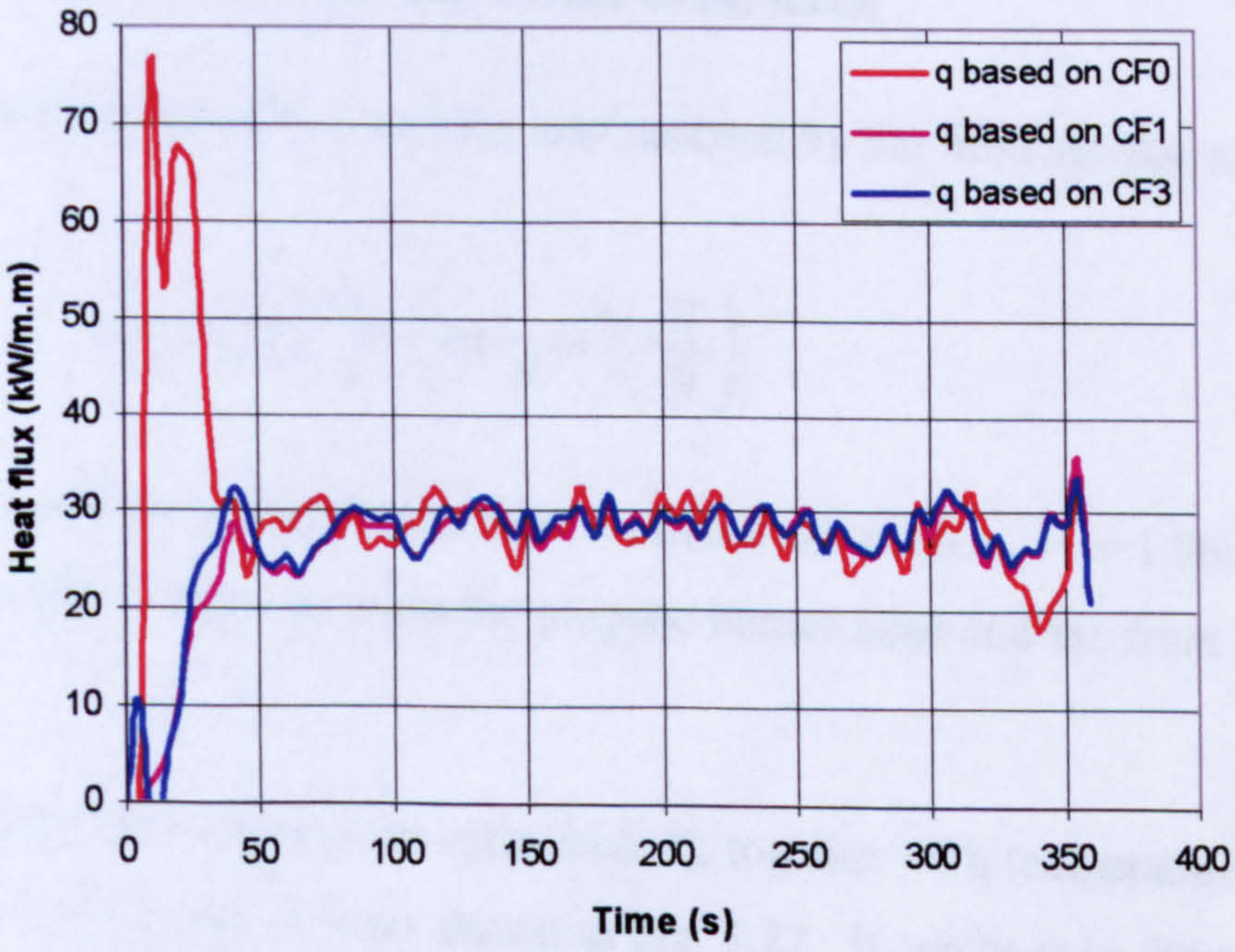

Figure 3.21 Derived heat flux levels using the meter

3.5 The Heat Flux Meter and Data Processing

The heat flux meter used in the calibration tests is the thermal capacitance type (ASTM E 456-96). It was designed for Vosper Thorneycroft Ltd. (VT) to fit with their purposes. The stepwise configuration of the cylindrical copper block was adapted to increasing the effective of the flux meter.

The temperature increase is directly related to the heat flux received, minus a small correction for losses, leading to the following equation:

$$q = \sigma\left(\varepsilon_r \alpha_m T_s^{\,4} - \varepsilon_m T_m^{\,4}\right) + h_c\left(T_s - T_m\right) = \frac{mCp}{A}\left(\frac{\partial T}{\partial t}\right) \qquad (3.10)$$

where

m = mass of the copper meter (kg)

A = front face area of the meter (m^2)

C_p = specific heat of the copper meter (J/kg/°K)

$\partial T/\partial t$ =copper meter temperature rise during the period of exposure to heat source

T_s = heat source temperature

T_m = temperature on the receiving surface of the meter

Neglecting convection effects and the heat radiated by the front surface of the meter gives:

$$\sigma\left(\varepsilon_r \alpha_m T_s^{\,4}\right) = \left(mC_p/A\right)\left(\frac{\partial T}{\partial t}\right) \qquad (3.11)$$

The following shows typical results from a calibration test (i.e., P_r = 1.0bar and D = 350mm, D is the distance between the propane burner head and the front surface of the meter).

The surrounding field temperature measured, T_s, together with temperature response profiles at TC1, TC2 and TC3 are shown in Fig. 3.22. It can be seen from Fig. 3.22 that after the initial response period (about 70 – 100 seconds long in the current case), the surrounding field temperature, T_s, becomes practically constant ($T_s \equiv$ 992°C).

In the meantime, at first examination, temperature responses at TC1, TC2 and TC3 look linear. In reality, however, this is not true.

Figure 3.23 shows the derived values of $(\partial T/\partial t)$ of the meter against time for 10 minutes. As one can see from this figure, $(\partial T/\partial t)$ declines all the time after the initial response time period (t_0 = 100s). No linear temperature response time period can be recognized during the 10 minutes long fire exposure.

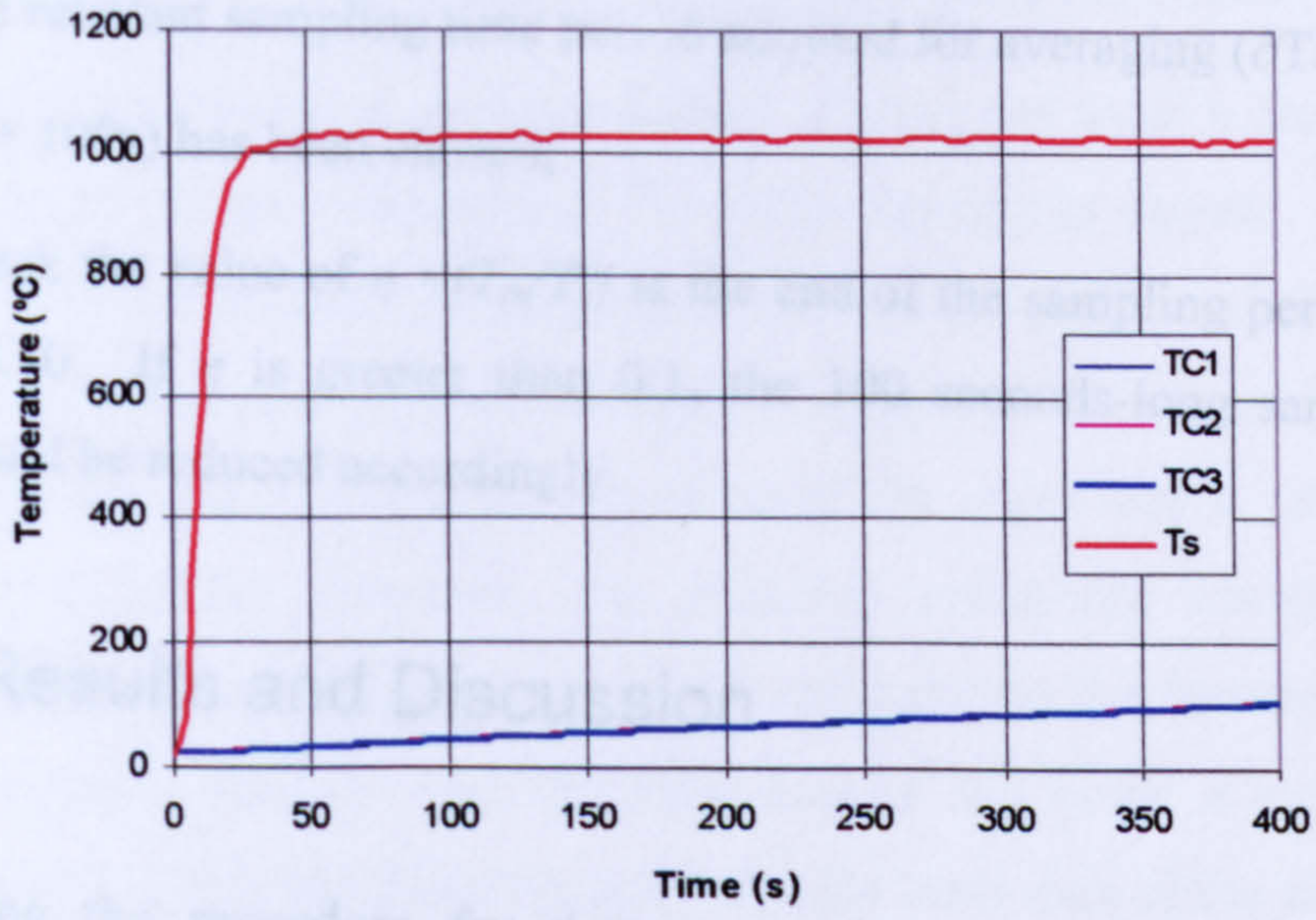

Figure 3.22 Temperature response profile of the meter (Pr = 1.0 bar, D = 35 cm).

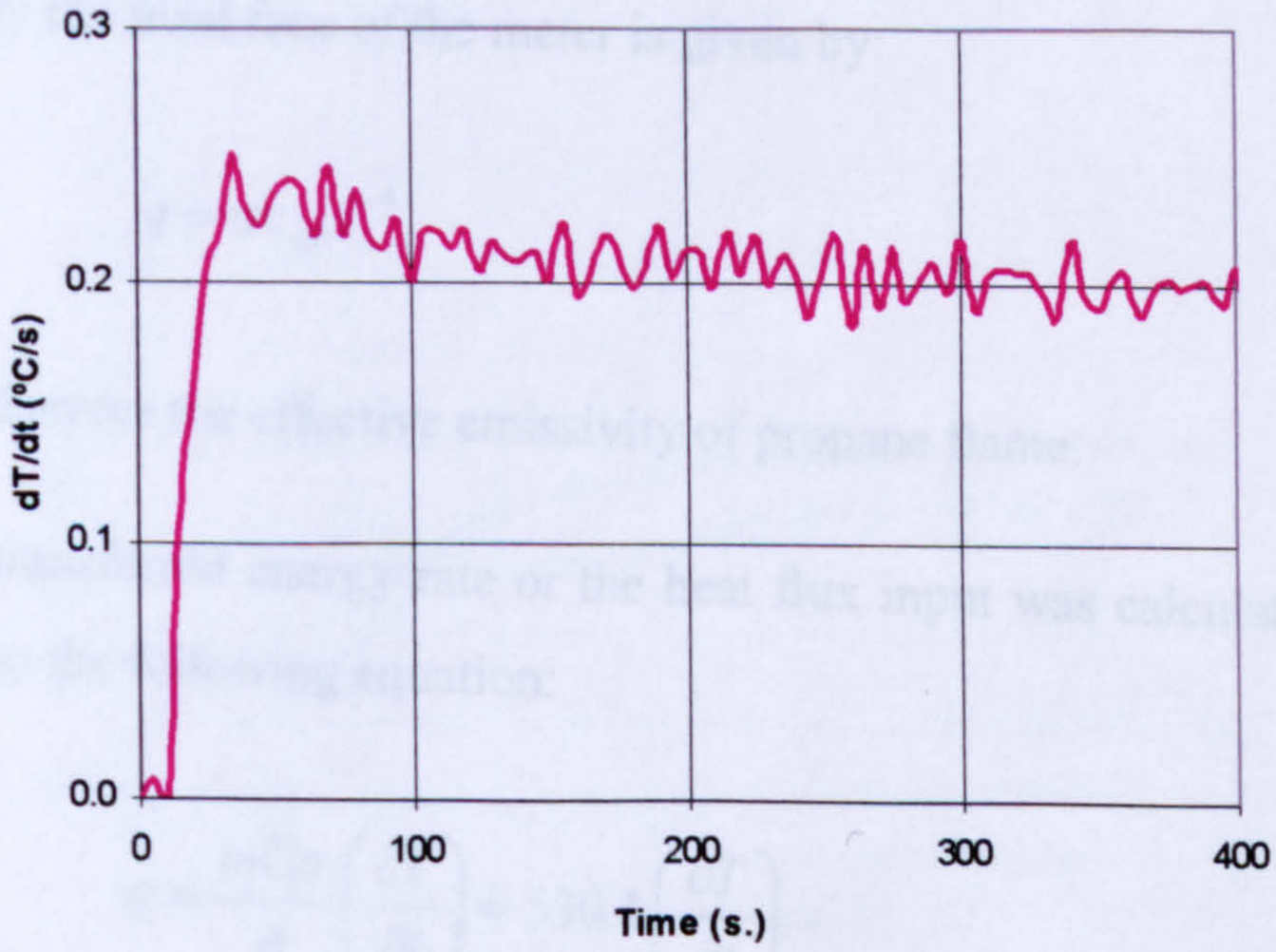

Figure 3.23 Derived values of (dT/dt) of the calibration test (Pr = 1bar, D = 350mm).

Based on the facts indicated above, in order to derive the incident heat flux input from the propane flame using the thermal capacitance type calorimeter, the following procedure was proposed and adopted in data processing:

- Based on the temperature response curve as shown in Fig. 3.22 of a calibration test, find out t_0, the initial response time period;
- To derive the heat flux received by the meter according to Eqn. (3.11).

  The relevant sampling time period adopted for averaging ($\partial T/\partial t$) from (t_0) to (t_0 + 100s) has been chosen;
- Check the value of $\eta = (T_m/T_s)$ at the end of the sampling period to ensure that $\eta \leq 0.10$. If η is greater than 0.1, the 100 seconds-long sampling time period should be reduced accordingly.

3.6. Results and Discussion

Following the procedure for data processing described above, two groups of calibration tests were conducted. The results are given below.

During the processing, it was assumed that $\alpha_m = 1.0$, so that the incident heat flux received by the front face of the meter is given by:

$$q = \sigma \varepsilon_{eff} T_s^4 \tag{3.12}$$

where ε_{eff} denotes the effective emissivity of propane flame.

Thus; the transferred energy rate or the heat flux input was calculated in each case according to the following equation:

$$q = \frac{mCp}{A}\left(\frac{\partial T}{\partial t}\right) = 530.1\left(\frac{\partial T}{\partial t}\right) \tag{3.6}$$

where:

$A = 4060.2$ (mm^2), $m = 5.605$ (kg), and $C_p = 384$ (J/kg. °C).

3.6.1. Results from Group I Tests: D ≡ 35 cm

A sequence of tests was conducted at D = 35, 30 and 25cm at different gas pressures (i.e. P_r 0.2, 0.3, 0.4, 0.5, 0.75, 1.0 and 1.25 bar). Figure 3.24 shows typical results from the test (i.e. at D = 350mm) in terms of a non-dimensional surrounding field temperature T_s, with the calibrated incident heat flux q and the effective emissivity of the propane flame as functions of pressure P_r. As can be seen from Fig. 3.24 the calculated effective emissivity, ε_{eff}, of the propane flame lies between 0.72 and 0.9.

The effective emissivity of propane flames appears not to be a monotonic function of pressure, P_r, or the temperature, T_s within the region shown. Under the given condition of D = 35 cm, starting from ε_{eff} = 0.73 at P_r = 0.4bar, the effective emissivity of the propane flame increases gradually with increasing pressure P_r, or temperature T_s,. At P_r = 1.2bar, the value of the emissivity is nearly 0.9. For P_r smaller than 0.4bar, however, the effective emissivity increases again with decreasing pressure P_r. This trend may be attributed to the fact that at D = 350mm, when P_r is lower than 0.4 bar, the front face of the meter is out of reach of the propane flame. Once the flame cannot reach the front face of the meter, there would be no forced convection effects during the heat exchange. As a result, heat transfer is achieved purely through heat radiation from the propane flame, leading to an increase in effective emissivity of the heating source.

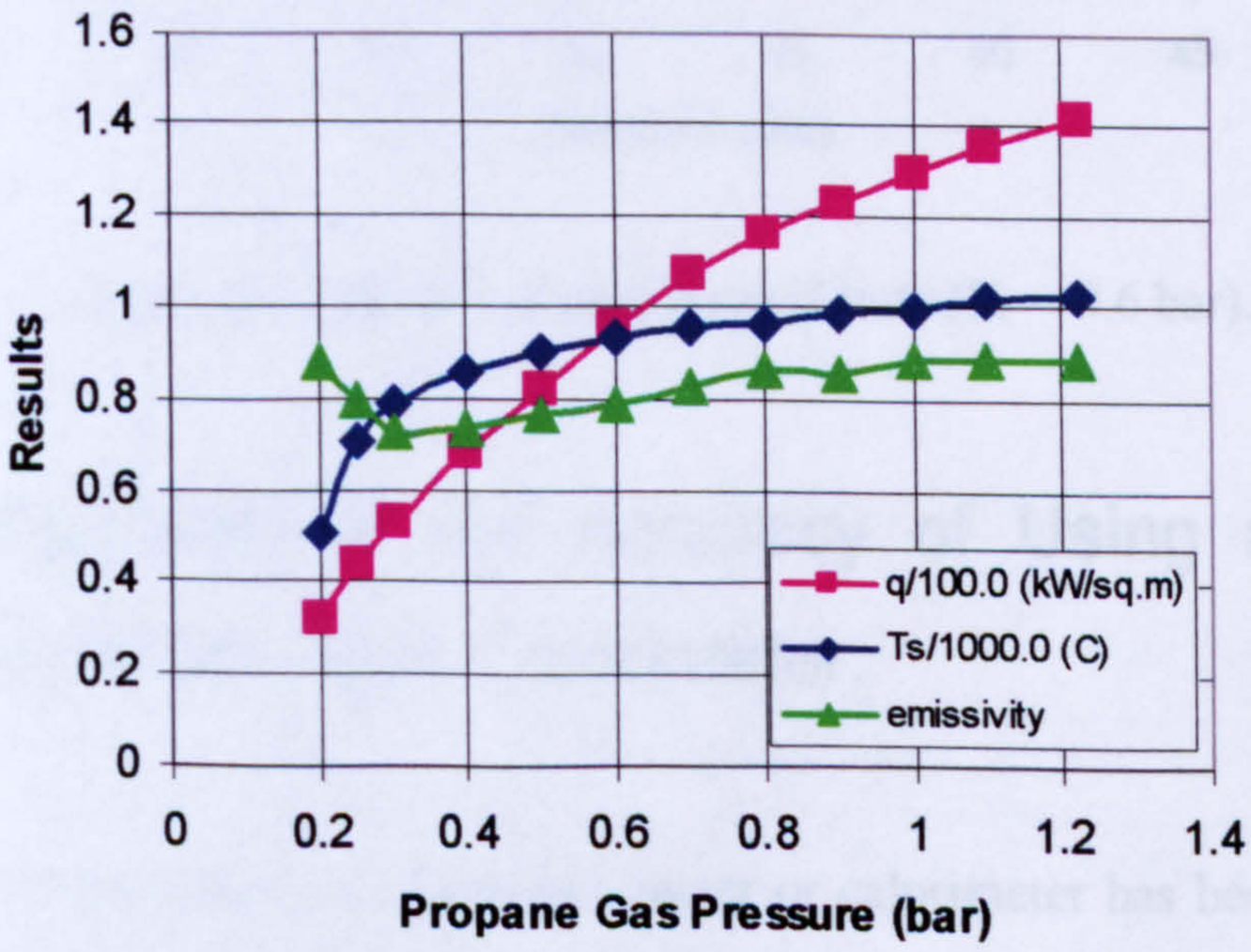

Figure 3.24 Results from Group I tests: D = 350mm.

3.6.2. Results From Group II Tests: Pr ≡ 0.6 bar

Group II tests were conducted at $P_r \equiv 0.6$ bar with different distances D between the propane burner head and the front face of the meter. The relevant results are shown in Fig. 3.25.

Once again, one can see from Fig. 3.25 that the effective emissivity is a complex function of temperature T_s. For distances of D smaller than 350mm, the effective emissivity of the flame is about 0.82, and once D is greater than 350~400mm, the emissivity increases gradually and obviously with increasing distance.

The results indicate that the exclusion of forced convection effects would lead to an increase in the effective emissivity of the propane flame.

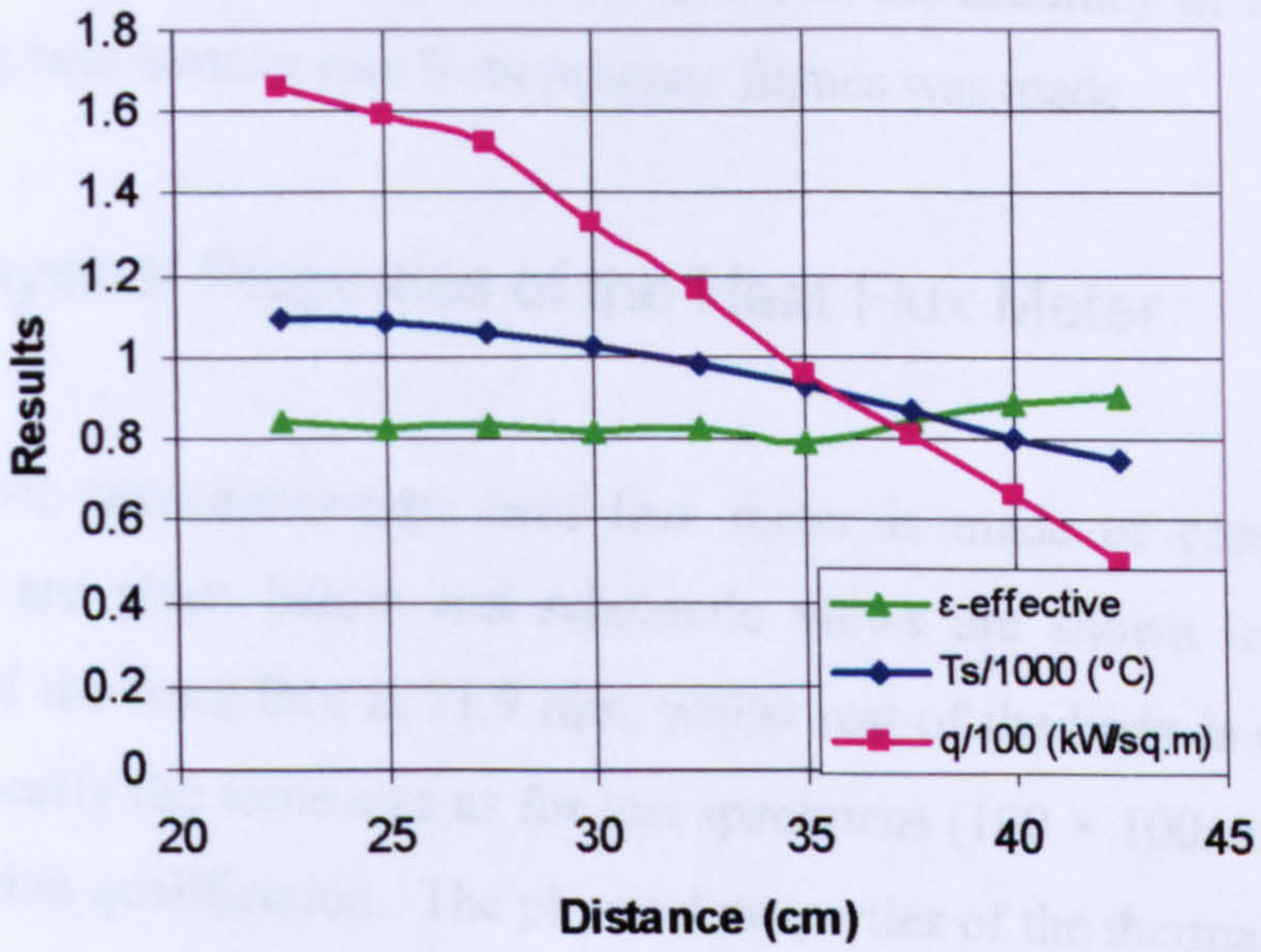

Figure 3.25 Results from Group II tests (Pr = 0.6 bar).

3.7 Assessment of the Accuracy of Using a Thermal Capacitance Type Calorimeter.

The thermal capacitance-type heat flux meter or calorimeter has been used indoors for measurements of the incident heat flux from propane flames. Also it is used for measurements of heat flux transferred from the back face of a composite laminate

during a fire test. As suggested in ASTM (Designation:E 457-96, 1996) when such a meter is exposed to a steady-state heating source with its front face, a linear temperature response of the meter is expected after a short time period of initial transient temperature response, and the relevant heat transfer rate is to be determined simply by the slope (linear portion) of the temperature-time curve and the physical properties of the meter.

The purpose of this experimental study was to examine and assess the accuracy of using this particular heat flux meter for measurements of heat transfer rates from propane flames. To achieve this, two natural cool-down tests were conducted with the meter under two different conditions. The heat transfer coefficient and emissivity of the front face of the meter at elevated temperature (60°C–140°C) were then derived according to Newton's Law of Cooling and the Stefan-Boltzmann law of thermal radiation. Finally an assessment of the accuracy of using the meter for calibrating heat transfer rate from propane flames was made.

3.7.1 Physical Properties of the Heat Flux Meter

The thermal capacitance-type heat flux meter is made of copper. Its physical properties are given below and schematic views are shown in Fig. 3.26. The diameter of the front face is 71.9 mm, whilst rest of the body is of the diameter of 99.5mm, nearly the same size as for test specimens (100 × 100mm) to be tested for fire protection qualification. The physical properties of the thermal capacitance-type heat flux meter are described in Table 3.1 as follows:

Table 3.1 Physical properties of the thermal capacitance-type heat flux meter

d	71.9 (mm)	C_p	384 (J/kg.°C)
D	99.5 (mm)	A_1 (front face area)	4060.2 (mm^2)
L_1	20.3 (mm)	A (total surface area)	41986.6(mm^2)
L_2	69.9 (mm)	V (total volume)	625959 (mm^3)
ρ	8954 (kg/m^3)		

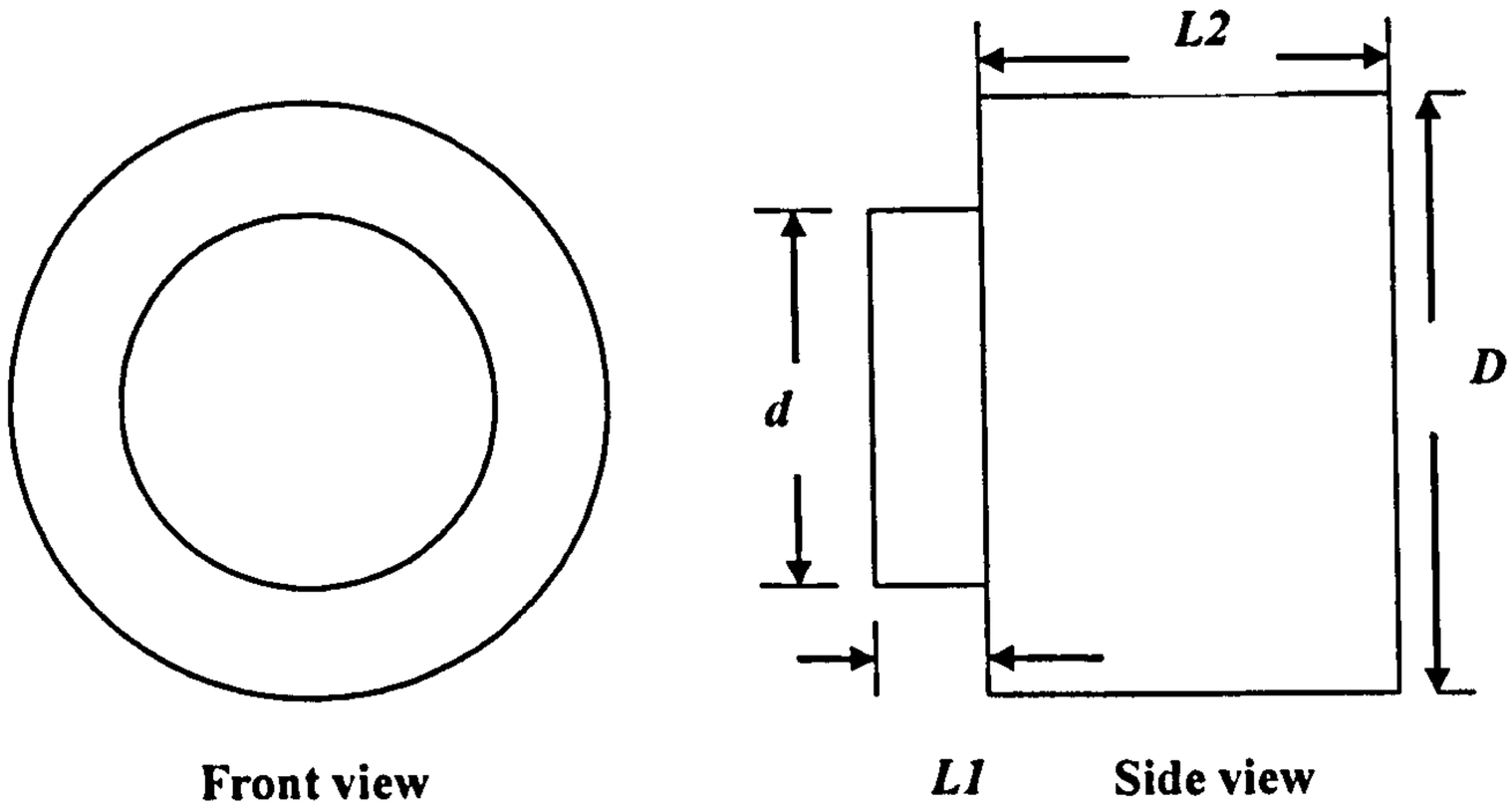

Figure 3.26 Heat flux meter used in the tests

3.7.2 Test Conditions

The expected linear temperature response of the meter when exposed with its front face to a steady-state heating source adopted from ASTM E 457-96 is actually based on the following two assumptions:

(A) Energy losses due to heat conduction through insulation layers of the meter are minimized and can be ignored;

(B) Energy losses due to heat radiation from the front face of the meter to the surrounding during measurements can be ignored in comparison with incident steady-state thermal energy input.

In the temperature vs. time curves of the meter recorded from a calibration test of propane flame (i.e. Fig. 3.22), T_s represents temperatures as a function of time measured at 10mm away and in front of the exposed surface of the meter in the calibration test (P_r = 1.0 bar, D = 350mm). It appears that in less than 100 seconds, the heating source became steady-state and, after that initial transient response period, all temperature responses of the meter body (from thermocouples TC1, TC2 and TC3) look linear. When the derived slope of the averaged temperature response curves is plotted out in Fig. 3.23, it becomes clear that the slope is not constant. The results indicated that, unlike the suggestion given in ASTM (Designation:E 457–96, 1996), the actual temperature response of the meter in this case can hardly be treated

as linear. Therefore, the two assumptions mentioned above have to be carefully re-examined in respect of this particular heat flux meter. To do so, the heat transfer coefficient of the meter in relation to assumption (A) and the emissivity of the front face of the meter in relation to assumption (B) have to be measured or derived.

When the front face of the meter is free from insulation, whilst the rest part of the surface is insulated by a vermiculate frame and Kaowool layers, the status of the meter is referred to as under the insulation condition (I) as schematically shown in Fig. 3.27a. In Fig. 3.27a, TC1, TC2 and TC3 denote three thermocouples installed inside the copper block: the tips of TC1 and TC3 are positioned 3mm from the back face of the meter, whilst the tip of TC2 is 30mm from the back face.

In addition to the thermal insulation imposed on the meter under condition (I), the front face of the meter is covered by a thick layer of Kaowool as schematically shown in Fig. 3.27b. Such a status of the meter is referred to as under insulation condition (II). Here, three thermocouples (i.e. TC1, TC2 and TC3) are located at the same positions as under condition (I).

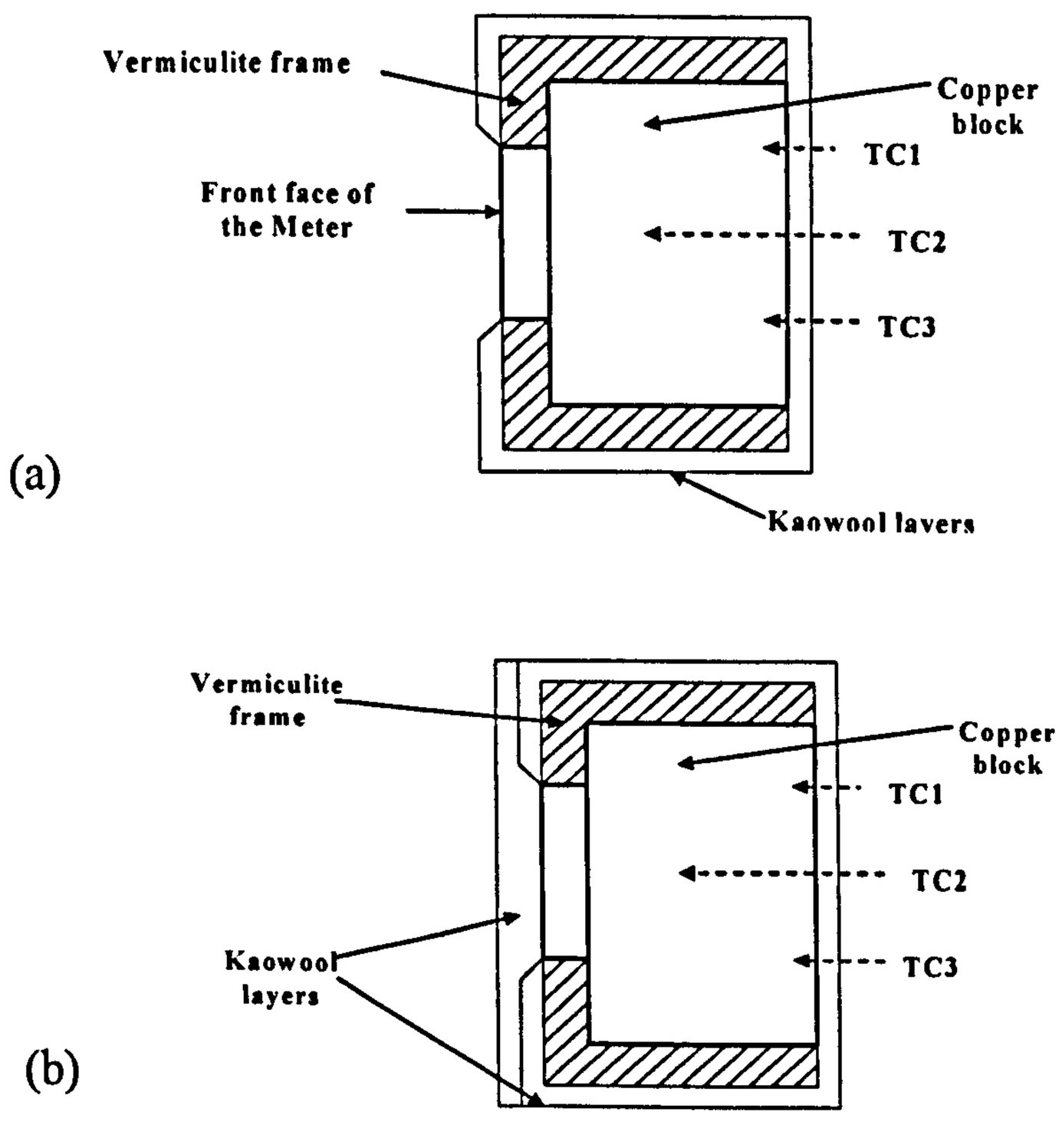

Figure 3.27 Schematic diagram of the meter rig for a) condition I, b) condition II.

3.7.3 Cooling-Down Test of the Meter under Testing Condition II

The meter with its front face exposed to a propane flame was first heated up to a temperature over 100°C and then naturally cooled down under testing condition (II) (i.e., front face insulated). During the course of the test the initial room temperature was 17.5°C. The measured cooling-down curve of the meter is shown in Fig. 3.28. It took more than three and half hours to get the meter body temperature from 104°C down to 75°C.

According to Newton's Law of Cooling, the total energy loss from the meter body under insulation condition (II) due to heat conduction through the insulation layers to the surrounding fluid (or air) at room temperature T_{room} with the meter's total surface area of A and body temperature of T_b, is given by

$$Q = hA\left(T_b(t) - T_{room}\right) \tag{3.13}$$

where h is the heat transfer coefficient under Testing condition (II). By considering thermal energy balance, the total energy loss to the surroundings, Q, is equal to the energy loss of the meter body:

$$Q = V\rho C_p \frac{\partial T_b(t)}{\partial t} \tag{3.14}$$

where V denotes total volume of the meter body.

Combining the two equations (3.13) and (3.14) leads to:

$$h = \left(\frac{V}{A}\right)\rho C_p \frac{\partial T_b}{\partial t}\left(T_b - T_{room}\right)^{-1} \tag{3.15}$$

Based on Eqn. (3.15) and the experimental data shown in Fig. 3.28, the derived heat transfer coefficients of the meter under condition (II), h, as a function of body temperature of the meter, T_b, are shown in Fig. 3.29. It can be seen from Fig. 3.29 that the derived values of the heat transfer coefficient of the meter under testing

condition (II) are nearly constant in the temperature range between 75°C and 105°C, with its averaged value being equal to 1.63 (W/m^2.°C).

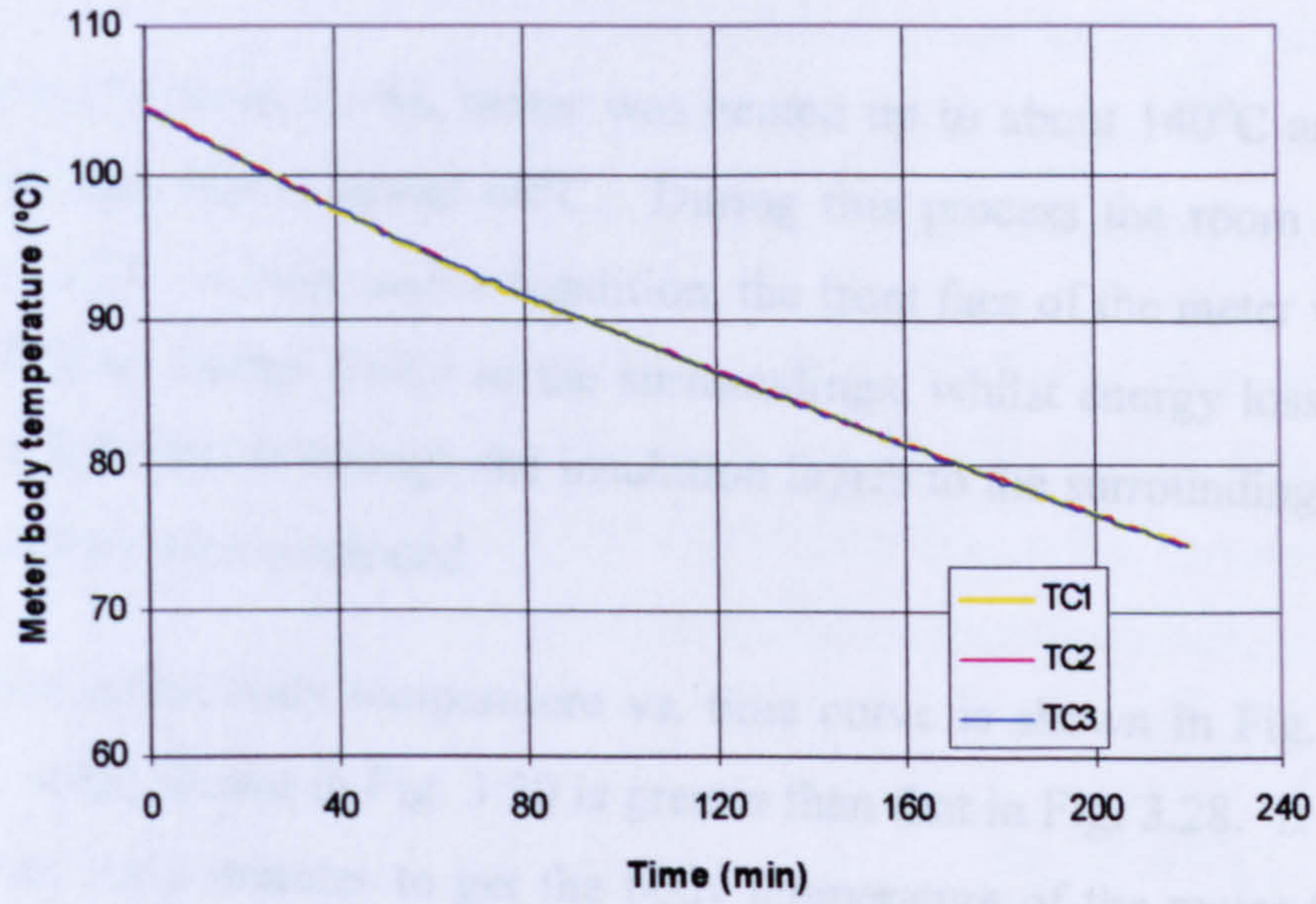

Figure 3.28 Cooling-down curve of the meter under testing condition II

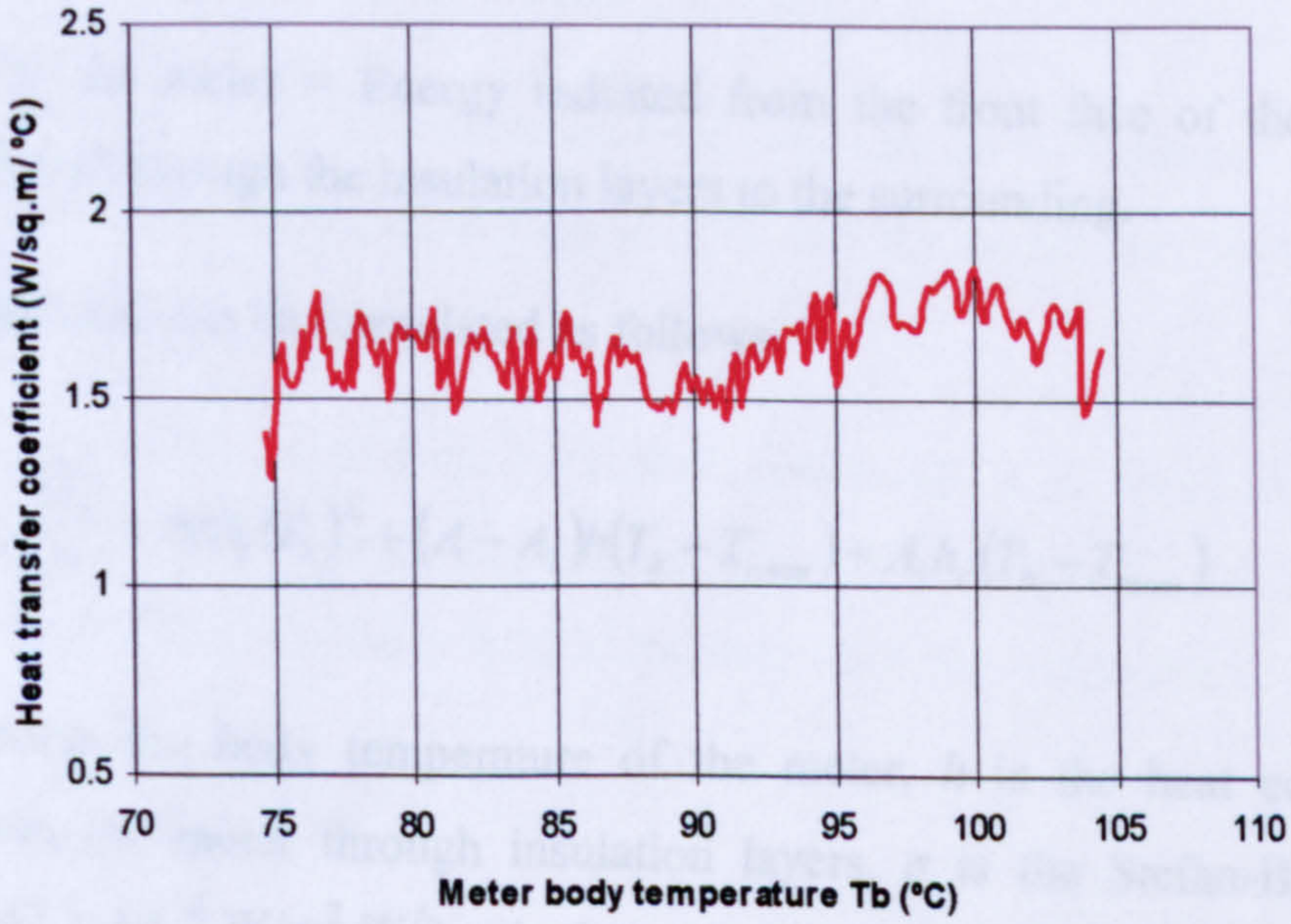

Figure 3.29 Derived values of heat transfer coefficient, h (W/m^2. °C)

3.7.4 Cooling-Down Test of the Meter under Testing Condition I

The second cooling-down test was carried out with the meter in order to derive the emissivity of the front face of the meter.

Under testing condition (I) the meter was heated up to about 140°C and then was cooled down naturally to about 60°C. During this process the room temperature recorded was 20°C. Under such a condition, the front face of the meter was allowed to radiate thermal energy freely to the surroundings, whilst energy losses from the meter due to conduction through the insulation layers to the surroundings of the rest of its total surface area continued.

The measured meter body temperature vs. time curve is shown in Fig. 3.30. The temperature range shown in Fig. 3.30 is greater than that in Fig. 3.28. It took nearly five hours and forty minutes to get the body temperature of the meter from 140°C down to 57°C.

Under the given condition, the thermal energy balance of the meter can be stated as follows;

Energy lost by the meter = Energy radiated from the front face of the meter + Energy transferred through the insulation layers to the surrounding.

The above statement can be formulated as follows:

$$V\rho C_p \frac{\partial T_b}{\partial t} = \sigma\varepsilon A_1 (T_b)^4 + (A - A_1)h(T_b - T_{room}) + A_1 h_c (T_b - T_{room}) \qquad (3.16)$$

where T_b denotes the body temperature of the meter, h is the heat convection coefficient from the meter through insulation layers, σ is the Stefan-Boltzmann constant (= 5.67×10^{-8} W/m^2 °K^4), ε is the emissivity of the front face of the meter and hc is the heat coefficient from the front face of the meter during the cooling-down test.

Once heat transfer coefficients h and h_c are known, one can derive the emissivity ε of the front face of the meter easily from Eqn. (3.16):

$$\varepsilon = \frac{1}{A_1 \sigma (T_b)^4}\left[V\rho C_p \frac{\partial T_b}{\partial t} - (A - A_1)h(T_b - T_{room}) - A_1 h_c (T_b - T_{room})\right] \qquad (3.17)$$

Based on the results given in the previous section, it is assumed in this study for simplicity that $h \equiv 2.0$ (W/m^2.C) within the temperature range of concern.

Estimation of the heat convection coefficient from the front face of the meter during the cool-down test, h_c, may be achieved by using an approximate equation.

As suggested by Eastop and McConkey, (1978) for natural convection from a vertical surface like the front face of the meter in this cooling-down test, it is reasonable to assume the air flow or circulation over the surface remaining laminar. The following equation can then be used for the estimation of the heat coefficient:

$$h_c = 1.42\left[\frac{(T_b - T_{room})}{l}\right]^{1/4} \qquad \text{(in: W/m}^2\,^{\circ}\text{C)} \qquad (3.18)$$

where l (in: m) denotes the characteristic length of the heat transfer problem. Under the present cases it may be selected as the typical height of the front face of the meter from the ground floor during the test (l = 1.0m).

Having adopted Eqn. (3.18) for evaluation of h_c, one can derive values of emissivity of the front face of the meter from Eqn. (3.17), and the results are shown in Fig. 3.31.

It can clearly be seen from Fig. 3.31 that emissivity is a function of body temperature. In the body temperature range from 60°C to 140°C, the emissivity increases from about 0.42 to nearly 0.70 as increase the body temperature.

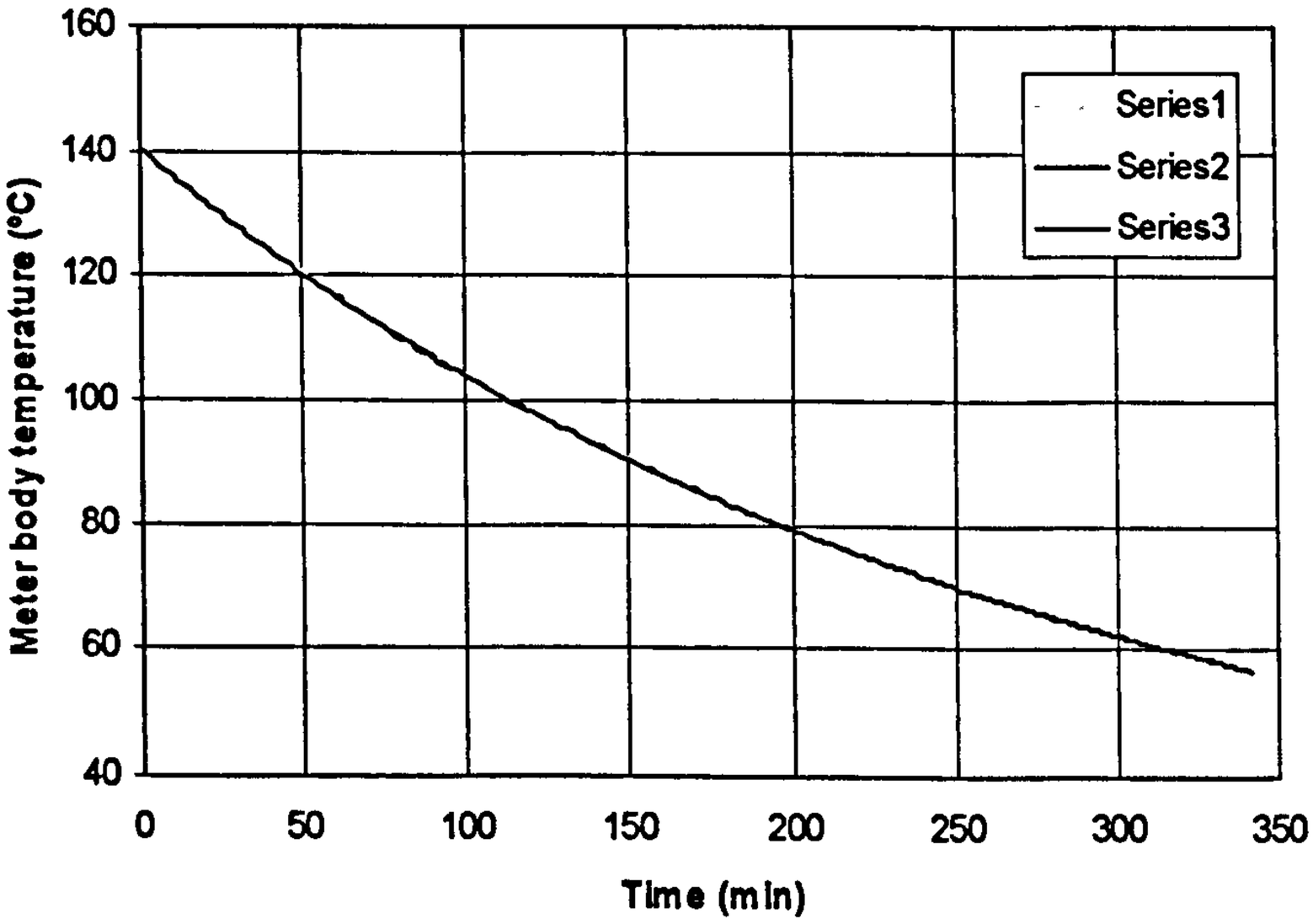

Figure 3.30 Cooling-down curve of the meter under testing condition (I).

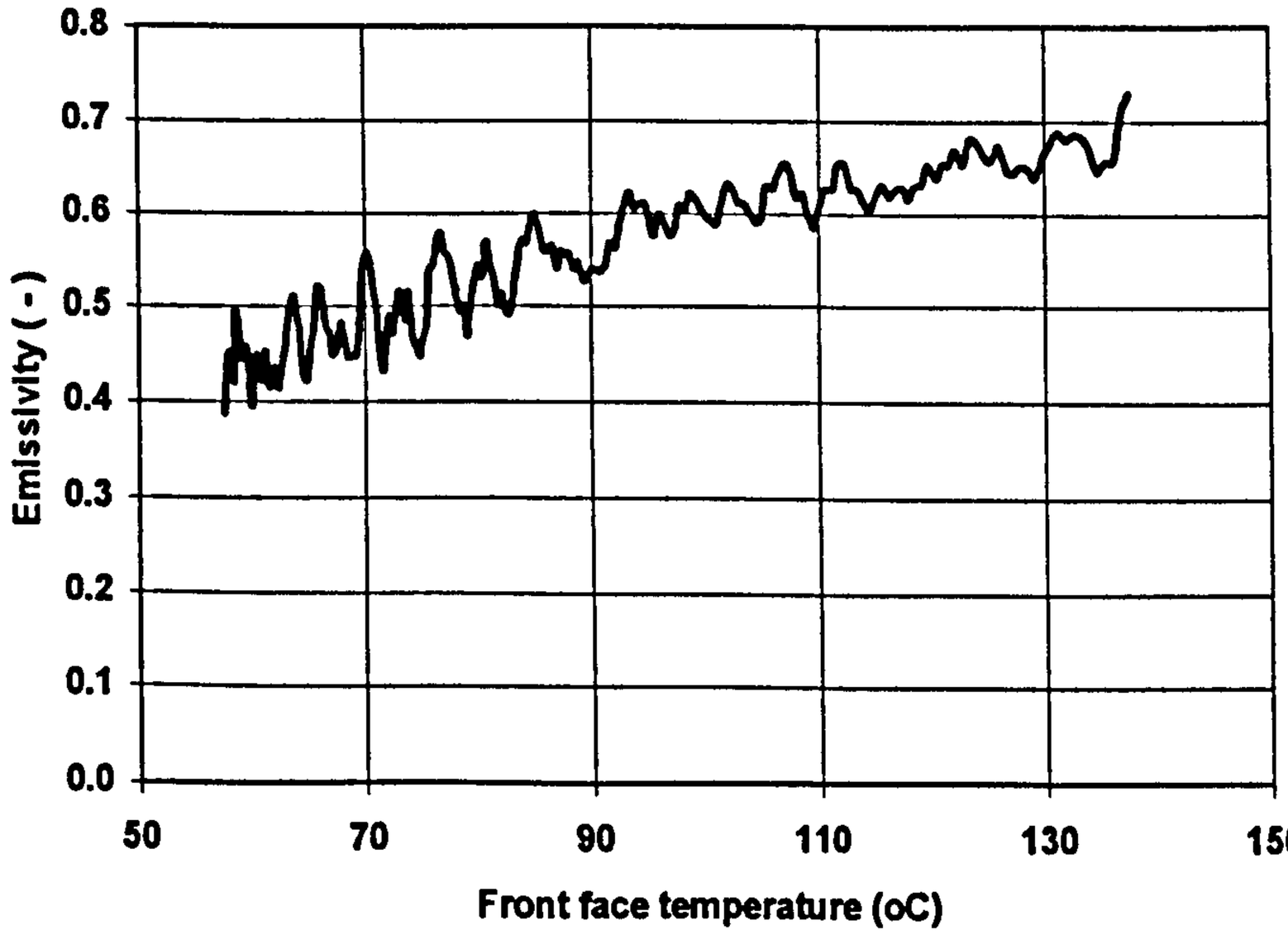

Figure 3.31 Derived emissivity of the meter

3.8 Assessment of the Accuracy of the Calibration Tests Using the Meter

The thermal capacitance-type calorimeter or heat flux meter has been used for calibrating incident steady-state heat transfer rates from propane flames. As stated in ASTM E 457-96, a linear temperature response of the meter is expected upon consideration of thermal energy balance. The incident steady-state heat transfer rate is then calculated straightforward from the measured slope of the linear temperature response of the meter.

In reality, as mentioned above, consideration of the thermal energy balance of the meter in a calibration test would lead to:

$$V\rho C_p \frac{\partial T_b}{\partial t} = \sigma\left(\varepsilon_f \alpha T_s^4 - \varepsilon T_b^4\right)A_1 - h\left(T_b - T_{room}\right)\left(A - A_1\right) \quad (3.19)$$

where

T_b = body temperature of the meter;

T_{room} = room temperature;

T_s = surrounding field temperature;

ε_f = efficient emissivity of propane flame;

ε = emissivity of the front face of the meter;

α = absorptivity of the front face of the meter;

h = heat transfer coefficient of the meter through insulation layers ($W/m^2\ ^oC$).

It can be seen from Eqn. (3.19) that only when thermal energy losses due to both heat conduction through the insulation layers and heat radiation from the front face of the meter to the surrounding are negligible, would a linear temperature response of the meter would be expected for a steady-state incident thermal energy input. Based on the derived values of h and ε, the accuracy of using the meter for calibration of a steady-state incident heat transfer rate can be assessed:

$$\left[\frac{\left(V\rho C_p \frac{\partial T_b}{\partial t}\right)_{actual}}{\left(V\rho C_p \frac{\partial T_b}{\partial t}\right)_{ideal}}\right] = \frac{\sigma A_1\left(\varepsilon_f \alpha T_s^{\,4} - \varepsilon T_b^{\,4}\right) - h\left(A - A_1\right)\left(T_b - T_{room}\right)}{\sigma A_1 \varepsilon_f \alpha T_s^{\,4}} = \xi \quad (3.20)$$

The upper term in the left hand of the above equation denotes the energy transfer rate actually received for raising the body temperature of the meter only, whilst the lower term of the left hand of the equation denotes the incident energy transfer rate from the steady-state heat radiation source. ξ may be regarded as an accuracy coefficient.

During the course of a calibration test on propane flames for a given distance D and pressure P_r, the surrounding field temperature T_{sK} can soon reach a constant level, but the body temperature of the meter would rise very gently all the time. This is the reason why the initial temperature response of the meter in a calibration test is not linear.

Equation (3.20) can be reduced to a simpler form. According to Kirchhoff's Law of Thermal Radiation, the emissivity of a body radiating energy at a temperature, T, is equal to the absorptivity of the body when receiving energy from a source at a temperature, T (Eastop and McConkey, 1978). Therefore, $\varepsilon=\alpha$ for the meter at any temperature and so equation (3.20) can be re-written as:

$$\xi = \left[1 - \frac{1}{\varepsilon_f}\left(\frac{T_b}{T_s}\right)^4\right] - \frac{h\left(T_b - T_{room}\right)}{\sigma\varepsilon_f \varepsilon T_s^{\,4}}\left(\frac{A}{A_1} - 1\right) \quad (3.21)$$

Estimation of accuracy coefficient, ξ, in three cases of calibration tests are given below as examples.

(1) Case I: (D = 250mm, releasing pressure of the burner P_r = 1.0bar; T_s = 1268°K; $T_{b\,\max}$ = 62.3 °C; T_{room} = 20.0°C; ε_f = 0.89; ε = 0.45 and h = 2.0 (W/m^2 °C)).

Substitution of the above data into Eqn. (3.21) leads to: $\xi = 0.981$.

(2) Case II (distance D = 400mm, releasing pressure of the burner P_r = 0.6 bar):

T_s = 1070.6°K; $T_{b\ max}$ = 58.0°C; T_{room} = 20.0°C; ε_f = 0.89; ε = 0.42 and h =2.0 (W/m^2 °C).

Substitution of the above data into Eqn. (3.21) leads to: ξ = 0.964

(3) Case III (distance D = 350mm, releasing pressure of the burner P_r = 0.30 bar):

T_s = 1061.5°K; $T_{b\ max}$ = 48.4°C; T_{room} = 20.0°C; ε_f = 0.73; ε = 0.40 and h = 2.0 (W/m^2 °C).

Substitution of the above data into Eqn. (3.21) leads to: ξ = 0.963.

3.9 Conclusions

- The small propane burner can be used to provide a constant heat flux input of up to 150kW/m^2 for the fire testing of composite laminates in a laboratory.
- For heat transfer from the propane flame to the receiving surface of the material being tested, although thermal radiation is the main mechanism, forced thermal convection effects may also be involved, depending on: the distance between the burner head and the front face of the material being tested; and the pressure at which the propane gas is released.
- Propane flames are selective emitters. The effective emissivity ε_{eff}, is a complex function of the 'surrounding field temperature', T_s, which is the temperature measured at a position about 10mm away from the receiving surface.
- Having adopted the 'surrounding field temperature', T_s, the Stefan-Boltzmann law can still be applied for describing the heat flux from propane flames: $q = \sigma \varepsilon_{eff} T_s^4$.
- It was found in this study that propane flames have an effective emissivity between 0.73 and 0.88 under the given environmental conditions in the lab. This finding is nearly the same as those reported in Perry & Chilton (1973) and Buchanan (2001).
- The results from cooling down tests have proven that the use of such thermal capacitance-type meters in calibrating incident heat transfer rate from propane

flames can produce accurate enough measurements with an estimated error of not more than 5%.

- The averaged heat transfer coefficient due to conduction from the meter through the insulation layers to the surroundings under testing condition I is about 2.0W/m^2 °C in the temperature range from 60°C to 100°C, and the derived emissivity of the front face of the meter is a function of body temperature. Its value increases gradually with increasing body temperature from: ε = 0.42 at body temperature = 60°C, to ε = 0.70 at body temperature = 140°C.
- Based on the quantitative results from the two cooling-down tests with the meter, the estimated error of using the thermal capacitance-type meter for calibration of incident steady-state heat transfer rates from propane flames is less then 5%.
- The surface condition of the front face of the meter may be come oxidised and also some products generated from the decomposition reactions of GRP laminates to different types of resin system may become attached.
- It is suggested from this experimental study that the thermal capacitance–type meter should be used for measurements of any heat flux input with the body temperature of the meter rising to not more then 70°C in order to ensure the accuracy of the testing method.

CHAPTER 4

MEASUREMENT OF THERMAL CONDUCTIVITY OF DRY FIBRE-MATS AT HIGH TEMPERATURE

4.1 Introduction

The mechanical strength of composite materials during a fire is strongly dependent on temperature, decreasing rapidly once temperature exceeds the glass transition temperature of the matrix material (Ott, 1981). As a result, accurately modelling the heat transfer through a composite is a critical part of conducting a structural analysis on the composite when exposed to fire.

One of the major difficulties encountered in modelling the thermal response of GFP composites in fire is the lack of material property values at high temperatures. In general, when a composite is exposed to fire, its density, thermal conductivity and specific heat change. This is attributed not only to the changes in composition contents of the composite due to decomposition, but also to changes in the material properties of the matrix and reinforcement materials them selves with increasing temperature at high temperatures.

The Rule of Mixture has been used to derive the thermal properties of composites at room temperatures when they can be treated as a solid material or a continuum. During fire exposure the composite will become a skeleton that is a new composite material consisting of three elements: (A) the reinforcement fibres, (B) the resin undergoing decomposition, and (C) a void filled with air and gases. The Rule of Mixture may be adopted again for deriving the thermal properties of the composites at high temperature. But, investigations have indicated that the application of the Rule is in particular not accurate for the evaluation of thermal conductivity of FRP composites.

A simple transient response method is introduced in this chapter for measuring the thermal conductivity of dry fibre-mats at high temperature using the small scale fire testing facility. The experimental results are then compared to (1) those derived from

the Rule of Mixture, and (2) those obtained from the literature. Having indicated its restrictions, it is concluded from the investigation that the method is a useful and reliable means for measuring the thermal properties of dry fibre-mats.

4.2 The Transient Response Method

Consider a set of dry E-glass fibre sheets (WR) forming a dry fibre mat, as schematically shown below in Fig 4.1.

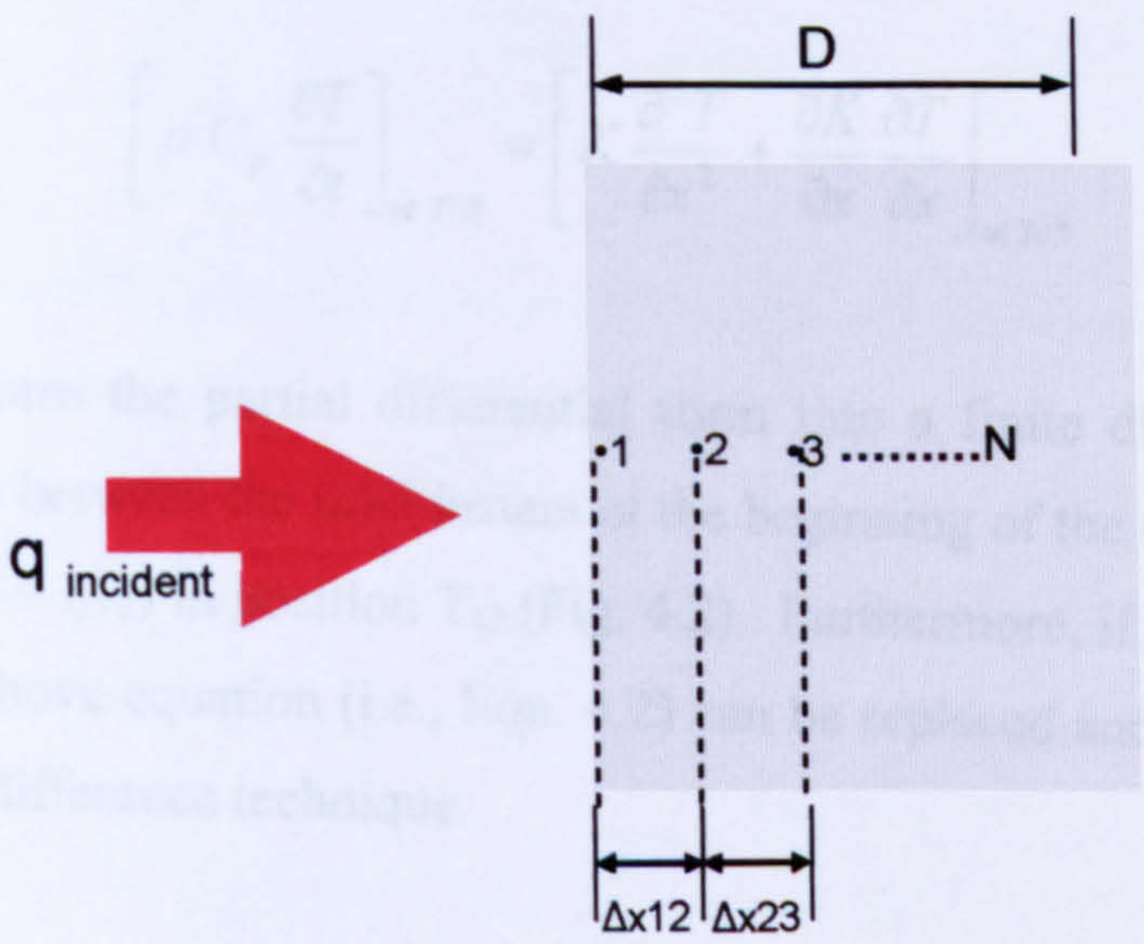

Figure 4.1 Dry fibre-mats

The mat is exposed to a fire or an incident heat flux (q) at its front side. It is assumed that the heat transfer inside the mat can be treated as a one-dimensional problem.

In assembling the fibre-mat, a number of thermocouples are inserted into the sheets, where the distances between the adjacent two thermocouples are Δx_{12}, Δx_{23}, Δx_{34}...$x_{i\ i+1}$.

It is assumed that the mat can be regarded as a uniform composite consisting of dry fibre and air in the through-thickness direction with density ρ and known specific heat Cp.

Based on the above assumptions, the 1D transient heat transfer equation can be given as follows:

$$\rho C_p \frac{\partial T}{\partial t} = \frac{\partial}{\partial x}\left(K \frac{\partial T}{\partial x} \right) \tag{4.1}$$

where: ρ (kg/m^3), C_p (J/kg °K) and K (W/m °K), are the density of the mat, the specific heat of the mat and the thermal conductivity of the mat, respectively. $T(x, t)$ is the temperature (°C) as function of (x) in through thickness and time (t).

Suppose that three thermocouples (i.e., T_{c1}, T_{c2} and T_{c3}) are inserted into the mat and $\Delta x_{12} = \Delta x_{23} = \Delta x$. Equation (4.1) is held at T_{c2}, and can be written as:

$$\left[\rho C_p \frac{\partial T}{\partial t} \right]_{at\ Tc2} = \left[K \frac{\partial^2 T}{\partial x^2} + \frac{\partial K}{\partial x} \frac{\partial T}{\partial x} \right]_{at\ Tc2} \tag{4.2}$$

To transform the partial differential form into a finite difference form, consider a small step between the time instant at the beginning of the step $t = t_j$ and at the end of the step ($t = t_{j+1}$) in position T_{c2} (Fig. 4.2). Furthermore, if (Δx) is also small enough, then the above equation (i.e., Eqn. 4.2) can be replaced and solved numerically using the finite difference technique.

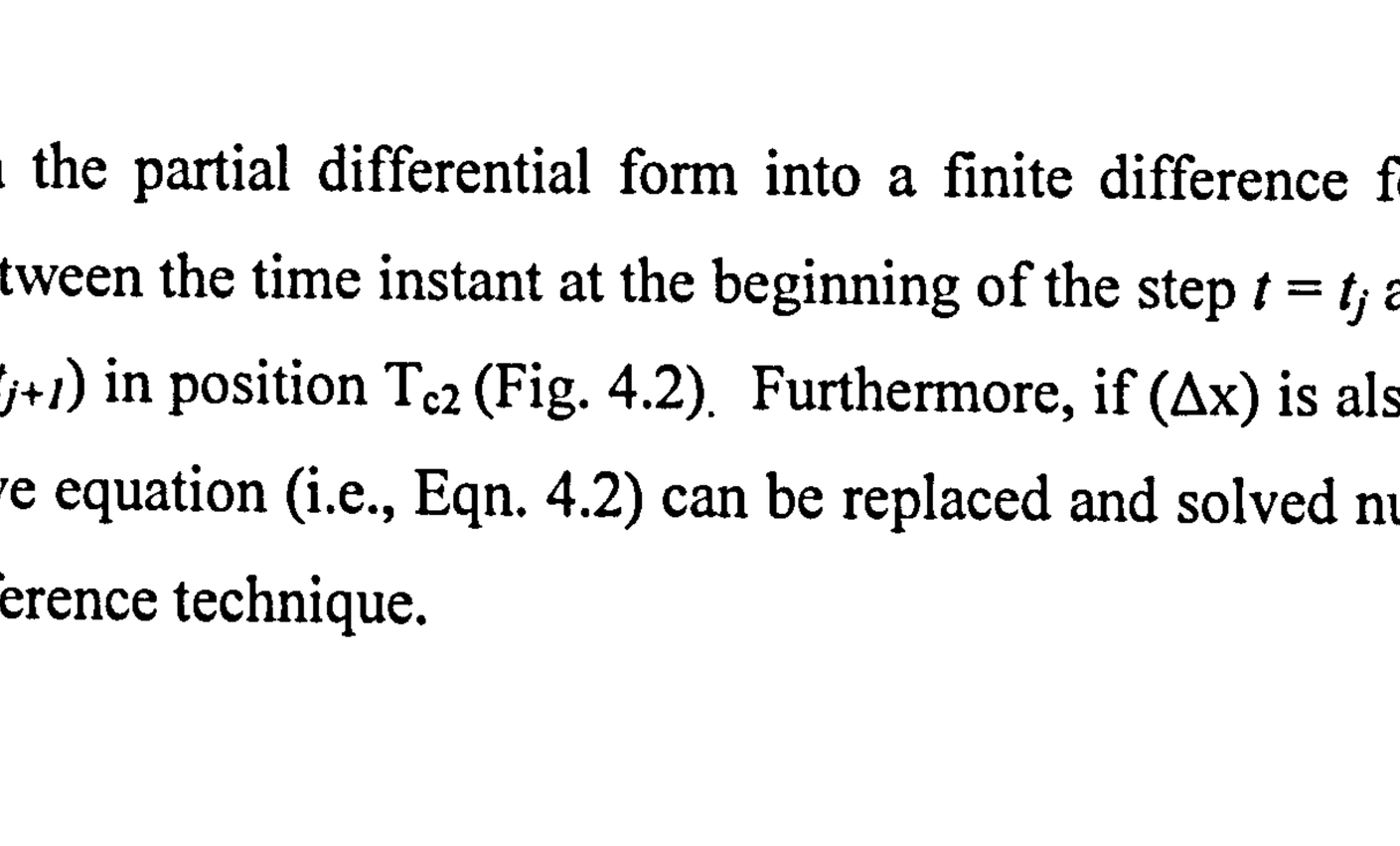

Figure 4.2 Discretisation in time and space domains

(i) Forward difference

$$\left.\frac{\partial T}{\partial x}\right|_{xi+1\to xi} \to \frac{T_{i+1}-T_i}{x_{i+1}-x_i} = lim_{x_{i+1}\to x_i}\ \frac{T_{i+1}-T_i}{x_{i+1}-x_i} = \frac{T_{i+1}-T_i}{\Delta x} \tag{4.3}$$

(ii) Backward difference

$$\left.\frac{\partial T}{\partial x}\right|_{xi-1\to xi} \to \frac{T_i-T_{i-1}}{x_i-x_{i-1}} = lim_{xi-1\to xi}\ \frac{T_i-T_{i-1}}{x_i-x_{i-1}} = \frac{T_i-T_{i-1}}{\Delta x} \tag{4.4}$$

(iii) Central difference

$$\left.\frac{\partial T}{\partial x}\right|_{i} \to \frac{T_{i+1}-T_{i-1}}{x_{i+1}-x_{i-1}} = lim_{xi-1\to xi+1}\ \frac{T_{i+1}-T_{i-1}}{x_{i+1}-x_{i-1}} = \frac{T_{i+1}-T_{i-1}}{2\,\Delta x} \tag{4.5}$$

The central difference form has been used to find the second derivative.

$$\left.\frac{\partial^2 T}{\partial x^2}\right|_{i} \to \frac{\left.\frac{\partial T}{\partial x}\right|_{i+1} - \left.\frac{\partial T}{\partial x}\right|_{i-1}}{\Delta x} = lim_{x\to xi}\ \frac{\frac{T_{i+1}-T_i}{\Delta x} - \frac{T_i-T_{i-1}}{\Delta x}}{(\Delta x)}$$

$$= \frac{T_{i+1}-2T_i+T_{i-1}}{(\Delta x)^2} \tag{4.6}$$

Equation (4.2) can be transformed into the following for numerical analysis:

$$\rho C_p \frac{\Delta T_2}{\Delta t} = K\ \frac{\Delta^2 T_2}{(\Delta x)^2} + \left(\frac{\Delta K}{\Delta T_2}\right)\left(\frac{\Delta T_2}{2(\Delta x)}\right)^2 \tag{4.7}$$

Re-arranging Eqn. (4.7), thus:

$$\rho C_p \frac{T_2^{\,j+1}-T_2^{\,j}}{t^{j+1}-t^{j}} = K_2^{\,i}\ \frac{T_3^{\,i}-2T_2^{\,i}+T_1^{\,i}}{(\Delta x)^2} + \frac{\partial K_2^{\,i}}{\partial T_2}\left[\frac{T_3^{\,i}-T_1^{\,i}}{2(\Delta x)}\right]^2 \tag{4.8}$$

Here, the term (Δx) is the distance between any two adjacent Tcs. The superscripts j and j+1 represent the time instants at the beginning and at the end of the time step

involved. Since (ρ Cp) is assumed to be known, one may obtain $\Delta K/\Delta T_2$ from measurement if an initial value of K, (i.e., Ko), is known or assumed. Meanwhile, we have, at a given time $t = t_j$.

$$\left(\frac{\Delta K}{\Delta T_2}\right)_j = \frac{K_{j+1} - K_j}{\Delta T_2} \tag{4.9}$$

Thus $$K_{j+1} = K_j + (\Delta T_2)\left(\frac{\Delta K}{\Delta T_2}\right)_j = K_j + \left(\frac{\Delta K}{\Delta T_2}\right)_j \left(T_2^{i+1} - T_2^{i}\right) \tag{4.10}$$

Step by step, the value of K_{j+1} can be derived from Eqn. (4.10) as a function of temperature T_2. By repeating such an evaluation loop at each time step, values of the thermal conductivity of the mat at high temperature have been derived.

The advantage of this method is its simplicity. The incident heat flux can be of any type, for example, constant or stepwise. The disadvantages of this method are that: (i) ρ and Cp have to be known; (ii) the initial value of K has to be known or assumed; and (iii) accuracy is highly dependent on Δx (i.e., the smaller Δx is, the more accurate the results are).

4.3 Fire Testing on Dry Fibre-Mats

4.3.1 Layout of the Sample

The experimental work was carried out using the small scale fire test facility; that is, a propane burner providing a constant heat flux input to a composite sample for measurement.

A series of fire tests were conducted to measure the thermal conductivities of such WR glass fibre mats at high temperatures up to 800°C. Tests were conducted with incident heat fluxes of approximately 24, 32, 53, 68, 82, 95, 107 and 116kW/m^2.

One of the sample mats was of 0.01 square meters and 11.8mm thick consisting of 23 layers of 0.130 kg E-glass woven roving. The arrangements made for this purpose

are shown schematically in Fig. 4.3. The sample (WR) sheets were kept inside a Sindanyo frame of 11mm thick with a side-gap for the Tcs wires for the fire test using the propane burner as a heating source. A steel plate of 1.0mm thick is put on top of the fibre-mat to ensure that the thickness of the mat is kept fixed. An insulation material such as vermiculate is kept attached on the back face of the mat to ensure that there are no gas flow effects inside the mat during a tests so that only the heat conduction effect is to be considered. The Kaowool material was placed surrounding the mat to ensure a 1-D case.

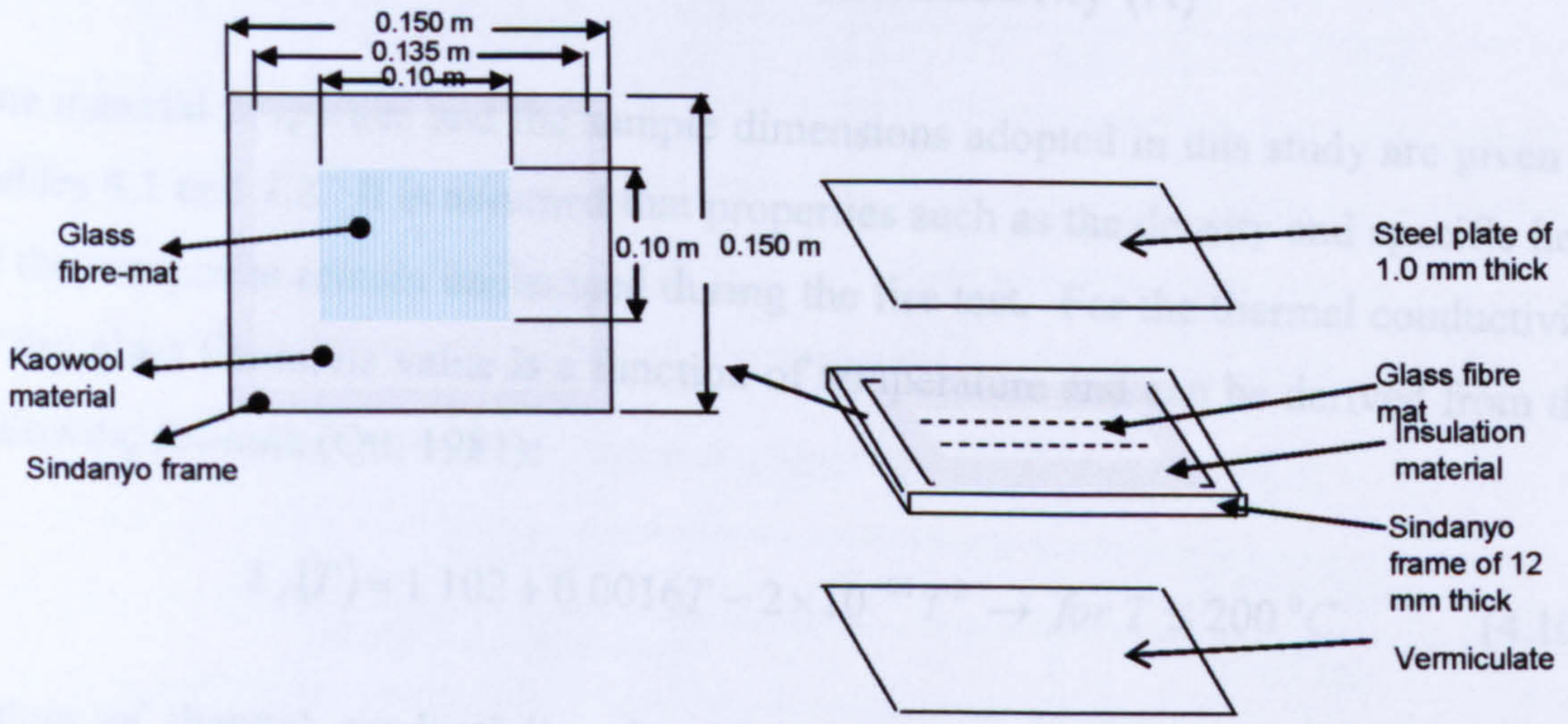

Figure 4.3 Specimen used for fire test (framed glass fibre mat and the front and the rear covers).

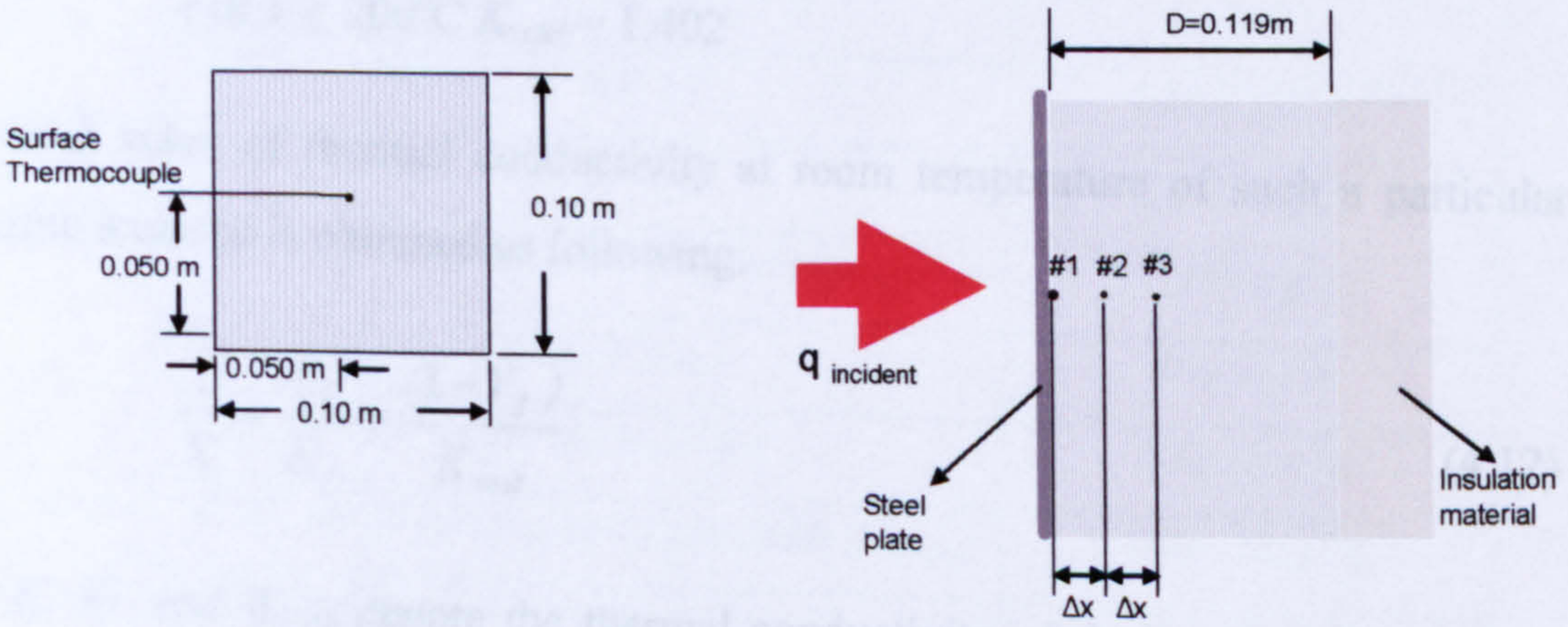

Figure 4.4 Sample used in thermal conductivity testing.

Three K-type thermocouples (i.e., Tcs_1, Tcs_2 and Tcs_3) were placed inside the fibre mat through Sindanyo side-gaps as indicated in Fig. 4.3, to record the mat temperature profile at 3 different depths of the mat as following: (i) one thermocouple (Tcs_1) is installed at the interface between the mat and the front steel plate; (ii)Two thermocouples were fixed inside the sample, one (Tcs_2) was placed between layers 5 and 6 at depth 0.002 m and the other (Tcs_3) was fixed between layers 10 and 11 at depth 0.004m. Before assembly the mats were weighed to estimate the mass density of the mat. The joint sample was held by the U-shaped channels.

4.3.2 The Initial Value of Thermal Conductivity (K)

The material properties and the sample dimensions adopted in this study are given in Tables 4.1 and 4.2. It is assumed that properties such as the density and specific heat of the composite remain unchanged during the fire test. For the thermal conductivity of dry glass fibres, its value is a function of temperature and can be derived from the following formula (Ott, 1981):

$$k_f(T) = 1.102 + 0.0016T - 2\times10^{-06}T^2 \rightarrow for\ T \le 200\ ^0C \qquad (4.10)$$

Values of thermal conductivity of voids (or air at atmospheric pressure) at high temperatures (up to 1200°C) can be derived from the following formula based on published data (Bejan, 1993):

$$k_{void} = 0.0239 + 8.0\times10^{-05}T - 3.0\times10^{-08}T \quad \text{for } T \le 200°C \qquad (4.11)$$

For $T \ge 200°C$ $K_{void} = 1.402$

The initial value of thermal conductivity at room temperature of such a particular composite material is obtained as following:

$$\frac{1}{K} = \frac{V_f}{K_f} + \frac{(1-V_f)}{K_{void}} \qquad (4.12)$$

where K, K_f and K_{void} denote the thermal conductivity of the particular composite material, the thermal conductivity of glass fibre and the thermal conductivity of the void respectively, whilst V_f, $(1.0 - V_f)$ denotes the fibre and void volume fractions

respectively. Both K_f and K_{void} are functions of temperature and the data adopted in this study for numerical studies are given in the next section.

Table 4.1 Set point temperature at the evaluated point

Test No	Sample of 1(23 layers)		Test No	Sample 2(20 layers)	
	Pr (bar)	Set point temp. °C		Pr (bar)	Set point temp. °C
1	0.1	225	9	0.2	450
2	0.2	498	10	0.3	580
3	0.3	600	11	0.4	654
4	0.4	652	12	0.5	705
5	0.5	701	13	0.6	740
6	0.6	738	14	0.7	773
7	0.7	777	15	0.8	790
8	0.8	792			

Table 4.2 The characteristic and thermal properties of the material used

property	Dimensions
Sample thickness (t)	0.033m
Mat thickness (D)	0.011m
Mat front area (A)	0.01 m^2
Distance between any two adjacent Tcs (Δx)	0.002m;
Weight of 23 layers of dry fibre mat (wt_1)	0.130 kg
Weight of 20 plies of dry fibre mat (wt_2)	0.138 kg
Fibre volume fraction of the mat (V_f)	0.4
Volume of the fibre mat (V)	0.000108 m^3
Density of glass fibres (ρ_f)	2560 $kg.m^3$
Density of dry air at atmospheric pressure (ρ_{air})	1.205 kg/m^3
Density of the fibre mat (ρ_{mat})	800 kg/m^3
Specific heat of glass fibres (Cp_f)	760 J/kg °K
Specific heat of dry air at atmospheric pressure (Cp_{air})	1006 J/kg °K
Specific heat of glass fibres mat (Cp_{mat})	760 J/kg °K
Initial thermal conductivity of the mat composite (k_{mat})	0.0375 (W/m. °K)

4.4 The Derived Value of K of the Dry Fibre-Mat

Two burner jet fire tests were conducted for the purpose of deriving the thermal conductivity of dry fibre mat at high temperature. This aimed at simulating a degraded glass fibre WR reinforced composite laminate with resin content completely depleted.

4.4.1 Effect of Incident Heat Flux

In the first fire test, twenty three layers of dry E-glass WR were assembled to form a mat of 100mm × 100mm of 12mm thick for testing. Figure 4.5 shows the typical measured temperature of the heating source (HF) and the temperatures profile at positions Tcs_1, Tcs_2 and Tcs_3 within the glass fibre mat. The distance between the front steel face and the propane burner during the test was set and kept fixed for all tests at a position of 30 cm away from the flame aperture. The initial temperature at these three positions was 20°C. In Fig. 4.5 the red line represents the hot face temperature, while the other lines (i.e. black, pink and blue) represent the mat temperature results.

Using a transient method the typical derived values of thermal conductivity of the dry glass fibre mat at high temperatures (up to 600°C) from the 1st fire test (i.e. Pr = 0.3bar and $q = 53$ kW/m^2) are shown in Fig. 4.6.

It is seen that in all the cases thermal conductivity increases with increases in temperature. As one can see from figure 4.6, the changes found in the thermal conductivity of the mat are significant; from the initial lowest value of about 0.038 W/m°K at room temperature to the highest value of about 0.125 W/m°K at high temperatures.

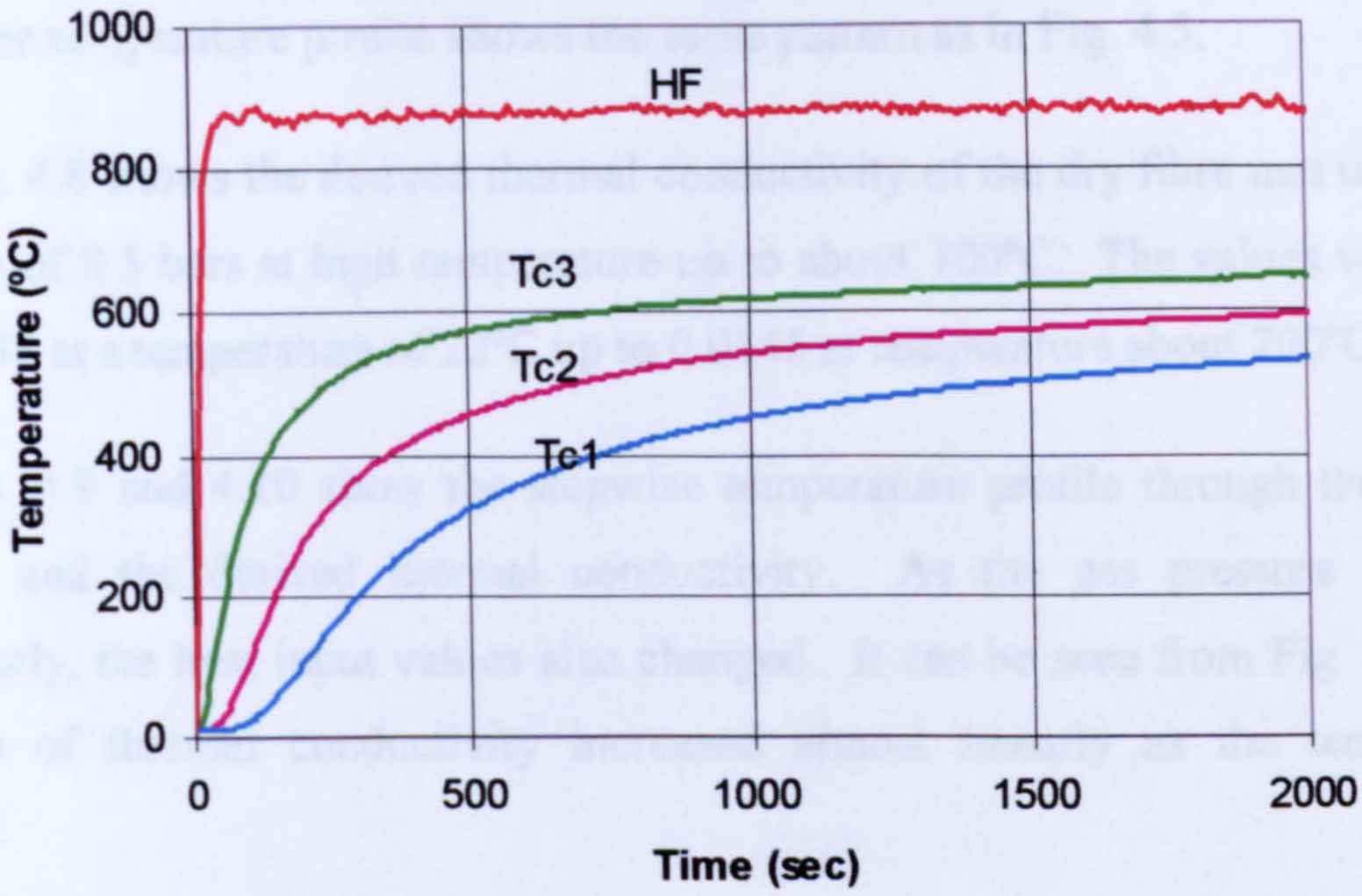

Figure 4.5 Measured temperature profiles through the dry fibre thickness, (Pr = 0.3 bar).

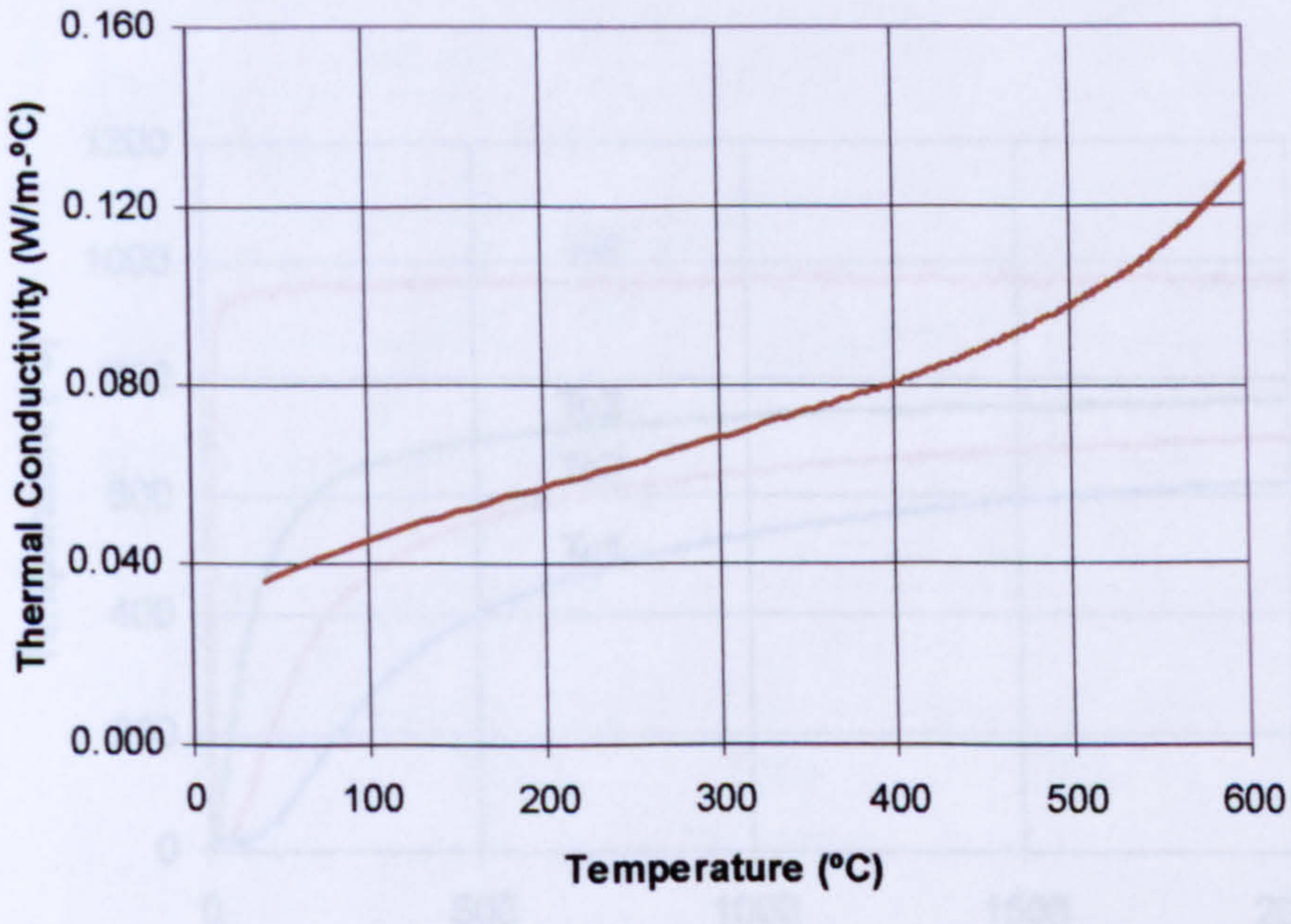

Figure 4.6 Derived values of thermal conductivity of the dry glass fibre mat with initial value of $K = 0.0375$W/m °K and Pr = 0.3 bar.

Figure 4.7 shows the temperature recorded from the fire test (i.e., Pr = 0.5 bar and q = 82 kW/m^2). Although the temperature has risen from 875°C up to 975°C as shown in Fig. 4.7, the temperature profile shows the same pattern as in Fig. 4.5.

Again Fig. 4.8 shows the derived thermal conductivity of the dry fibre mat under test conditions of 0.5 bars at high temperature up to about 700°C. The values vary from about 0.038 at a temperature of 22°C up to 0.0145 at temperature about 700°C.

Also Figs. 4.9 and 4.10 show the stepwise temperature profile through the sample thickness and the derived thermal conductivity. As the gas pressure changed, consequently, the heat input values also changed. It can be seen from Fig. 4.10 that the value of thermal conductivity increased almost linearly as the temperature increased.

Figure 4.11 demonstrates a comparison between two the results obtained from different tests typically with gas pressure of 0.3 bars and 0.7 bars. The figure shows that the variation of thermal conductivities of both cases is almost similar. It can be seen that both lines are in good agreement with each other. It is quite clear from Fig. 4.11 that the value of thermal conductivity is independent of the level of heat input.

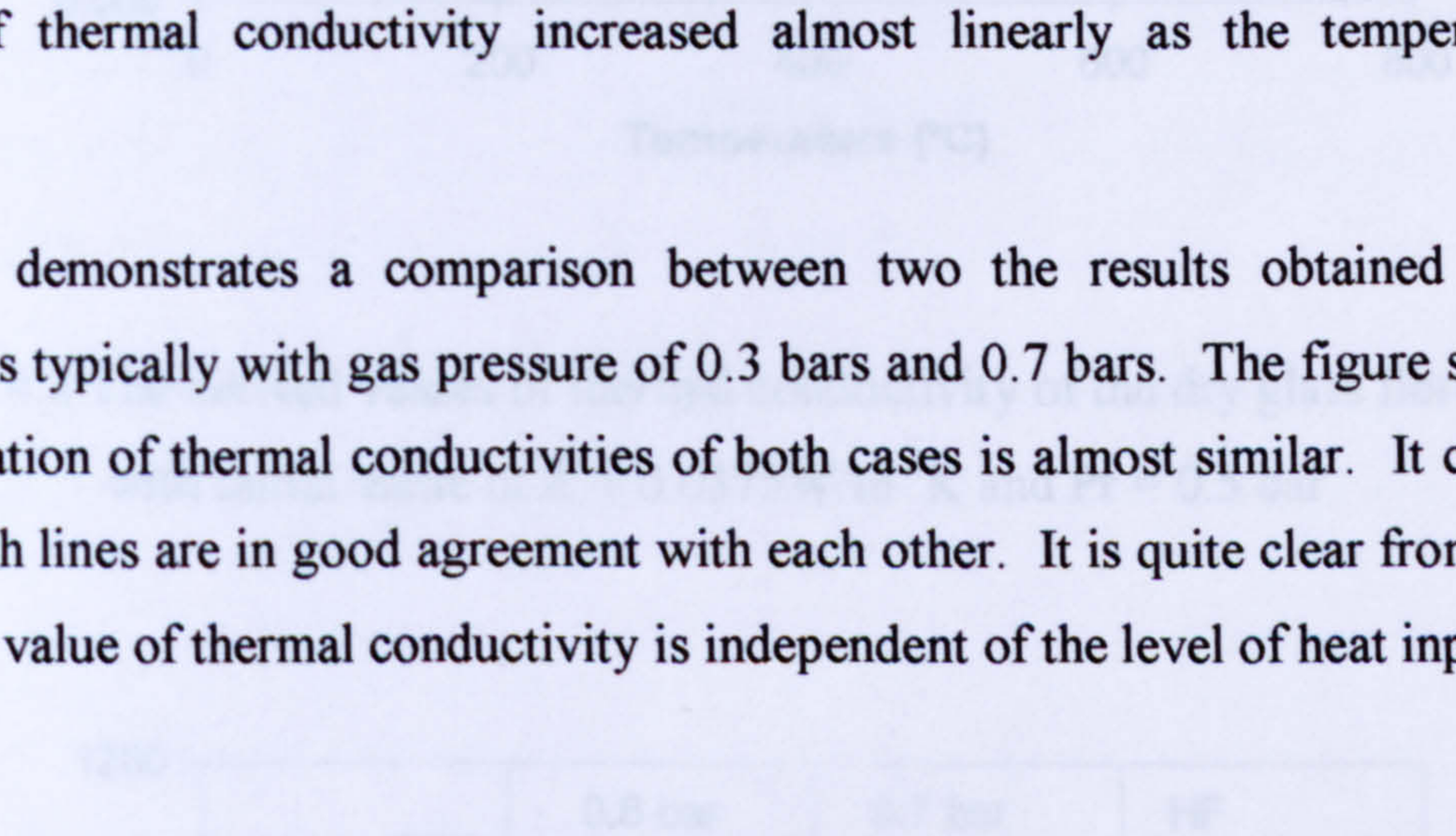

Figure 4.7 Measured temperature profiles through sample thickness, (Pr = 0.5 bar)

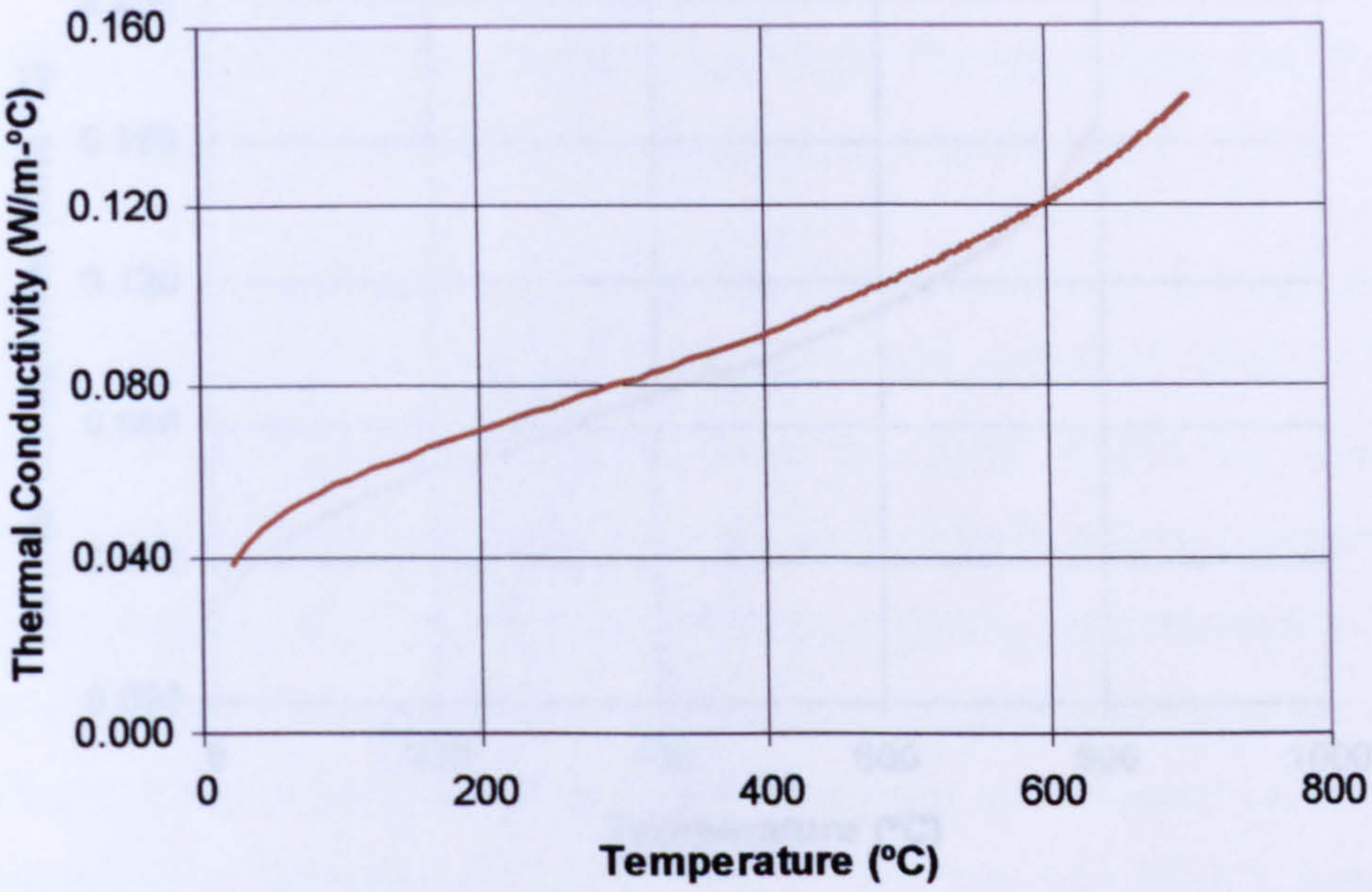

Figure 4.8 The derived values of thermal conductivity of the dry glass fibre mat with initial value of K = 0.0375W/m °K and Pr = 0.5 bar

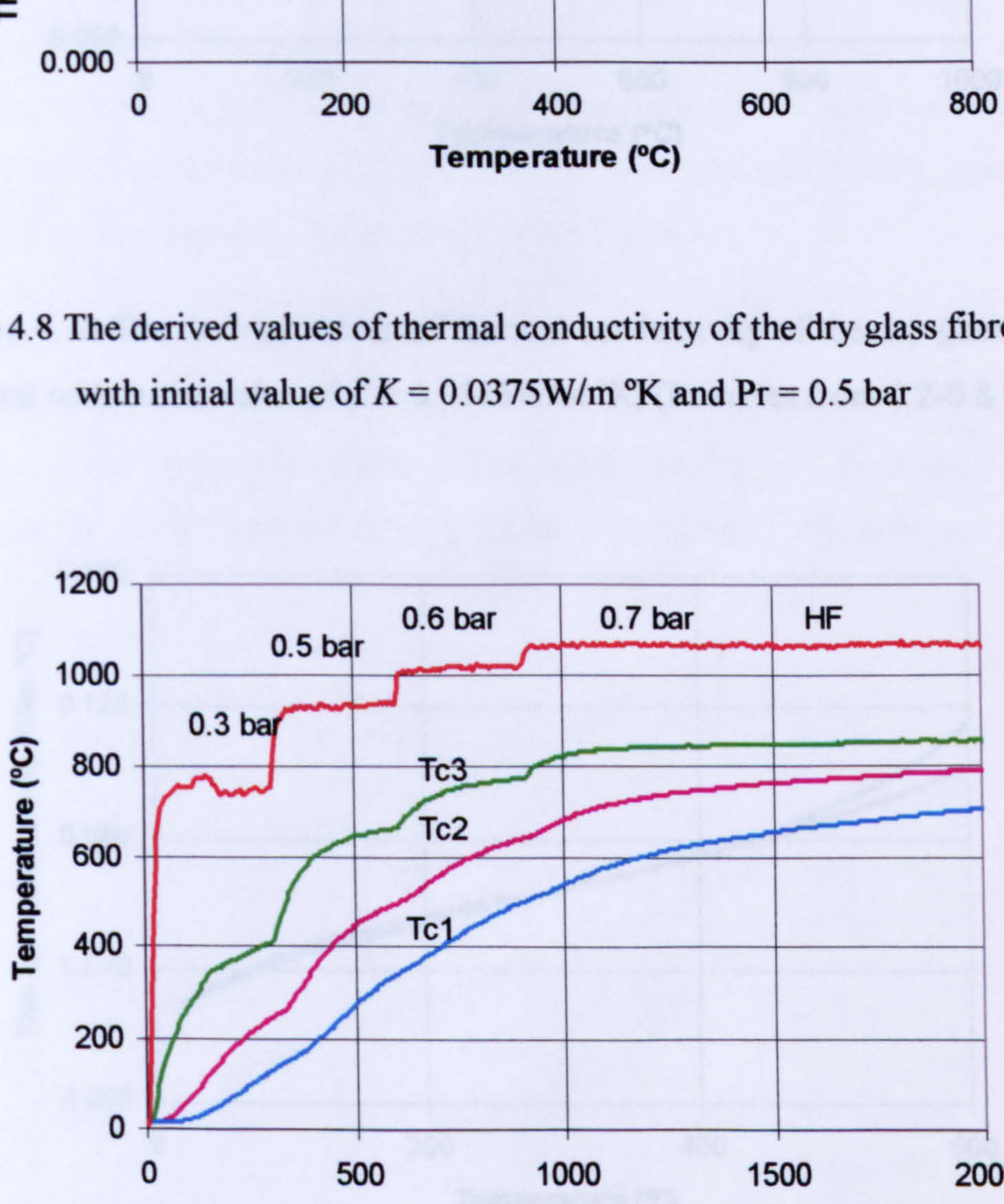

Figure 4.9 Measured temperature profiles from the stepwise gas pressure, (Pr = 0.3 to 0.7 bar).

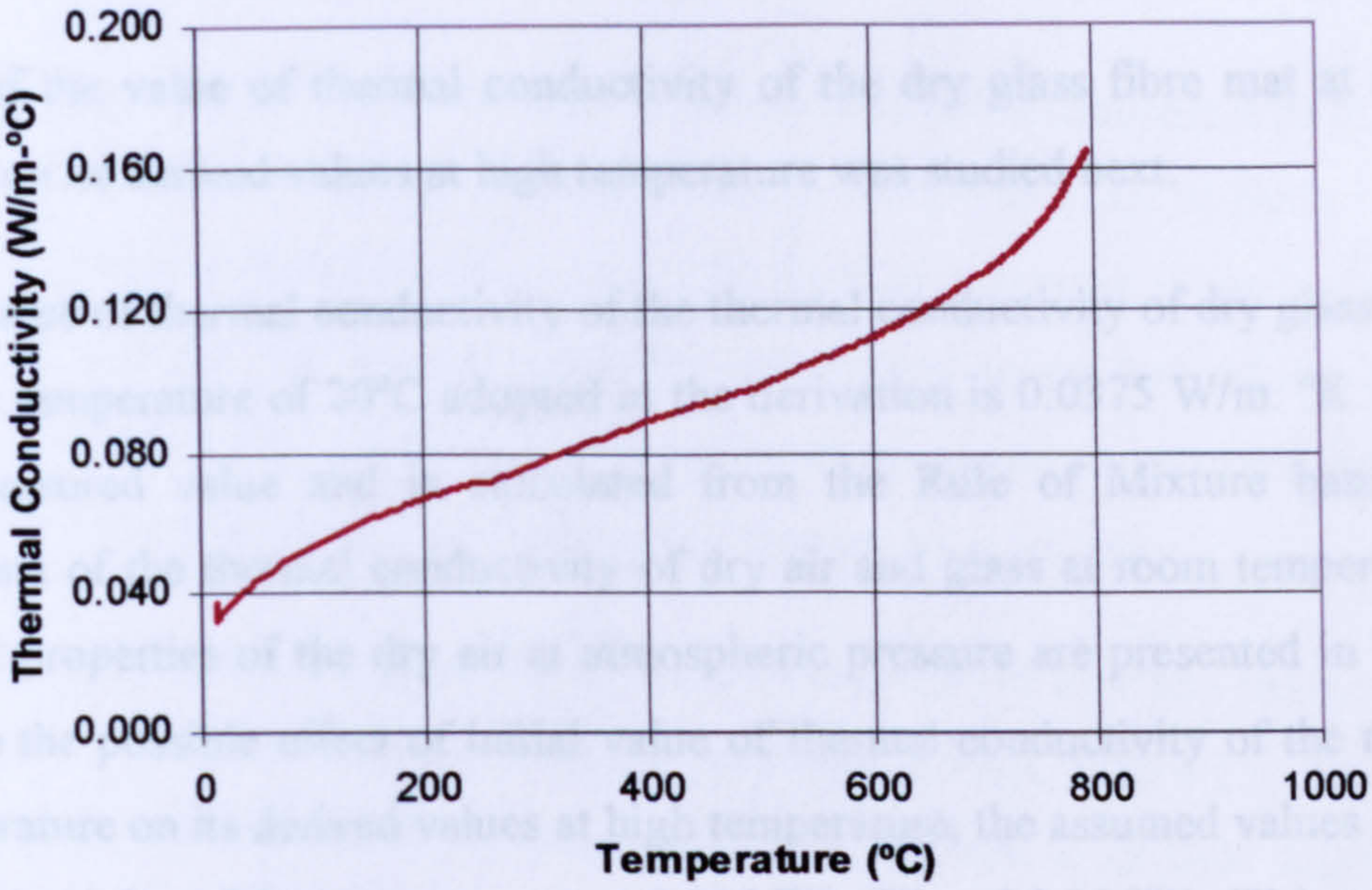

Figure 4.10 The derived values of thermal conductivity of the dry glass fibre mat with initial value of $K = 0.0375$W/m °K, (Pr varies from 0.2-0.8 bar).

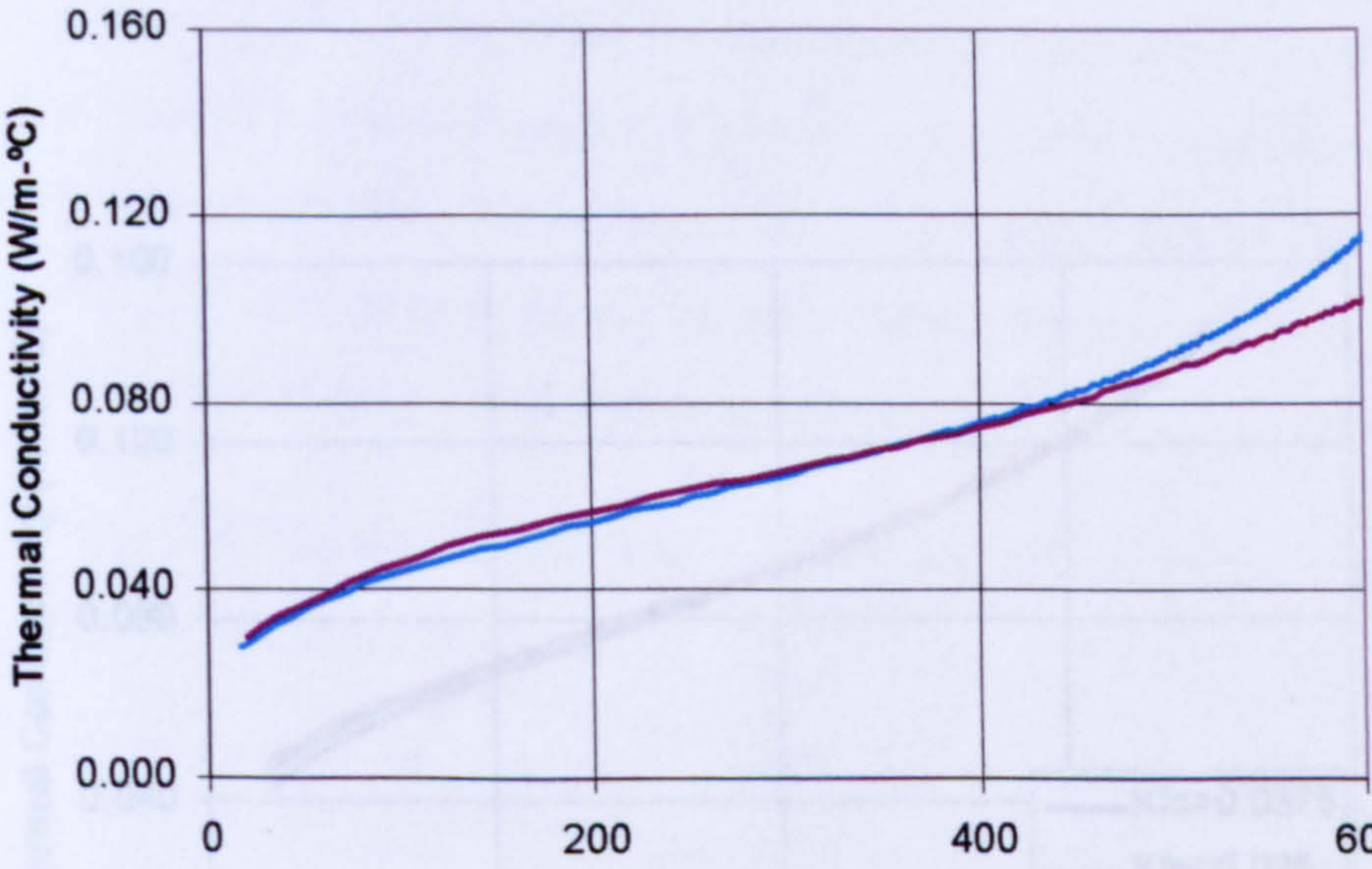

Figure 4.11 The derived thermal conductivity. The light blue line refers to the results obtained from the fire test at gas pressure of 0.4 bars and the brown line represents the relevant results from gas pressure set at 0.7 bars.

4.4.2 Effects of Initial Value of K

The effect of the value of thermal conductivity of the dry glass fibre mat at room temperature on its derived values at high temperature was studied next.

The initial value of thermal conductivity of the thermal conductivity of dry glass fibre mat at room temperature of 20°C adopted in the derivation is 0.0375 W/m. °K. This is not a measured value and is calculated from the Rule of Mixture based on published data of the thermal conductivity of dry air and glass at room temperature. The thermal properties of the dry air at atmospheric pressure are presented in Table 4.3. To see the possible effect of initial value of thermal conductivity of the mat at room temperature on its derived values at high temperature, the assumed values of the thermal conductivity of the mat were set at 0.025 W/m°K and 0.05 W/m°K instead of 0.0375 (W/m°K). The relevant results are shown in Fig. 4.12.

By comparing the three curves plotted in Fig. 4.12, one may conclude that the derived property values are not affected by the input initial value of the property at room temperatures. Such initial values may affect results at the very beginning of the heating-up process only. Ignoring this particular part of the results allows a simple conclusion.

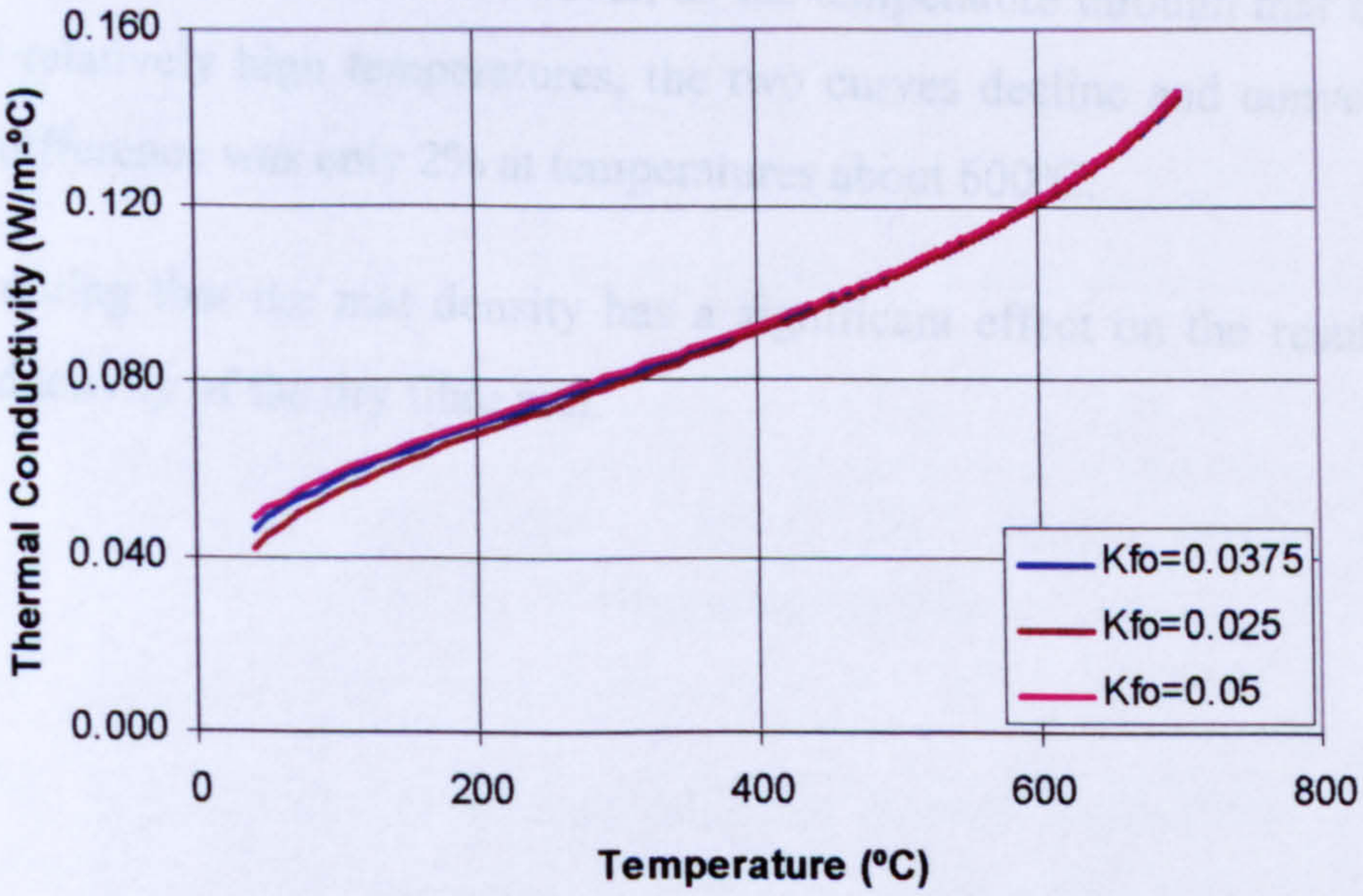

Figure 4.12 Derived values of *K* of the dry glass fibre mat from three different initial value of *K*, (i.e., 0.025, 0.0375 and 0.05W/m °K), (Pr at 0.5 bar).

4.4.3 Effect of Mass Density of Glass Fibre-Mats

A second series of tests was conducted with the same test arrangement as test one, to measure the temperature profile through a thinner sample in order to further examine the effect of the mat thickness on deriving the thermal conductivity, and to provide a data set to validate the thermal property determined using the thicker 23 layer samples. These samples consisted of twenty layers of woven roven glass fibre. These samples were assembled together in the same manner as in test one.

In the tests conducted, the glass fibre was not measured to lose any mass. Typical results from such fire tests (i.e. test 2) are presented in Figs. 4.13-4.15. Figure 4.13 shows the relevant measured temperature profile for test 2 at heat input of gas pressure (Pr = 0.4 bar).

Figure 4.14 show the change in mass density affects the result of the mat thermal conductivity. A comparison between the results obtained from test one at mat density (ρ) of 1300 kg/m^3 and the results from the second test at a density of 1388 kg/m^3 are plotted together in Fig. 4.15.

As can be seen from Fig. 4.15, the changes in the thermal conductivity of the mat are clear. The relative difference between the two curves at low temperature or at the start of the test was about 24%. However, as the temperature through mat thickness increases at relatively high temperatures, the two curves decline and converge, and the relative difference was only 2% at temperatures about 600°C.

It is worth noting that the mat density has a significant effect on the result of the thermal conductivity of the dry fibre mat.

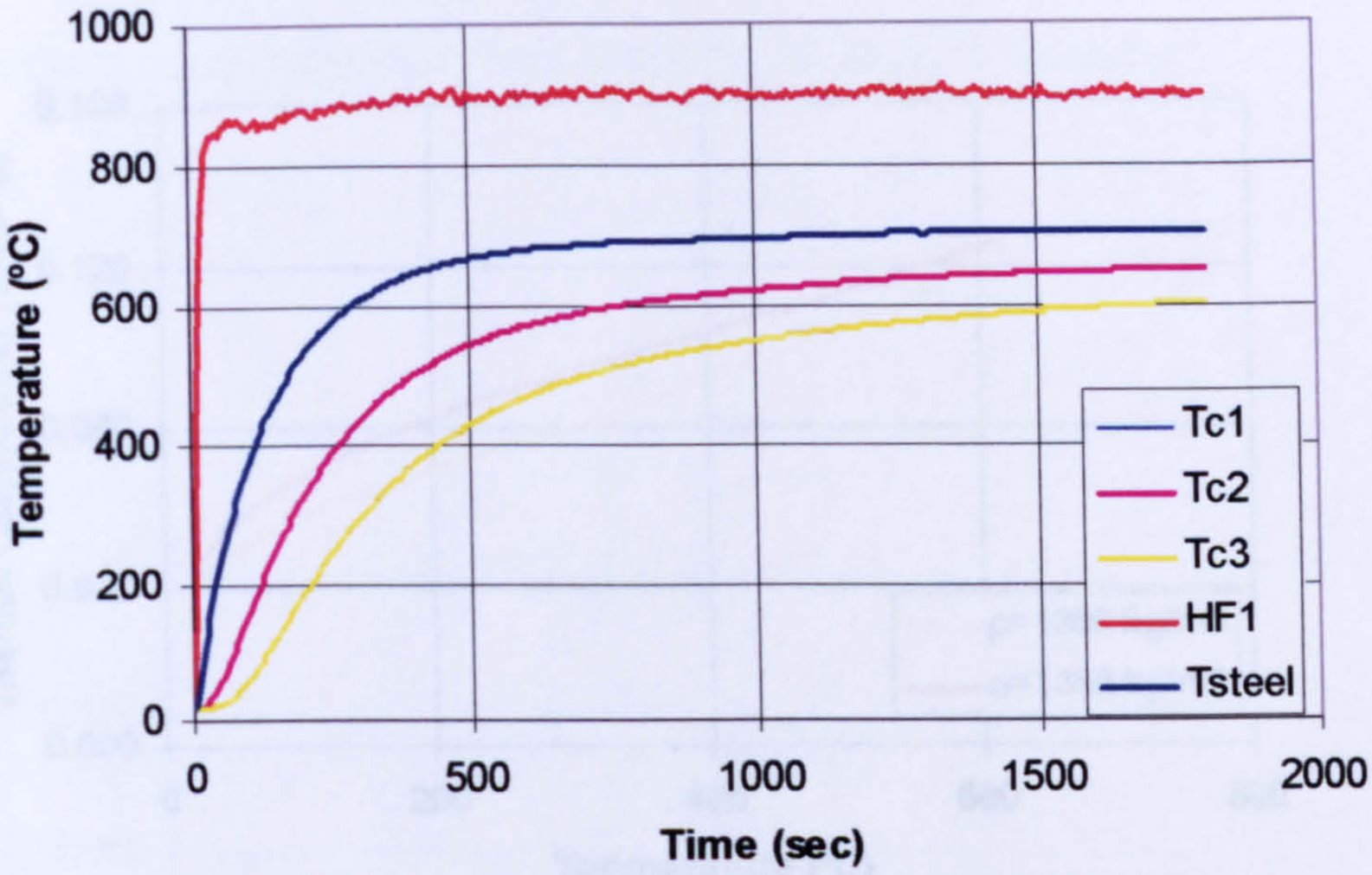

Figure 4.13 Measured temperature profiles from, (Pr = 0.4 bar).

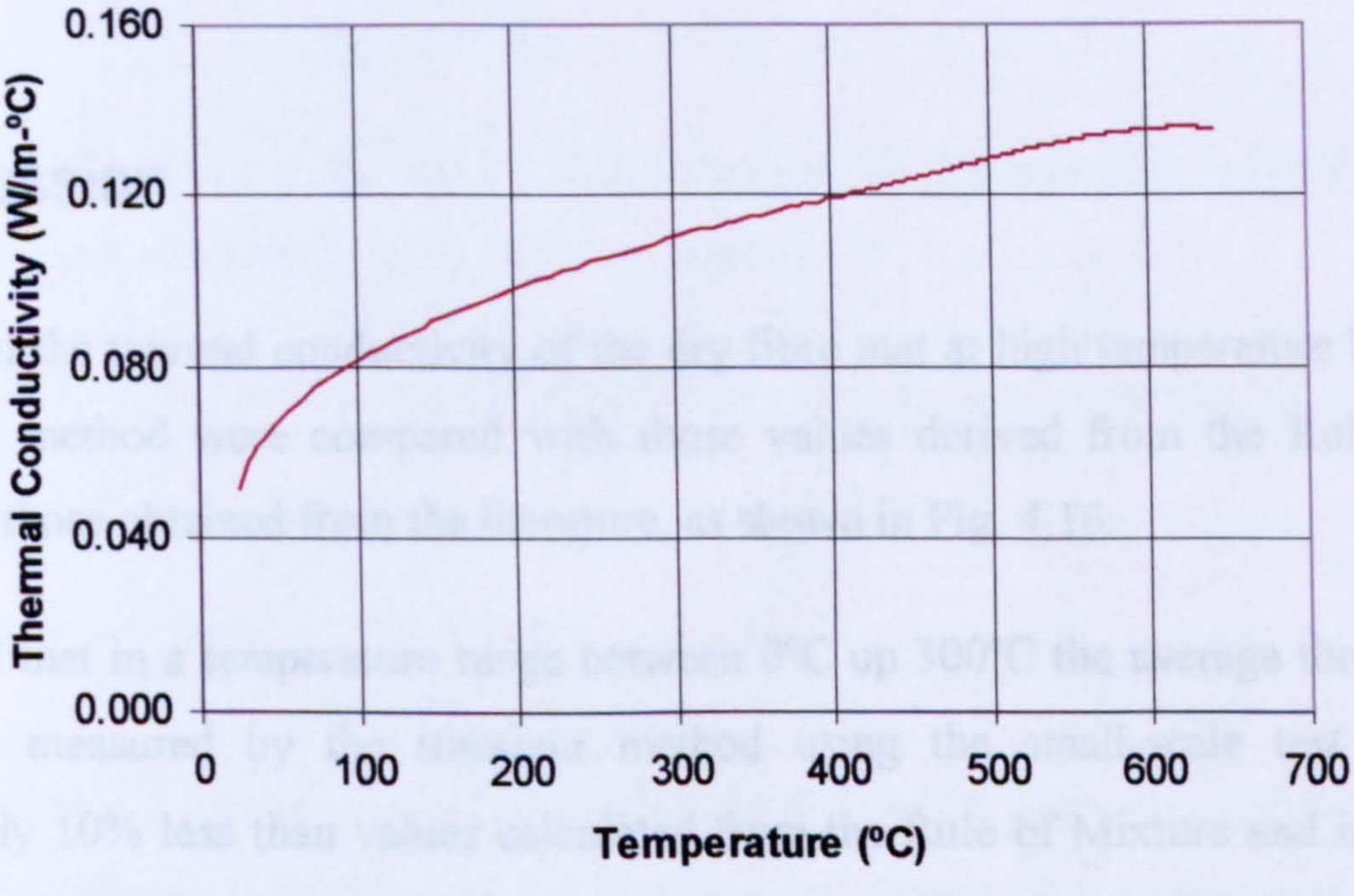

Figure 4.14 The derived values of thermal conductivity of the dry glass fibre mat. ($K = 0.0375$ and Pr = 0.5 bar).

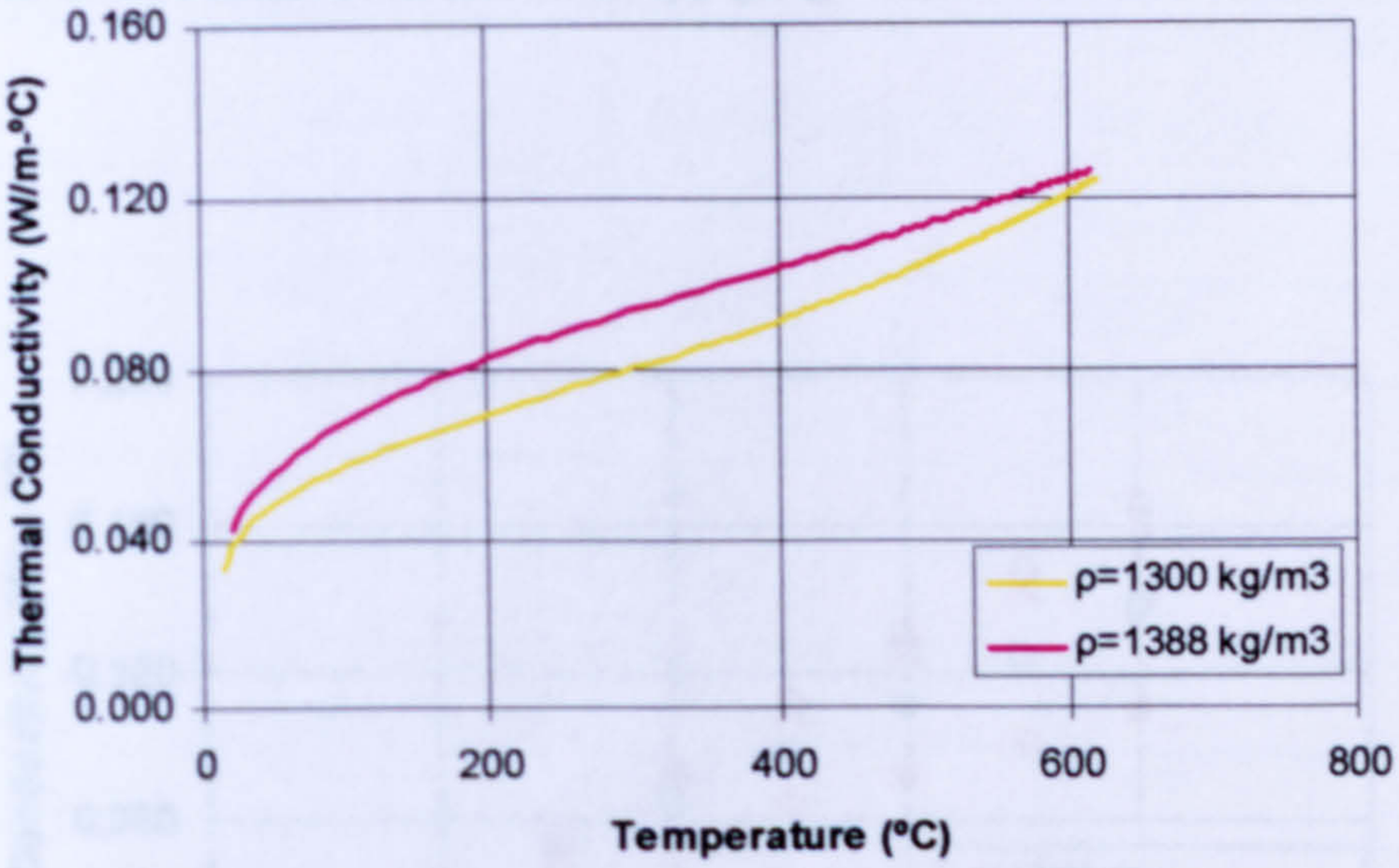

Figure 4.15 Derived values of thermal conductivity of the dry glass fibre mat from two results at different mat density. The lower curve represents the results at ρ = 1300 kg/m3 and the upper curve represents the results obtained at ρ = 1388 kg/m3. Both tests were derived at K = 0.0375 and Pr = 0.5 bar).

4.5 Discussion

The values of the thermal conductivity of the dry fibre mat at high temperature from the transient method were compared with those values derived from the Rule of Mixture and those obtained from the literature, as shown in Fig. 4.16.

It was found that in a temperature range between 0°C up 300°C the average thermal conductivity measured by the transient method using the small-scale test was approximately 10% less than values calculated from the Rule of Mixture and in the range of 10-17% higher in temperature range between 400°C and 800°C. However, by comparing the derived results with those from available published data, the difference is less than 13% in the temperature range between 300°C and 800°C.

On the other hand, it is quite clear from Fig. 4.16 that this difference is relatively high compared with these results obtained from applying the Rule of Mixtures.

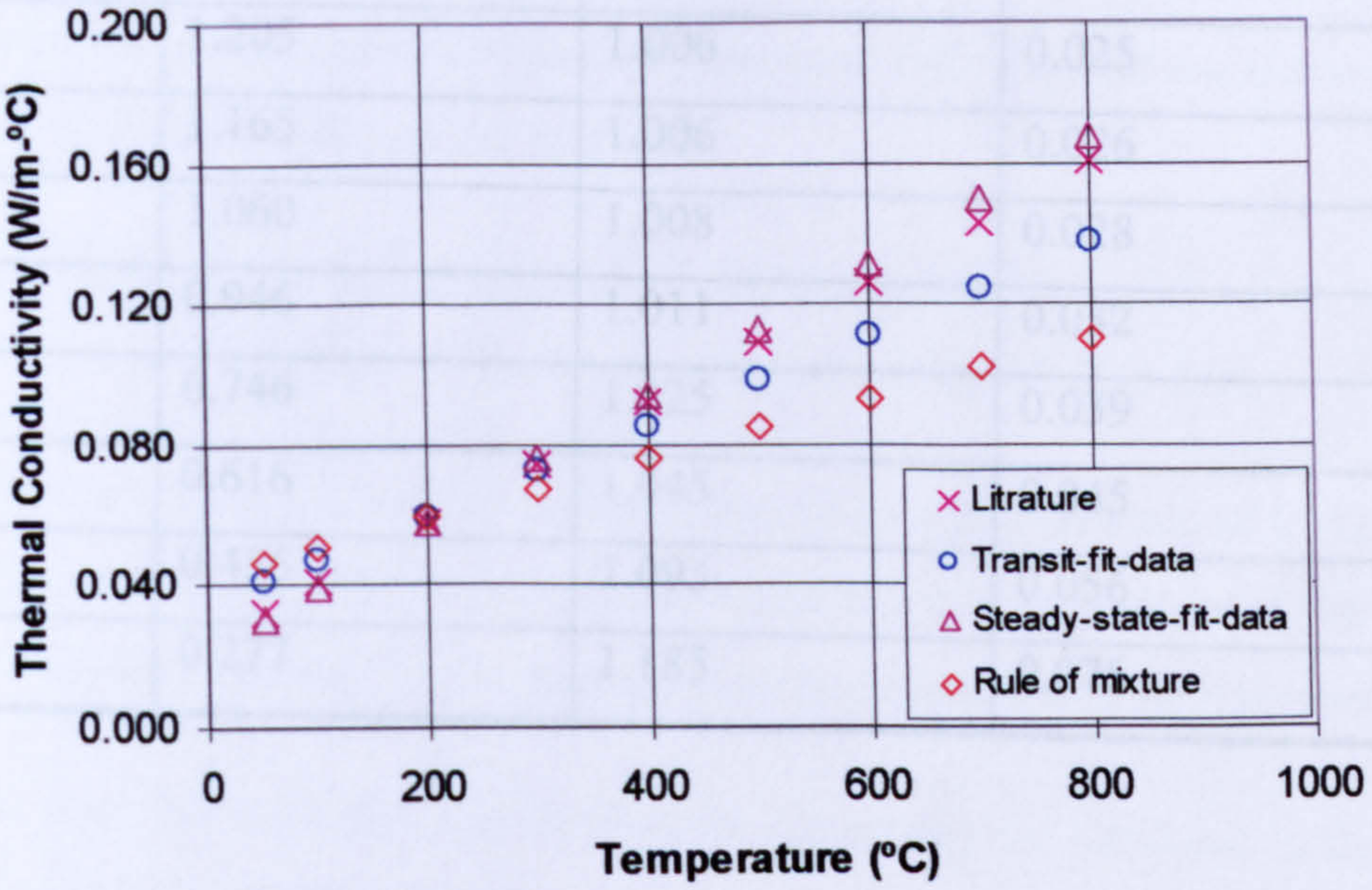

Figure 4.16 A comparison of thermal conductivity results at high temperature.

The thermal conductivity in the small-scale testing using the transient method was found to vary approximately linearly with temperature.

Their experimental values can be described according to the following empirical equations:

$$K = 0.0001290\,T + 0.03414 \tag{4.13}$$

where K represents the value of thermal conductivity of the dry fibre mat, and T is the local sample temperature (in °C); and which has a correlation of $r^2 = 0.994$ with the transient test data.

The above equation is found to fit very well compared to the experimental values. These values of thermal conductivity compared to those reported in the literature are presented in Table 4.4.

Table 4.3 Properties of dry air at atmospheric pressure.

Temperature °C	Density (ρ) kg/m^3	Specific heat (Cp) (KJ/kg. °K)	Thermal conductivity (k) (W/m. °K)
0	1.293	1.006	0.024
10	1.247	1.006	0.025
20	1.205	1.006	0.025
30	1.165	1.006	0.026
60	1.060	1.008	0.028
100	0.946	1.011	0.032
200	0.746	1.025	0.039
300	0.616	1.045	0.045
500	0.456	1.093	0.056
1000	0.277	1.185	0.076

Table 4.4 Thermal conductivity values obtained from different results

Temperature °C	Literature-results (Brian and Jason, 2004)	Transient-method	Steady-state method	Rule of mixtures
0	0.024	0.034	0.021	0.042
50	0.032	0.041	0.030	0.047
100	0.041	0.047	0.039	0.051
200	0.058	0.060	0.058	0.059
300	0.075	0.073	0.076	0.068
400	0.092	0.086	0.094	0.076
500	0.109	0.099	0.113	0.085
600	0.126	0.112	0.131	0.094
700	0.144	0.124	0.150	0.102
800	0.161	0.137	0.168	0.111

4.6 Conclusion

- The transient response method as introduced here can be adopted to determine the thermal conductivity of the dry glass fibre mat as a function of temperature from 20-800°C. A well-characterized small-scale test apparatus can be used to produce the thermal response data required for determining the thermal conductivity of the material;

- The derived thermal properties of the particular composite mat (dry glass fibres + air) are in good agreement with relevant published data;

- The results from this study indicate that, in general, the Rule of Mixture is not sufficient to evaluate the thermal conductivity of the particular fibre mat as a 'composite material' in the through-thickness direction at high temperatures;

- An empirical equation was derived for estimating the variation in the thermal conductivity of dry glass fibre mats.

CHAPTER 5

SMALL-SCALE FIRE TESTING

5.1 General Introduction

The design of structures against fire is important, demanding increasing attention as fire risk and isolation of the structure increases, and their qualification and acceptance in fire risk applications depends on satisfying standard tests. These involve small-scale tests such as for non-combustibility, ignitability, surface spread of flame and cone calorimetery (ISO 834, 1975). These are combined with large scale testing which includes furnace tests under specified temperature/time such as the SOLAS curve (ISO 5660-1, 1993), or the more severe Hydrocarbon fire curve (SOLAS, 1974).

Current interest in most industries is devoted to the response of materials to tests such as jet-fire, furnace fire and pool fire tests.

Within this study, small scale furnace and small scale jet-based fire resistance testing has been adopted, to simulate the SOLAS and hydrocarbon fire conditions.

A series of furnace fire tests on composite laminates have been carried out using a small scale indoor furnace. The panels tested were of dimensions 300mm × 170mm with thicknesses between 9.6mm and 10.5mm manufactured by the hand lay-up technique to be used for the purpose of the tests. Also, another part of the testing involved using a small-scale furnace, in which the composite panels were supplied by DML, attempting to achieve the A60 requirements of fire protective layers on top of a specified CFRP pipe repair. During the tests the samples were exposed to specified fire conditions defined by a furnace temperature versus time curve.

Another group of fire tests have also been conducted using a burner to provide a jet fire. In the tests, the composite samples were square laminates of 150 × 150mm and 8mm thick laminates were framed with an exposed front area of 100 × 100mm.

This chapter describes the main results from the two groups of fire tests and discussions of and conclusions from the results are also presented.

5.2. A small-scale Furnace Fire Testing

5.2.1 Fire Testing

The aim of such experimental work is to look for different types of laminates based on different types of matrix systems, in order to improve fire resistance.

Fire tests were carried out using a small scale furnace. The test arrangement is shown in Fig. 5.1. The test panels of dimensions 300 x 170mm were designed to fit into the front door of the furnace and were exposed to a specified temperature/time curve.

The furnace is designed to consume natural gas over a pressure range of approximately 7 inches water gauge (w.g) at the highest setting, down to 0.25 inches water gauge at the lowest setting. The furnace is computer controlled and initial adjustments of the furnace were made in order to find the highest gas pressure setting and operating procedure required to achieve as closely as possible the desired temperature regime such as SOLAS curve or the more severe hydrocarbon (H/C) curve. The hydrocarbon curve was derived from BS 476 Part 20 Appendix (BS 476, 1990) and governed by numerical Eqn. (5.1) as shown in Fig. 5.2

$$T(t') = 1080\left(1 - 0.325.e^{-0.167\frac{t'}{60}} - 0.675.e^{-2.5\frac{t'}{60}}\right) + T_o \qquad (5.1)$$

where T_o = Initial room temperature, t = Time (minutes).

The furnace reference temperature was measured using a K type thermocouple positioned inside the furnace, set at 100mm from the exposed hot face. A data acquisition system was used to convert the voltage signals to temperature, which was displayed digitally. Two thermal couples were fixed to the sample by drilling a hole through the thickness in the sample, with one hole drilled to a depth of half the

thickness, and the second to the depth of the through thickness. Copper disc thermocouples were used on the free side of the panel (i.e., cold face). The thermocouples were bonded on with epoxy resin. The output of each thermocouple was observed and recorded throughout the test runs using a data logging system of the 'Pico' type.

It must remembered that this is very small scale testing compared to standard fire tests conducted under BS 476 and IMO (International Maritime Organization) requirements, and is intended to offer quicker and cheaper initial screening tests. The furnace reaches a temperature of 1100°C in approximately 25 minutes, which is very close to the hydrocarbon curve, which reaches a temperature of 1100°C in approximately twenty minutes. This is a preliminary investigation which aims to show how such a furnace can simply, quickly and cheaply be used to give an indication of the insulating and fire resistance abilities of GRP panels.

5.2.2 Sample Preparation

The samples to be fitted in the furnace for fire tests were prepared and manufactured by hand lay-up. Panels were manufactured using woven roving glass reinforcements based on different types of resin such as orthophthalic, isophthalic polyester and vinyl ester resins. After curing, the laminates were cut to size to fit the furnace door. Inner and outer thermocouples were included after the manufacture of the laminates to enable measurement of the temperature through the thickness during fire testing. The glass volume fraction of each laminate was measured by carrying out a standard matrix burn-off test.

Another group of laminate samples, each approximately 8mm thick, was also prepared by DML for investigation as possible protection materials. The materials used and the type of laminated panels used in the fire tests are specified in Tables 5.1 and 5.2, respectively.

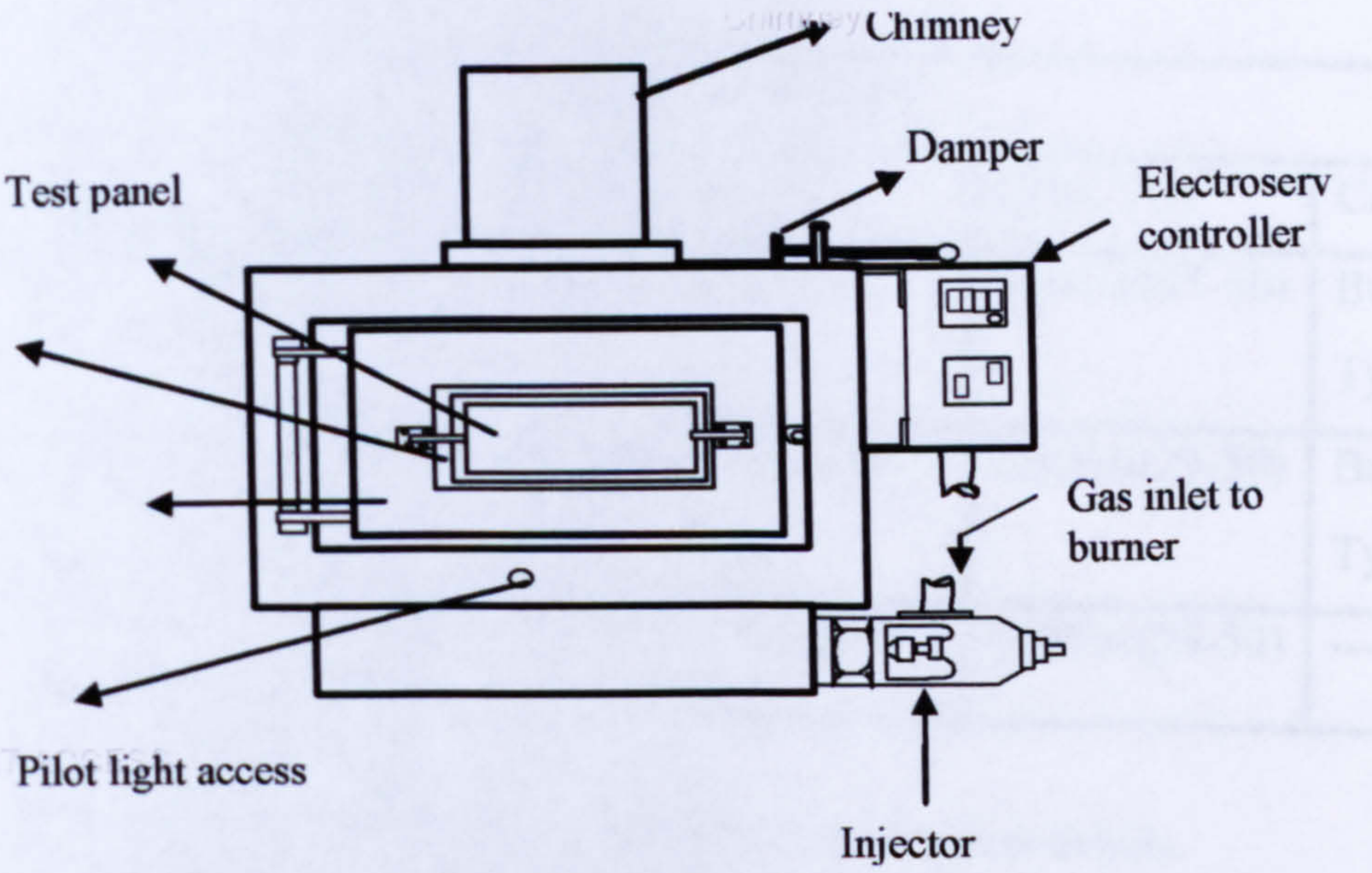

Figure 5.1 Schematic presentation of the front view of the furnace.

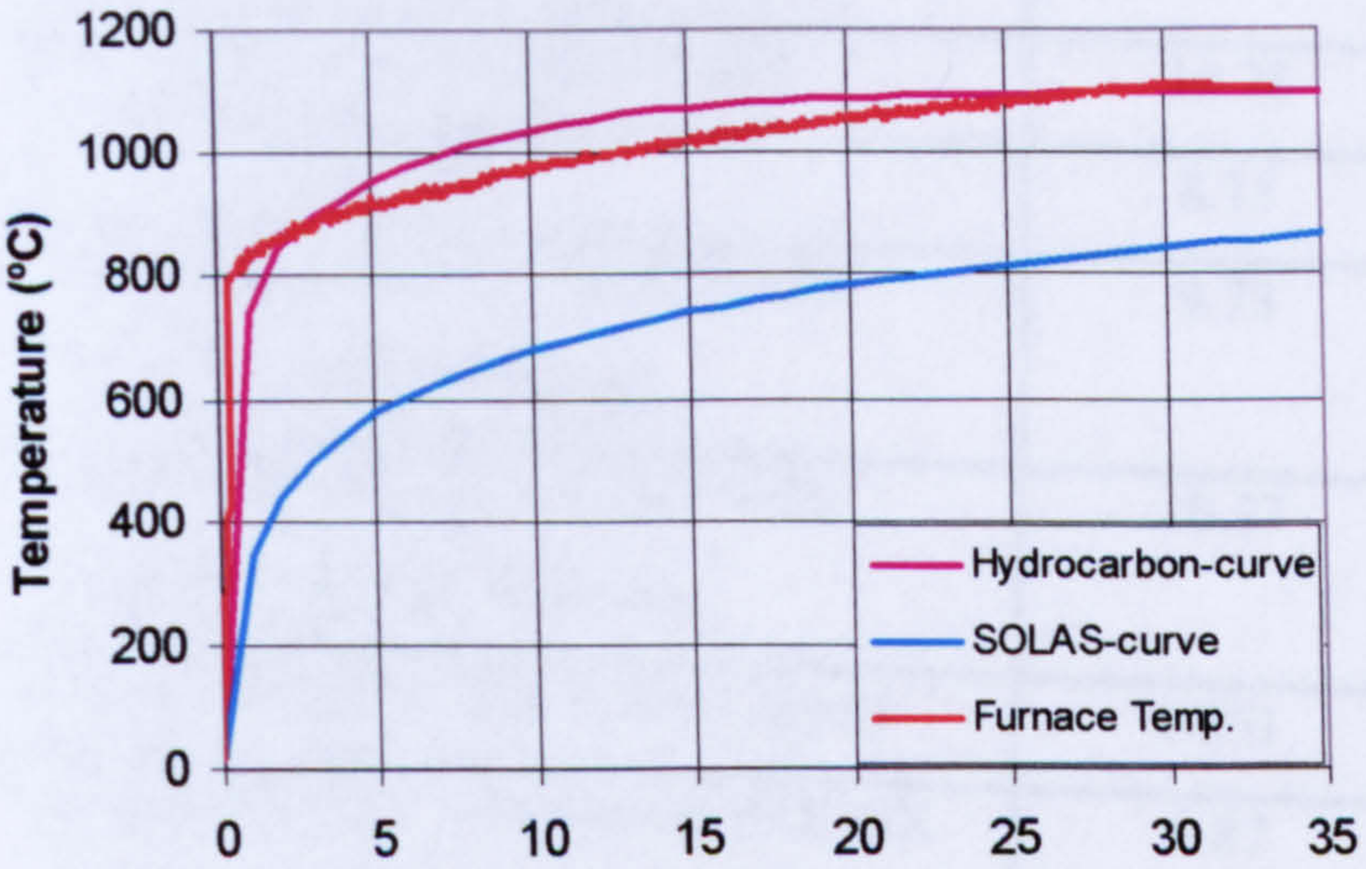

Figure 5.2 A comparison of furnace, hydrocarbon curve and the SOLAS temperature curves.

Table 5.1 Details of materials used.

Materials Details			
Resin	Reinforcement used	Conc. (%)	Catalyst
Isophthalic polyester	E-glass (WR, wt. of 600 g/m^2)	Styrene(25-50)	Butanox Type:MSO
Orthophthalic polyester	E-glass (WR, wt. of 600 g/m^2)	Styrene(25-50)	Butanox Type:MSO
Vinyl ester	E-glass (WR, wt. of 600 g/m^2)	Styrene(25-50)	--------

Table 5.2 Type of laminated panels and their volume fraction details.

Laminate Specification	Thick. (mm)	Vf %	Vv %
GRP / Orthophthalic PE + 4 layers of Al foil.	10.86	46	3.6
GRP / Orthophthalic PE + 3 layers of Al foil.	10.50	47	3.9
GRP / Orthophthalic PE + 2 layers of Al foil..	10.21	45	2.8
GRP / Orthophthalic and Isophthalic PE only.	10.09	46	2.3
Vinyl ester	10.71	45	2.9
GRP/ H polyester (unidirectional)	10.28	50	4.8
Phenolic	8.15	55	7.2
GRP / Orthophthalic PE + TXCV7076 (12 % Nominal coating).	9.73	49	4.1
GRP / Orthophthalic PE + TXCV7076 (Nominal coating, all layers).	10.33	48	3.4
GRP / Orthophthalic PE TXC7129 (1 layer)	10.51	43	3.1
GRP / Orthophthalic PE + Aluminised PRE-OX (1 layer).TXCV7076 (Nominal coating, all layers).	9.87	44	2.1
GRP / Orthophthalic PE + Superwood steel wire reinforced (1 layer).	10.63	49	2.6
GRP / Orthophthalic PE + TXC7138 (1 layer). (Nominal coating, all layers).	12.86	43	4

5.2.3 Test Limitations

Failure of the samples is deemed to have occurred when one or more of the following criteria are met:

Stability; failure is deemed to have occurred when the unloaded specimen under test collapses, or if deflection is beyond acceptable limits.

Integrity; failure is deemed to have occurred when a crack appears in the material through which flames or hot gases may pass to light a cotton wool pad held near the cold face, or if a fully developed crack exists.

Insulation; failure is deemed to have occurred when the temperature on the unexposed face increases on average by more than 160°C.

The hydrocarbon curve reaches a temperature of 1100°C in approximately twenty minutes whereas the current furnace takes 25 minutes. Hence it must be accepted that the fire testing will not necessarily give reliable results of how a material will perform in real fire situations. It is rather a way of testing for an acceptable level of performance, and for comparing different materials.

5.2.4 Experimental Furnace Tests Results

10mm thick polyester matrix panels constructed with woven roving reinforcement were tested with a range of fibre volume fractions. Figure 5.3 demonstrates the composite panel under fire testing. The composite panels were structurally stable during the fire tests, and no signs of violent or explosive delamination were observed. After about 10 minutes some smoke was observed from the cold face and delamination events took place, accompanied by noise and fumes, and a gradual blackening of the cold face of the panels was observed during the later stages of the tests. The resin component close to the hot face was completely spent after a few minutes' exposure to the hydrocarbon fire. The resin at the cold face started decomposition after about 30 minutes into the test.

Typical results for a 10mm thick glass woven roving panel based on different matrix systems are shown in Figs 5.4 and 5.5. The figures represent the temperature profile through the composite panels against time. The upper curve represents furnace temperature, while the lower three curves represent the hot face, the mid-plane and the cold side (i.e., free side) temperature response through the composite panel respectively. It can be seen from Figs. 5.4 and 5.5 that the temperature rise recorded at the cold face of the panel shows a stable increase almost linearly throughout the fire tests.

The output from the inter-laminar thermocouple tends to level out to a steady state value in the later stages of the test, whilst the cold face temperature continues to rise. In the later stages of the tests the inter-laminar temperature outputs are more uncertain due to separation of the reinforcement layers as the resin is depleted. There is useful information to be gained by continuing the test for as long as possible in order to be able to follow the final process of failure. Safety considerations, however, dictated the need to terminate the test at cold face temperatures a little in excess of 200°C.

Figures 5.6 and 5.7 shows typical results for composite panels laminated with some additive product, such as aluminum trihydrate (ATH) and aluminum foil respectively

Figure 5.8 shows a plot of temperature profile responses for different types of laminates for comparison. In general, all laminates exhibit similar behaviour in terms of temperature response; however, some show better fire resistance. This is most obvious with those laminated with additive products such as ATH.

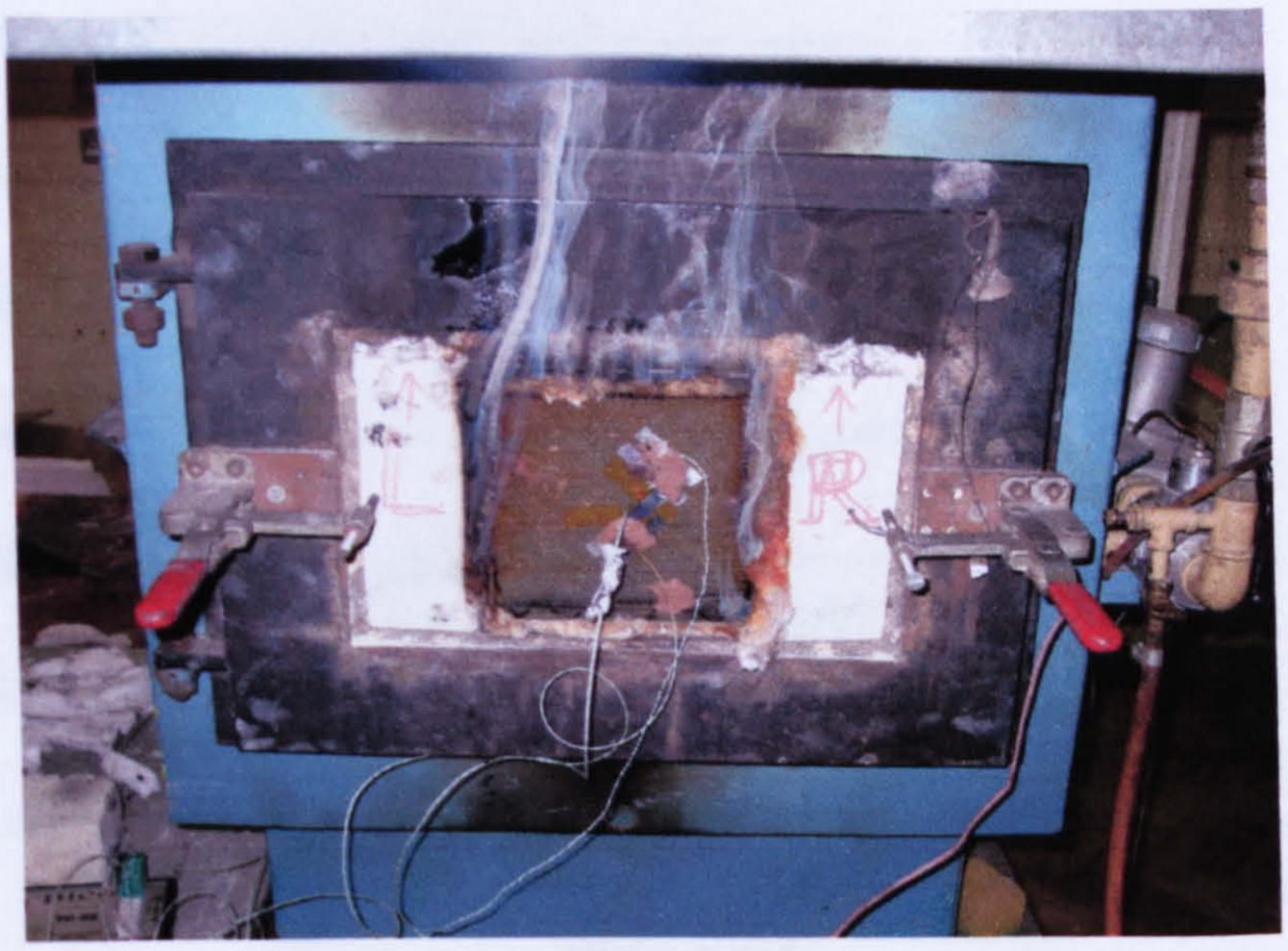

Figure 5.3 Cold side of the composite panel under testing.

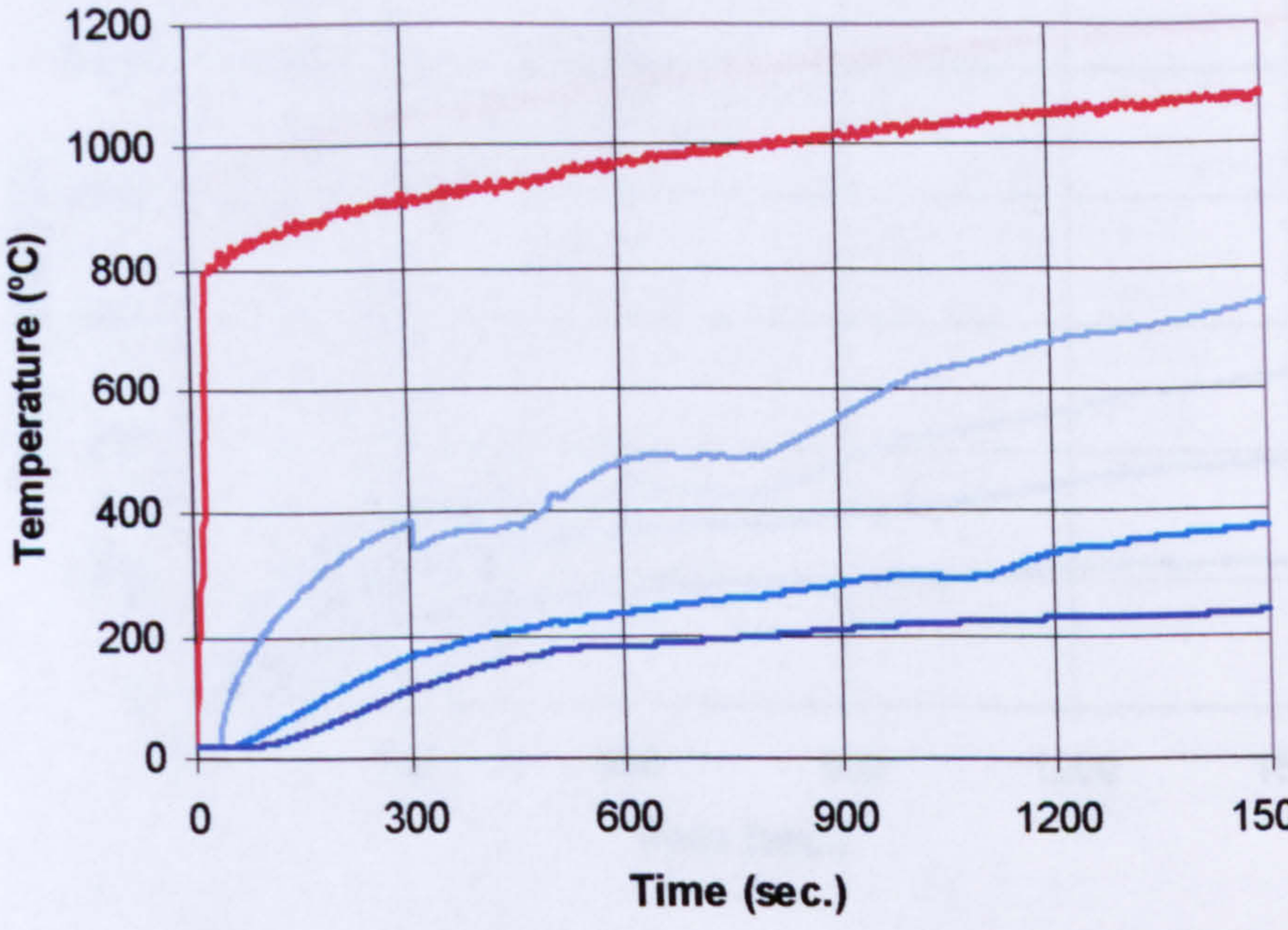

Figure 5.4 Experimental furnace fire test results for orthophthalic polyester/glass woven roving laminated panel (V_f = 45%).

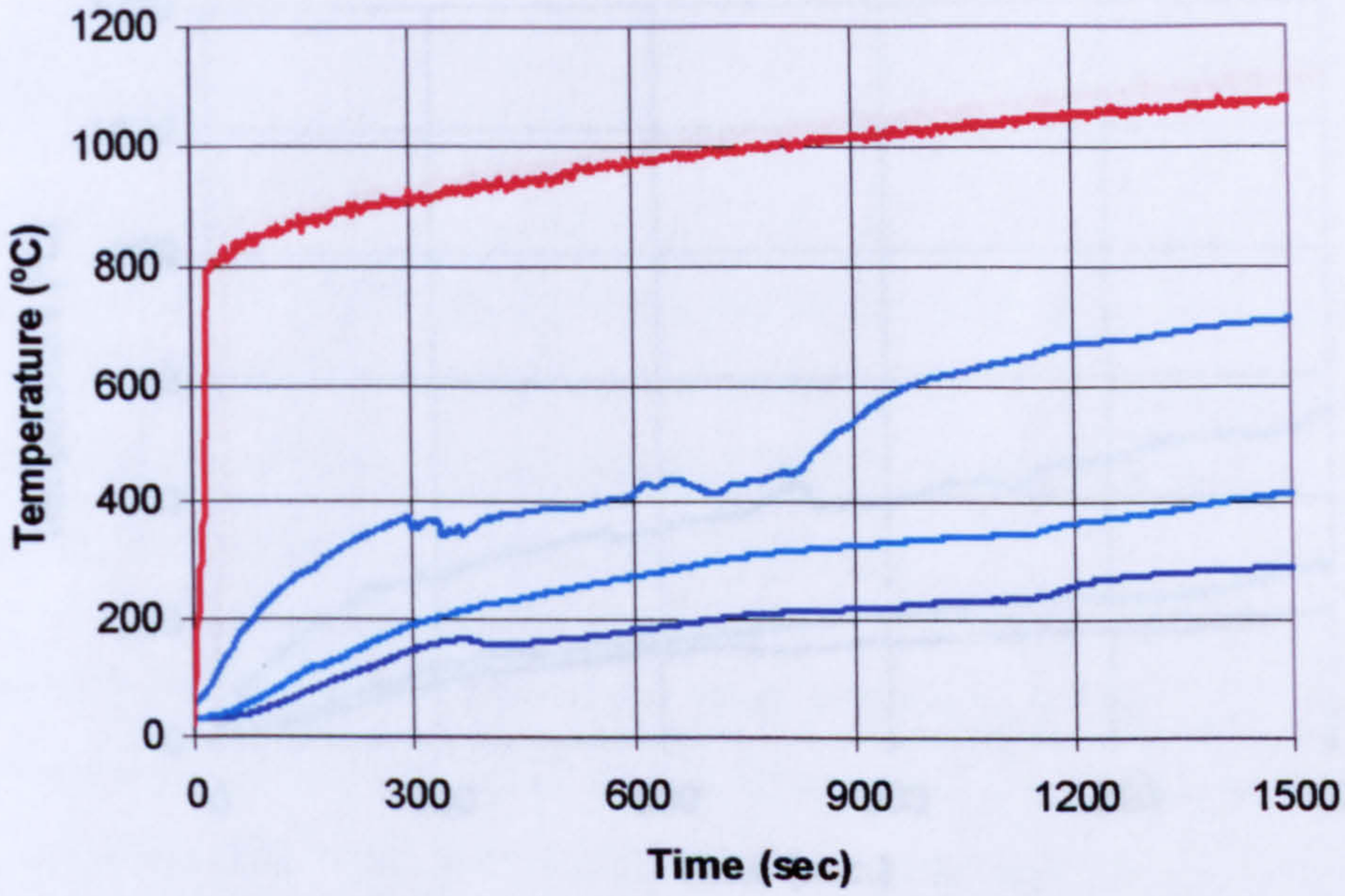

Figure 5.5 Experimental furnace fire test results for vinyl ester/glass woven roving laminated panel ($V_f = 49\%$).

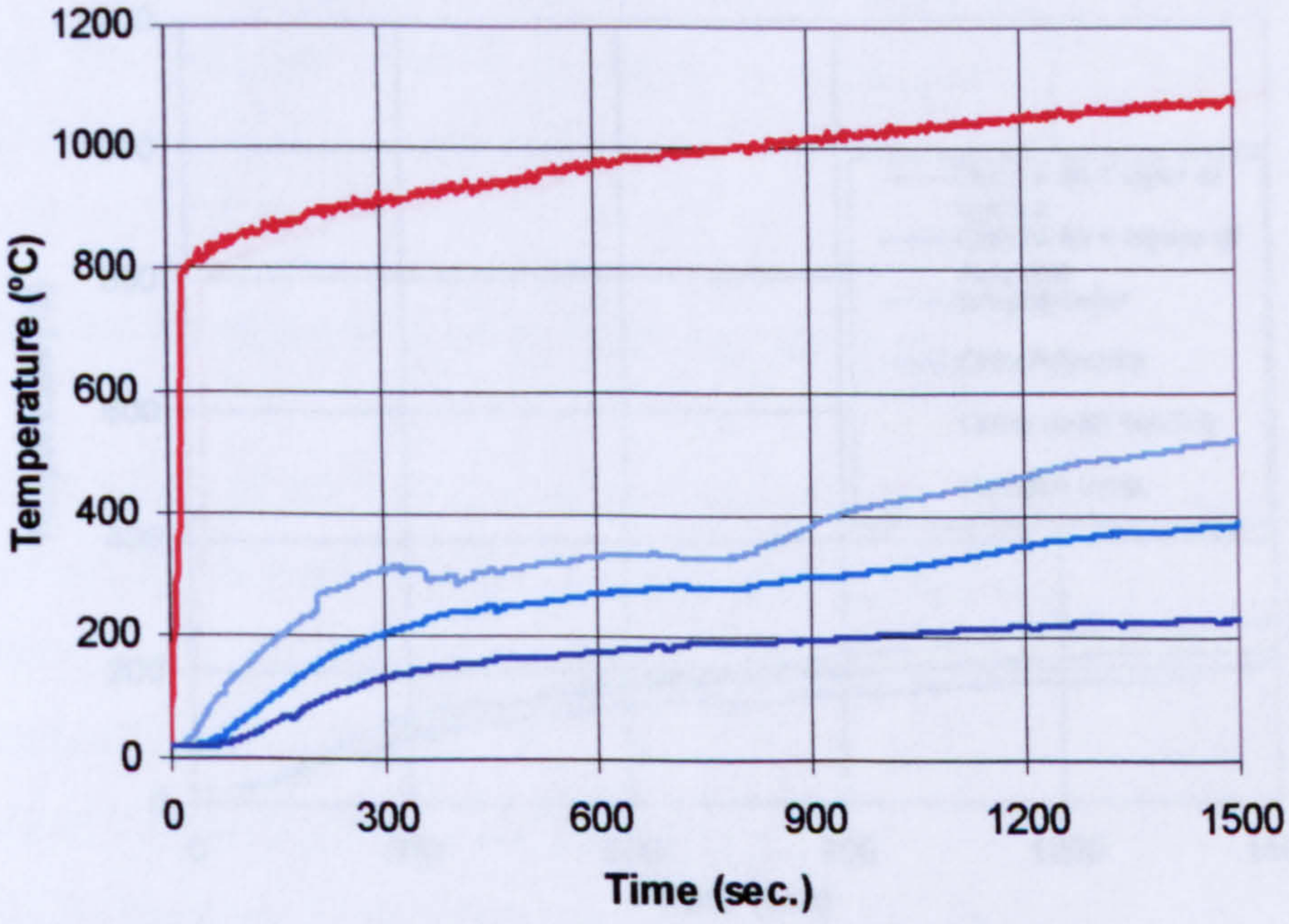

Figure 5.6 Experimental furnace fire test results for orthophthalic polyester/glass woven roving with %ATH ($V_f = 53\%$).

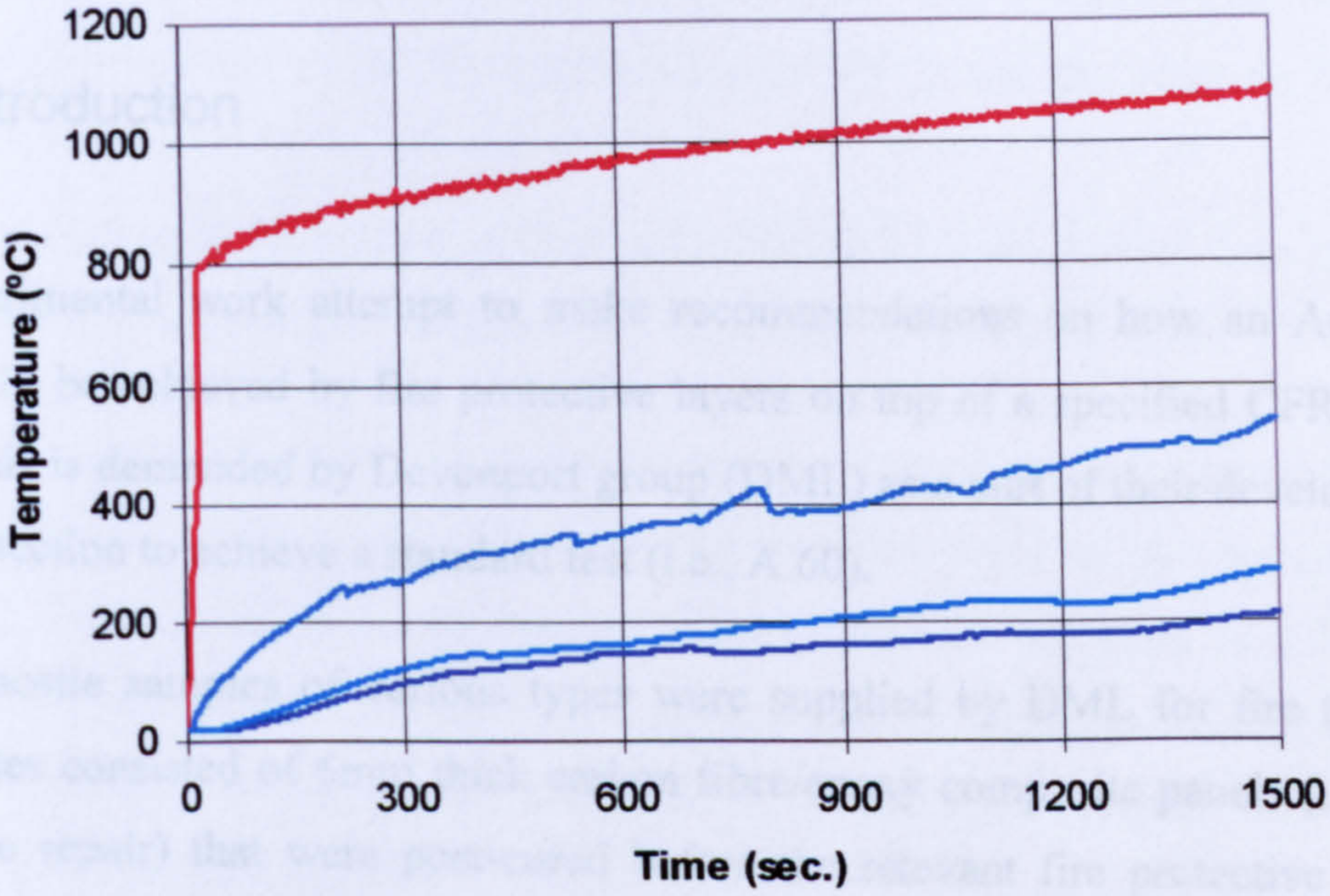

Figure 5.7 Experimental furnace fire test results for orthophthalic polyester/glass WR laminated panel with 2 layers of aluminium foil (V_f = 51%).

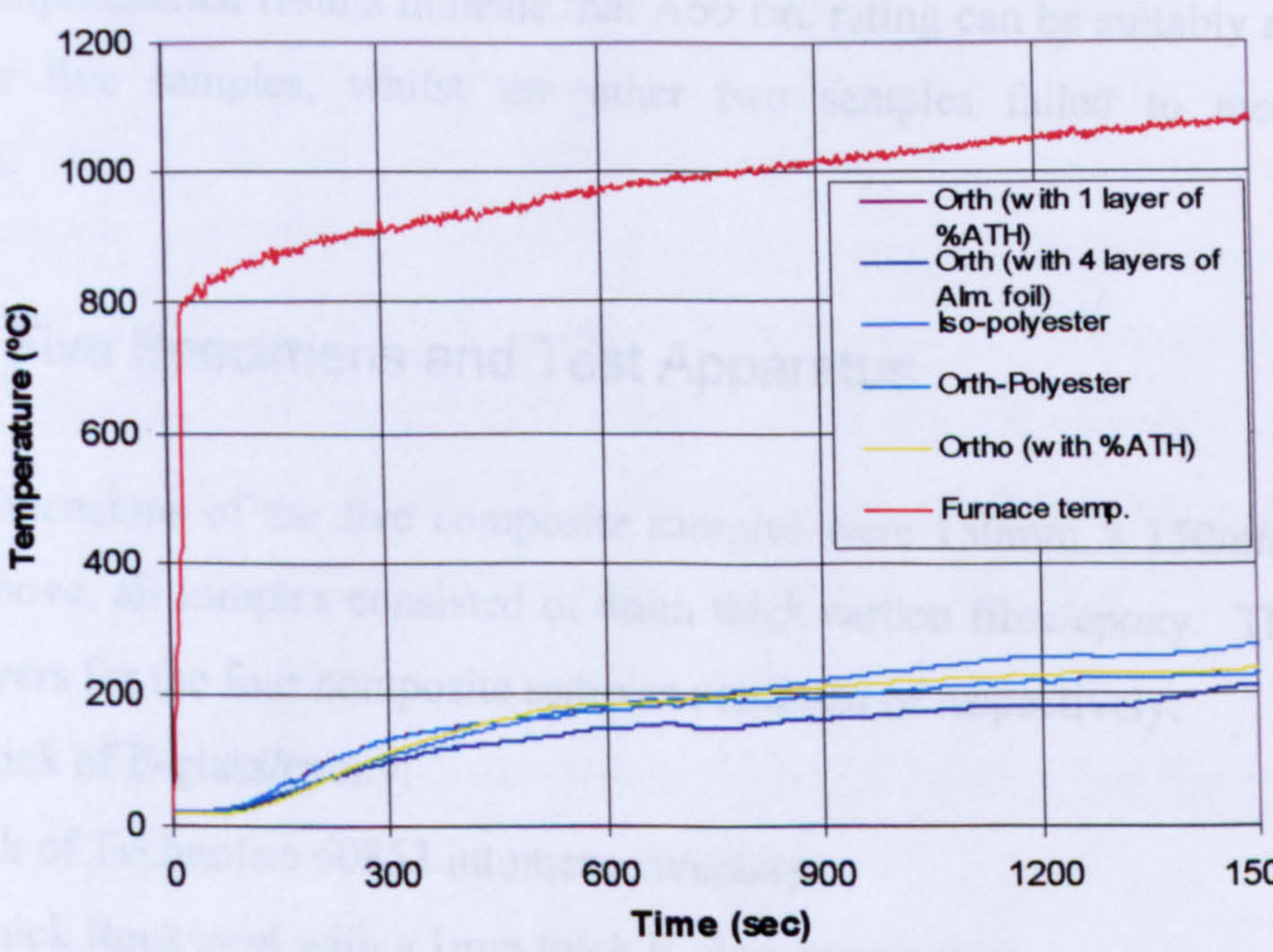

Figure 5.8 Experimental hydrocarbon curve furnace fire tests results of E-glass WR panels for different types of laminate, (i.e. orthophthalic polyester resin, orthophthalic polyester with %ATH, orthophthalic polyester with aluminium foil and isophthalic polyester resin).

5.3 SOLAS Fire Testing on Five Composite Panels

5.3.1 Introduction

This experimental work attempt to make recommendations on how an A60 fire rating could be achieved by fire protective layers on top of a specified CFRP pipe repair. This is demanded by Devonport group (DML) as a part of their development of fire protection to achieve a standard test (i.e., A 60).

Five composite samples of various types were supplied by DML for fire testing. The samples consisted of 6mm thick carbon fibre/epoxy composite panels (i.e., the CFRP pipe repair) that were post-cured before the relevant fire protective layers were applied.

The fire resistance performance of the five composite samples was tested using a small scale fire test furnace according to the standard 'SOLAS' time-temperature curve. The experimental results indicate that A60 fire rating can be suitably met by three of the five samples, whilst the other two samples failed to meet the requirements.

5.3.2 The Five Specimens and Test Apparatus

The panel dimensions of the five composite samples were 150mm × 150mm. As mentioned above, all samples consisted of 6mm thick carbon fibre/epoxy. The fire protective layers for the four composite samples consisted of respectively:

(1) 20 mm thick of E-glass/epoxy;

(2) 4mm thick of Technofire 60853 intumescent/epoxy;

(3) 100mm thick Rockwool with a 1mm thick E-glass/epoxy skin;

(4) 35mm thick syntactic phenolic foam with 5mm thick E-glass/phenolic skin;

(5) 40mm thick of wool + 0.5mm thick Unifram.

The total thickness, therefore, for each of the five composite panels tested was 26mm, 10mm, 106mm, 46mm, and 46.5mm respectively.

Two welded tip glass fibre insulated thermocouples of type K were installed before fire testing on each of the five samples to measure the temperatures of the samples: one at the interface of the CFRP/protection layers (INT), and the other on the cold face (CF).

Before fire testing in each case, a thermocouple (INT) was inserted into position through a hole of 6mm depth vertical to the back face of the CFRP layer.

One type N mineral insulated thermocouple was positioned inside the small furnace 10mm away from the front face of the samples to measure the furnace temperature. During fire testing the measured furnace temperature was fed back to a PC and compared to the standard SOLAS curve, for the control of furnace conditions by varying the gas flow to the furnace main burner. A computer program was written using Lab View for this purpose.

The small furnace used is a standard gas heated oven modified to meet the requirements of the specified fire testing and was fuelled by the main natural gas supply.

Originally, the refractory lined door frame of the furnace allowed test panels of dimensions 300mm × 170mm to be clamped securely into place and exposed to the required temperature/time curve. The door frame was then modified to keep a steel frame of dimensions 160 × 160 mm in place, with the opening dimensions being 130mm × 130mm. A panel sample of dimensions 150mm × 150mm could be then tightly inserted into the steel frame for fire testing by insulating a thick layer of Kaowool material around the four sides of the panel to be tested.

5.3.3 Thermal Boundary Conditions on Cold Face of the Samples and A60 Requirements.

It was agreed with DML that the cold face of the samples (i.e. the cold face of the CFRP panels) during fire testing would be open to the surroundings. Free radiation plus and natural convection were the thermal boundary conditions applied to the cold face of the composite samples during testing. Figure 5.9 shows E-glass/epoxy composite panel at the end of the fire testing.

The A60 requirements for fire-resisting structural divisions under the Provisions of the 1974 SOLAS Convention state that "they should have thermal properties such that the average temperature on the unexposed side will not rise more than 139°C above the original temperature, nor will the temperature at any one point, including any point, rise more than 180°C above the original temperature during the appropriate fire protection time", and A60 means that the "appropriate fire protection time" is 60 minutes.

The SOLAS time-temperature curve is defined by the following equation:

$$T = 345 \log_{10}(8t + 1) + To \tag{5.2}$$

where t is the time (in: minutes) and T_0 is the ambient temperature (in: °C).

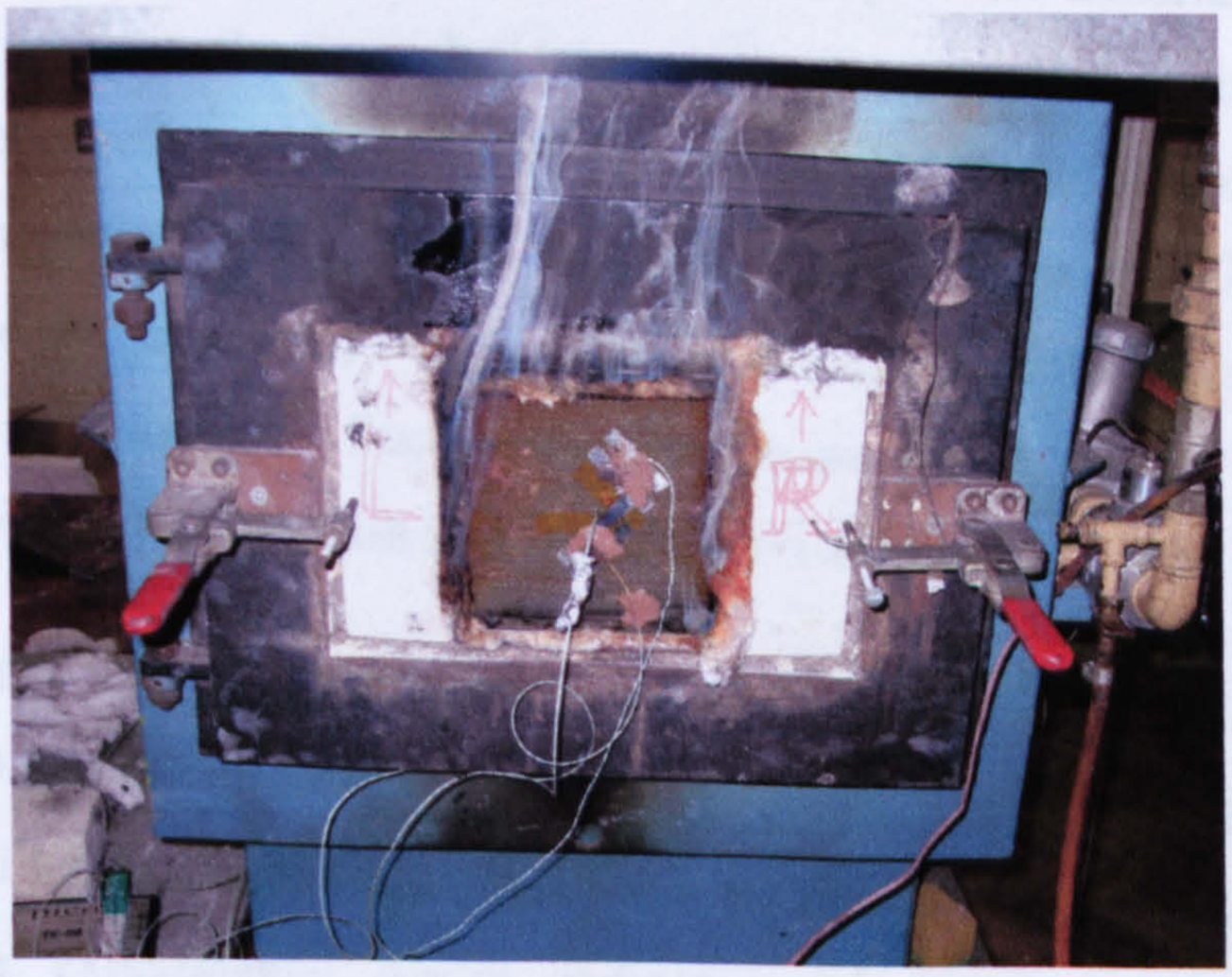

Figure 5.9 Fire testing on 20mm thick of E-glass/epoxy at the end of 45 minutes of fire testing.

5.3.4 Experimental Results for 5 DML Composite Panels

The measure temperature profiles from the fire testing of the 4 of the samples together with the standard SOLAS curve are shown in Figs. 5.10 to 5.13. The initial room temperatures during the tests were between 21-24°C.

It can be seen from Figs. 5.10 and 5.13 that the measured furnace temperatures in general follow the standard SOLAS time-temperature curve quite closely. At some moments, differences between them are clearly seen, as in the case of figure 5.10 which was caused by flash-over from the hot surface of the sample during the test. Effects caused by flash-over are, in general, only local, but would affect the furnace temperature control process. In case of the test on specimen #2 (i.e. 6mm carbon fibre/epoxy +4mm thick of Technofire 60853 intumescent/epoxy), the test had to be stopped after 32 minutes when it was found that very severe material expansion of the protection layer in the through-thickness direction resulted in that part of the protection layer together with the CFRP panel being out side of the protection band of Kaowool insulating layers around the four sides of the sample, leading to hot gases generated due to decomposition escaping directly from the sides (not the cold face) into the surroundings. Such a situation meant that it was no longer a one-dimensional thermal transfer case and any further results would not be valid.

The detailed fire resisting performance of the specimen #1 (i.e 6mm carbon fibre/epoxy+20 mm thick of E-glass/epoxy) is shown by the data listed in Table 5.3. If the measured temperatures are regarded as averages on the unexposed face of the specimens, the experimental results indicated that specimen #1 meets A30 requirements only. The performance of specimen #3 meets A60 requirements. To just meet A60 requirements, the thickness of the Rockwool layer might be largely reduced. No severe flash-over effects were found during the test.

Also, the experimental results show that the thermal response behaviour of samples #4 (i.e. 6mm carbon fibre/epoxy +35mm thick syntactic phenolic foam with 5mm thick E-glass/phenolic skin) and #5 (i.e. 6mm carbon fibre/epoxy +40mm thick of wool + 0.5mm thick Unifram) meets A60 requirements. No flash-over effects were found during the test.

A lot of strong explosive cracking noises were heard during the fire testing. Material expansion in the through-thickness direction of the sample was also observed. A simple holding support was applied to keep the specimen in place.

Table 5.3 The measured fire-resisting performance.

Time to reach 160°C (min)	Temp. on the CF (in: °C)	Temp. on the INT (in: °C)
Sample #1 (i.e. 6mm carbon fibre/epoxy+20 mm thick of E-glass/epoxy)		
32.6	160	191
38.0	180	217
40.9	190	230
44.1	200	243
Sample #3 (i.e. 6mm carbon fibre/epoxy +100mm thick Rockwool with a 1mm thick E-glass/epoxy skin)		
30	29	32
40	37	44
50	53	67
60	70	86
Sample #4 (i.e. 6mm carbon fibre/epoxy +35mm thick syntactic phenolic foam with 5mm thick E-glass/phenolic skin)		
30	27	28
40	34	38
50	45	50
60	58	67
Sample #5 (i.e. 6mm carbon fibre/epoxy +40mm thick of wool + 0.5mm thick Uniform).		
30	91	100
40	110	123
50	136	146
60	159	170

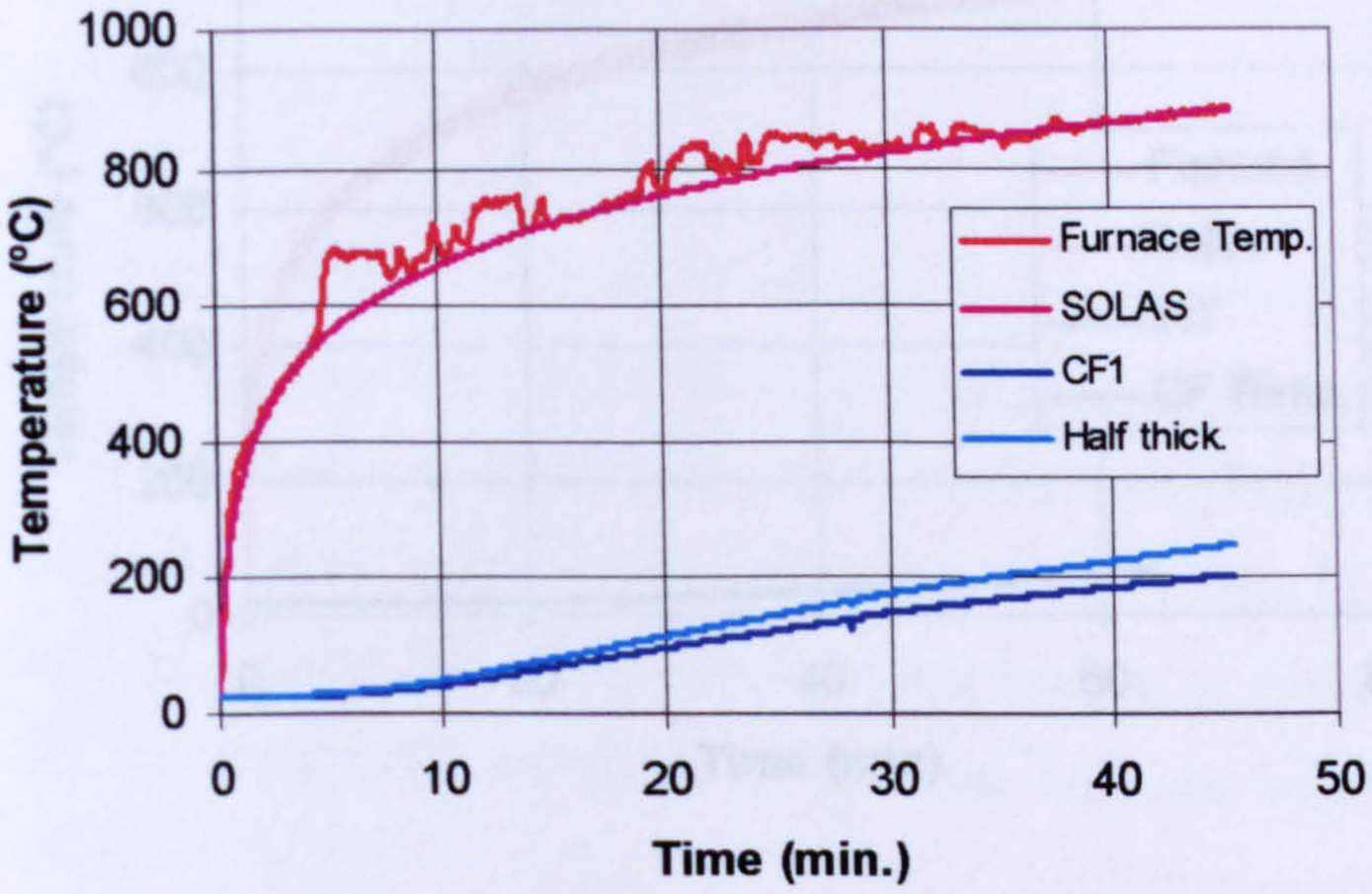

Figure 5.10 Measured temperature profiles of panel #1 for the first 45 minutes

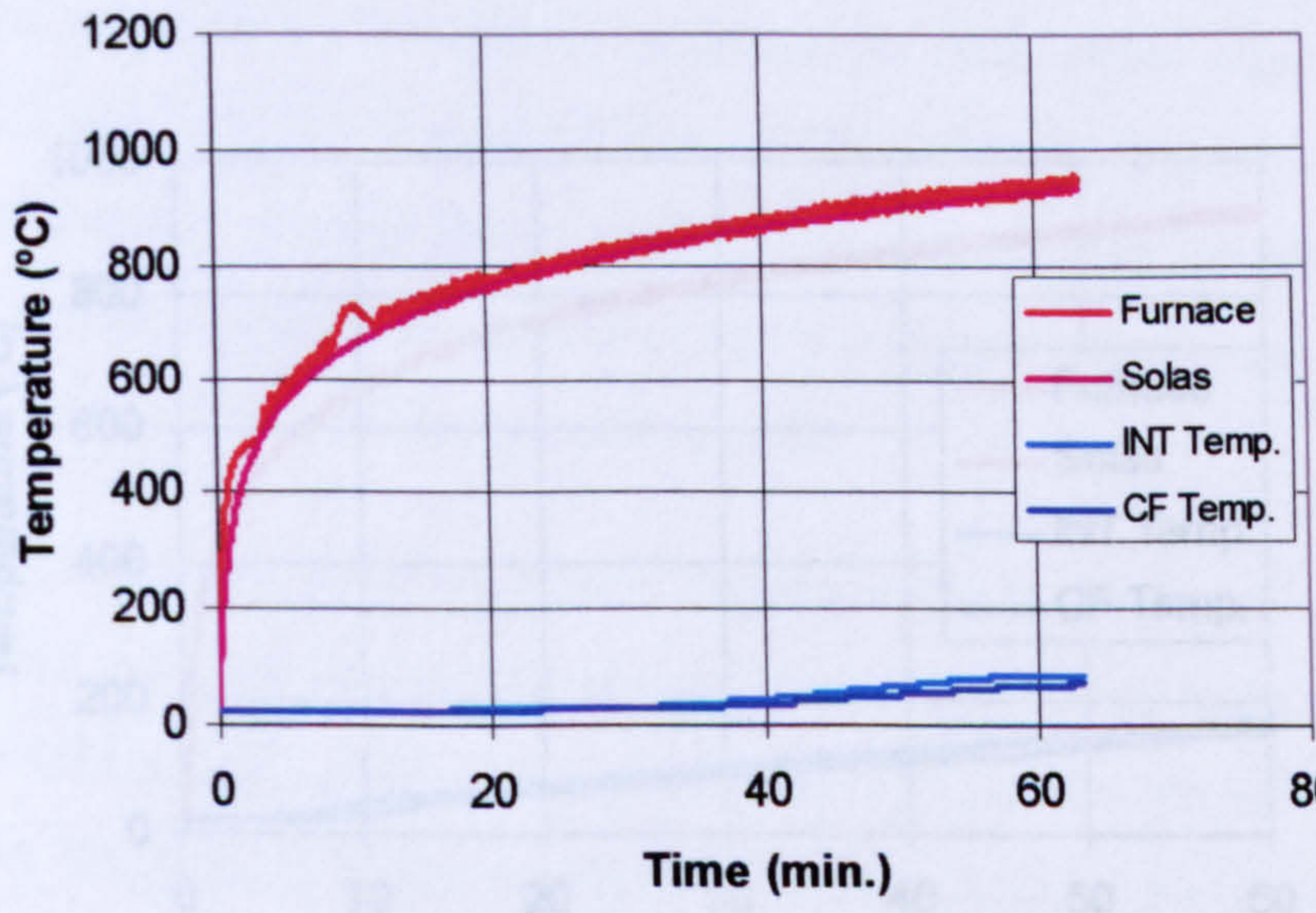

Figure 5.11 Measured temperature profiles of specimen #3 for the first 63 minutes

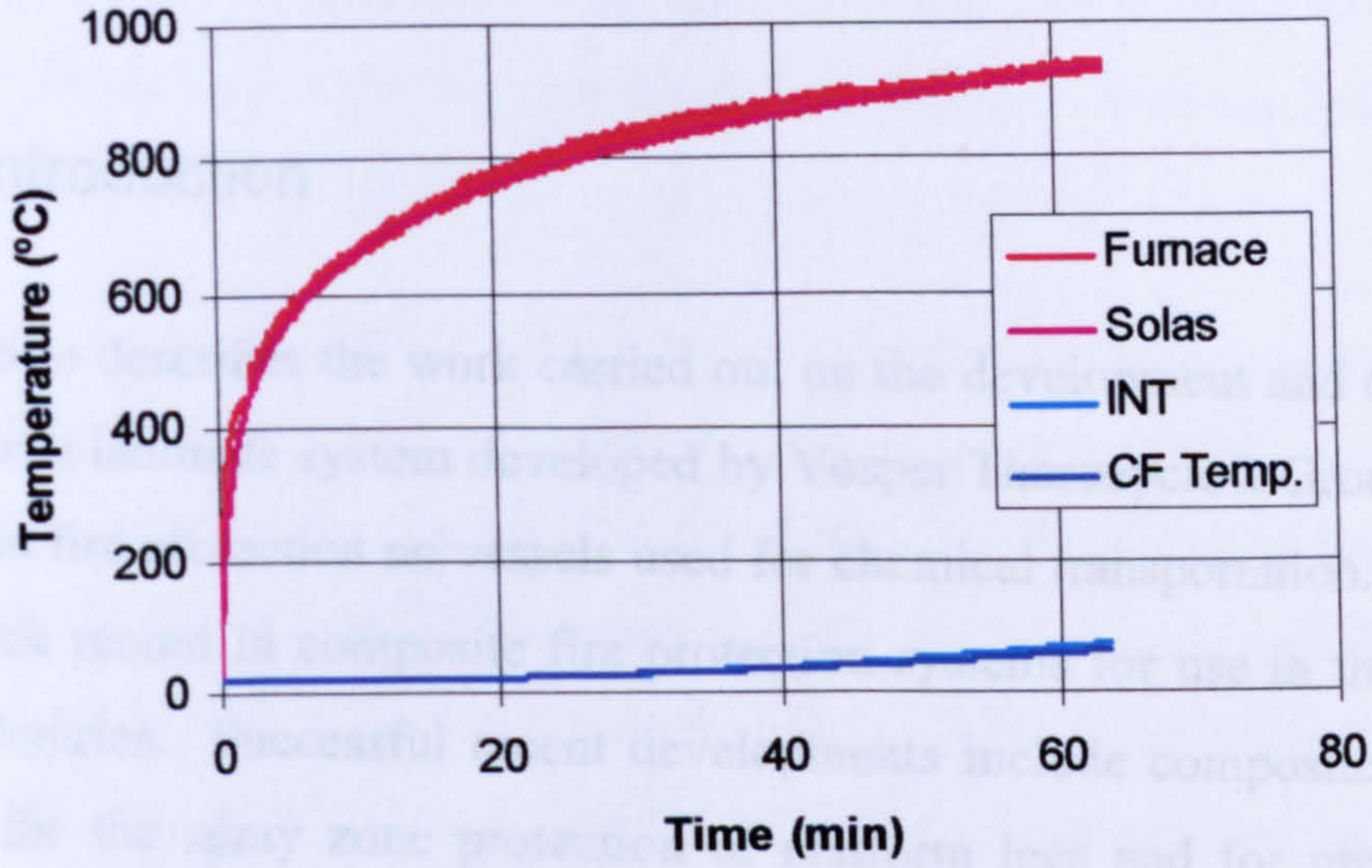

Figure 5.12 Measured temperature profiles of specimen #4 for the first 63 minutes

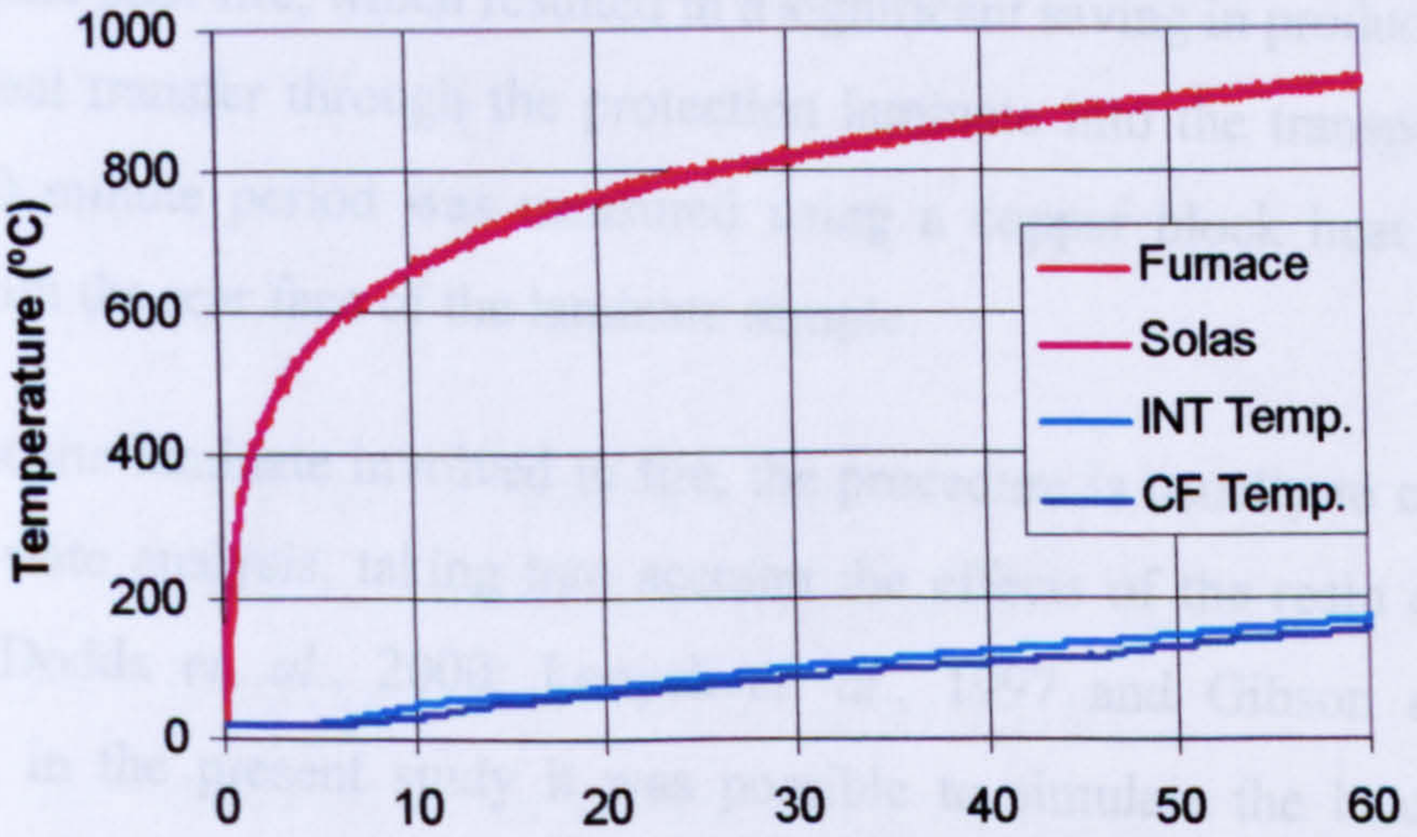

Figure 5.13 Measured temperature profiles of specimen #5 for the first 63 minutes

5.4 Qualification of the Thermal Performance of Composite Fire Protection Laminates

5.4.1 Introduction

This section describes the work carried out on the development and qualification of a composite laminate system developed by Vosper Thorneycroft Group Plc (VT). to be used in fire protection on vessels used for chemical transportation. VT (UK) Ltd has a track record in composite fire protection systems for use in the offshore and other industries. Successful recent developments include composite encapsulation systems for the spray zone protection of platform legs and for pressurised risers (Gibson, 2000).

The worked involved a performance-based approach in which specially developed laminates were subject to a heat flux representative of the type of fire that was demonstrably in excess of the design conditions. The design conditions refer to the behaviour of a cylinder with heat protection in place, in a 30 minute full-scale pool fire.

In the qualification tests a small-scale calibrated propane burner was used to replace the full-scale pool fire, which resulted in a significant saving in product development costs. Heat transfer through the protection laminate into the transportation vessel over a 30 minute period was measured using a copper block heat flux meter in contact with the rear face of the laminate sample.

For composite laminate involved in fire, the procedure is usually to carry out a full unsteady state analysis, taking into account the effects of the resin decomposition process (Dodds *et. al.*, 2000; Looyeh *et. al.*, 1997 and Gibson *et. al.*, 2003). However, in the present study it was possible to simulate the heat transmission behaviour of the laminate with a simple unsteady state heat transfer analysis of the type generally applied to materials that do not decompose. This leads to a relationship that can be used in the design of a wider range of lightweight fire protection systems.

5.4.2 Laminate Development

The transportation of hazardous chemical species as gases, liquid or solids in sealed metallic containers usually requires a full risk analysis. Such analysis usually takes into account scenarios involving fire.

According to the standard IAEA fire-test conditions, with the insulating system fitted, the specification requirements of composite laminate for protecting the type of cylinder in question were to limit to 50% as far possible the heat transfer coefficient (HTC) and the average heat flux (q) over the whole cylinder area into an existing class of widely used cylindrical vessels (i.e. without insulation) during a 30 minute pool fire, which should also be easily and frequently removed for handling and processing operations.

The laminate thickness was limited to 7mm, which is much thinner than most previously used fire protection laminates. The testing programme developed was therefore aimed at representing whether the required levels of fire protection and integrity during fire could be achieved.

For design purposes and according to the IAEA standard fire test conditions, the possible heat flux into an unprotected vessel in a pool fire would be calculated from the following relationship (IAEA Standard fire test conditions):

$$q = \sigma \varepsilon_{Fire} \varepsilon_{Cylinder} \left(T_{Fire}^4 - T_{Cylinder}^4\right) + h_{Cylinder} \left(T_{Fire} - T_{Cylinder}\right) \qquad (5.3)$$

where:

q = the heat flux into the cylinder, W/m^2

σ = the Stefan-Boltzmann Law constant = 5.67 x 10-8, $W/m^2{}^oK^{-4}$

ε_{Fire} = emissivity of the fire, being equal to 0.9

$\varepsilon_{cylinder}$ = emissivity of the cylinder being equal to 0.8

$h_{cylinder}$ = convective heat transfer coefficient from the fire to the cylinder

= $10 W/m^2 {}^oK$

T_{Fire} = fire temperature

$T_{Cylinder}$ = cylinder temperature.

In numerical terms, therefore:

$$q = 4.0824 \times 10^{-8} \times \left(T_{Fire}^4 - T_{Cylinder}^4\right) + 10\left(T_{Fire} - T_{Cylinder}\right) \qquad (5.4)$$

Equation (5.3) can be seen to contain terms representing both the radiation and convective components; however, the radiation term dominates.

Although pool fires vary in intensity according to weather and other conditions, a fire temperature of 800°C (1,073°K) was assumed. It is also assumed that the cylinder temperature at the start of exposure is no lower than 38°C. The heat flux into an unprotected cylinder under these conditions from Eqn. (5.4), is 61kWm^{-2}, and the corresponding heat transfer coefficient, therefore, is 81W m^{-2} °K^{-1}. To qualify as fire protection laminate, therefore, the overall heat flux and the heat transfer coefficient into the vessel should be no higher than 50% of these values during a 30 minute exposure to a fire at least as severe as this (i.e. a pool fire).

Because of the surface features mentioned above, it is assumed that the protection laminate would cover only 80% of the surface of the cylinder. So, if the heat transferred through the protection into the cylinder is a proportion, x, of the heat that would be transferred without protection, an overall reduction of 50% would give the condition:

$$0.5 = 0.2 + 0.8\,x, \qquad \text{so } x = 0.375.$$

The target values of heat flux and heat transfer coefficient to qualify the protection laminate are therefore 0.375 of the values mentioned above, (i.e. 22.9kWm^2 and 30.4Wm^{-2} °K^{-1}, respectively). For the protection laminate to qualify, these values should not be exceeded at any point during a 30 minute fire test. This standard was further refined by specifying that the HTC, averaged over any 1 minute period, should not be exceeded during the test.

5.4.3 Experimental Procedure

The qualification measurements of the development laminates were carried out using a 30 minute constant heat flux test. The experimental arrangement is shown in Fig. 5.14. 150 mm square laminates were placed in a steel 'picture frame' that enabled a 100mm square central region to be exposed to a constant heat flux. The purpose of the frame was to minimise any effects due to the burning of volatiles around the edge of the laminate sample. The samples were thermally insulated from the frame by a layer (3mm approximately) of Kaowool.

The composite sample was lightly clamped to the front face of a 72 mm thick copper block which acted as a heat sink or a heat flux meter. The rear surface of the specimen was in contact with one end of the cylinder. The degree of thermal contact between the flat test sample and the copper block was intended to be equivalent to or better than the expected contact between the fire protection and the vessel. It is assumed that, due to curvature, fitting tolerances and surface irregularities, the overall closeness of contact would be less than that encountered here. One run was carried out in which a 1.8mm gap was maintained between the specimen and the block, to simulate the effect of poor thermal contact. The remainder of the exterior of the copper block and the rear face of the sample were insulated with cape board and Kaowool.

It was assumed that, during the test, heat would go into the block only through the 72mm diameter face. In order to quantify the small heat loss through the insulation, a correction was made by carrying out the experiment on Newton's Law of Cooling, in which the block was heated and the front face was insulated, then the system allowed to cooling naturally. This correction was relatively small (i.e. 2°C overall by the end of a typical test).

The front face temperature of the sample was measured during the test with a k-type thermocouple. During the earlier measurements the gas supply was adjusted during each run to keep the front face thermocouple reading a steady value. Later on, however, the gas supply was fixed and not adjusted during the test. In order to examine the effect of varying the hot face temperature, one run was carried out at a

lower hot face temperature (average 788°C) and one at a higher temperature (average 1000°C).

A burner-to-sample distance of 350 mm was used throughout the tests. The fuel supply was adjusted to maintain the desired hot face temperature. For most of the runs the steady state hot face temperature was maintained at a value just below below 1000°C. A net heat flux of 85kWm^{-2} was measured for a front face temperature of 1000°C.

The test duration was 30 minutes, during which the three copper block thermocouples were recorded, along with the front face temperature, at 5 second intervals. There was very little difference between the three copper block sensor temperatures, indicating that the heat flux between the exposed part of the sample and the block was uniform. These three temperatures were therefore averaged when calculating the test results. Experimental scatter was reduced by applying a 5-point mean smoothing formula to the averaged temperatures.

5.4.4 Materials

The laminates tested were all supplied by Vosper Thornycroft. They measured 150mm square by approximately 7mm thick. They all contained principally chopped strand mat reinforcement in some particular grade of orthophthalic polyester resin. Other components (one ply of silica fabric and one of expanded steel mesh) were included to improve mechanical integrity at high temperatures. Also, measurements were made on samples with and without gel-coat.

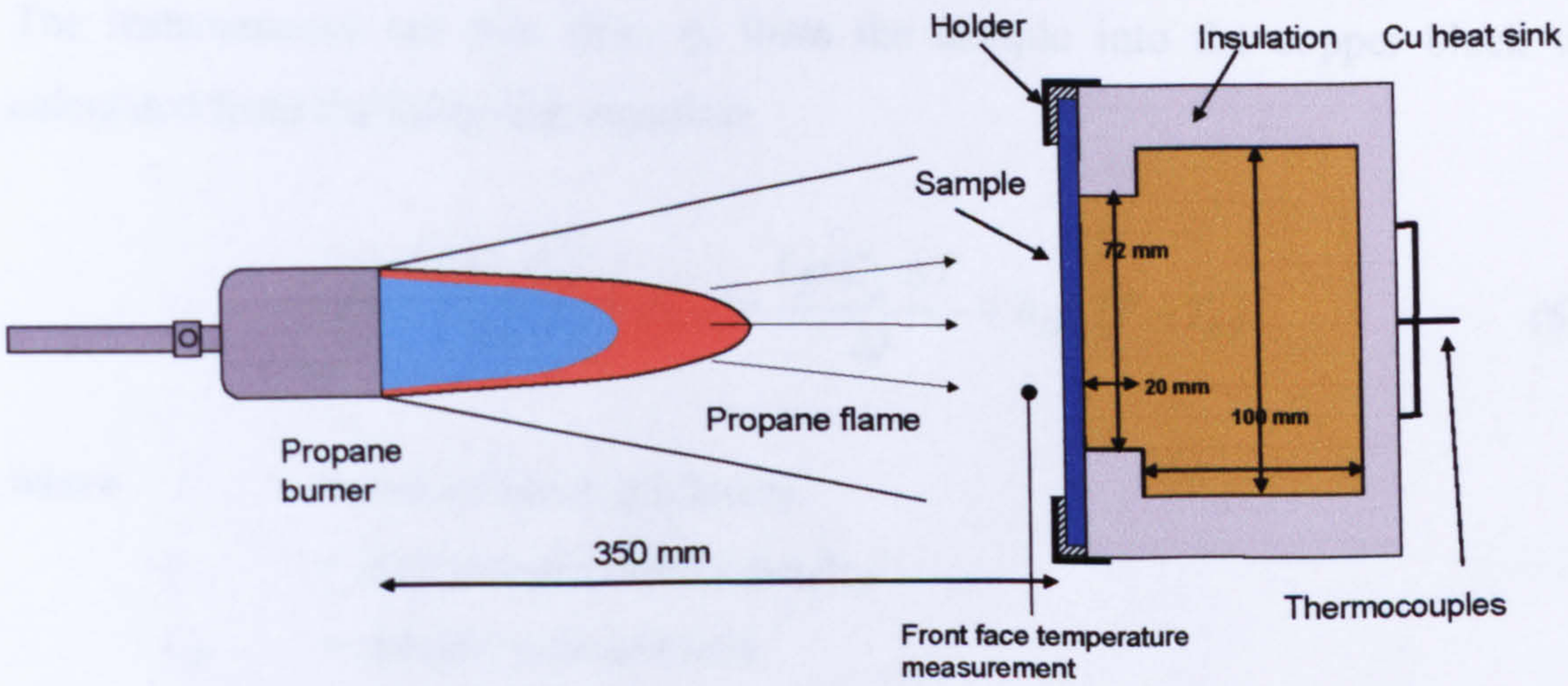

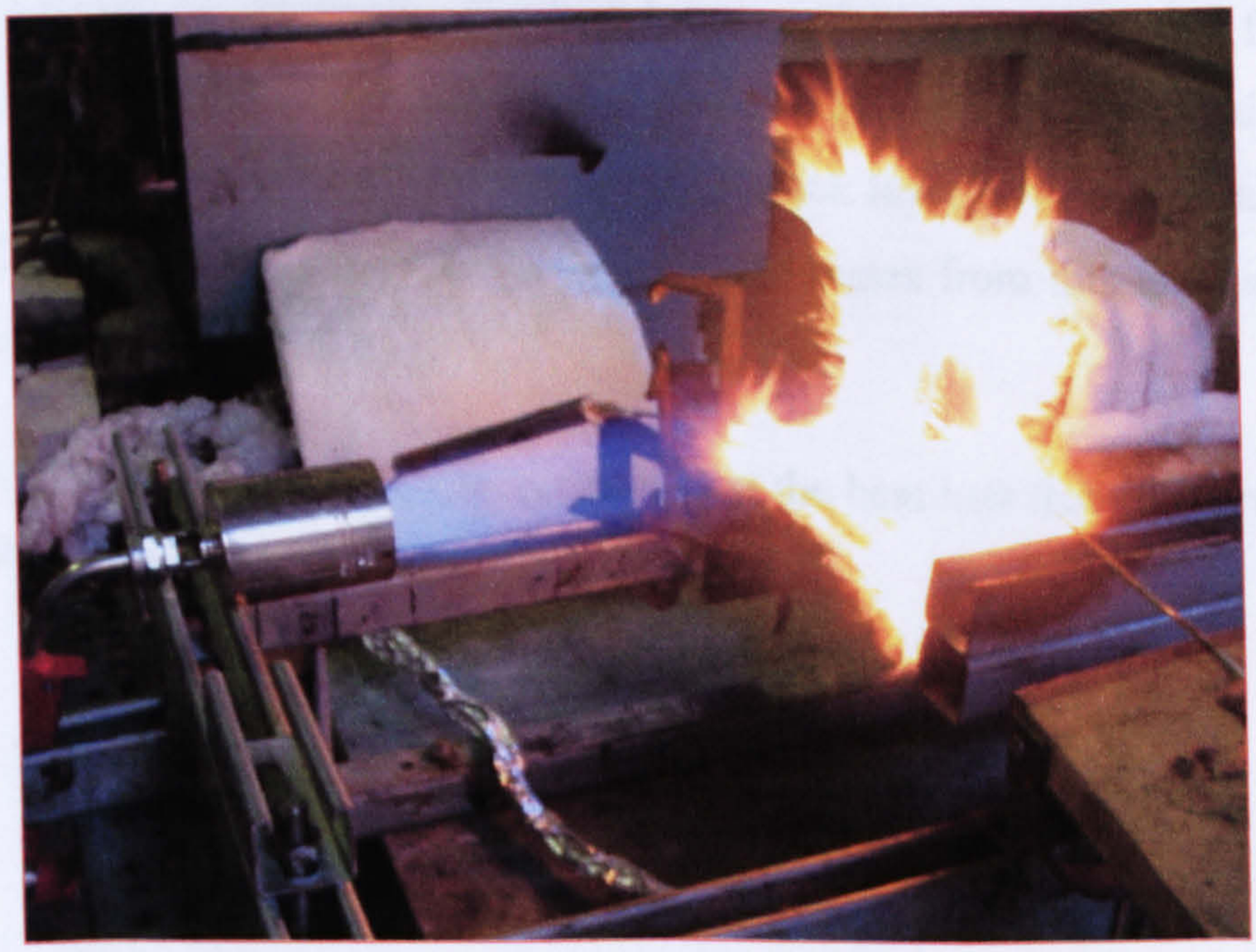

Figure 5.14 Experimental rig used to determine the heat flow into the copper block via the laminate, for a particular hot face temperature.

5.4.5 Rig Calibration and Treatment of Results

The instantaneous net heat flux, q, from the sample into the copper block was calculated from the following equation:

$$q = \frac{l\rho C_p \Delta T}{\Delta t} + q_{Loss} = \frac{l\rho C_p \Delta T}{\Delta t} + h_{Loss}(T - T_0) \qquad (5.5)$$

where l = sink or block thickness

ρ = sink (cooper block) density

C_p = specific heat of block

T, ΔT = sink material temperature, increment

Δt = time increment;

T_o = environmental temperature at rear of rig.

The second term in Eqn. (5.5) (i.e., q_{Loss}) is the correction for the heat losses from the heat sink to the environment. The heat loss transfer coefficient, h_{Loss}, from the block was measured by means of cooling curves. Following a conventional 30 minute heat flux test, the burner was turned off, a thick layer of Kaowool insulation was applied to the front face of the rig to minimise losses from this face, and then the cooling curve was recorded.

During the cooling experiment it was assumed that the heat loss from the sink to the environment was given by:

$$q_{Loss} = l\rho C_p \frac{dT}{dt} = -h_{Loss}(T - T_0) \qquad (5.6)$$

Re-arranging, this gives

$$\int_{t=tR}^{t} dt = -\frac{l\rho C_p}{h_{Loss}} \int_{TR}^{T} \frac{dT}{T - T_0}$$

where T_R is the heat sink temperature at a reference time, t_R. Integrating this gives

$$t - t_R = -\frac{l\rho C_p}{h_{Loss}} ln\left(\frac{T - T_0}{T_R - T_0}\right)$$

which, on re-arranging, becomes

$$\frac{T - T_0}{T_R - T_0} = exp\left(-\frac{h_{Loss}}{l\rho C_p}(t - t_R)\right), \text{ so}$$

$$T = T_0 + (T_R - T_0)exp\left(-\frac{h_{Loss}}{l\rho C_p}(t - t_R)\right) \tag{5.7}$$

Figure 5.15 shows the fitted prediction of Eqn. (5.7), from the cooling curve. This fit was achieved by pinning the curve to the experimental value at a reference time value of 100 minutes. The fit was achieved with a heat transfer coefficient of 10.98 W/m^2°C. Subsequently, the value obtained for the heat transfer loss was then used in the correction term of Eqn. (5.5) for derived the net heat flux from the sample under question into the copper block meter (i.e. .the second term).

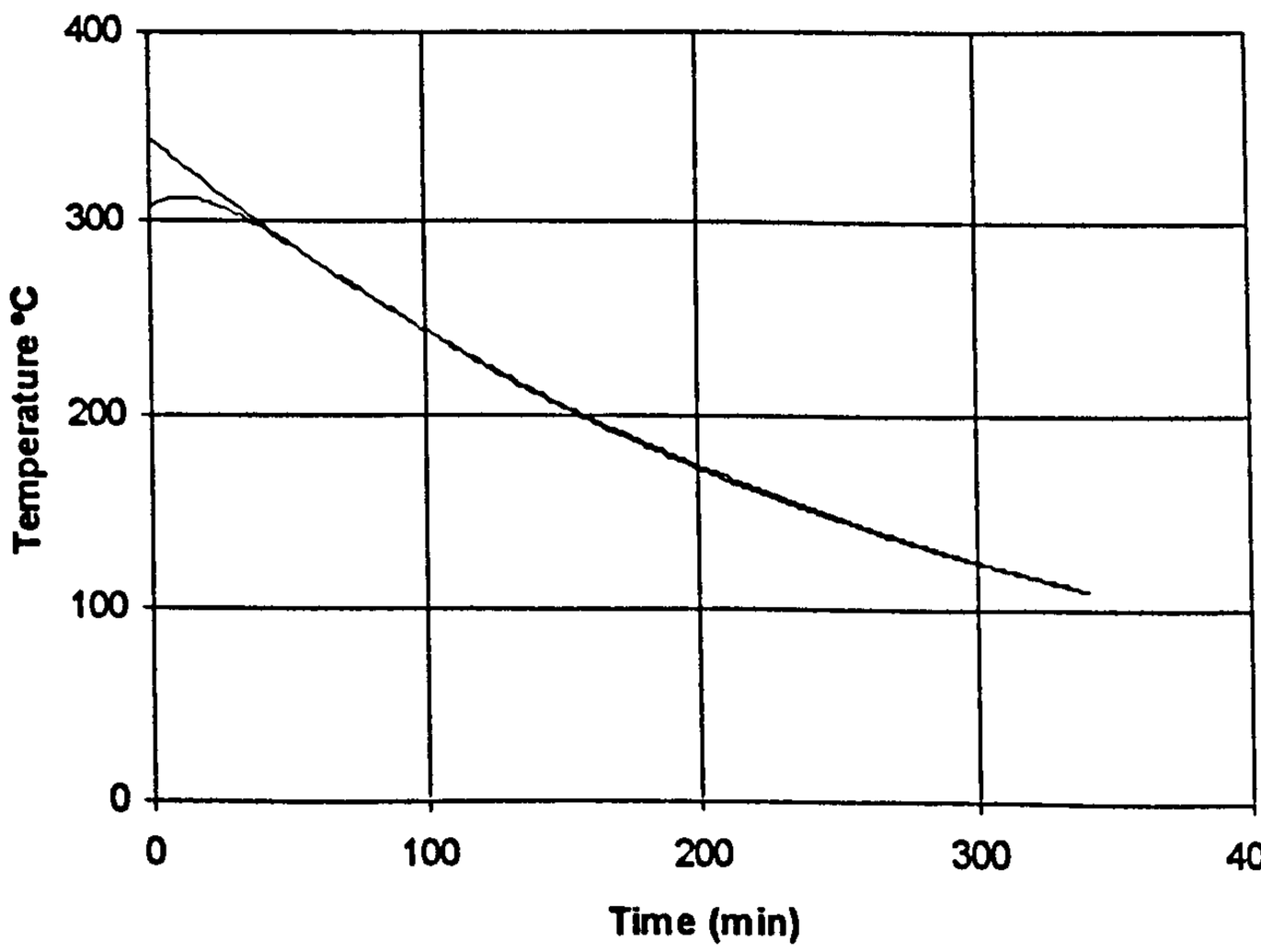

Figure 5.15 Recorded temperatures (blue line) during the heat loss calibration experiment. The model curve (pink) was fitted by pinning the curves at a reference point at 100 minutes.

An 'apparent' overall heat transfer coefficient, h, for fire protection was calculated from the net heat flux value into the copper block, using the relationship

$$h = \frac{q}{T_1 - T} \tag{5.8}$$

where T_1 is the measured hot face temperature, and T is the cold face temperature. This was plotted as a function of time along with the other test results in the accompanying Excel spreadsheet and PowerPoint figures.

In addition, an average heat transfer coefficient for the 30 minute test was calculated by using the average hot and cold face temperatures in Eqn. (5.8).

It was agreed that, for design and qualification purposes, the maximum apparent heat transfer coefficient, rather than the average, would be used. This value, averaged over a period of 1 minute, should not exceed a value of 30.4 $Wm^{-2}°C^{-1}$.

5.4.6 Heat Flux Calibration

The heat flux into the copper block was calibrated for four different hot face temperatures in an experiment involving step changes in the hot face temperature. The results are given in Fig. 5.16, which shows the hot face temperature, the block temperature and the heat flux calculated from the rate of change of block temperature using Eqn. (5.3).

Figure 5.17 shows the heat flux values measured in the calibration test, plotted against the measured hot face temperature. For comparison, a line has been added representing the predictions of the IAEA Pool Fire relationship from Eqn. (5.4). It can be seen that the measured hot face temperature in the burner test needed to produce a particular heat flux is significantly lower (by approximately 100°C in most cases) than the pool fire temperature needed to produce the same flux. The most probable reason for this is that the measured temperature in front of the hot face in the burner test was reduced by the presence of the cool copper block. The copper block had high thermal conductivity and never exceeded a temperature of

160°C in the calibration tests. By contrast, the laminate has a much lower conductivity and will reach higher temperatures.

This effect was counted in test runs 12-17. For these runs the propane flame was adjusted to give a measured hot face temperature of 800°C using the copper heat flux block. The same gas setting was then maintained, without adjustment, in a heat flux test on a laminate specimen. It was found that the measured hot face temperature in the test could exceed the initial 800°C value by up to 100°C. It was therefore concluded that most of the difference between the heat flux vs. hot face temperature curves, and the IAEA Pool fire equation in Fig. 5.17 could be accounted for by this effect. The key factor on which the qualification relies is that the propane burner rig should give a heat flux intensity which is at least as great as that in the IAEA Pool fire. It was therefore decided that, for final qualification purposes, the results of runs 12-17 would be used.

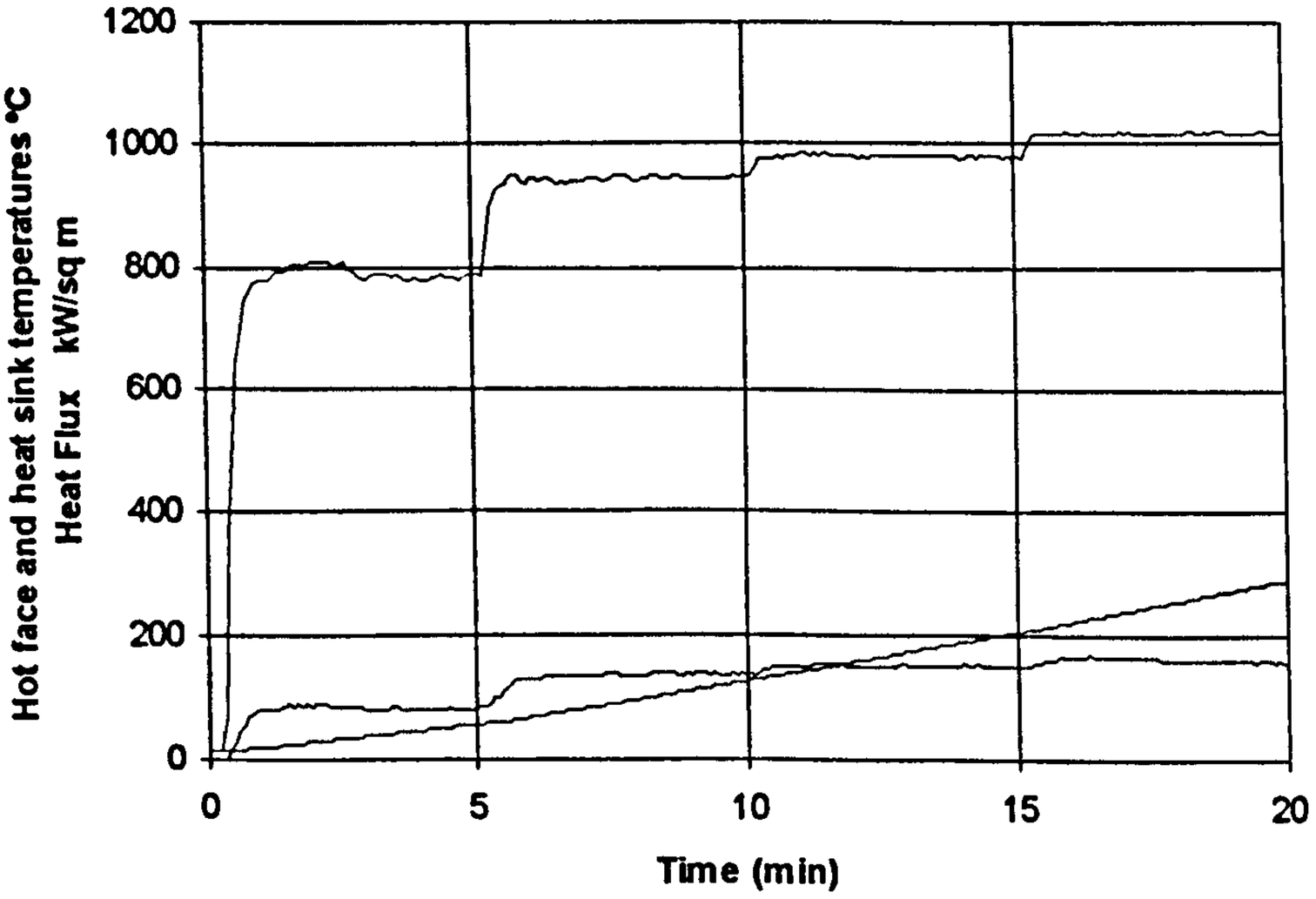

Figure 5.16 Results of the heat flux calibration on the copper block meter, showing the hot face temperature (upper curve), the block temperature (pink) and the calculated heat flux (red).

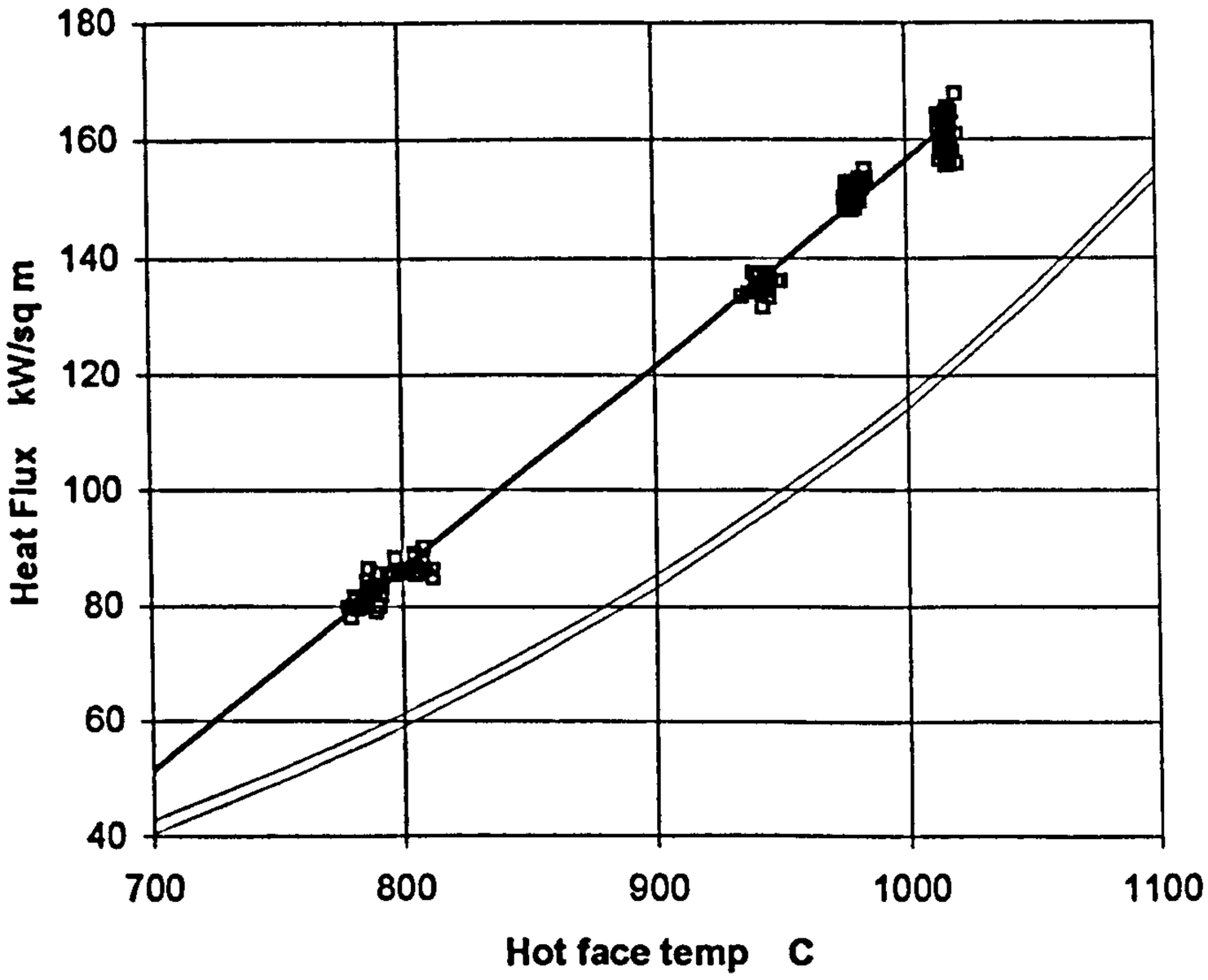

Figure 5.17 Heat flux data plotted against hot face temperature during the copper block calibration test (squares). The predictions of the IAEA pool fire model (Eqn. 5.2), for block temperatures of 38°C (upper curve) and 160°C (lower curve) have been added for comparison.

5.4.7 Results and Discussion

Figures 5.18-5.20 shows an example of a set of data from the test results. The hot face temperature rises to an almost constant value within a very short time after lighting the burner. The majority of the curves of copper block temperature vs. time were similar in appearance to this. In most tests, following a short initial delay there was a transient region, presumably corresponding to the removal of the resin from the laminate. This usually occurred during the first few minutes of the test. Following this, the copper block temperature rose smoothly during the remainder of the test period.

The maximum heat flux occurred close to or at the end of the test. Comparing Figs. 5.18 and 5.19, it can be seen that the heat flux for the steel mesh reinforced samples was slightly greater than those for the plain laminates due, probably, to the heat conducted by the steel. As already mentioned, the heat sink temperature itself rises

fairly steadily, with relatively little experimental noise. In some of the runs, however, more noticeable scatters can be seen, probably corresponding to thermally induced movements of the specimen and other events such as delamination or cracking, and the differentiation process used to calculate heat flux from the block temperature rise.

Comparing the results in Fig. 5.20, with the earlier ones obtained at a higher hot face temperature, it can also be seen that heat flux increases with increasing hot face temperature. Figure 5.21 shows an example of one of the qualification tests in which the hot face temperature was set at 800°C with the thermocouple in contact with the copper block. The general form of the results is similar to the others, but the hot face temperature can be seen to rise significantly above 800°C when testing the laminate specimens. This procedure was used in tests Q-12 to Q-17 for the final qualification.

Table 5.4 shows a summary of all the results, expressed as maximum heat flux. It can be seen in tests Q-12 to Q-17 that there is no systematic difference between the samples with and without gel-coat. Because these tests were carried out under conditions demonstrated to have been equivalent to or more damaging than a pool fire, they were chosen for use in the final case for qualification.

Table 5.5 shows the qualification values of heat transfer coefficient calculated from results Q-12 to Q17, assuming an overall temperature difference of 762°C in each case, as discussed previously. The mean value of HTC from these six results is 24.1 $Wm^{-2}K^{-1}$. The 95% upper confidence limit on the mean is 26.4$Wm^{-2}K^{-1}$ and the 95% upper confidence limit on any individual measurement is 29.8$Wm^{-2}K^{-1}$, both of which are lower than the qualification criterion of 30.4$Wm^{-2}K^{-1}$.

In terms of integrity, the laminates performed well. Between 10 and 50 seconds after propane ignition, depending on the hot face temperature, the decomposition products of the resin ignited and the surface of the laminate exhibited flashover.

Figure 5.22 shows the front and rear faces of a test specimen following cooling after the test. The front face still shows traces of the gel coat pigment, and much of the chopped strand reinforcement is visible and intact, though friable. Resin and char appear to have been removed from the front surface layers by heat and oxidation,

leaving a residue of clean glass. The conditions of Fig. 5.22, however, were above the design temperature.

Table 5.4 Summary of qualification test results.

Sample	Details	Max. HF Temp.°C	Max. q kWm^{-2}	Sample	Details	Max. HF Temp.°C	Max. q kWm^{-2}
Q-1	Laminate	980	22.5	Q-9	Laminate	791	18.2
Q-2	Laminate	944	27.0	Q-10	Lam. w. mesh, with 1.2mm gap.	795	14.1
Q-3	Laminate w. mesh	966	35	Q-12	Laminate w. mesh	871	17.6
Q-4	Laminate w. mesh	966	35.2	Q-13	Laminate with mesh	883	17.8
Q-5	Laminate	958	32.5	Q-14	Laminate w. mesh	868	19.0
Q-6	Laminate w. mesh	980	33.9	Q-15	Laminate/mesh no gel coat	852	19.9
Q-7	Laminate	960	28.2	Q-15	Laminate/mesh no gel coat	852	19.9
Q-8	Laminate w. mesh	802	18.7	Q-16	Laminate/mesh no gel coat	852	15.8
				Q-17	Laminate/mesh no gel coat	833	20.3

Table 5.5 Qualification values of heat transfer coefficient.

Sample	Details	Max. H. T. C. (kWm^{-2} °C^{-1})
Q-12	Laminate w. mesh	23.1
Q-13	Laminate w. mesh	23.4
Q-14	Laminate w. mesh	24.9
Q-15	Laminate/mesh no gelcoat	26.1
Q-16	Laminate/mesh no gelcoat	20.7
Q-17	Laminate/mesh no gelcoat	26.6

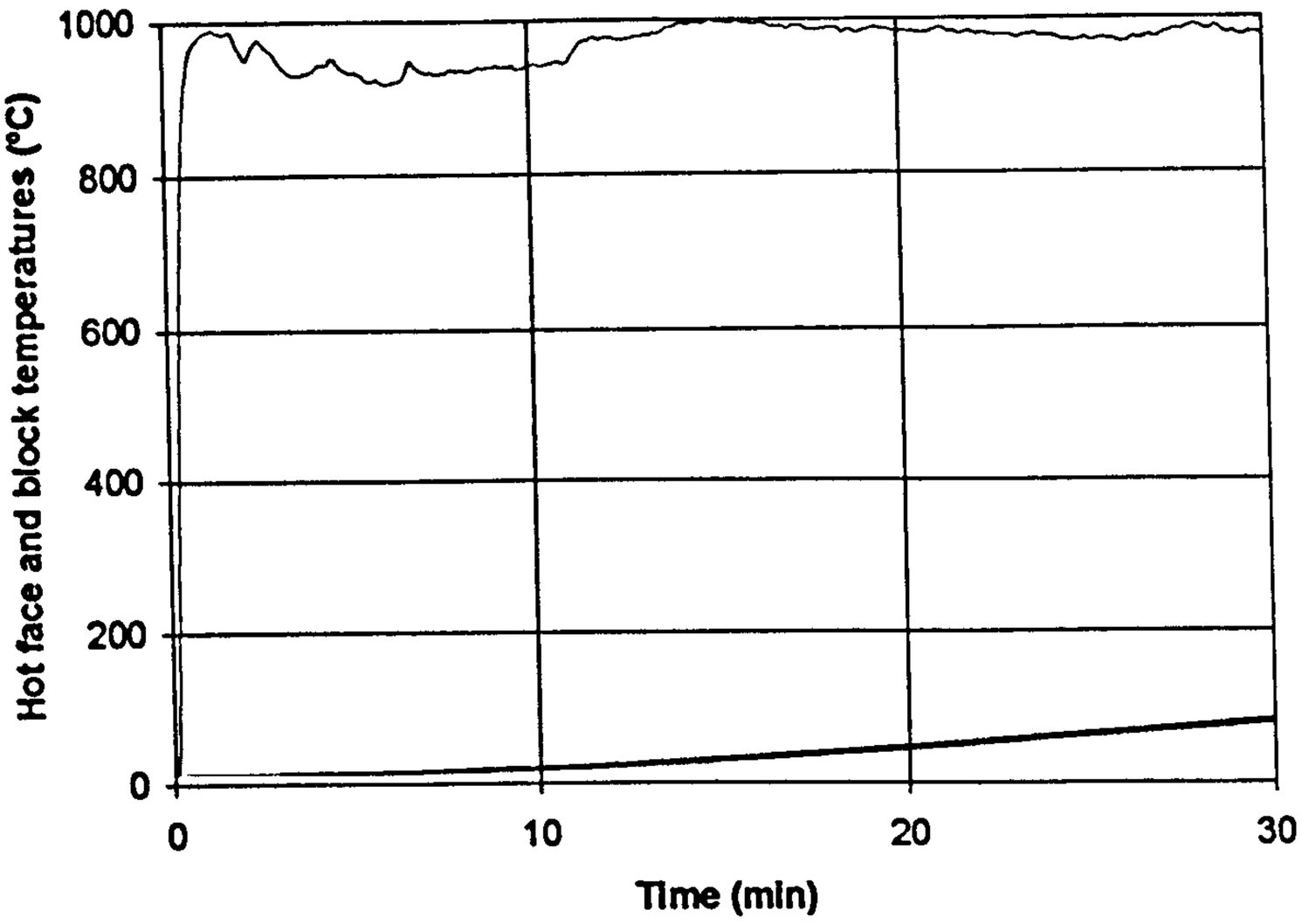

(a)

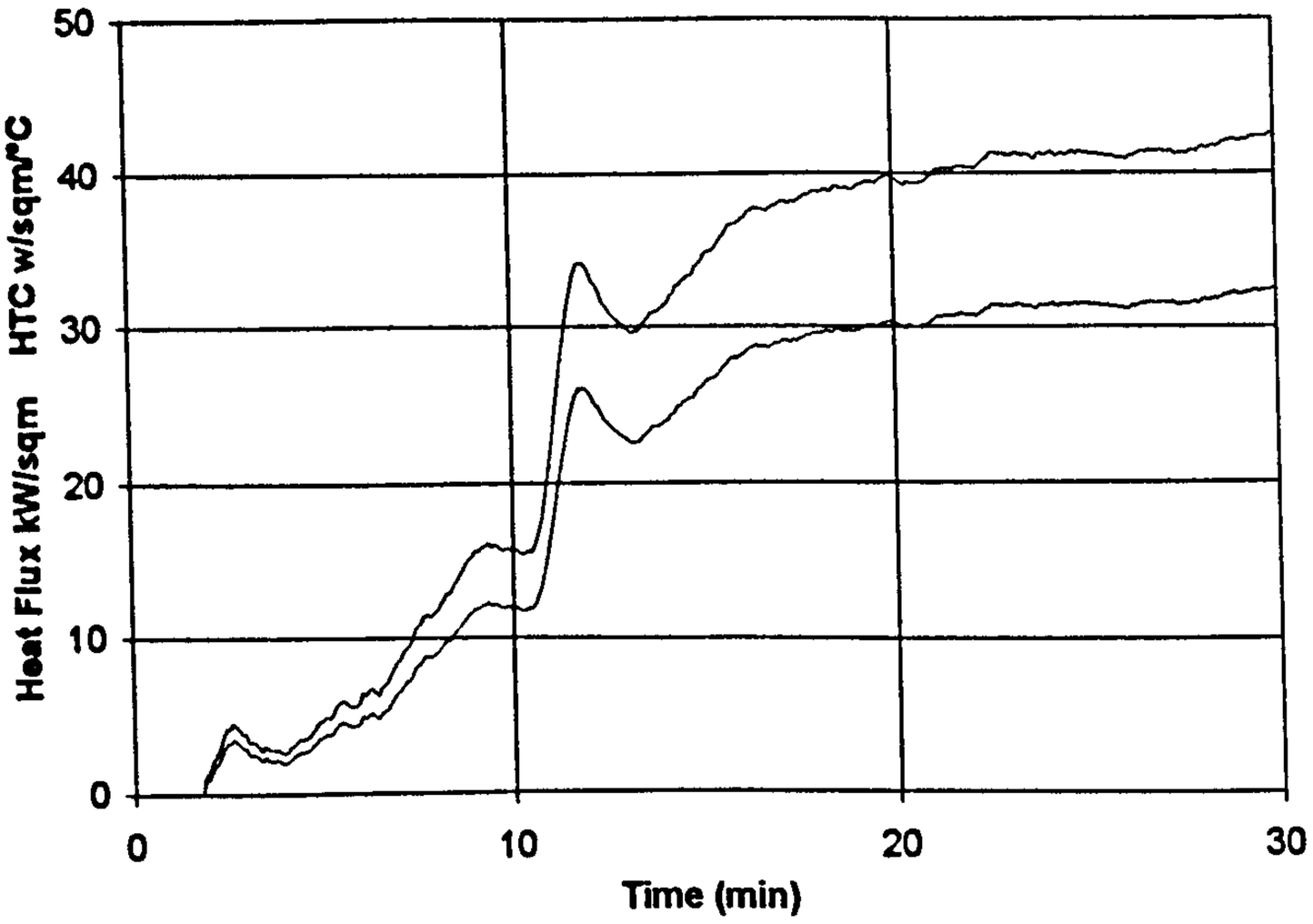

(b)

Figure 5.18 Results of the test on laminate, Q-5, nominal hot face temperature 950°C. The upper curves show hot face and block temperature vs. time. The lower figure shows the heat flux (lower curve) and apparent heat transfer coefficient (upper curve) vs. time. The HTC was calculated assuming a temperature difference of 762°C.

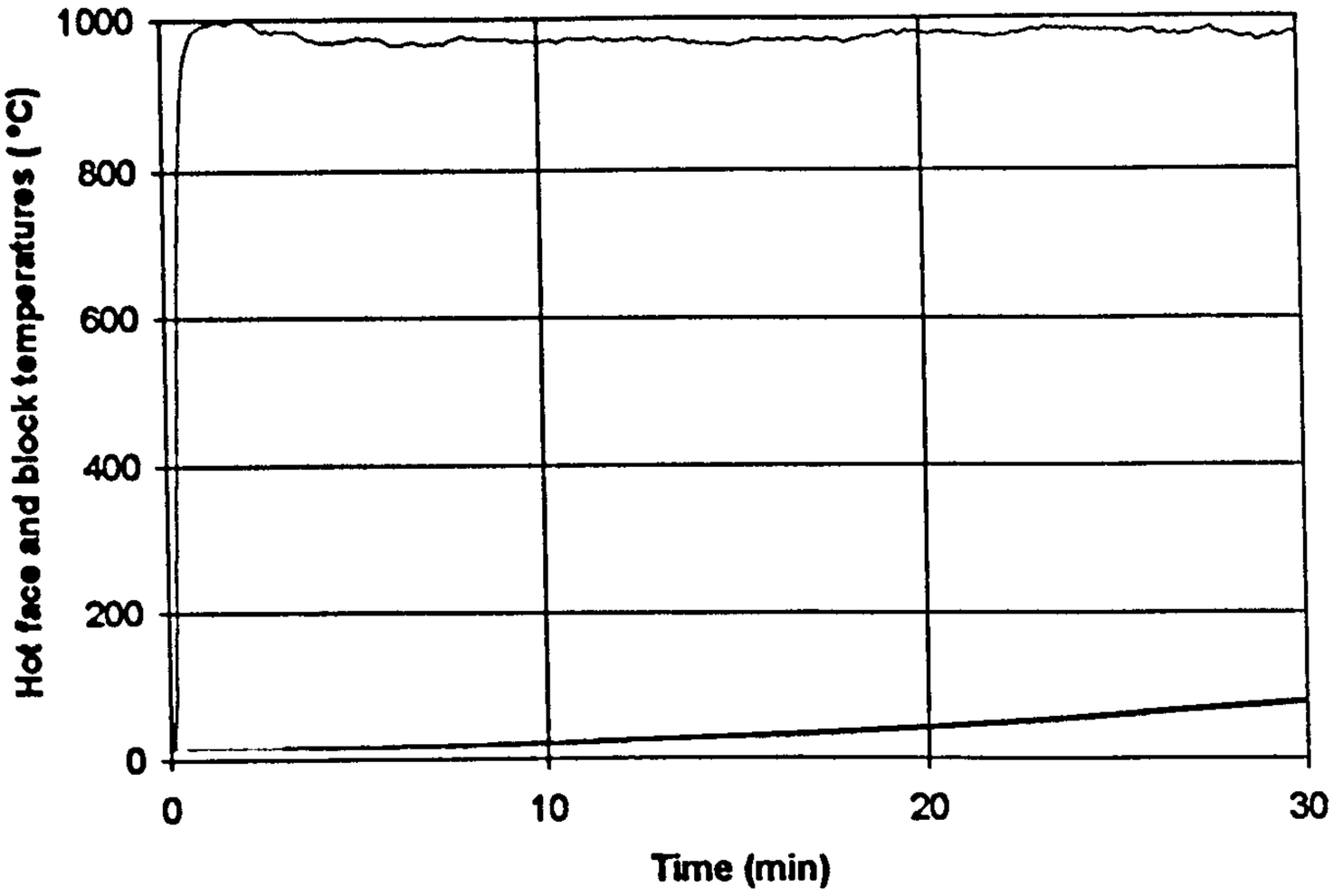

(a)

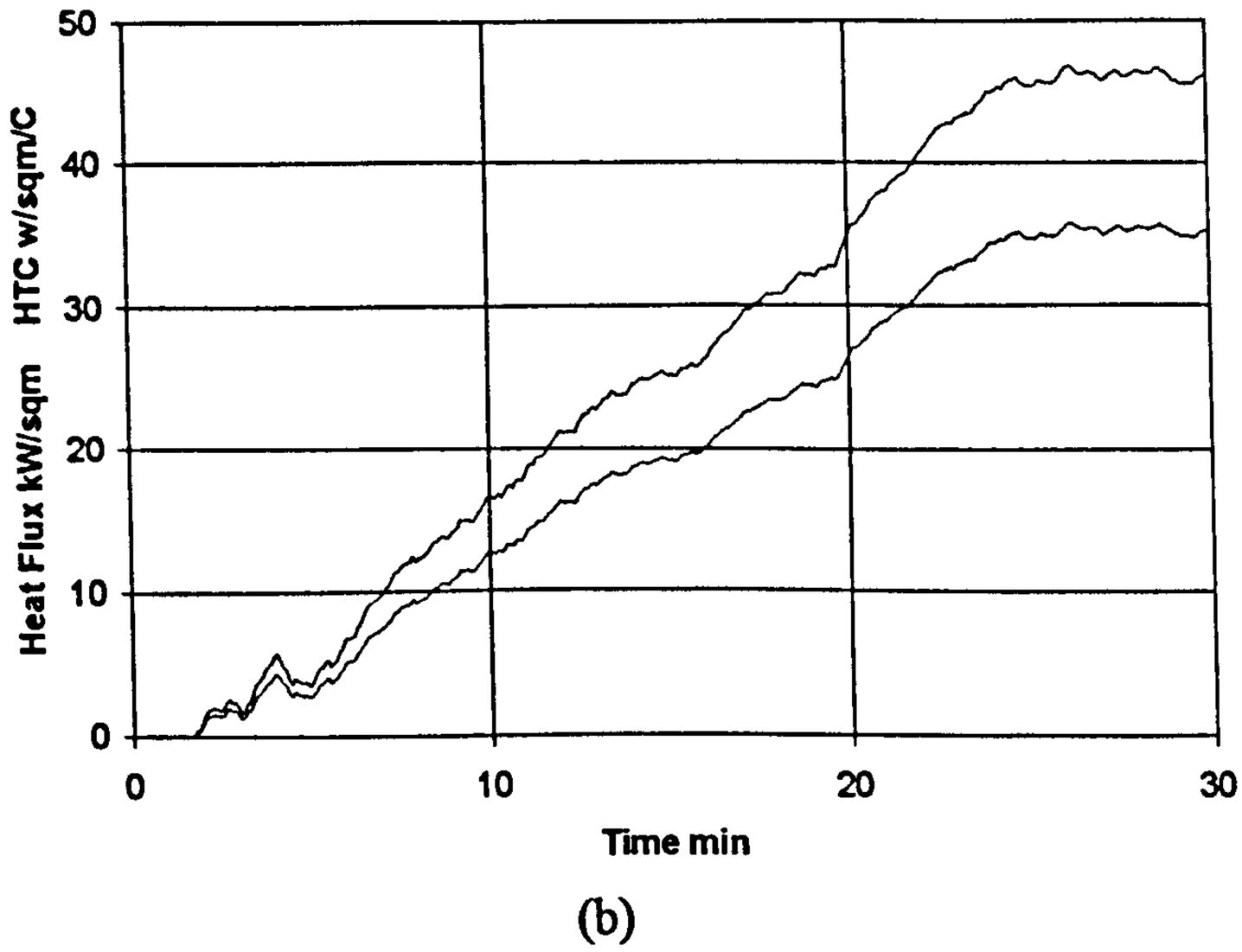

(b)

Figure 5.19 Results of the test on laminate with mesh, Q-4, nominal hot face temperature 950°C. The upper curves show hot face and block temperature vs. time. The lower figure shows the heat flux (lower curve) and apparent heat transfer coefficient (upper curve) vs. time. The HTC was calculated assuming a temperature difference of 762°C.

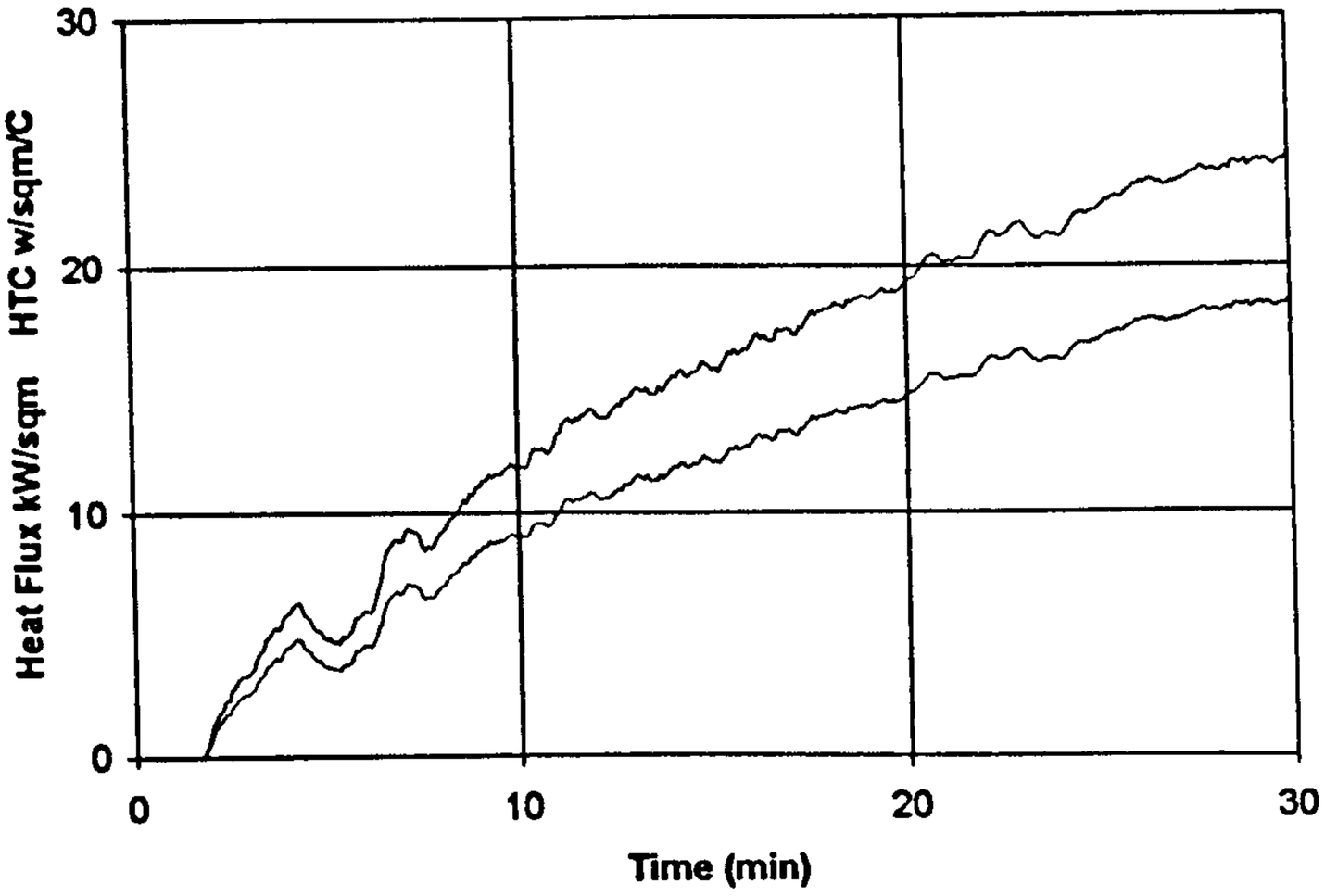

(a)

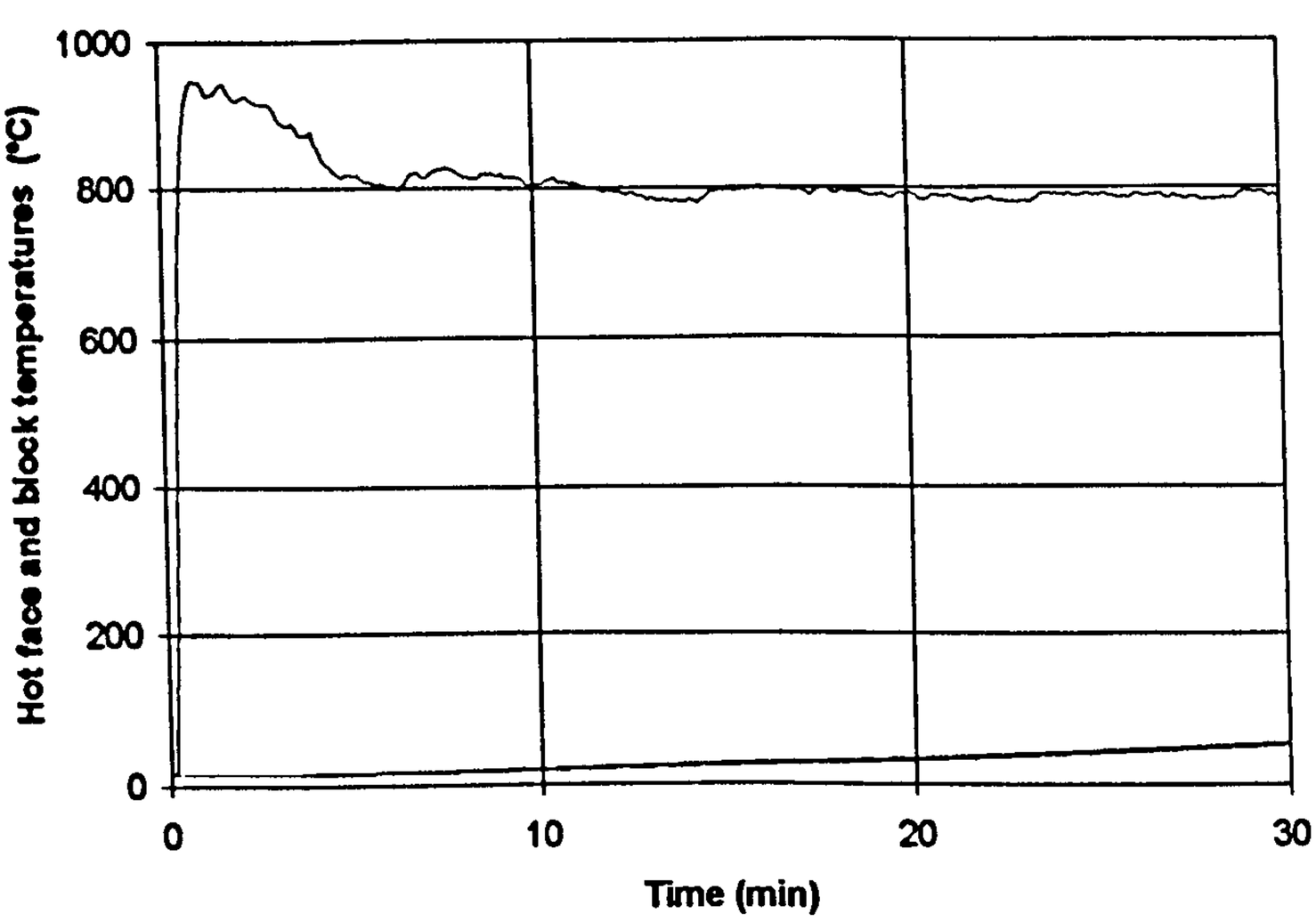

(b)

Figure 5.20 Results of the test on laminate with mesh, Q-8, nominal hot face temperature 800°C. Upper curves show hot face and block temperature vs. time. The lower figure shows the heat flux (lower curve) and apparent heat transfer coefficient (upper curve) vs. time. The HTC was calculated assuming a temperature difference of 762°C.

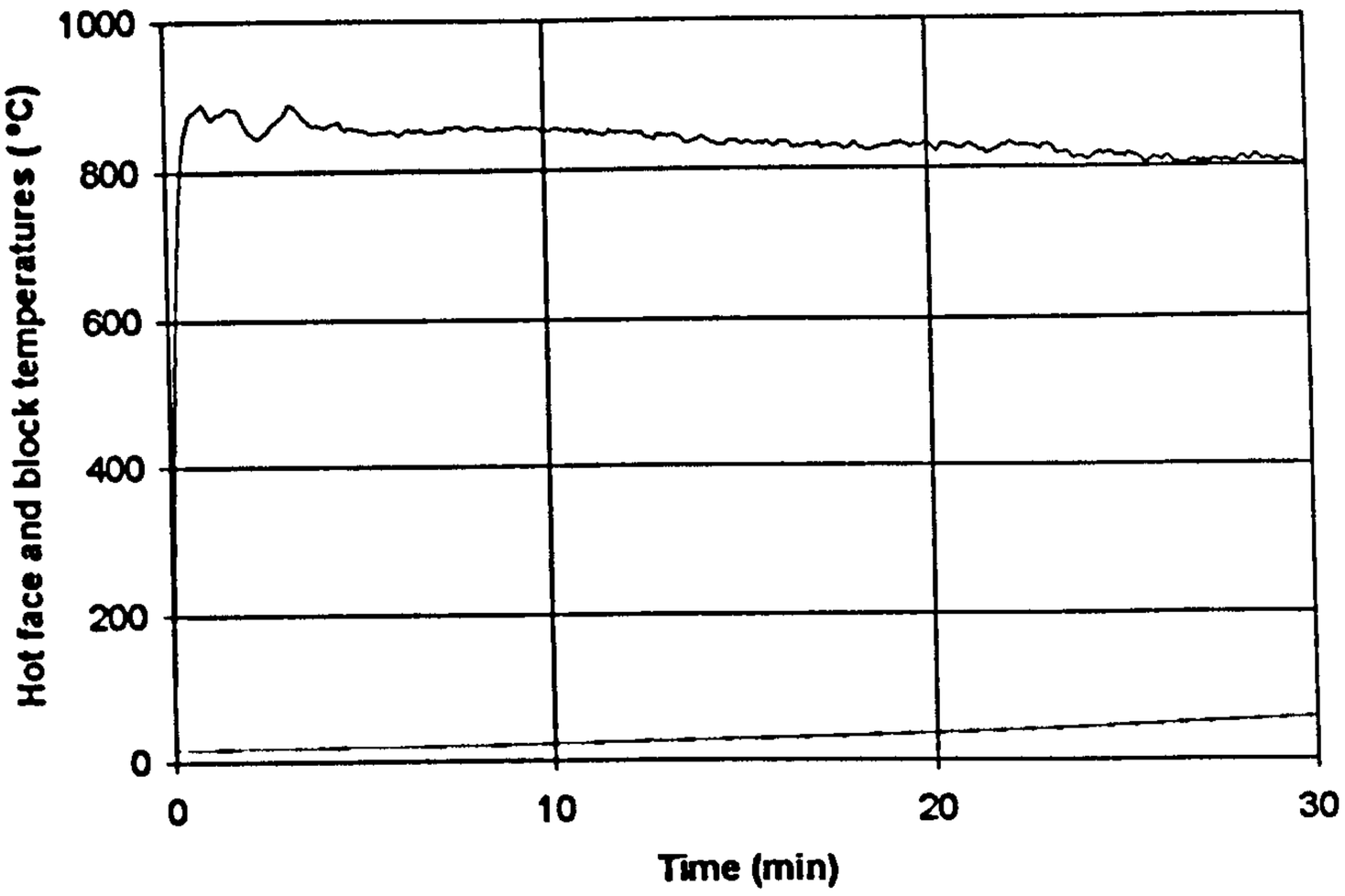

(a)

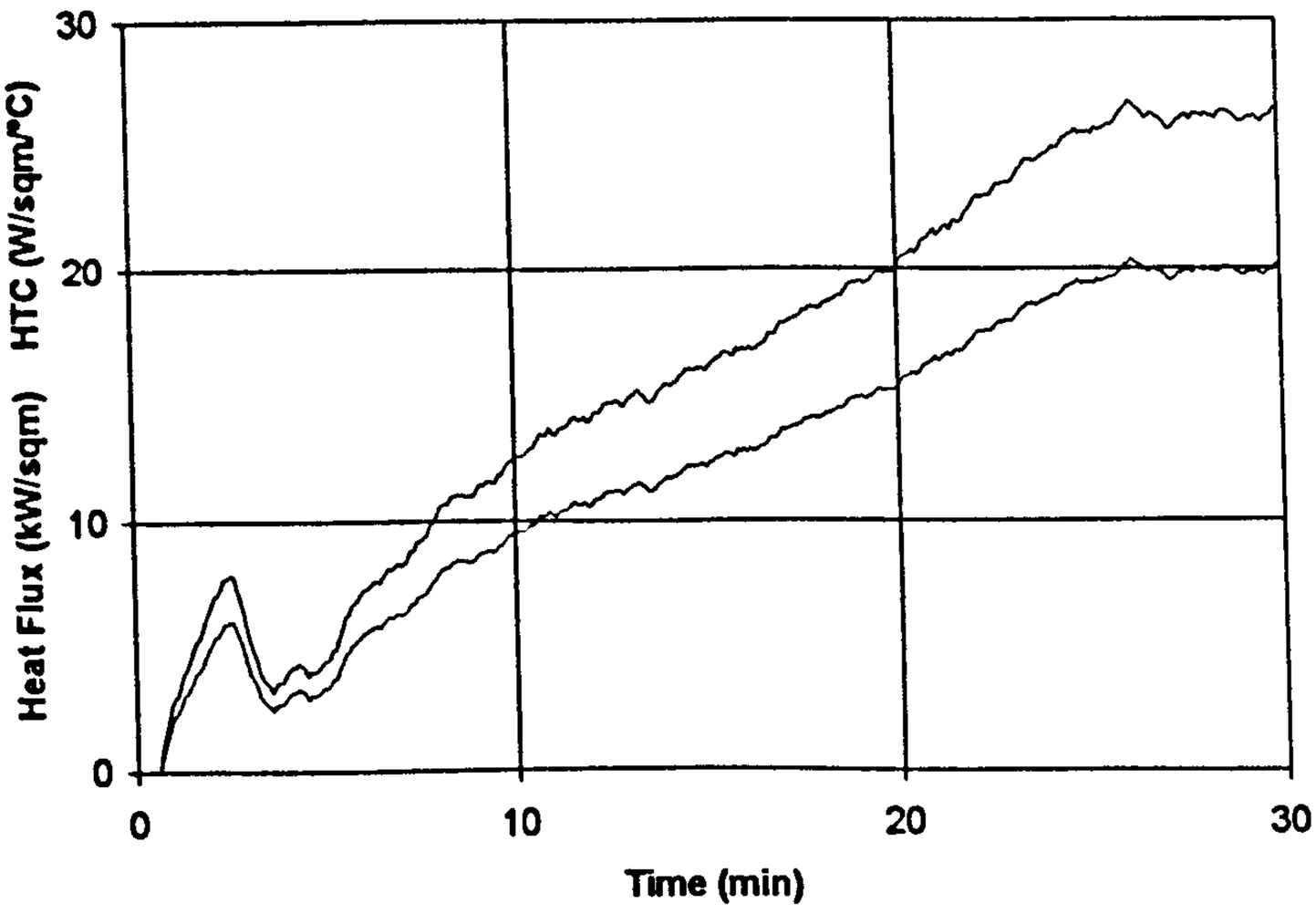

(b)

Figure 5.21 Results of the qualification test on laminate with mesh and no gel-coat, Q-17. For tests Q-12 to Q-17, the gas was adjusted to achieve a hot face temperature of 800°C with the thermocouple in contact with the copper block. The heat flux test was then carried out without changing the gas setting. The upper curve shows hot face temperature vs. time (which rises significantly above 800°C. The lower figure shows the HTC (upper curve) and the heat flux (lower curve) vs. time. The HTC was calculated assuming a temperature difference of 762 °C.

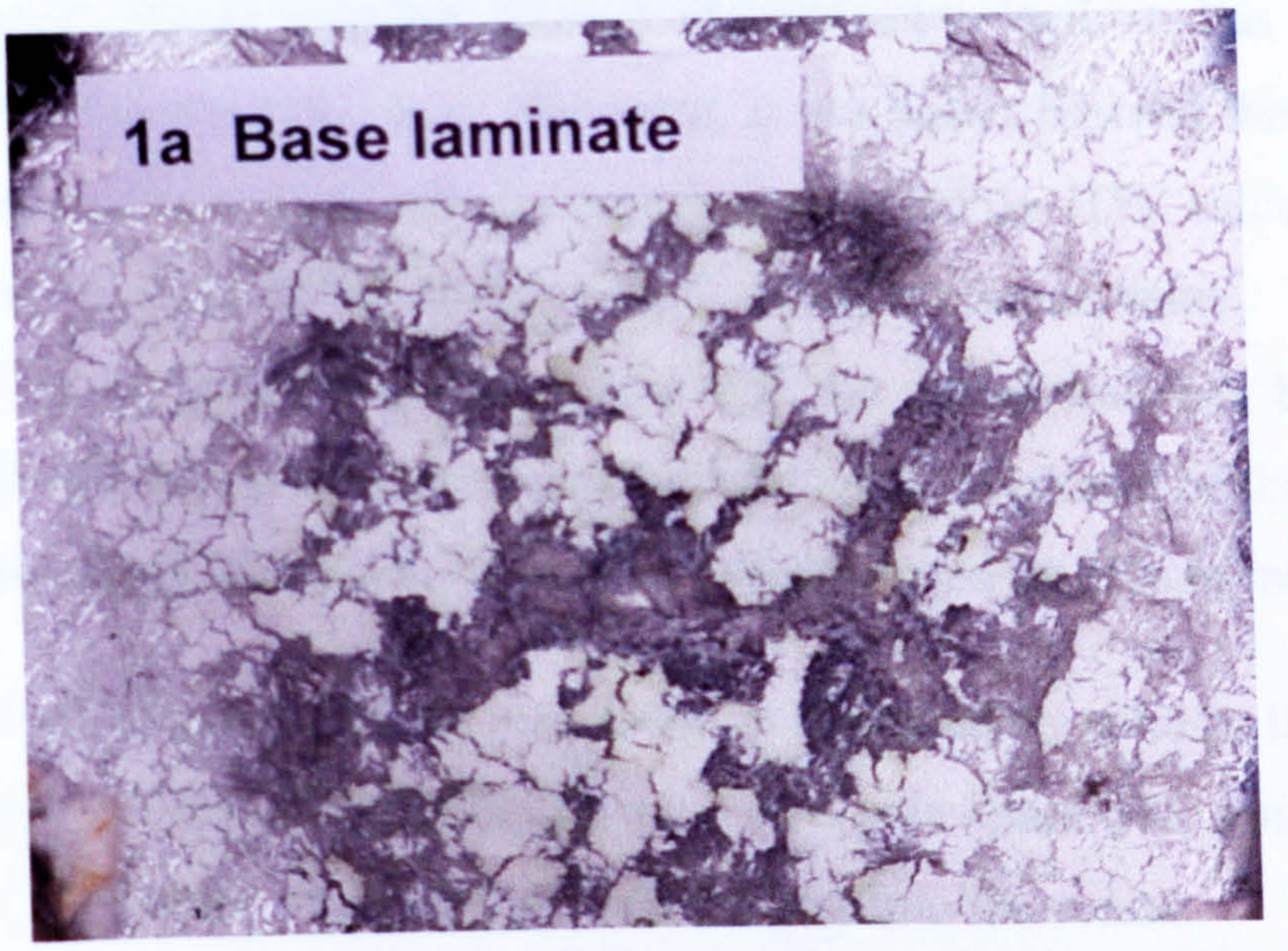

Figure 5.22 Front (upper photo) and rear face (lower photo) of a laminate sample after testing.

It should be noted that the results are regarded as conservative for the following reasons:

- The maximum test heat flux through the protection laminate has been assumed to apply throughout the test. However, it has been observed that this quantity rises throughout the test. The average heat flux and the HTC calculated over the full test period would be only about 75% of the maximum value.

- Good contact between the protection and the vessel wall has been assumed, when in fact poor contact or no contact will apply over most of the surface. This could mean that the heat flux has been overestimated by 25% or more.

- It has been assumed that the vessel wall is contacted by solid or liquid contents, when in fact there will probably be a gas or vapour space over some of the upper surface. This is the worst case for heat transfer into the vessel.

- The burner procedure produces an almost constant heat flux early in the test. By contrast, a pool fire would take a few minutes to reach its full intensity.

The main factor limiting the speed and accuracy of the experimental procedure appeared to be the achievement of a steady block temperature, equal to the specimen temperature, at the start of each experiment. Because a well insulated block of large mass was chosen, it was found that a period of 12 hours or more was needed for the block cool to reach ambient temperature after each run.

5.5 Conclusion

The form of the cold face response of samples was prepared and manufactured by hand lay-up using WR glass reinforcements based on different types of resin such as orthophthalic and isophthalic polyesters. Vinyl esters resins are similar with slightly difference responses from those laminated with aluminum foil which provide a delay in the transmission of heat into the zone or component protected by the laminate.

Despite the loss of most of the resin, the material close to the cold face remains undamaged and the panel remains structurally sound. The laminate showed good integrity of the front face material, and only a very small amount of glass fibre was

lost. Also the rear face was undamaged and becomes black, indicating a certain level of char formation.

The fire resistance performance of the five composite samples tested as a part of the DML development of fire protection according to the standard 'SOLAS' time-temperature curve, indicated that A60 fire rating can be well met by two of the five samples. For instance, the performance of 100mm Rockwool with 1mm E-glass/epoxy skin and the 35mm syntactic phenolic foam with 5mm E-glass/phenolic skin specimens can meet A60 requirements. It is noted that to just meet A60 requirements, the thickness of the Rockwool layer might be largely reduced. On the other hand, the experimental results show that the 20mm E-glass WR/epoxy meets A30 requirement only, whilst the 4mm Technofire 60853 intumescent/epoxy failed to meet the requirements.

The qualification and performance of the composite laminate system developed by VT (UK) Ltd. for possible fire protection was examined. All the test laminates performed in a similar manner and gave maximum HTC values during the test of less than the target value of $30Wm^{-2}\,°C^{-1}$. Any of the laminates would therefore be of suitable construction, from a purely thermal viewpoint, for the application.
The actual mean value was $24.1Wm^{-2}K^{-1}$, with a 95% upper confidence limit of $26.4Wm^{-2}K^{-1}$, which is significantly lower than the required value. Qualification has therefore been achieved.

There is no systematic difference between gel-coated and non-gel-coated samples, so the gel-coat used is unlikely to damage fire protection performance. The laminates containing steel mesh are slightly less effective than those without it. Since the main qualification was achieved with the mesh samples, both types of laminate qualified from a thermal performance viewpoint.

CHAPTER 6

DATA PREPARATION FOR MODELLING

6.1 Arrhenius Equation and Kinetic Parameters.

6.1.1 Introduction

When composite components are exposed to fire, their polymeric matrix materials may undergo decomposition at high temperatures. To predict the thermal response behaviour of composites in fire, the kinetic parameters of pyrolysis reactions are required for the analysis. These include: (1) a rate factor, A (in 1/sec. or 1/hour); (2) the order of the pyrolysis reaction, n, (non-dimensional); (3) the activation energy of the polymeric material in decomposition, E, (in: J/mole) and (4) the non-dimensional ratio of final mass, m_f over initial mass of the material during decomposition process, (m_f/m_o). A 1D FD code (i.e. program COM_FIRE in FORTRAN) has been developed at Newcastle University for the prediction of the fire resistance of composite laminates in fires (Gibson *et. al.*, 1994). To run the code, the kinetic parameters of the relevant resin system of composite materials are required as a part of the input.

The kinetic parameters can be calculated from thermogravimetric data obtained from TGA tests of the sample materials under air or under nitrogen. The mass change rate of polymeric materials in decomposition is given by an n^{th} order Arrhenius equation of the following form (Friedman, 1965):

$$(-1/m_o)(\partial m/\partial t) = A\, e^{-E/RT}\; f(m/m_o) \tag{6.1}$$

In this chapter, a technique for deriving the kinetic parameters of a polymeric material from its TGA data of the material is described and a FORTRAN program is

used for the data processing based on this technique. The results derived for a group of polymeric materials or GRP composites are presented for further use.

6.1.2 The Freeman Method and the Modified Technique

The kinetic parameters of the relevant polymeric materials are evaluated from the resulting TGA curves based on the Freeman and Carroll (1957) method. This method allows one to derive the parameters with the use of a single experimental TGA curve. The method can be modified to process data based on multiple heating rate TGA curves.

The method and the modified technique adopted in this study are described as follows. In general, the Arrhenius equation (i.e. Eqn. (6.2)) is used to describe the pyrolysis reaction of a polymeric material at high temperatures:

$$\frac{dm}{dt} = -A\, m_0 \left[\frac{m - m_f}{m_0}\right]^n \exp^{-(E/RT)} \tag{6.2}$$

where; m, m_o and m_f (in: mg) are the instant mass of the sample, the original mass of the sample and final mass of the sample at the end of decomposition respectively; and t (in: s) and T (in: K) are the time and temperature variables respectively.

Or, in a more general form:

$$\frac{\partial w}{dt} = -A\,[w - w_f]^n \exp^{-(E/RT)} \tag{6.3}$$

where: $w = m/m_o$; $w_f = m_f/m_o$; and $f(w\text{-}w_f)$ = an unknown function of $(w\text{-}w_f)$.

By taking logarithms of the two sides of Eqn. (6.3) to base 10, this becomes:

$$\log\left[-\frac{\partial w}{\partial t}\right] = \log(A) + n \log[w - w_f] - \frac{E}{RT} \log e \tag{6.4}$$

Equation (6.4) is holds only within the temperature region T1 ≤ T ≤ T2 where decomposition takes place, and hence $(-\partial w/\partial t) > 0$. For any temperature outside the decomposition region $(\partial w/\partial t) = 0$.

Egnuation (6.4) can be led to:

$$\Delta \log\left[-\frac{\partial w}{\partial t}\right] = n\,\Delta \log\left[w - w_f\right] - \frac{E}{2.302R}\Delta\left(\frac{1}{T}\right) \tag{6.5}$$

Equation (6.5) can be re-written as:

$$\frac{\Delta \log\left(-\dfrac{\partial w}{\partial t}\right)}{\Delta \log\left(w - w_f\right)} = n - \frac{E}{2.302R}\frac{\Delta\left(\dfrac{1}{T}\right)}{\Delta \log\left(w - w_f\right)} \tag{6.6}$$

By defining the following two variables,

$$y = \frac{\Delta \log\left(-\dfrac{\partial w}{\partial t}\right)}{\Delta \log\left(w - w_f\right)}, \quad \textit{and} \quad x = \frac{\Delta(1/T)}{\Delta \log\left(w - w_f\right)}$$

then eq (6.6) shows a linear relationship between y and x:

$$y = n - \frac{E}{2.302R}x \tag{6.7}$$

Based on Eqn. (6.7), one may derive the kinetic parameters (n and E).

Having derived the two values n and E, the rate factor A can be further derived from Eqn. (6.4). Finally, the other parameter, w_f, can be easily calculated from the original TGA data: $w_f = m_f / m_o$.

6.2 TGA Data Processing

The TGA measurements under idealised, laboratory conditions provide enough data to fit an Arrhenius rate equation (i.e. Eqn. 6.2) to the material's behaviour, and also to provide a measure of the amount of carbonaceous char left behind when the resin is spent.

The samples were prepared from resin-impregnated glass sheets that were supplied by the Fibreline Company and the Norpol Company. The samples being tested were fibreglass-reinforced resins such as F4010 Phenolic, a P4506 fire retardant such as Halogenated polyester, and free glass fibre such as isophthalic and orthophthalic polyester resin and vinyl ester resin.

The specification data-sheets for all resins are presented in Table 6.1. The Thermo-balance Stanton Redcroft Model (STA 780 Series equipment, Chemistry Department, Newcastle University) as shown in Fig. 6.1, was used to measure changes in sample weight. The major advantages of the STA 780 system are its ease of operation and speed of use. In this investigation, loss in sample weight was recorded as a function of temperature and time, while furnace temperature was continuously increased at fixed rates of 25°C/min and 60°C/min.

In all cases, the thermogravimetric data refer to approximately 100 milligrams of representative resin material placed in (000) Coors glazed porcelain crucibles and heated at a rate of 25°C/min or 60°C/min after tarring the balance in a flow of $50cm^3$/min in an atmosphere of dry nitrogen. The mass of resin was recorded from ambient temperature, under the same flowing gas conditions, to the desired maximum heating temperature. The loss in mass was recorded as a function of temperature and time using Pico-log software, while furnace temperature was continuously increased at the desired fixed rate (i.e. 25°C/min or 60°C/min).

The total duration of such a test is about 20 minutes, but approximately 5 further minutes are required to cool the furnace and clean the crucible.

Table 6.1. Specification data sheet for all resin systems used in TGA tests.

Type of sample (glass-free)		
Type of Matrix System	Series no.	Supplier
Isophthalic polyester	420-100	NORPOL (V-TC)
Orthophthalic polyester	440-M750	NORPOL (V-TC)
Vinyl ester	9100-700	NORPOL (V-TC)
Type of sample (with glass-fibre)		
Type of Matrix System	Type of fibre-glass	Supplier
Phenolic	Unidirectional F 4010	FIBRELINE
Halogenated polyester	Unidirectional P4506 fire retardant	FIBRELINE

Figure 6.1 Experimental apparatus for thermal analysis (TGA) test (Chemistry Dept).

6.3 Useful Data Obtained From the Tests

A TGA (thermogravimetric analysis) data set of a sample is usually given in the form of remaining mass (in: mg) of the sample material as a function of time (in: seconds) or temperature (in: °C). Such a test may be conducted under air or under nitrogen at a constant heating rate. A TGA_PRO FORTRAN program was used for the TGA data processing to derive the four kinetic parameters (i.e. n, A, E and m_f/m_o), of a composite system required for running the 1D FD fire Code (i.e. COM_FIRE), which is to be used for the prediction of the thermal response behaviour of composite laminate in fire. The use of the TGA_PRO program involves two steps. The first step is to derive mass change rate as function of temperature, so that the main decomposition region of concern in terms of temperature can be properly defined. The second step is to get all four parameters, having input the defined decomposition region. For a resin system like phenolic, two separated phases of the chemical reaction may be involved. To derive the kinetic parameters for both phases, the second step of the program must be run twice based on the defined decomposition region.

Figure 6.2 shows a plot of the TGA data of the sample materials (i.e. isophthalic and orthophthalic polyester, vinyl ester, phenolic and halogenated polyester resin) cured according to the manufacture's specifications, where mass is given in a non-dimensional mode (i.e. $w = (m/m_o)$ as a function of temperature. The tests were carried out at nominal heating rates of 25°C/min and 60°C/min in nitrogen.

The initial weight loss curve presented in Fig. 6.2 was due to water (% moisture), and the reaction was initiated at a temperature approximately at 230°C/min., and was relatively rapid from 320 to 480°C. To define the decomposition region more clearly from the TGA data, the mass change rate of some resin systems, ($-dw/dt$) were calculated as a function of temperature. Apart from the phenolic system, it is quite clear that the major decomposition region takes place between $T_1 \approx 300$°C and $T_2 \approx 480$°C, and, in most cases, the rate of decomposition passes through a maximum at 430°C after which it decreases rapidly. After this point only slight change occurred and the decomposition was substantially complete when the temperature had risen above 600°C (for most resin systems). The weight loss which

occurs after that is equal to the carbon content, as carbon is burnt off in the oxygenated atmosphere.

Within the major decomposition region of the resin between T1= 300°C and T2 = 480°C, the calculated values of X and Y from the TGA data are shown in Fig. 6.3. It can be seen from the figure that the actual relationship between x and y is not exactly, but only approximately, linear.

The rates of change in sample weight of the phenolic resin as a function of temperature under nitrogen shows markedly different decomposition behaviour. The phenolic resin decomposes in two stages over a wider temperature range than other systems such as polyester and vinyl ester. The first stage of the reaction mainly occurs over the temperature interval of 150 to 370°C, while the second stage of the reaction occurs over the temperature range of approximately 440°C to 690°C. The maximum decomposition in this stage of the reaction occurred at temperatures above 555°C. After that, constant decomposition was observed and the reaction was completely finished when the temperature reached about 1200°C.

Based on the four kinetic parameters derived, the mass change rate of the resin sample can be calculated as a function of temperature from Eqn. (6.3):

$$w = \left[\frac{1}{A}\left(-\frac{\partial w}{\partial t}\right)e^{(E/RT)}\right]^{1/n} + w_f \tag{6.8}$$

The simulated TGA curve based on the Arrhenius equation is shown in Fig. 6.4 together with the original TGA curve for comparison. The discrepancy between the two curves is attributed mainly to varying heating rates during the course of TGA.

Figure 6.5 shows the heating rate derived from the TGA data. It can be seen from Fig. 6.5 that in the decomposition region 300°C-480°C, the heating rate was not kept constant and was generally higher than the nominal value of 25°C/min.

The kinetic parameters of the resins as derived are presented in Table 6.2.

From the intercept and slope of the line, the order of reaction for each system was obtained, and the corresponding orders of reaction and energies of activation were determined from the intercepts and slopes of the lines.

Table 6.2 Kinetic parameters for thermal degradation

Materials involved		*n*	*E* (J/mol)	*A* (1/sec)	*mf/mo*
Isophthalic PE resin		3	0.288E+06	0.539 E+24	0.040
Isophthalic PE/E-glass W/R		1.7	0.222E+06	0.118 E+11	0.644
Halogenated PE/CSM E-glass		1.1	0.104 E+06	0.79 E+08	0.533
Halogenated PE Unidirectional E-glass		1	0.111 E+06	0.579 E+09	0.791
Orthophthalic PE resin		1.8	0.144 E+06	0.989 E+13	0.041
Vinyl-ester resin		3.5	0.197 E+06	0.518 E+14	0.038
Phenolic resin	stage I	12	0.613 E+05	0.129 E+08	0.415
	stage II	3.1	0.134 E+06	0.739 E+26	0.776
Epoxy resin		5	0.431 E+06	0.662 E+38	0.080

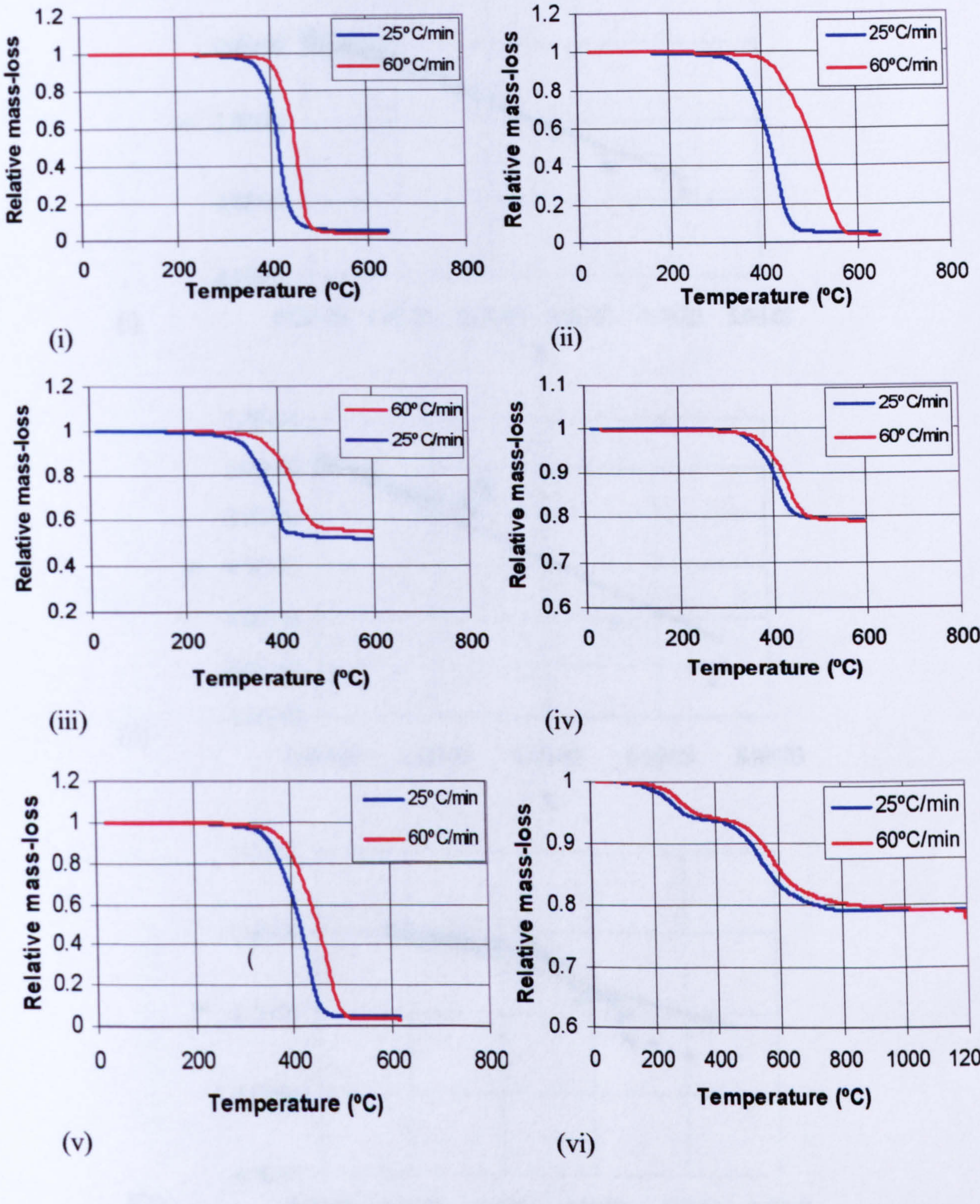

Figure 6.2 The Original TGA Data of the resin systems of (i) Isophthalic polyester, (ii) Orthophthalic polyester (iii) Vinyl ester resin, (iv) Phenolic (V_f= 36% iv), (v) Halogenated polyester/CSM E-glass and (vi) Halogenated polyester Unidirectional E-glass (P4506 lamina V_f= 49%).

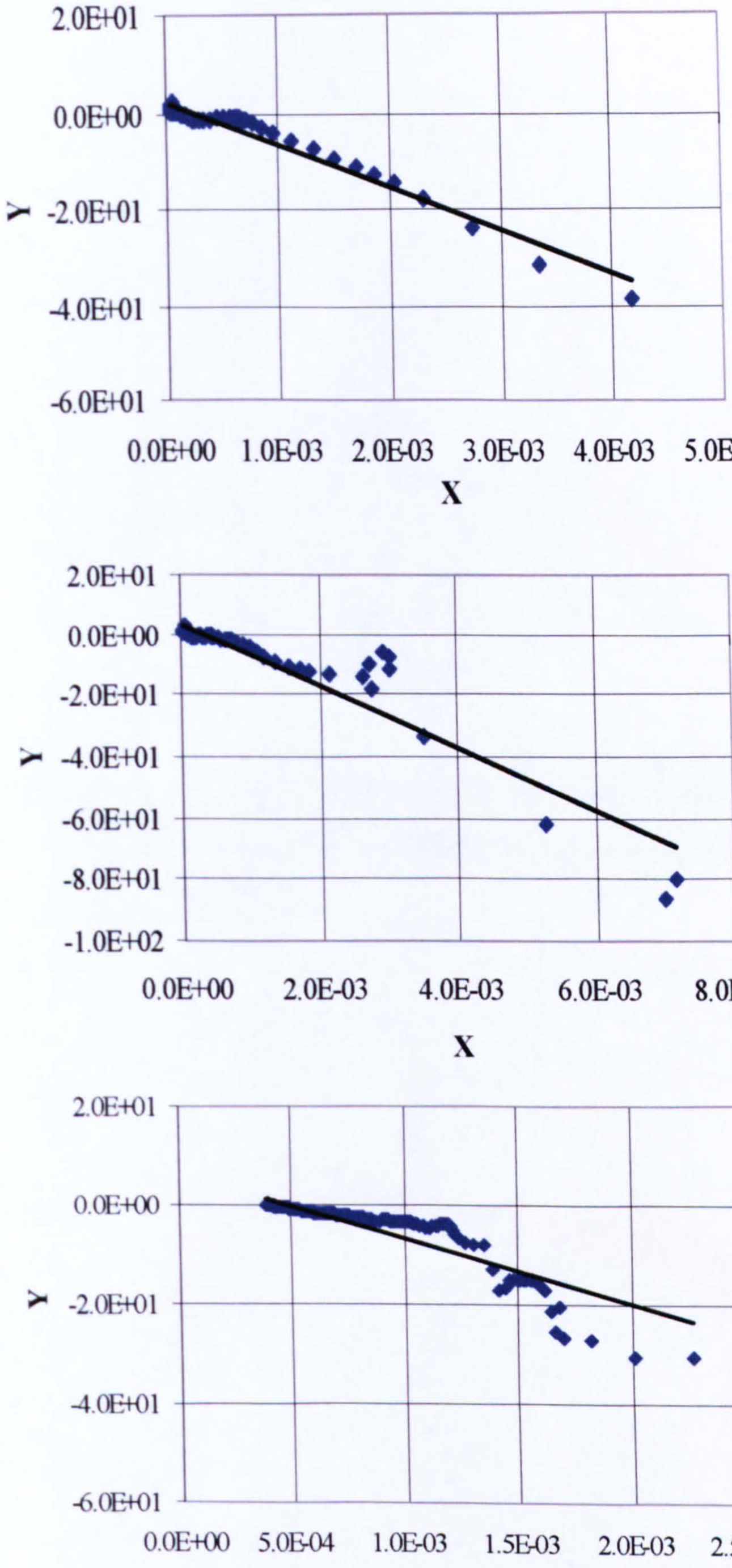

Figure 6.3 The calculated Y as a function of X for (i) Orthophthalic resin (ii) Vinyl ester resin (iii) Phenolic resin (V_f = 36%).

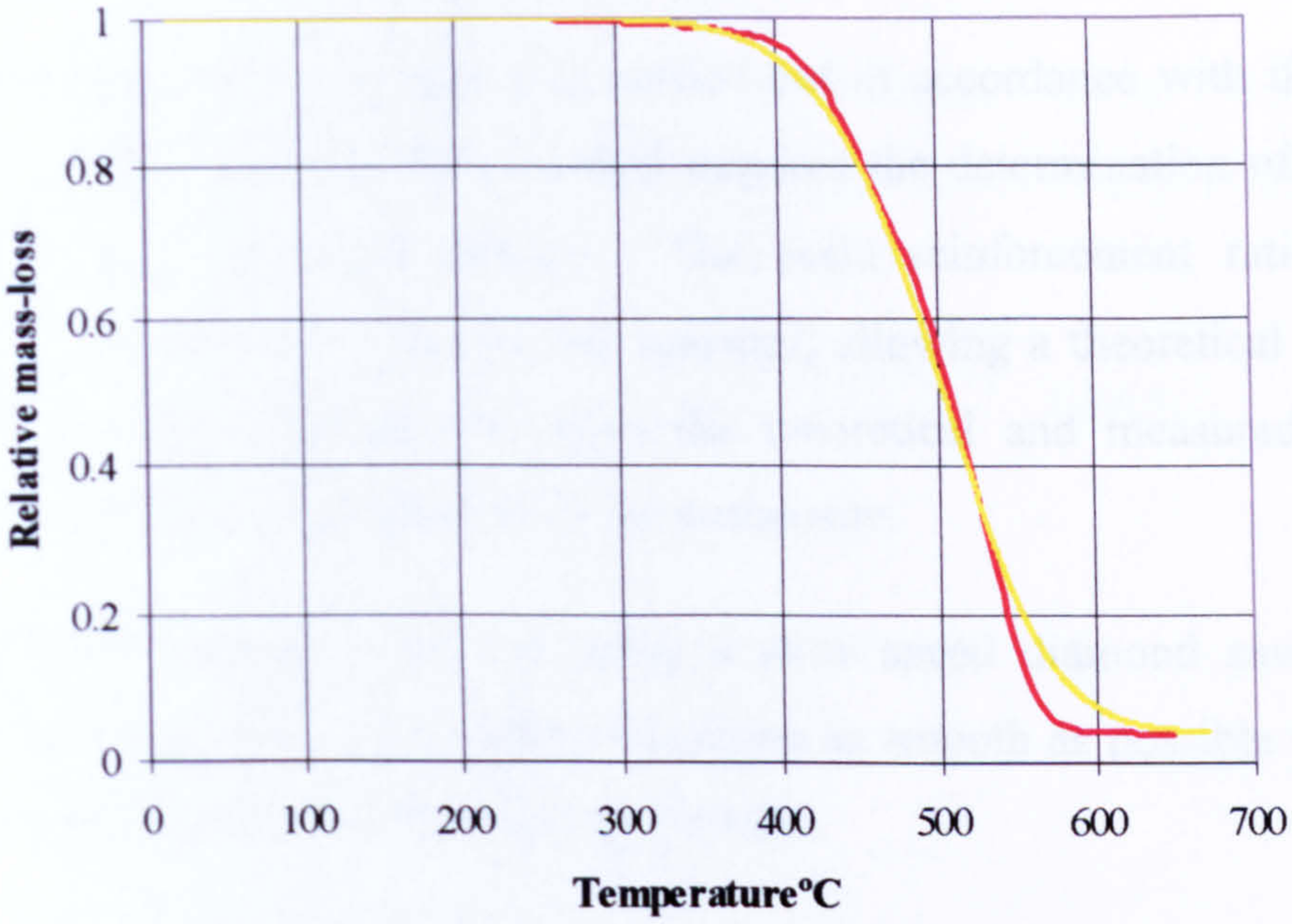

Figure 6.4 The original and derived mass-loss curves of the polyester resin. The red line represents the experimental data and the yellow line is the derived data.

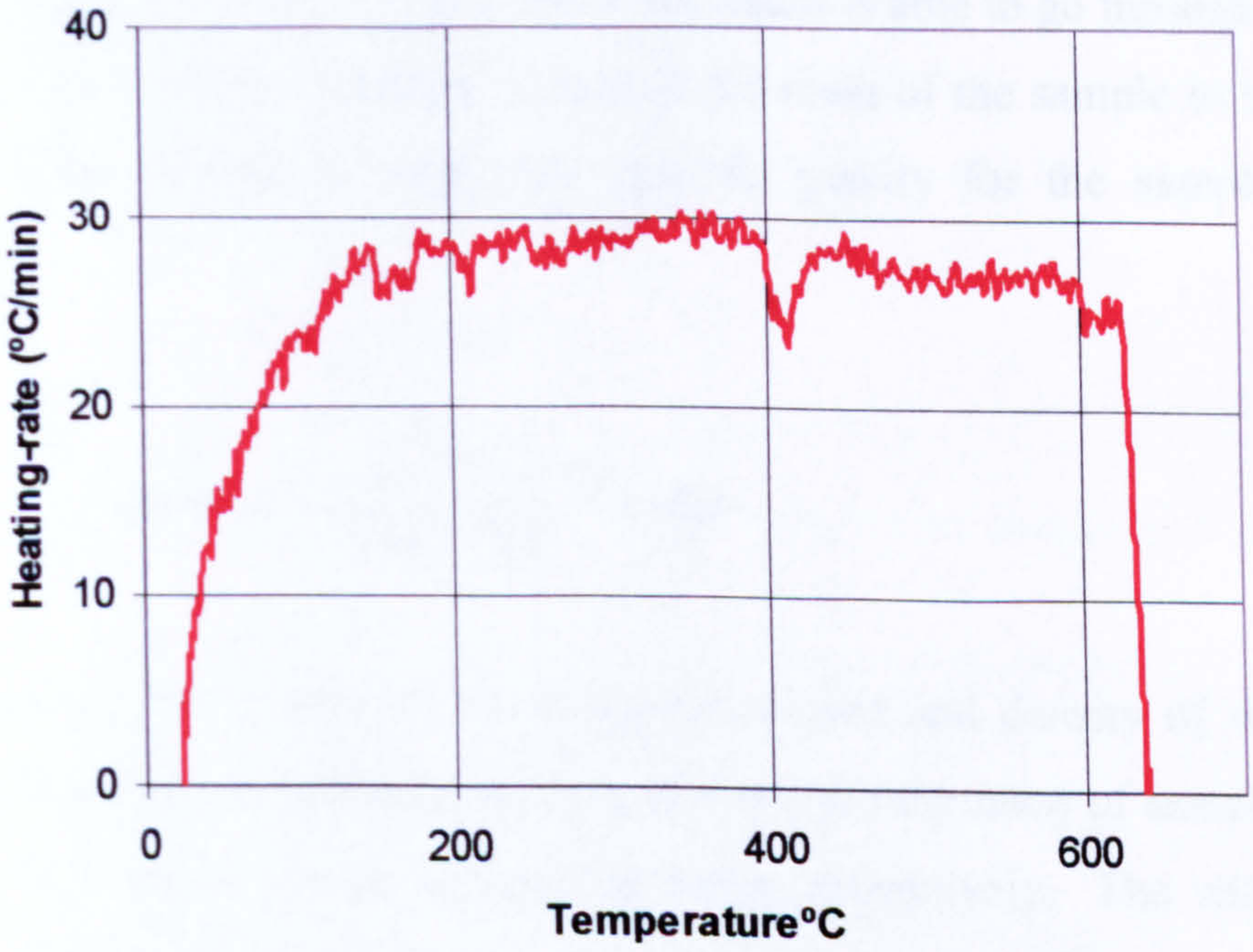

Figure 6.5 Typical derived heating rate of the TGA test

6.4 Fibre Volume Fraction Determination

The measurement of void content was carried out in accordance with the method described by Curtis, (1988). This method requires the determination of the resin, reinforcement and composite density. The resin reinforcement ratio is then determined by burning-off of the matrix material, allowing a theoretical density to be calculated. The difference between the theoretical and measured densities indicates the volume of voids present in the composite.

The samples of materials were cut using a slow speed diamond saw for each material tested to produce edges which would be as smooth as possible in order to prevent the trapping of air bubbles during the tests.

To calculate the composite specific gravity, the mass of the sample was measured both in the air and in a liquid of known density, typically water. It must be noted here that the void content values calculated may be subject to large error. This was caused by the fact that the samples immersed in the water were open ended, so that water would ingress into open voids. It was expected that this was likely to lead to a large error, particularly in poorly impregnated samples. The test routine as such is unable to distinguish between voids which the liquid is able to go through and those which it is not. From the recorded values of the mass of the sample in the air and the mass of the sample in water, the specific gravity for the sample may be calculated:

$$\rho_{c(meas)} = \frac{m_{s1}}{m_{s1} - m_{s2}} * \rho_{water} \tag{6.9}$$

where ρ_C, ρ_w are the density of the sample measured and density of water being equal to 1000 g/cm^3, respectively; and m_{S1} and m_{S2} are the mass of sample weighed in air and the mass of sample weighed in water, respectively. The value of Eqn. (6.9) is then corrected for the density of the liquid at the test temperature (for water at 25°C multiplied by 0.9975). The ratio of the glass matrix in the sample must also be measured; this was carried out on the same sample used for the measurement of the specific gravity. The sample is weighed and then burned-off at 550°C for five

hours. The weight of the glass which remains is then recorded, leading to the mass fraction of the polymer and glass in the sample.

Assuming matrix and fibre densities were known and constant, the respective volume fraction of the glass V_f and matrix V_m can also be determined using:

$$V_f = \frac{m_f/\rho_f}{m_s/\rho_{c(measured)}} = \frac{m_f * \rho_{c(measured)}}{m_s * \rho_f} \quad (100\,\%) \qquad (6.10)$$

Thus the volume fraction of the matrix can also be calculated by:

$$V_m = (1 - V_f) \qquad (6.11)$$

The theoretical density (for a material with zero void content) can be calculated for the sample composite using the rule of mixtures:

$$\rho_{C\,(theor.)} = [(V_f \rho_f + V_m \rho_m)\,(1000\ \mathrm{gcm^{-3}})] \qquad (6.12)$$

The void content (Vv) can be measured by the difference between the theoretical and measured densities:

$$V_v = \left[\frac{\rho_{c(theor.)} - \rho_{c(meas.)}}{\rho_{c(theor.)}}\right] \quad 100\,\% \qquad (6.13)$$

The mean value was then calculated for the five samples for each test conducted.

The density, fibre volume fraction and void content of the composite panels are shown in Table 6.3. It can be clearly observed in Table 6.3 that the results for volume fraction varied between 36% and 54%. The highest value of void content was exhibited by the phenolic system. This is probably related to the nature of this resin, which has a high void content due to condensed water formed during the reaction process which forms the resin. This water is trapped in the resin and forms micro-voids after resin curing.

Table 6.3 Volume fraction measurement on the majority of the materials used.

Sample Code	Sample Type	Sample thickness (mm)	V_f %	V_m %
1	GRP/orthophthalic polyester + 4 layers from aluminium foil	10.7	44	2
2	GRP/orthophthalic polyester + 3 layers from aluminium foil	9.62	37	2.1
3	GRP/orthophthalic polyester + 2 layers from aluminium foil	10	54	1.6
4	GRP/orthophthalic polyesterl	10		1.8
5	GRP/isophthalic polyester	10.8	44	1.4
6	GRP/Vinyl ester	10.1		2.3
7	Halohenated GRP/polyester	9.98	46	2.9
8	GRP/Phenolic	8.5		5
A	GRF/orthophthalic polyester + TXCV7076 Nominal coating all layers	9.73	41	1.6
B	GRF/orthophthalic polyester + TXCV7050 1 layer	10.33	42	1.1
C	GRF/orthophthalic polyester + TXCV7129 1 layer	10.51	46	3
D	GRF/orthophthalic polyester + Aluminised PRE-OX 1 layer	9.87	38	2.6
E	GRF/orthophthalic polyester + TXCV7161 Superwood steelwire reinforced 607 max fabric 1 layer	9.96		2.2

6.5 Conclusion

To run the COM_FIRE code, the kinetic parameters of the relevant resin systems of composite materials are required as a part of the input. These kinetic parameters were obtained by carried out TGA tests.

The Freeman technique was applied to calculate the kinetics of the thermal decomposition of the polyester, vinyl ester, phenolic and epoxy, which were investigated under heating rates of 25 and 60°C in an atmosphere of dry nitrogen. An A FORTRAN program was used for the data processing based on the Freeman technique.

It has been found that the form of the weight loss curve in nitrogen at 60 °C/min. is similar to that at a rate of 25°C/min., but the reaction is initiated and completed at slightly higher temperature. The decomposition begins at 200°C for most of the samples in question and is complete at 500°C approximately. The kinetics of the reaction were evaluated by the method of Freeman and Carroll.

The apparent activation energies of isophthalic polyester, orthophthalic polyester, vinyl ester, and epoxy were estimated to be 0.288E+06, 0.144E+06, 0.197E+06 and 0.431E+06 (J/mol) respectively. However, phenolic resin has two stage of reaction, and it was found that E = 0.613E+05 for the first stage and E = 0.134E+06 for the second stage.

The density, fibre volume fraction and void content of the composite panels were determined according to the testing method described earlier in this chapter. It was observed that the results for volume fraction from the tests varied between 36% and 54%. The highest value of void content was exhibited by the phenolic system. This is probably related to the nature of this resin, which has a high void content due to condensed water which is formed during the reaction process which forms the resin.

CHAPTER 7

ONE-DIMENSIONAL MODELLING OF COMPOSITES IN FIRE

7.1 The 1-D Finite Difference Model

7.1.1 Introduction

The computer program COM_FIRE, version 3.4, 2004 (developed at the Centre of Composite Materials Engineering (CCME), School of Mechanical, and System Engineering, University of Newcastle, UK), is used in this chapter for the predictions of the thermal responses of composite laminates in fire.

Program COM_FIRE was initially developed in 1994 for predictions of the thermal resistance of thick GFRP laminates when exposed (with one of its two faces) to hydrocarbon fire only, based on the one-dimensional (1D) model (Gibson e*t al*, 1995) using a finite difference (FD) numerical analysis approach. Now the new version of the program can be used to predict the thermal responses of composite laminates exposed to different heating sources, and the resin systems and fibre reinforcements involved can be of different types.

7.1.2 The Non-linear Governing Equation in Heat Transfer

The 1-D FD thermal model accounts for the total energy transfer through a composite laminate by taking into consideration a number of factors which contribute to the slow burn through effect observed in thick composite laminates.

The derivation of the governing equation is given as following:

- A 1D FD element cut from the composite laminate under examination with a unit cross-sectional area and a length of (Δx) in the through-thickness direction is shown below:

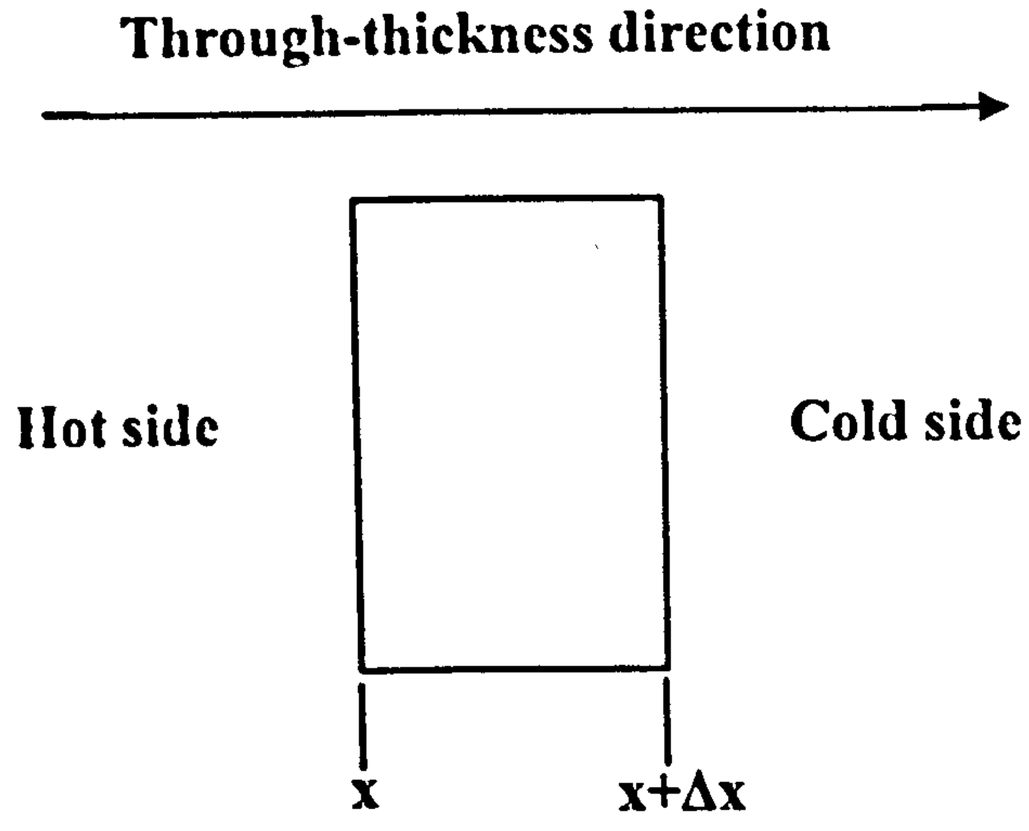

Figure 7.1 One 1D FD element

- Rate of change of internal energy inside the 1D FD composite element:

$$\frac{\partial}{\partial t}(\rho_{com} h_{com})(\Delta x) \tag{7.1}$$

where ρ_{com} denotes density of the composite material, whilst h_{com} represents enthalpy of the material.

- Internal energy change of the element due to conventional heat conduction:

$$\frac{\partial}{\partial x}\left(k_{com}\frac{\partial T}{\partial x}\right)(\Delta x) \tag{7.2}$$

where k_{com} represents thermal conductivity of the composite material and T (in:^{o}C) denotes temperature of the body.

- Internal energy change of the element due to gaseous mass flow (from the cold side to the hot side):

$$\frac{\partial}{\partial x}\left(\dot{M}_g h_g\right)(\Delta x) \tag{7.3}$$

where $\dot{M}_g$ denotes gaseous mass flux, or rate of gaseous mass flow, and h_g denotes enthalpy of the gases generated during decomposition.

- Internal energy change of the element due to heat generation or absorption:

$$-Q_p \frac{\partial \rho_{com}}{\partial t}(\Delta x) \tag{7.4}$$

where Q_p denotes heat of decomposition and is negative for endothermic reaction.

Having assumed that there is no accumulation of gases generated in the composite during fire exposure, a consideration of the energy conservation of the element under examination leads to the following non-linear partial differential equation:

$$\frac{\partial}{\partial t}(\rho h)_{com} = \frac{\partial}{\partial x}\left(k_{com} \frac{\partial T}{\partial x}\right) + \frac{\partial}{\partial x}\left(\dot{M}_g h_g\right) - Q_p \frac{\partial \rho_{com}}{\partial t} \tag{7.5}$$

The term on the left hand side of Eqn. (7.5) can be re-written as:

$$\rho_{com} \frac{\partial h_{com}}{\partial t} + h_{com} \frac{\partial \rho_{com}}{\partial t} = \left(\rho C_p\right)_{com} \frac{\partial T}{\partial t} + h_{com} \frac{\partial \rho_{com}}{\partial t} \tag{7.6}$$

and the second term on right hand side of Eqn. (7.5) can be re-written as:

$$\dot{M}_g \frac{\partial h_g}{\partial x} + h_g \frac{\partial}{\partial x}\left(\dot{M}_g\right) = \dot{M}_g \left(C_{pg}\right) \frac{\partial T}{\partial x} + h_g \frac{\partial}{\partial x}\left(\dot{M}_g\right) \tag{7.7}$$

Here, $\left(C_{pg}\right)$ represents the specific heat of the gases generated.

Through considering mass conservation over the element, one may derive the following equation:

$$\frac{\partial}{\partial x}\left(\dot{M}_g\right)=\frac{\partial \rho_{com}}{\partial t} \tag{7.8}$$

and therefore, the gas mass flux, $\dot{M}_g$, at any position, x, and at any time, t, may be calculated by integrating Eqn. (7.8):

$$\dot{M}_g = \int_{solid\,surface}^{x} \frac{\partial}{\partial t}(\rho_{com})dx \tag{7.9}$$

Substitution of Eqns. (7.6-7.9) into Eqn. (7.5) leads to the following governing equation adopted in the program:

$$(\rho C_p)_{com}\frac{\partial T}{\partial t}=\frac{\partial}{\partial x}\left(k_{com}\frac{\partial T}{\partial x}\right)+\dot{M}_g C_{pg}\left(\frac{\partial T}{\partial x}\right)-\frac{\partial \rho_{com}}{\partial t}\left(Q_p+h_{com}-h_g\right) \tag{7.10}$$

where: T, t and x are temperature, time and through thickness coordinates, respectively.

When the hot surface of a composite sample exposed to a fire reaches a sufficiently high temperature, chemical reactions within the composite body may begin to occur and its resin component degrades to form gaseous products. The following n^{th} order Arrhenius equation is adopted in the thermal analysis to simulate the decomposition process of the resin system involved:

$$\frac{\partial m}{\partial t}=-Am_0\left[\frac{m-m_f}{m_0}\right]^n \exp(-E/RT) \tag{7.11}$$

where:

m	=	mass of the resin (kg),
m_o	=	initial mass of the resin (kg),
m_f	=	final mass of the resin at the end of decomposition (kg),
A	=	pre-exponential factor (1/sec),
T	=	temperature of the resin (^oK),
n	=	order of the chemical reaction (non-dimensional real),

E = activation energy (J/mole),

R = gas constant (= 8.314 J/mole/°K).

The governing equation (i.e. (7.10)) must be solved simultaneously with Eqn. (7.11).

The four kinetic parameters appearing in Eqn. (7.11) (i.e. activation energy, E, pre-exponential factor, A, order of the chemical reaction, n and final mass of the resin at the end of decomposition, m_f) can be derived from processing the thermogravimetric data using Anderson's single heating rate technique as described in Chapter 6.

7.2 The Fire Modelling Program

The non-linear partial differential equation (i.e. Eqn. (7.10)) governing the heat transfer process from a heating source to a composite laminate is numerically solved using a straightforward explicit finite difference method and iteration procedure. The iteration procedure is required in dealing with thermal boundary conditions.

Thermal boundary conditions on the hot face (HF) of the laminate are specified in the analysis as natural convection combined with free radiation when exposed to a heating source. In the numerical analysis, the values of emissivity and absorptivity of the front face of composite laminate under examination have to be input, whilst the value of the emissivity of the heating source is also required in the input.

The heat exchange process or the energy transfer from a heating source to a composite laminate sample during the exposure time period is controlled by thermal interaction between the specified heating source surrounding the front hot face (HF) and the hot face of the sample itself through thermal radiation and natural convection. In fire situations, radiation is always the main mechanism in energy transfer and no forced heat convection is assumed in the analysis.

The total heat flux, q, into the front hot face of a composite sample is determined according to the following equation:

$$q = \sigma\left(\varepsilon_s \alpha_m T_s^4 - \varepsilon_m T_m^4\right) + h_c\left(T_s - T_m\right) \tag{7.12}$$

where

q = heat flux into the hot face of the material sample (W/m^2);

T_s = surrounding temperature of heating source;

T_m = temperature on hot face of the material sample;

h_c = heat transfer coefficient through natural convection ($W/m^2/C$);

ε_s = emissivity of heating source (-);

α_m = absorptivity of the HF material of the sample;

ε_m = emissivity of the HF material of the sample;

σ = Stefan-Boltzmann constant (56.7×10^{-12} $W/m^2/K^4$).

The first term on the right hand side of Eqn. (7.12) represents the energy transfer to the sample from the heating source through thermal radiation, which follows the familiar Stefan-Boltzmann law. The second term represents the energy transfer to the sample through natural thermal convection from the heating source.

For prediction purposes, the evaluation of flame emissivity under specified conditions is necessary, since its value is usually a complex function of field temperatures.

To measure the surrounding temperature of a heating source in a fire test, T_s, thermocouples should be placed in such positions which are close to the front hot face of the sample within the boundary layer thickness of the fluid flow.

As indicated by Buchanan (2001), in fire situations most hot surfaces, smoke particles or luminous flames may have an emissivity between 0.7 and 1.0. This was also the finding revealed by Gibson *et al*, (2003).

In general, the emissivity of the hot face of an FRP composite laminate sample, ε_m, can be taken as 0.8, and in most practical cases, the absorptivity of the hot face of the sample, α_m, can be taken as 1.0.

There are three options in this program for thermal boundary conditions on the cold face of the laminated sample under examination: (1) thermally insulated; (2) natural convection plus free radiation; (3) connected with a steel plate of a given thickness. Thermal boundary condition on the back face of the steel plate can be either thermally insulated or natural convection combined with free radiation.

7.2.1 Thermal Properties

It is clear that the thermal properties of FRP composites are resin volume fraction-dependent. These properties may vary considerably at high temperatures due to: (1) changes in resin volume fraction; and (2) changes in the composition of the materials due to chemical reactions.

In this program (version 3.4), the initial density, thermal conductivity and specific heat of a given virgin composite material are evaluated for a specified fibre volume fraction, V_f, according to the Rule of Mixture:

$$\rho_{com} = \rho_f V_f + \rho_m V_m$$

$$C_{p,com} = \frac{C_{p,f}\,\rho_f\,V_f + C_{p,m}\,\rho_m\,V_m}{\rho_f\,V_f + \rho_m V_m}$$

$$\frac{1}{K_{com}} = \frac{V_f}{K_f} + \frac{V_m}{K_m}$$

Re-evaluation of the density of the composite material is repeated at each node and each time step during computation to account for changes caused by resin decomposition. The predicted remaining resin content (in: %) at a time and for a layer at a given depth in the through-thickness direction of the composite is called RRC in the analysis.

No density change in E-glass fibres is expected for temperatures up to about 1000°C.

Although it has been found to be unsatisfactory to use the above formulae for estimating the thermal conductivity and specific heat of composites at high temperatures; for simplicity, it is assumed in this program (version 3.4) that the derived initial values of k_{com} and $(C_p)_{com}$ are independent of temperature.

7.2.2 Type of Heating Source

Five different types of heating source are considered in this program and these include:

- The hydrocarbon (HC) curve, which is automatically defined by the program;
- The SOLAS fire curve, which is automatically defined by the program;
- A constant incident heat flux, which is specified by the value of heat flux and the relevant emissivity of the heating source;
- An experimentally or theoretically defined temperature vs. time curve in an input data file describing the thermal environment surrounding the front surface of the composite sample under examination.
- An experimentally or theoretically defined temperature vs time curve in an input data file describing temperatures on the front hot surface of the composite sample.

The final type above is associated with no particular heating source. This special type of 'heating source' is designed for predictions to be compared with predictions obtained from running commercial FEA or FDA packages in a conventional thermal analysis, where thermal boundary conditions are usually defined as temperatures on boundary surfaces as a function of time. For thermal analysis in most commercial packages, the effects of decomposition reactions in materials at high temperatures are usually not included.

7.2.3 Input and Output Data Required for Running the Program

The main input data files to the program are (unit = 31, file = fort.31) and (unit = 32, file = fort.32). The input data file (unit=31, file=fort.31) is used to define the job title, the dimensionless Fourier number in heat transfer analysis, the initial room temperature specified, the resin system involved (such as polyester resin, vinyl ester

resin or phenolic resin). It is also used to define the type of glass reinforcement involved (such as E-glass fibres, carbon fibres or Kevlar fibres). Also the fire exposure time period (in minutes) and the thickness of the GFRP laminate under examination (in: mm) as well as the fibre volume fraction of the GFRP laminate under examination are to be specified in this input.

For printing out the relevant results, seven node numbers (chosen from 2 to 51) are to be specified. For example, ND4 = 26 means that the corresponding results for the mid-plane node or for the 25th layer of the laminate are those in the middle column of the file.

The three kinetic parameters of the first stage of the reaction (such as AA, EE and H) are also to be specified. The type of heat source under examination also has to be specified; for instance; = 0 for HC curve; = 1 for the case where the heating source is defined by the input data file (unit=32); = 2 for a constant heat flux; = 3 for SOLAS fire curve. Finally, the emissivity of the heating source, and both the emissivity and the absorptivity of the GRP laminate's front surface have to be specified.

The input data file (unit=32, file=fort.32) is used for the case where the heating source is defined from experimental data. This contains four main inputs. The first input is used for identification of the job, the second input is the total number of data lines, the third input indicates the time unit adopted (i.e. = 1 if the time unit adopted in this input file is minutes; = 2 if the time unit adopted in this input file is seconds). The last input from input unit 32 indicates the environmental temperature at a given time.

There are five output files from running this program. However, the main output files are the temperature profiles in the through-thickness direction of the laminate at the chosen seven node positions for the specified fire exposure time period, and the predicted RRCs as functions of time at the chosen seven layers of the laminate. The RRCs are expressed as the percentage of remaining resin content over the initial resin weight.

The input and output data files are described in detail in Appendix 1.

7.3 Some Experimental Results of Composite Laminates in Fires

Fire tests were conducted with some hand lay-up WR specimens using a small furnace and the results are illustrated in Fig. 7.2.

Values for the kinetic parameters of the samples were taken as standard from previous work (i.e. in Chapter 6). The pre-exponential factor in the stage one reaction was 0.98E+13 (1/sec.), the activation energy 0.144E+06 (J/mol), and the heat of decomposition 2344600 (J/kg). The heat input was taken from the experimental data, or assumed to be constant, and the rear face was assumed to either be thermally insulated (no heat transfer) or free to radiation and natural convection. The emissivity and absorptivity of the samples were given arbitrary values based upon past experience of 0.8 and 1.0 respectively. Figure 7.3 shows the typical model output for 10mm thick WR based laminates for (a) orthophthalic polyester resin, (b) isophthalic polyester resin, and (c) vinyl ester resin. The test conditions yielded similar temperature profile behaviour throughout the laminates regardless of the resin type. After a rapid temperature rise in the first 200 seconds, the gradient of the temperature profile can be seen to become gentler. This is attributed to the cooling effect of the volatile products of the resin decomposition moving towards the flame.

Both the gas flow and the endothermic effects are neglected. The gas flow term in Eqn. (7.10) requires a significant amount of computation. Current work on the extension of the model from one to two dimensions means that the possibility of neglecting gas flow will considerably simplify computation. Another very significant result predicted by the model observed here concerns the effect of glass content. Up till now, for fire protection applications, great efforts have been made by several companies to achieve laminates with the highest possible glass content. Of course, the greater structural integrity of WR will be of prime importance when laminates are under load in a fire. One of the main reasons for developing the fire model was to save on the cost of fire testing when developing laminates for specific fire protection applications.

(a)

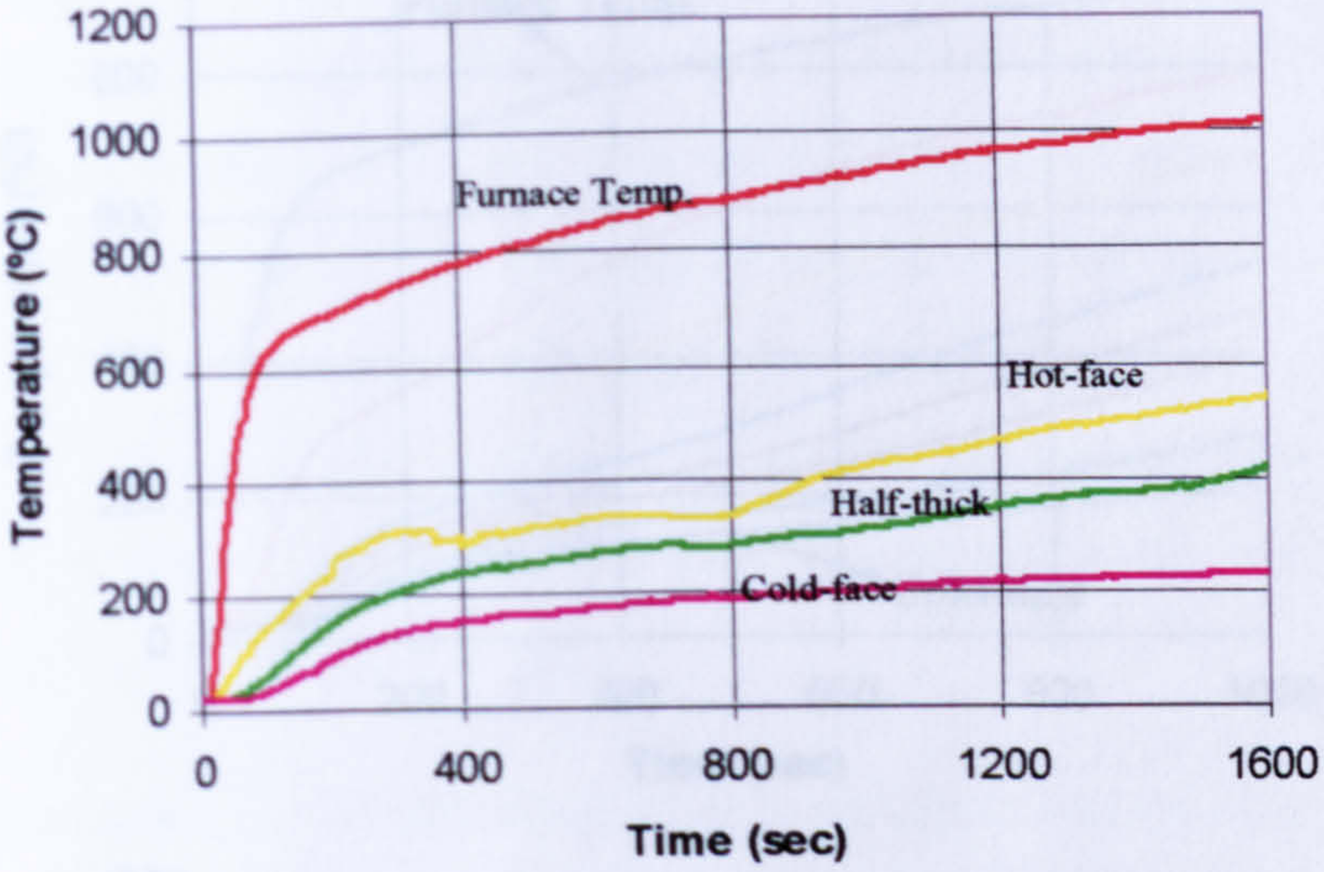

(b)

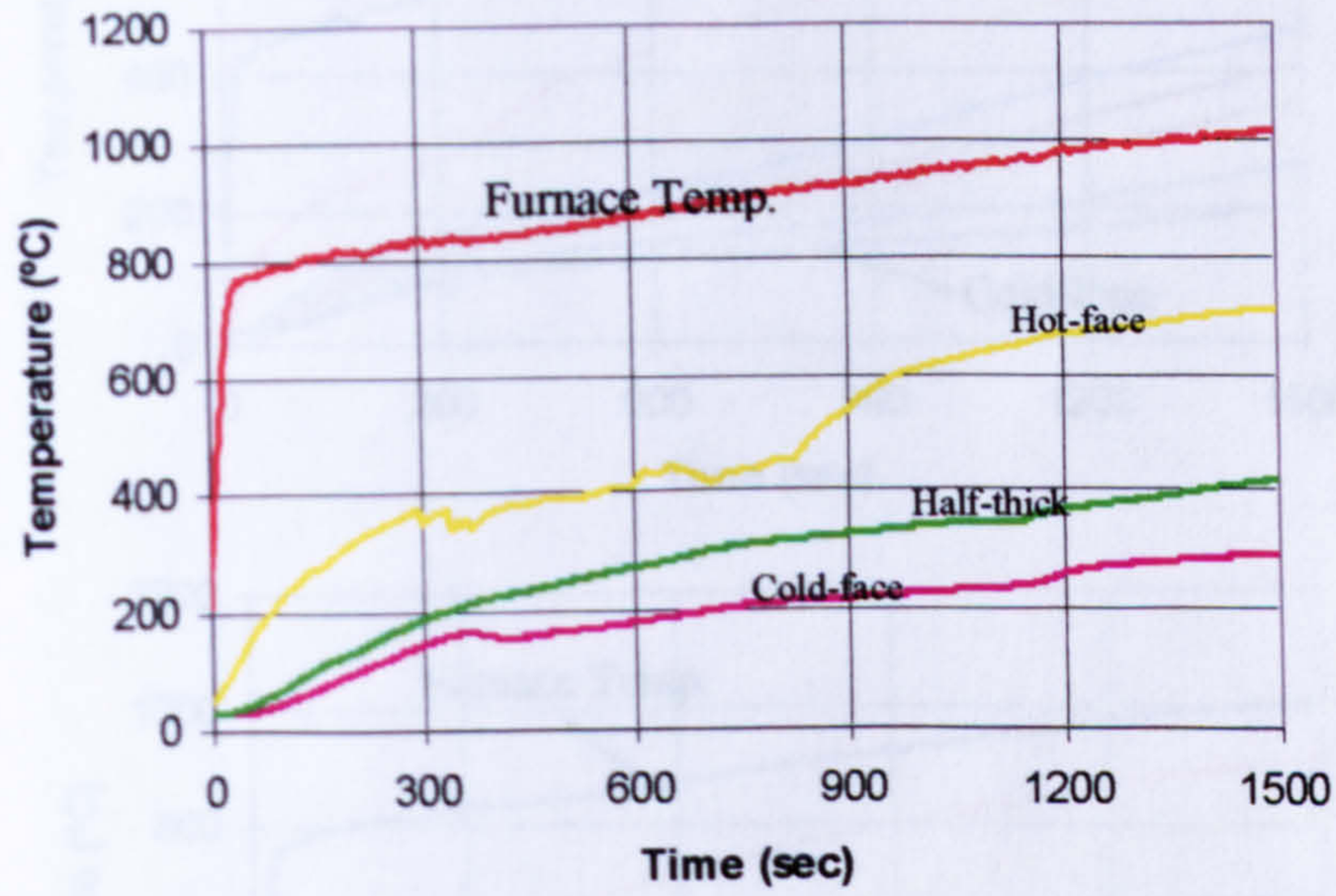

Figure 7.2 Experimental furnace fire test results on WR laminates for: (a) orthophthalic polyester (V_f = 48%), (b) Vinyl ester resin (V_f = 50%).

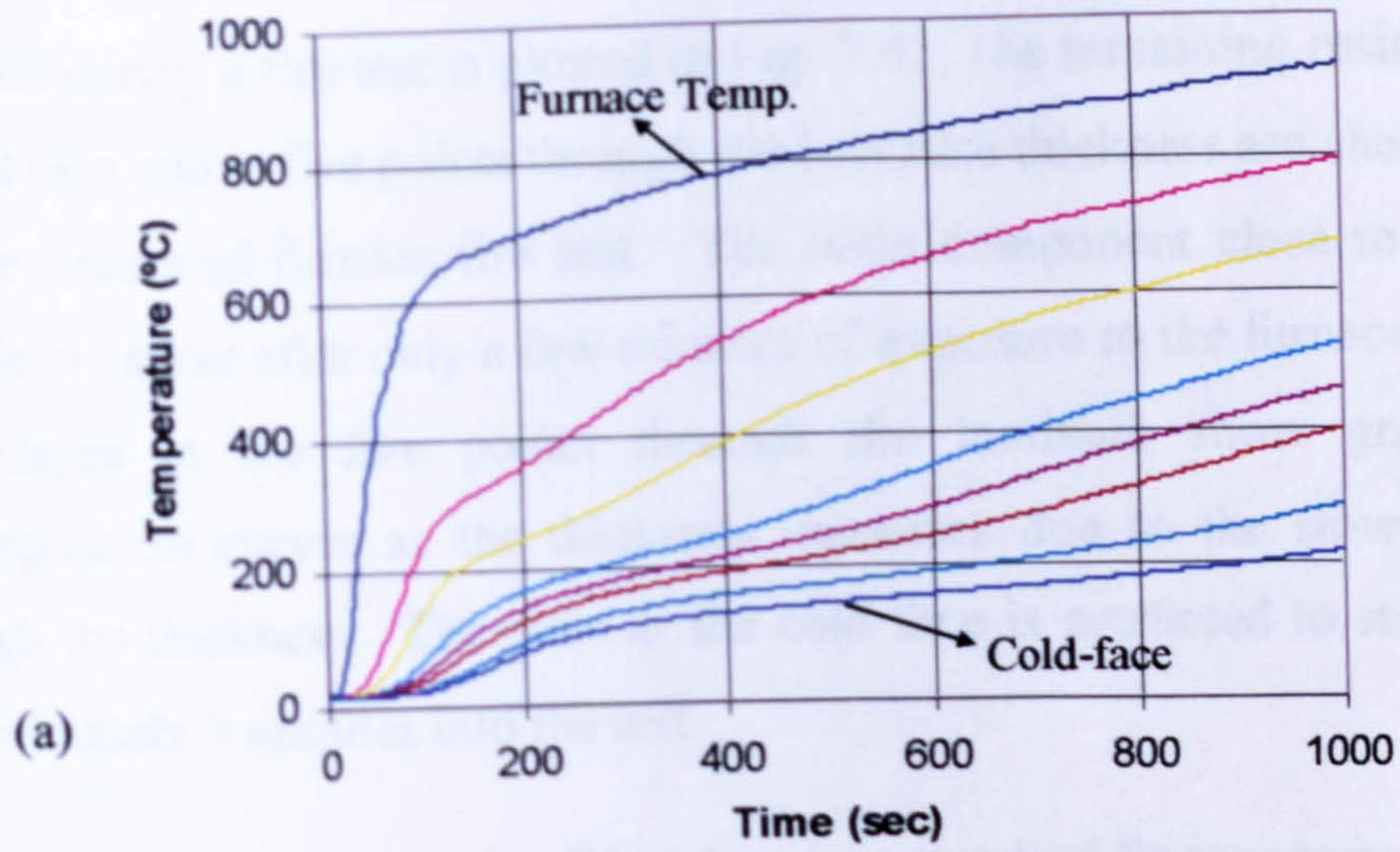

(a)

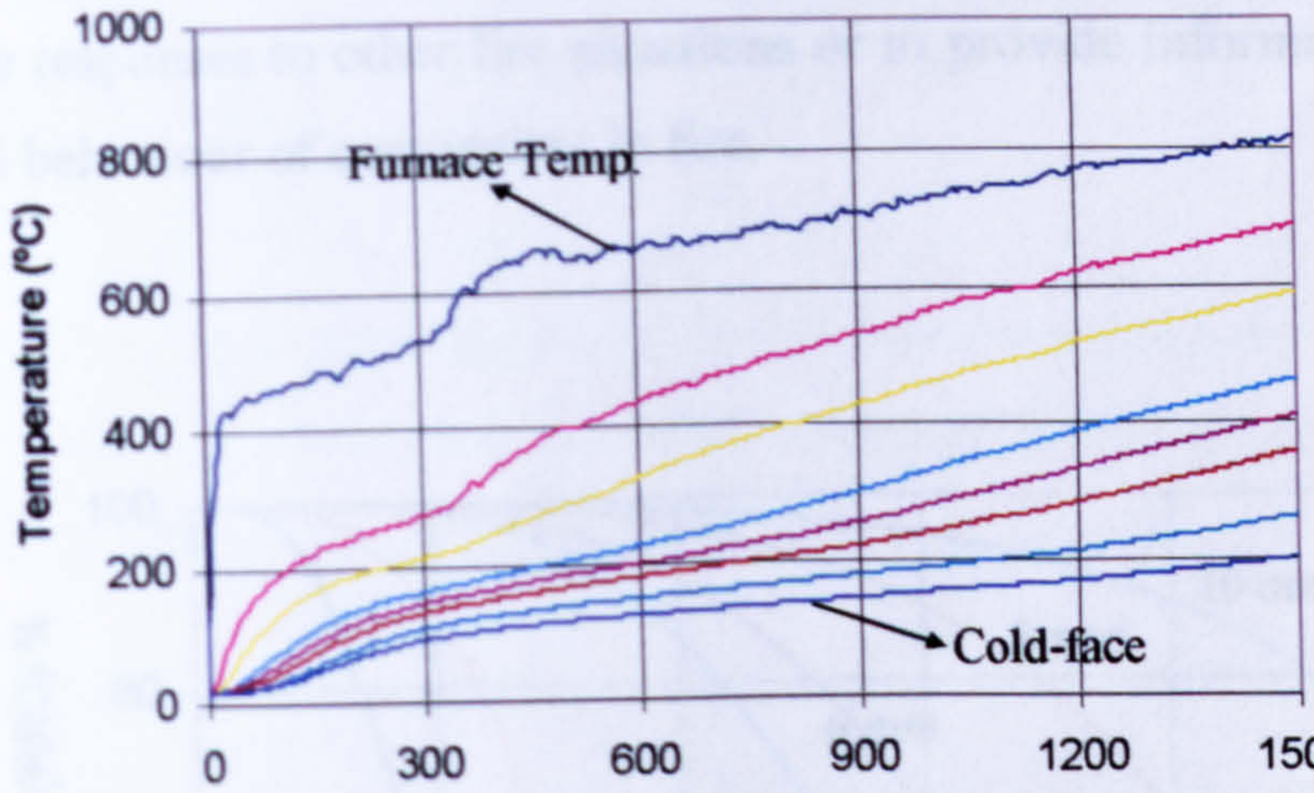

(b)

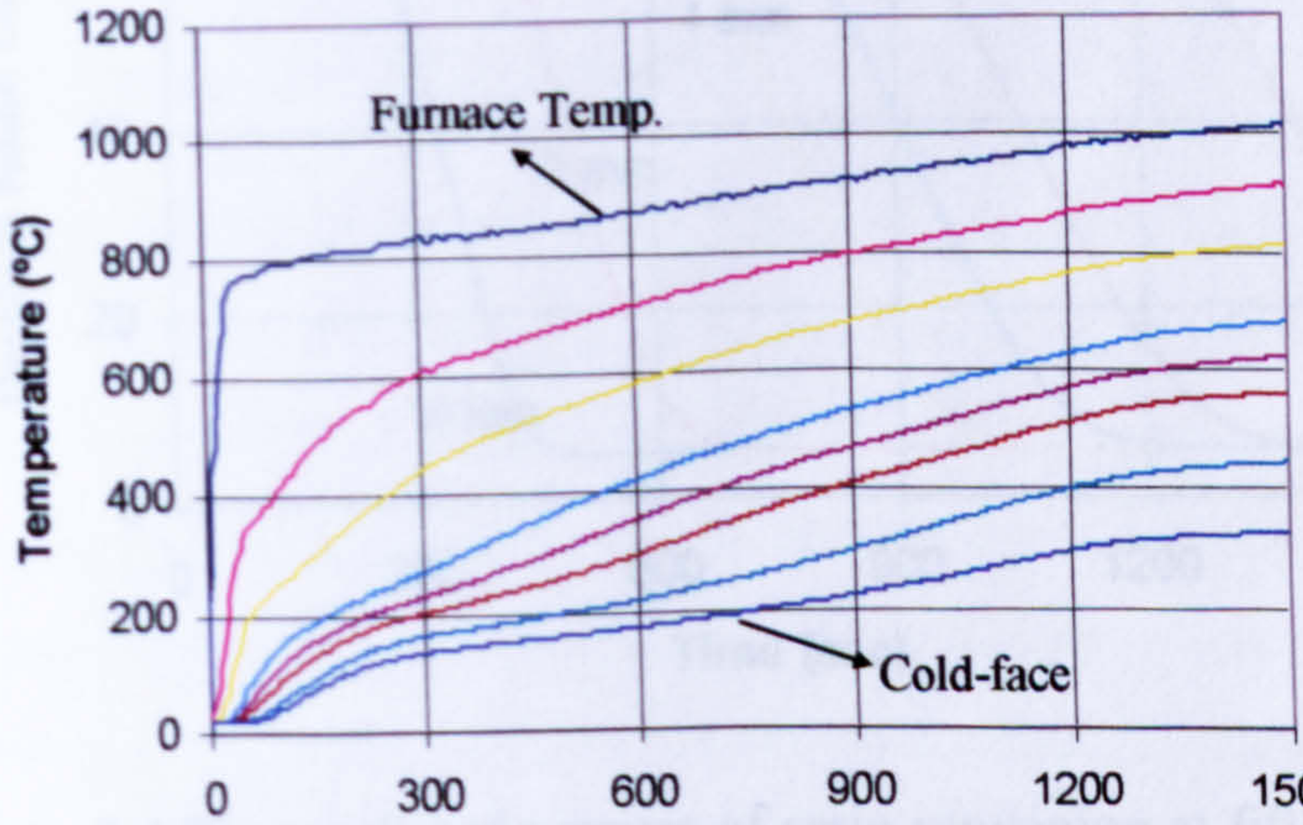

(c)

Figure 7.3 Modelled thermal profiles for composite panels of three different laminates: (a) WR/orthophthalic polyester resin (V_f = 48%, (b) Isophthalic polyester resin (V_f = 45%)and (c) Vinyl ester resin system (V_f = 50%).

The predicted ablation of a 10mm thick 45% volume fraction polyester/glass laminate during a fire test is plotted in Fig. 7.4. The remaining resin percentages at the hot face and at five points through the laminate thickness are shown against time for the simulated furnace fire test. The resin component close to the hot face is completely spent after only a few minutes of exposure to the furnace fire. The resin percentages at the five points through the laminate show gradually broader decomposition curves as the thickness increases due to the slower heating rates through the thickness. The resin at the cold face is predicted to start decomposing approximately 9 minutes into the test.

The thermal response model validated against standard furnace tests can be extended to predict the responses to other fire situations or to provide information relevant to the structural behaviour of composites in fire.

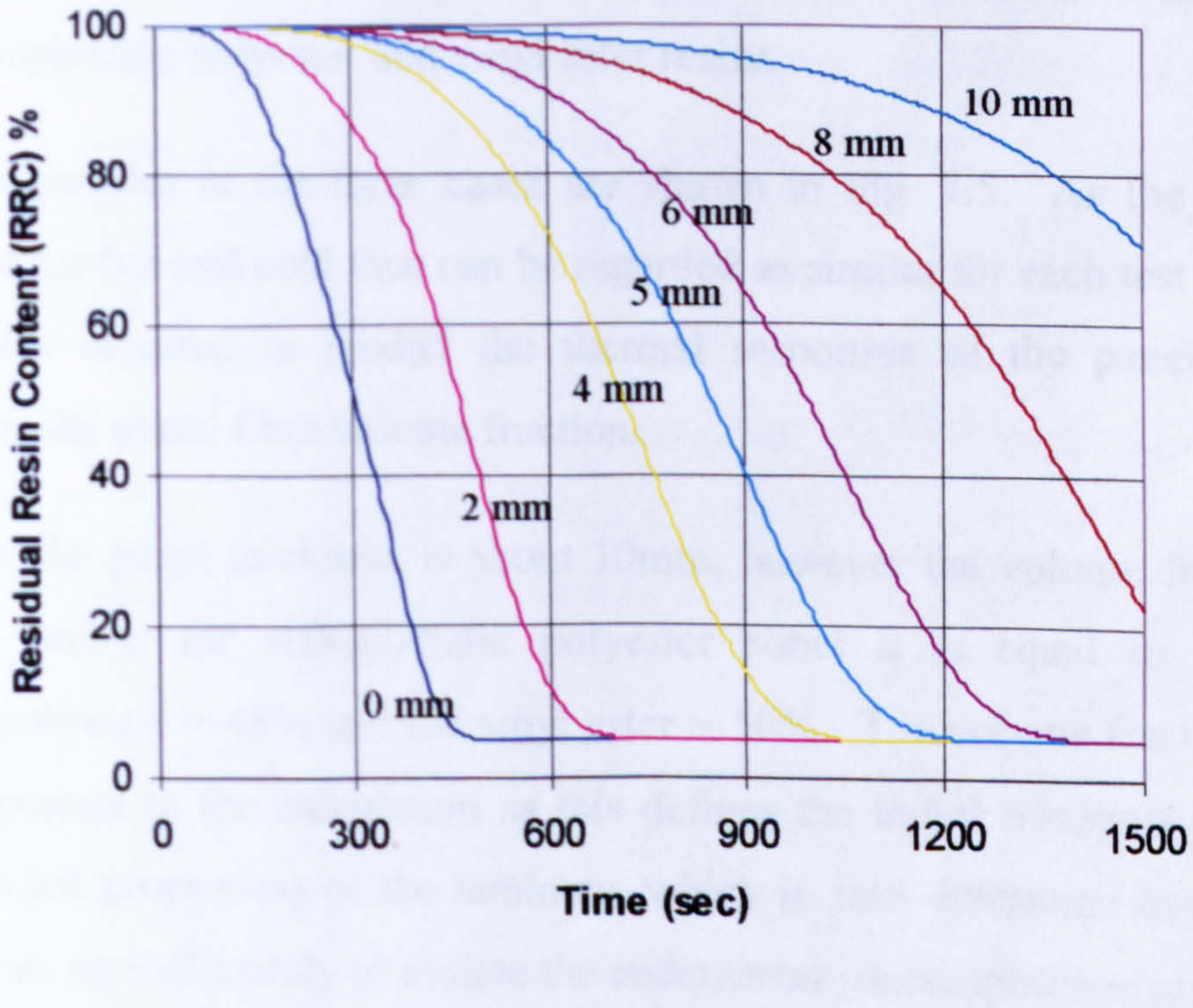

Figure 7.4 The predicted amount of resin remaining at fifth points through the thickness for a 10.0mm thick, 48% volume fraction polyester / glass laminate during furnace fire test.

Extension of the one-dimensional thermal model to higher dimensions would allow a complete prediction of the temperature distribution in a complex shaped component. This knowledge would allow calculation of the thermal stresses in the structure due to the fire; thus assisting in risk assessment for an overall structure.

Subject to a knowledge of the relevant boundary conditions, the model may be used to predict the responses of composite materials to pool fires, jet-fires or other fire incidents. An example of the use of the thermal model is the preparation of design information for the use of composite materials in fire sensitive applications.

7.4 Comparison of Results from Fire Testing and Predictions

Comparison of the experimental measurements and the predicted thermal responses are presented in Fig. 7.5 for E-glass WR reinforced laminates with orthophthalic polyester, isophthalic polyester and vinyl ester resins.

Temperature profiles in the three cases are shown in Fig. 7.5. As the boundary conditions at the hot and cold face can be regarded as similar for each test setup, the only variables required to predict the thermal responses of the panels are the thickness and the initial fibre volume fraction.

In each case the panel thickness is about 10mm, however the volume fraction for each panel varies; for orthophthalic polyester panel it is equal to 48%, for isophthalic polyester = 45% and for vinyl ester = 50%. The volume fraction of the panel is important to the calculation as this defines the initial transport properties (i.e. undamaged properties) of the laminate, which in turn determine how quickly the panel heats up sufficiently to initiate the endothermic decomposition reaction.

It can be seen that, despite the complexity of some of the processes occurring in fire, reasonable agreement can be obtained between the model and the measured data for the three composites over a range of volume fractions.

It should, however, be pointed out that laminates of thinner thickness would not in any case be expected to behave in the same way as thick ones (i.e. >12mm) since a critical thickness is needed for the progressive degradation process to take place (Gibson and Wu, 1994). It has been found for thicker specimens (> 10mm) that the cold face temperature response is reproduced very accurately. This size effect can be explained by the reduced structural integrity of thinner sections of laminates. The model does not account directly for delamination of the composite layers. The slow burn-through effect caused by the endothermic decomposition of the resin is allowed to develop as the panel maintains its structural integrity. For thinner panels, the insulation failure criterion of a temperature rise of 140°C is breached very rapidly, and the structural integrity of the laminate is quickly reduced as the surface reinforcement layers are delaminated.

The form of the cold face response is similar in all the samples tested. Following an initial temperature rise there is a prolonged plateau, corresponding to the removal of the volatile material from the laminate. The main significance of the results is the presence of this plateau, which in the field would provide a delay in the transmission of heat into the zone or component protected by the laminate. The temperature of the plateau region, and most especially the time it lasts, are of course key features of the fire resistance of a laminate.

It was probable that the Arrhenius constants for the decomposition reaction, calculated from TGA data, would require adjustment in order to fit the model predictions to realistic fire test results. The experimental scatter is seen in the inter-laminar thermocouple outputs, due to delamination of the panels as resin is decomposed locally to the thermocouples. The predicted inter-laminar temperatures do not follow the thermocouple outputs exactly, due to the modelling of the delaminations by averaging the transport properties, but the cold face temperature prediction is accurate.

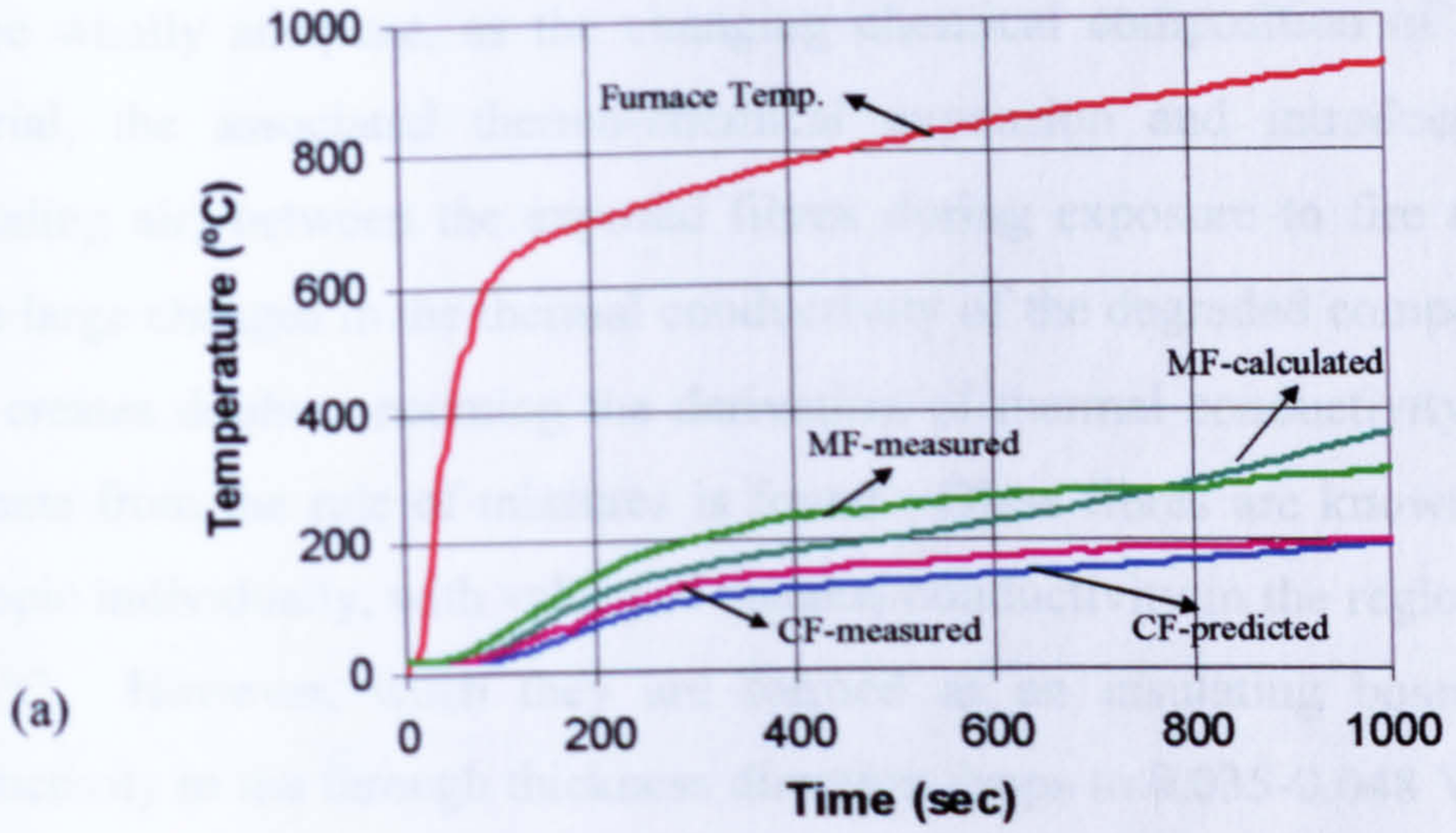

(a)

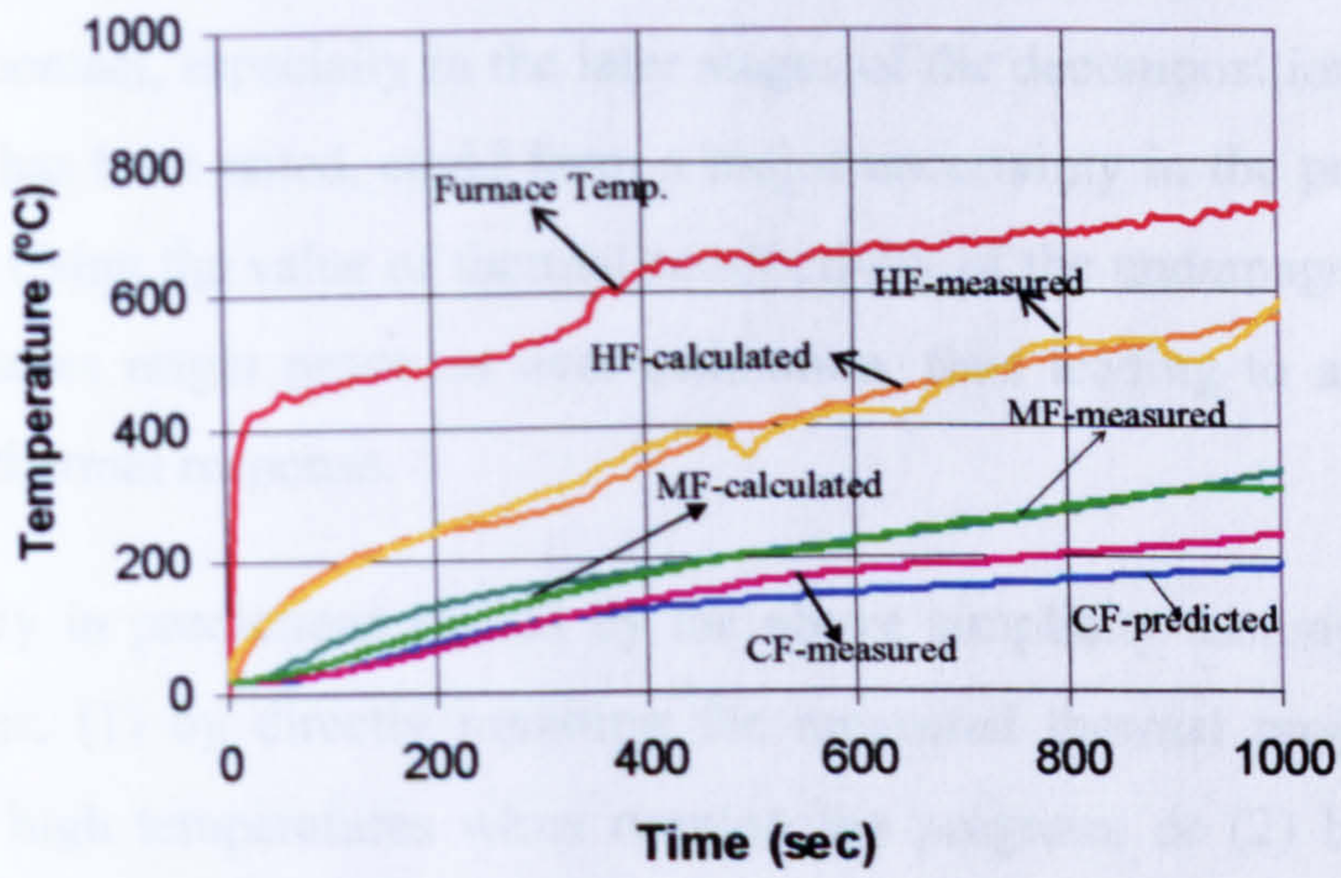

(b)

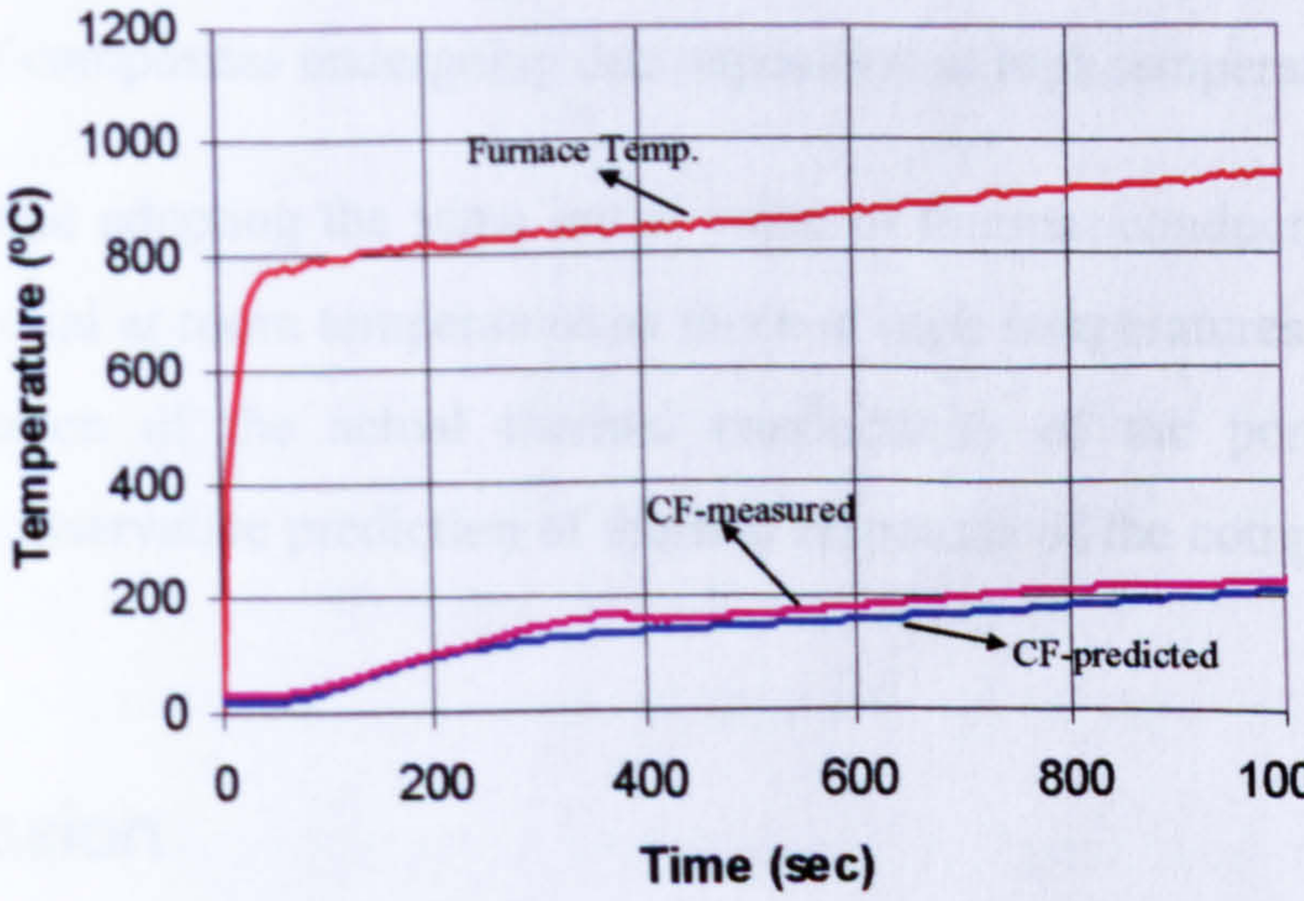

(c)

Figure 7.5 A comparison of the experimental and calculated fire test results for: (a) WR/orthophthalic polyester resin (V_f 48= %, (b) Isophthalic polyester resin (V_f = 45%)and (c) Vinyl ester resin system (V_f = 50%).

The use in the modelling of constant thermal properties at high temperatures may not be wholly adequate, as the changing chemical composition of the laminated material, the associated thermo-chemical expansion and introduction of gases (including air) between the exposed fibres during exposure to fire are thought to cause large changes in the thermal conductivity of the degraded composite laminate. This creates doubt concerning the derivation of thermal conductivity for degraded laminate from the rule of mixtures is found. Glass fibres are known to be almost isotropic individually, with values of thermal conductivity in the region of 1.05-1.09 W/m°C. However, when they are formed as an insulating board the thermal conductivity in the through thickness direction drops to 0.035-0.048 W/m°C (Bejan, 1993). The elimination from the model of the change in thermal conductivity of the fibres due to contact, especially in the later stages of the decomposition where some fibre melting has been noted, could form a major uncertainty in the prediction (Wu *et al.*, 2004). Using the value of thermal conductivity of the undamaged laminate at high temperatures might prove an over-estimation, thus leading to a conservative prediction of thermal response.

The inaccuracy in predictions caused by the above simplicity assumption is to be resolved either; (1) by directly inputting the measured thermal properties of the composite at high temperatures when running the program; or (2) by adopting a modified Rule of Mixture in the program for evaluating the thermal conductivity and specific heat of composites undergoing decomposition at high temperatures.

It is expected that adopting the same initial value of thermal conductivity of virgin composite material at room temperature as those at high temperatures might lead to an over-estimation of the actual thermal conductivity of the porous laminate, resulting in a conservative prediction of thermal responses of the composite material in fires.

7.5 Discussion

Despite vibrant debate over the approximations of input parameters and assumptions made in the computations of the thermal model presented for analysis, the agreement between modelled and measured responses is considered very good indeed.

It can be seen that significant heat transfer occurs through the samples with a non insulated rear face, thus slowing the decomposition of the composite resin and the breakdown of the ablative protection. Therefore, under the conditions and laminate thicknesses tested vinyl ester would be a more suitable fire barrier than polyester. However at lower heat fluxes polyester may perform equally well. Under the conditions tested the polyester would outlast the vinyl ester by 100 seconds, with decomposition behaviour up to that point being almost equal.

A modification to the program that truly represents the two dimensional heat transfer effects in the laminates would improve the agreement of the model and measured results.

It is suggested that the existence of gases or air in the voids generated during decomposition of the composite material is taken into account in formulating a modified Rule of Mixture:

7.6 Conclusions

- A simple one dimensional F D model has been found to be capable of modelling the thermal response behaviour of polyester/WR and vinyl ester/WR laminates subject to fire tests.
- The most important term in the model and the most significant effect is that of the resin decomposition endotherm, which delays heat conduction through the panel and produces a plateau in the cold face response.
- Extension of the 1D thermal model to 2D or 3D allow a complete prediction of the temperature distribution in a complex shaped component. This knowledge allows calculation of the thermal stresses in the structure due to the fire, and would assist in risk assessment for an overall structure.
- Subject to a knowledge of the relevant boundary conditions, the model may be used to predict the responses of composite materials in pool fires, jet fires or other fire incidents. An example of the use of the thermal model is the preparation of design information for the use of composite materials in fire sensitive applications.

CHAPTER 8

CONCLUSIONS AND FUTURE WORK

8.1 Conclusions

From the study conducted using the small scale propane burner as the fire testing facility, the following conclusions can be drawn:

- The small scale propane burner can be used to provide a constant heat flux input of up to 150kW/m^2 for the fire testing of composite laminates in a laboratory with an exposed surface area of about 100x100mm.
- Flames are selective emitters. The effective emissivity ε_{eff} of the flames produced by the propane burner in a fire test is a complex function of the 'surrounding field temperature', T_s, which is the temperature measured at a position about 10mm away from the receiving surface. The emissivity is a function of (i) pressure, and (ii) the distance between propane burner and the objective.

- It was found from this study that the effective emissivity ranged from 0.7-1.0 for the given environmental conditions in the laboratory. This finding is nearly the same as those reported by Perry and Chilton (1973) and Buchanan (2001).

- It was found from this experimental study that a thermal capacitance–type meter suggested by ASTM E:457-96 should be used only for measurements of a heat flux level resulting in a body temperature not higher then 70°C, mainly in order to ensure that the heat radiation effect from the meter receiving surface can be ignored.

Based on the small scale fire testing facility, the transient response method proposed in this study can be adopted to determine the thermal conductivity of dry glass fibre mats as a function of temperature from about 20°C-800°C. The derived thermal conductivity of the particular composite mats (dry glass fibres +

air) are in a good agreement with relevant published data. Furthermore, an empirical equation was derived for estimating the variation in the thermal conductivity of dry glass fibre mats.

- Five composite samples have been fire tested to examine fire resistance performance. Those are produced from the DML. The samples were exposed to the standard 'SOLAS' time-temperature curve. The results indicate that A60 fire rating can be well met by two of the five samples. For instance, the performance of 100mm Rockwool with 1mm E-glass/epoxy skin and the 35mm syntactic phenolic foam with 5mm E-glass/phenolic skin specimens can meets A60 with requirements. It is noted that to just meet A60 requirements, the thickness of the Rockwool layer might be largely reduced. On the other hand, the experimental results show that the 20mm E-glass WR/epoxy meets A30 requirements only, whilst the 4mm Technofire 60853 intumescent/epoxy was failed to meet the requirements.

- Another series of composite laminated samples produced by VT were tested. All the test laminates performed in a similar manner and gave maximum HTC values during the test of less than the target value of $30 Wm^{-2} °C^{-1}$. Any of the laminates would therefore be of suitable construction, from a purely thermal viewpoint, for the application.

The actual mean value was $24.1 Wm^{-2}K^{-1}$, with a 95% upper confidence limit of $26.4 Wm^{-2}K^{-1}$, which is significantly lower than the required value. Qualification has therefore been achieved.

There is no systematic difference between gel-coated and non-gel-coated samples, so the gel-coat used is unlikely to damage fire protection performance. The laminates containing steel mesh are slightly less effective than those without it. Since the main qualification was achieved with the mesh samples, both types of laminate qualified from a thermal performance viewpoint.

- To run the 1D FD fire code in FORTRAN, COM_FIRE, the kinetic parameters of a relevant resin system of composite materials are required as a part of the program input. These kinetic parameters of polyester, vinyl ester, phenolic and

epoxy were obtained by carrying out TGA tests using the Freeman technique under a heating rate of 25 and 60°C in an atmosphere of dry nitrogen, and the FORTRAN program, i.e., TGAP2, was used for the data processing based on the Freeman technique.

The apparent activation energies of isophthalic polyester, orthophthalic polyester, vinyl ester, and epoxy were estimated to be 0.288E+06, 0.144E+06, 0.197E+06 and 0.431E+06 (J/mol), respectively. However, phenolic resin has two stages of reaction, and it was found that E = 0.613E+05 for the first stage and E = 0.134E+06 for the second stage.

- Through comparison between the experimental results and predictions, it can be concluded that the existing one dimensional finite difference model is capable of modelling the thermal response behaviour of polyester/WR and vinyl ester/WR exposed to fires, including heating source like the small furnace or the small scale propane burner used in the CCME, University of Newcastle lab.

8.2 Future Work

- The work carried out in this study has proved that the small scale fire testing facility based on the use of a simple propane burner for examining thermal response of FRP laminates in fires provides a cost-effective way of conducting experimental assessments of the thermal resisting performance of composites in fire. Although incident heat flux levels have been calibrated, the outcome of the calibration tests are to be further confirmed using other approaches such as the cone calorimeter.

- The small scale fire testing facility developed can be used not only for examining the fire resistance of composites exposed to a heating source, but also to measure thermal properties for example, the thermal conductivity of composite material at high temperatures, as shown in this study, based on the transient response method. Further improvement of the transient response method adopted and also other potential methods can be explored to use this

facility for measuring thermal properties (including both K and C_p) of composite laminates at high temperatures which are usually not available in the literature.

- The small scale fire testing facility for composite laminates could be further modified to carry out fire testing on composite in fire under loads to further develop the capacity of this novel facility as schematically shown in Fig. 8.1.

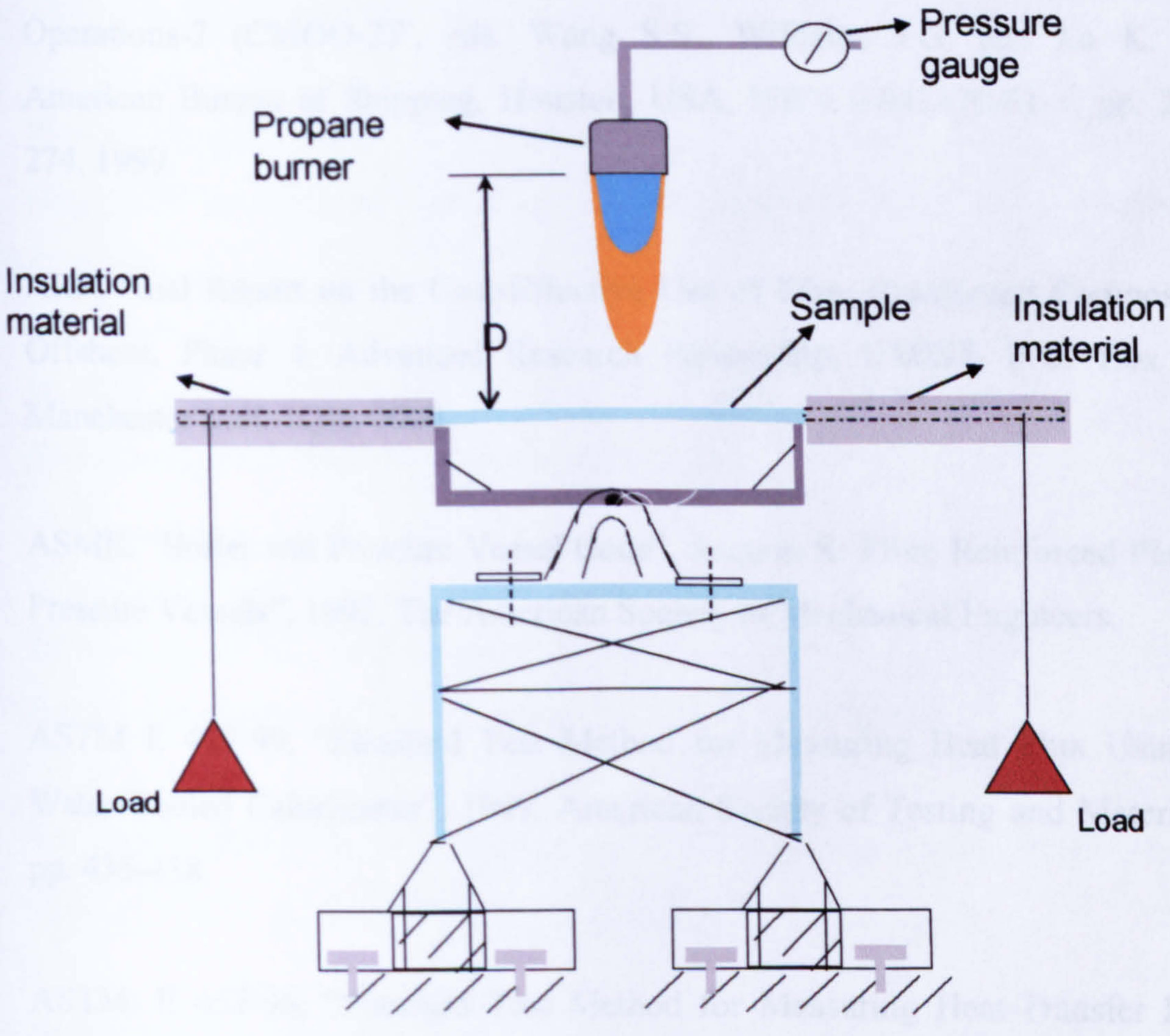

Figure 8.1 Front view of the layout of the testing facility including a sample.

References

Adams M.C., "Recent Advances In Ablation" American Rocket Society, 1959. vol. 29: pp. 625-631.

Anderson D.A. and Freeman E.S., "The Kinetics of the Thermal Degradation of the Synthetic Styrenated Polyester, Laminac 4116", Journal of Applied Polymer Science, 1959. vol. 1(2): pp. 192-199.

Anisdahl D.T.; Wang w. and Stokke R., "In Composite Materials for Offshore Operations-2 (CMOO-2)", eds. Wang S.S., Williams J.G. and Lo K. H., American Bureau of Shipping, Houston, USA, ISBN 0-943870-01-1, pp. 261-274, 1999.

ARP, Final Report on the Cost-Effective Use of Fibre Reinforced Composites Offshore, Phase 4, Advanced Research Partnership, UMIST, P.O. Box 88, Manchester M60 1QD, 2000.

ASME, "Boiler and Pressure Vessel Code", Section X: Fibre Reinforced Plastic Pressure Vessels", 1992. The American Society of Mechanical Engineers.

ASTM E 422-99, "Standard Test Method for Measuring Heat Flux Using a Water-Cooled Calorimeter", 1999. American Society of Testing and Materials, pp. 435-438.

ASTM: E 457-96, "Standard Test Method for Measuring Heat-Transfer Rate Using a Thermal Capacitance (Slug) Calorimeter", 1997. American Society of Testing and Materials, pp. 454-458.

Bamford C. H., Crank J. and Malan D.H., "The Combustion of Wood. Part1" Cambridge Phil. Soc. Proc., 1946. vol. 42: pp. 166.

Bejan A., "Heat Transfer", Appendix D: Properties of Gases, John Wiley & Sons, Inc., 1993.

Boyer G. T., "An Analytical and Experimental Investigation of the Thermophysical Properties of a Swelling Charring Composite Material" MSc. Dissertation, 1984. Virginia Polytechnic Institute and State University.

Brian Y. L. and Jason O., "Thermal Properties of Composites for Heat Transfer Modelling During Fires", in SAMPE 2004. May 16-20, 2004. Long Beach, CA. USA.

Brown J. R, Mathys Z., "Reinforcement and Matrix Effects on the Combustion Properties of Glass Reinforced Polymer Composites" Composites (Part A), 1997. vol. 28: pp. 675-681.

Brown N.A. and Tipping G. " Fire Safe Polyester Composites Using Aluminium Hydroxide" in Composite in Fire 1. 1999. Newcastle University, Newcastle, England.

BS 476 part 20, "British Standard Fire Tests on Building Materials and Structures", 1987. British Standards Institution.

Browne T. N. A. abd Gibson A. G. "Structural Composites in Fire" in Postgradute Confrence. 2004. Newcastle upon Tyne, England

BS 4994, "Design and Construction of Vessels and Tanks in Reinforced Plastics", 1987. British Standards Institution.

BS 5950: "The Structural use of Steel in Buildings Part 8: Code of Practice for Fire Resistant Design", 1990. British Standards Institution.

BS 6336, "Development and Presentation of Fire Tests and their Use in Hazzard Assessment", 1982. British Standards Institution.

Buchanan A. H., "Structural Design for Fire Safety", Wiley J. & Sons Ltd, 2001. pp. 35-56.

Cantrill J. and Gibson A. G. "Reinforced Thermoplastic Pipe: Performance and Applications", in ninth international conference on fibre reinforced composite, 2002. Newcastle upon Tyne, England.

Childs R.N., Greenwood J.R., and long C., "Heat flux measurement techniques", Proc Instn Mech Engrs, 1999. vol 213 part c: pp. 655-677.

Convention for Safety of Life at Sea (SOLAS) 1974, Consolidated Edition 1992, IMO London.

Crank J. "The Mathematics of Diffusion" Clarendon Press, 2nd Edition Oxford, 1975.

Cullen H. L., "The public Inquiry into The Piper Alpha Disaster" HMSO, London, V. 2, 1990.

Curtis, P.T. "Crag Test Methods for the Measurement of the Engineering Properties of Fibre Reinforcement Plastics". Royal Aerospace Establishment, Technical report, 1988.

Dewhurst D.W., "The Influence of Fire on the Design of Polymer Composite Pipes and Panels for Offshore Structures", PhD 1997. Civil and Environmental Engineering University of Salford, UK.

Diller T. E. "Heat Flux Calibration-Progress Towards National Standards", In Advances in Heat Transfer, pp. 325-335, 1995.

Dodds N. and Gibson G., "Modelling the Fire Response of Composite Structures for a Range of Thermal Conditions" in Second International Conference on Composite Materials for Offshore operations (CMOO-2), 1997, Houston, USA.

Dodds N., Gibson A. G., Dewhurst D. and Davies J M, "Fire Behaviour of Composite Laminates", 2000. Composites A, vol. 31: pp. 689-702.

Doyle C. D., "Kinetic Analysis of Thermogravimetric Data" Journal of Applied Polymer Science, 1961. vol.15: pp. 285-292.

Eastop T. D. and McConkey A., "Applied Thermodynamics" Longman, London and New York, 1978. p. 687.

Freeman, E.S. and Carroll B., "The Application of Thermoanalytical Techniques To Reaction Kinetics. The Thermogravimetric Evaluation of The Kinetics of the decomposition of Calcium Oxalate Monohydrate", Phys J. Chem., 1957. vol. 62: pp. 394-397.

Friedman, H. L. "Kinetics of Thermal Degradation of Char-Forming Plastics from Thermogravimetry Application to a Phenolic Plastic", 1965. Journal of Polymer Science: Part C, 6: pp. 183-195.

Gibson A. G. "Composite Materials in the Offshore Industry" Metals and MAterials, 1989. pp. 590-594.

Gibson A. G., Wu Y. S., Chandler H. W., Wilcox J. A. D. and Bettess P. "A Model for the Thermal performance of Thick Composite Laminates in Hydrocarbon Fires" Revue de L'Institute Francais du Petrole, 1995. vol. 50 (1): pp. 69-74.

Gibson A. G. "Review of Applications of Composite Materials in the Oil Gas Industry" Centre for Composite Materials Engineering, University of Newcastle upon Tyne, Newcastle, 2000.

Gibson A. G. and Fahrer A. "Reinforced Thermoplastic Tubes for Pressure Applications" in eight international conference on Fibre reinforced Composites, Ed. A. G. Gibson, 2000, pp. 201-209.

Gibson A.G., editor, Proceedings of Composites in Fire Conferences, University of Newcastle upon Tyne, 15-16 September 1999 and 12-13 September 2001, ISBN 0-9540459-1-2.

Gibson A G, Wright P. N H, Wu Y-S, Mouritz A P, Mathys Z and Gardiner C P, "Modelling the Residual Mechanical Properties of Polymer Composites after Fire", Plastics, Rubber and Composites, 2003. vol. 32 (2), pp. 81-90.

Gibson A. G., Wu Y-S and Naas A. L., "A Low Cost Burner Technique for the Development and Modelling of Laminates in Fire", in Composites in Fire 3, 2003. Newcastle upon Tyne, England.

Henderson J. B., Wiebelt J. A. and Tant M. R., "A Model for the Thermal Response of Polymer Composite Materials with Experimental Verification" Journal of Composite Materials, 1985. vol. 19: pp. 579-595.

Hill P. S. and White G. C., in Composite Materials for Offshore Operations-2 (CMOO-2)', eds. S.S. Wang, J, J.G. Williams and K.H. Lo, American Bureaue of Shipping, Houston TX 77060, ISBN 0-943870-01-1. pp. 623-634, 1999.

Hull D. and Clyne T. W. "An Introduction to Composite Materials", Cambridge University Press, 1996.

Irvine D. J. and McCluskey J. A., "Fire Hazards and Some Common Polymers" Polymer Degradation and Stability, 2000. vol. 67: pp. 383-396.

ISO 5660-1, "THE CONE CALORIMETER TEST", 1993. International Standards Organization.

ISO 834-1, "Fire resistance tests, Elements of building construction, Part 1: General requirements" 1975. International Standards Organization.

Kansa E. J., Perlee H. E. and Chaiken R. F. "Mathematical Model of Wood Pyroloysis Including Forced Convection" Combustion and Flame, 1977. vol. 29: 311-324.

Kanury, A. M., "An Evaluation of the Physico-Chemical Factors Influencing the Burning Rate of Cellulosic Fuels and a Comprehensive model for Solid Fuel Pyrolysis and Combustion." PhD Dissertation, 1969. University of Minnesota, Minneapolis.

Kung, H. C., "A Mathematical Model of Wood Pyrolysis", Combustion and Flame, 1972. vol. 18: pp. 185-195.

Lawson R. M. "Fire Engineering Design of Steel and Composite Building", Journal Constructional Steel Research, 2001. vol. 57: pp. 1233-1247.

Lay F. L and Gutierrez J. "Fire Retardant Composites for Naval Applications" The Use of Alumina Trihydrate (ATH), SAMPE Journal, 2001. vol. 37 (4): pp. 59-63.

Longstaff J. R. "Measurement and modelling of the fire ablation of composites at different levels of heat flux" final year project. 2004. Newcastle University, Newcastle, England.

Looyeh M. E., Bettes P. and Gibson A. G. "A One-Dimensional Finite Element Simulation for the Fire-Performance of GRP Panels for Offshore Structures". International Journal of Numerical Methods for Heat & Fluid Flow, 1996. vol.7 (6): pp. 609-625.

MacInally A., and Miller A. H., "The Use of Epoxy Vinyl ester Resin System in Marine, Offshore, Chemical and Construction Industries". 1998.

Mazumdar S. K., Composites manufacturing: Materials product and process Engineering. CRC press, Boca Raton, Florida, USA, 2002.

McManus HLN, Springer GS., "High Temperature Thermomechanical Behaviour of Carbon-Phenolic and Carbon-Carbon Composites, I. Analysis". J. Comp. Mats., 1992. vol. 26: pp. 206-209.

Mouritz A. P., Gibson A. G. Wu Y-S. Mathys Z. and Gardiner C.P. "Modelling Char Formation in Burning Polymer Laminate Composites" Composites A, 2004.

Oil And Gas Journal "Explosion, Fire Heavily Damage North Sea Platform"., July 11, 1988. p. 20.

Ott H.-J. "Thermal Conductivity of Composite Materials" Plastic and Rubber Processing and Applications, 1981. vol. 1 (1): pp. 9-24.

Panova L. G., Artemenko S. Y. E., Besshaposhnikova V. I. and Andreyev V. V., "Behaviour Features of Composite Polymer Materials Based on Fire-Resistance Polyester Fibres During Pyrolysis and Burning". Polymer Science 1988. vol.10 (30): pp. 2318-2323.

Perry R. H and Chilton C. H. "Chemical Engineers Handbook", McGraw-Hill Book Company, 1973.

Powell P. C., Engineering with Polymers. Chapman and Hall, 1983.

Scudamore M. J. "Fire Performance Studies on Glass-Reinforced Plastic laminates" Fire and Materials, 1994. vol 18: 313-325.

Sorathia U., and Beck C, "Fire Protection of Glass/Vinyl Ester Composites for Structural Applications" in Int. SAMPE Symp, 1996. p. 687.

Sorathia U., Rollhauser CM and Allen Hughes W., "Improved Fire Safety of Composites for Naval Applications" Fire and Materials, 1992. vol. 16: pp. 119-125.

Stringfellow W.D., "Fibreglass Pipe Handbook" Fibreglass Pipe Institute, New York, 1992.

Tavman I. H., Akinci H., "Transverse Thermal Conductivity of Fibre Reinforced Polymer Composites", Int. Comm. Heat Mass Transfer, 2000. vol. 27 (2): pp. 253-261.

Tewarson, "SFPE Handbook of Fire Protection Engineering" NFPA, Chapter 4, pp. 3-53, 1995.

The Engineer: Fire Fighting with Passive Resistance, vol. 18, 1990. p. 31.

Tolukian and Goldsmith, "Thermophysical Properties of High Temperature Solid materials" TPRC, Purdue University, or Hand book of Thermophysical Properties, MacMillan Press, 1961.

Troitzsch J., International Plastics Flammability Handbook, Hanser, 1983.

Van Krevelen, D. W., Van Heerden C., and Huntjens F. J., "Physicochemical Aspects of the Pyrolysis of Coal and Related Orgainc Compounds" Fuel, 1951. vol 30: p. 253.

Varma I. K. and Gupta V. B., "Thermosetting Resin Properties. Chapter 2.01 of comprehensive Composite Materials", Eds A Kelly and C Zweben, Elsevier, 2000.

Wickstom U and Goransson U, "Predition of Heat Release Rates of Surface Materials in Large-Scale Fire Tests Based on Cone Calorimetery Results" ASTM J. of testing and evaluations, 1987. vol. 15 (6): p.64.

Wu Y-S., Wilcox J. A. D., Gibson, A. G. and Bettess, P., "Design of Composite Panels for Mechanical and Fire Performance" Final Report for British Gas plc, University of Newcastle-upon-Tyne, 1993.

Appendix

COM_FIRE PROGRAM INPUT AND OUTPUT DATA

The main input data file to the program are(unit = 31, file = fort.31) and (unit = 32, file = fort.32).

The main input data file (unit=31, file=fort.31)

Set 1. **JOB:** the first set is used as the title of the job.

Set 2. **FNUM:** The dimensionless Fourier number in heat transfer analysis. A value of 0.05 is recommended in most of cases.

Set 3. **TEMP_ROOM:** The room temperature (in: °C) specified. It is assumed that the initial temperatures at all the 51 nodes are the same as the specified room temperature.

Set 4. **NRESIN**: This set used to define the resin system involved:

= 1, for polyester resin;

= 2, for vinyl ester resin;

= 3, for epoxy resin;

= 4, for phenolic resin.

Set 5. **NFIBRE**: Is used to define the type of the glass reinforcement involved:

= 1, for E-glass fibres;

= 2, for carbon fibres;

= 3, for Kevlar fibres.

Set 6. **TIMED, THICK, VOLFR**: In this set, the **TIMED** is the required fire exposure time period (in minute) for examination. The set **THICK** is the thickness of the GFRP laminate under examination (in: mm). **VOLFR** is the fibre volume fraction of the GFRP laminate under examination.

Set 7. **ND1, ND2, ND3, ND4, ND5, ND6, ND7**: **ND1, ND2,** and **ND7** are the seven node numbers (chosen from 2 to 51) for printing out relevant results with these nodes. For example, ND4 = 26 means that the corresponding results for the mid-plane node or for the 25th layer of the laminate are those in the middle column of the file.

Set 8. **KDEGRA:** This set is used to specified whether the parameter of material degradation effects included in the analysis or not.

= 0, (Not including);

= 1, (Yes including.

Set 9. **KMASFL**: Is controlling parameter for gas mass flow effects

= 0, the effects are not included in the analysis;

= 1, the effects are included in the analysis.

Set 10. **AA, EE, H**: This set is used to define the three kinetic parameters of the first stage of the reaction.

AA The pre-exponential factor in the Stage–1 reaction (in: 1/sec)

EE The activation energy in the Stage–1 reaction (in: J/mol).

H The heat of decomposition in the Stage–1 reaction (in: J/kg).

Set 11. **AA2, EE2, H2**: This set has to be used to define the kinetic parameters for the second stage of reaction. This set used for the case of Phenolic resin.

Set 12. **RC12**: The residual resin content (RRC) value at the end of stage I reaction during the decomposition process is specified in this set. This is only applying for phenolic resin system.

Set 13. **K FUR, K CF**: The **K FUR** input indicator for the control of the type of the heat source under examination:

= 0, for HC curve;
= 1, for the case where the heating source is defined by the input data file (unit=32);
= 2, for a constant heat flux;
= 3, for SOLAS fire curve.

The **K_CF** input indicator for the control of thermal boundary conditions on the CF of the laminate:

= 0, the CF is thermally insulated;

= 1, natural convection combined with free radiation for the CF;
= 2, connected to a steel plate of a given thickness.

Set 14. **EMIS_HTSO, EMIS_GRP, ABSORP_GRP**: In this set, the emissivity of the heating source **EMIS_HTSO**, the emissivity of the GRP laminate's front surface **EMIS_GRP** and the absorptivity of the GRP laminate's front surface **ABSORP_GRP** have to be specified.

Set 15. **K_WATER**: The input indicator for including effect of water (moisture) content on energy transfer due to water vaporization:

= 0, the effect is not included in the analysis;
= 1, the effect is included in the analysis.

Set 16. **Q_FLUX**: Is the constant heat flux input (in: kW/m^2). This set has to be omitted if type of heat source is not as a constant heat flux.

Set 17. **THICK_STEEL, K_CFST**: It has to be omitted if the thermal boundary conditions on the CF of the laminate is not connected to a steel plate of a given thickness.

For **THICK_STEEL** the thickness of the steel plate connected with the CF of the laminate under examination (in: mm);

For **K_CFST** the input indicator for the control of the type of thermal boundary conditions on the CF of the steel plate:

= 0, the CF of the steel plate is thermally insulated;
= 1, natural convection combined with free radiation for the CF of the steel plate.

Set 18. **CNT_WATER, HTD**: Omitted if effect of water (moisture) content on energy transfer is not included in the analysis.

For **CNT_WATER** the initial percentage of water (moisture) content absorbed in the composite laminate (in: %);

For **HTD** one half of the temperature range centred at 100 ° C, in which water vaporization process is assumed to take place.

The input data file (unit=32, file=fort.32)

The input data from this unit is used for the case where the heating source is defined from experimental data result.

Set 1. **JOB**: Is used for identification of the job.

Set 2. **N_FUR**: Is the total number of the data lines in this input file. Each of the data lines indicates the environmental temperature at a given time.

Set 3. **MOS**: The input indicator of the time unit adopted in Set 3 of this file:

= 1, the time unit adopted in this input file is minute;
= 2, the time unit adopted in this input file is second.

Set 4. **TIME_FUR(I), TEMP_FUR(I)**:

TIME_FUR a given time (in second or in minute);
TEMP_FUR the environmental temperature at the given time (in: ^{o} C).

One should note that the input maximum value, **TIME_FUR**, in this file has to be either equal to or greater than the input value of **TIMED** defined in the main input file (unit=31).

The input data file (unit=32, file=fort.32)

There are five output files from running this program. These include files of unit=30, unit=40, unit=50, unit=60 and unit=70. All output files are self-explained.

Unit=30, file='fort.30'

The main part of the print-out in this file is the temperature profiles in the through-thickness direction of the laminate at the chosen seven node positions for the specified fire exposure time period.

Unit=40, file='fort.40'

This output file shows the predicted RRCs (Remaining Resin Contents) as functions of time at the chosen seven layers of the laminate. The RRCs are expressed as the ratio of remaining resin content over the initial resin weight in percentage.

Unit=50, file='fort.50'

This output file shows the predicted RTMs (Remaining Total Mass) as functions of time at the chosen seven layers of the laminate. The RTWs are expressed as the ratio of remaining total mass over the initial value of the layer in percentage.
Through combining the data in this output file with those contained in output file 'fort.30', one may obtain the messages on RTMs as functions of temperature at the chosen seven layers, which are very similar to the experimental data obtained from TGA tests.